ANTHRACYCLINE-INDUCED CARDIOTOXICITY: THE ROLE OF PROTEOLYTIC PATHWAYS

by

Balindiwe JN Sishi

Dissertation presented for the Degree of

DOCTOR OF PHILOSOPHY
(Physiological Sciences)

In the Department of Physiological Sciences

At Stellenbosch University

Promotor: Prof Anna-Mart Engelbrecht

Co-Promotors: Dr Benjamin Loos and Prof Jacques van Rooyen

Faculty of Science

Department of Physiological Sciences

March 2012

Declaration

By submitting this thesis electronically, I declare that the entirety of the work contained therein is my own, original work, that I am the owner of the copyright thereof (unless to the extent explicitly otherwise stated) and that I have not previously in its entirety or in part submitted it for obtaining any qualification.

Date: March 2012

Abstract

Introduction: The anthracyclines (ACs), daunorubicin (DNR) and doxorubicin (DXR) are two of the most effective drugs known for the treatment of systemic neoplasms and solid tumours. However, their clinical use is often hampered by their dose-dependent cumulative cardiotoxicity, which leads to irreversible and fatal drug-induced congestive heart failure. The mechanism by which ACs induces heart damage is not fully understood. Recent reports have indicated that DXR activates autophagy and ubiquitin proteasome-mediated degradation of specific transcription factors, however, no reports exists on the effect of ACs on the E_3 ubiquitin ligases, MuRF-1 and MAFbx. The aim of the first part of the study was therefore to investigate the effect of DNR treatment on the protein and organelle degradation systems in the heart and to elucidate the signalling mechanisms involved.

Although this model was ideal in allowing the investigation of the signalling pathways which are affected by DNR, it did not allow for further exploration or manipulation of signalling pathways that may be of potential benefit in this context. The *in vitro* model was therefore used to validate the hypothesis that increased autophagy alleviates AC-induced cardiotoxicity and delays the onset of cardiomyocyte death. The aims for the second part of the study were (i) to characterize the effect of DXR in H_9C_2 cells, (ii) to determine whether the induction/inhibition of autophagy in combination with DXR alleviates cytotoxicity and (iii) to investigate the influence of increased/decreased autophagy in combination with DXR on reactive oxygen species (ROS) production, mitochondrial function, endoplasmic reticulum (ER) stress and the ubiquitin proteasome pathway. In the final part of this study, an *in vivo* model was used to assess the potential benefit of autophagy in a novel GFP-LC-3 tumour bearing mouse model of acute DXR-induced cardiotoxicity.

Material and Methods: Adult rats were divided into two groups where one group received six intraperitoneal injections of 2 mg/kg DNR on alternate days and the other group received saline injections as control. Hearts were excised and perfused

on a working heart system the day after the last injection and freeze clamped for biochemical analysis.

H_9C_2s were cultured and treated with Bafilomycin A1 (10 nM, inhibitor of autophagy) for 6 hrs, Rapamycin (50 μM, inducer of autophagy) for 24 hrs, DXR (3 μM) for 24 hrs or a combination of these drugs. Following treatment, cells were harvested and assessed for cell death, proteolytic activity and oxidative stress using western blotting, fluorescence microscopy and flow cytometry.

In the final phase of the study, twenty-four female mice were injected at 8 weeks with a mouse breast cancer cell line (EO771) and after observation of tumour growth, animals were either treated with one injection (i.p.) of Rapamycin (4 mg/kg), two injections (i.p.) of DXR (10 mg/kg) or a combination of the two drugs. After the experimental protocol, mice were terminated and their hearts were rapidly excised. The hearts were divided cross-sectionally and utilized for biochemical and histological analyses.

Results and Discussion: DNR treatment significantly attenuated myocardial function and increased apoptosis in the *ex vivo* heart model. DNR-induced cardiac cytotoxicity was associated with the upregulation of two E_3 ubiquitin ligases, MuRF-1 and MAFbx as well as a significant increase in two markers of autophagy, beclin-1 and LC-3. These changes observed in the heart were also associated with attenuation of the PI3-kinase/Akt signalling pathway.

The augmentation of autophagy with rapamycin before DXR treatment significantly reduced cell death in the *in vitro* model. Indeed, rapamycin treatment demonstrated to be a vital survival mechanism for acute DXR-induced cardiotoxicity as it decreased cellular ROS production, improved mitochondrial function and prevented nuclear translocation of DXR. Moreover, these changes in cardiomyocytes were also associated with a reduction in the ubiquitin-proteasome pathway (UPP).

In the final part of this study, a novel tumour bearing GFP-LC3 mouse model was developed to confirm the results obtained in the *in vitro* study. It was demonstrated that acute DXR-induced cardiotoxicity resulted in increased apoptosis, the inhibition of autophagy and increased proteolysis via the UPP. These findings were associated with a reduction in body weight and cardiomyocyte cross-sectional area. The cardiotoxic effects of DXR were substantially reduced when autophagy was induced with rapamycin. Taken together, our data strongly indicates that it is possible to attenuate the cardiotoxic effects of doxorubicin in cancer patients by carefully controlling the levels of autophagy using rapamycin as adjuvant therapy.

Uittreksel

Inleiding: Die antrasikliene (AC's), daunorubisien (DNR) en doksorubisien (DKS), is twee van die mees effektiewe AC wat bekend is vir die behandeling van sistemiese neoplasmas en soliede tumore. Hulle kliniese gebruik word egter deur dosis afhanklike kumulatiewe kardiotoksisiteit benadeel, wat tot onomkeerbare en dodelike kongestiewe hartversaking kan lei. Die meganisme waardeur AC's hartversaking kan veroorsaak, word nog nie ten volle verstaan nie. Onlangse navorsing het aangetoon dat DKS autofagie en die ubikwitienproteosoom-bemiddelde degradasie van spesifieke transkripsie faktore aktiveer. Daar is egter geen literatuur wat die effek van AC's op die E_3-ubikwitienligases, MuRF-1 en MAFbx beskryfnie. Die doel van hierdie eerste afdeling van die studie is om die effek van DNR behandeling op die proteïen- en organel degradasie sisteme in die hart te ondersoek en om van die betrokke seinmeganismes te bepaal.

Alhoewel hierdie model ideaal is om sommige seinweë wat deur DNR geaffekteer word, te ondersoek, kon seinoordragpaaie wat potensieël voordelig in hierdie konteks is, nie in bg. model gemanipuleer word nie. Die *in vitro* model is gebruik om die hipotese dat verhoogde outofagie AC-geïnduseerde kardiotoksisiteit verlaag en sodoende seldood verminder, te bevestig. Die doel van hierdie afdeling van die studie was: (i) om die effek van DKS op H_9C_2 selle te karakteriseer, (ii) om te bepaal of die induksie/inhibisie van outofagie in kombinasie met DKS kardiotoksisiteit verbeter (iii) om die invloed van verhoogde/verlaagde outofagie in kombinasie met DKS op reaktiwe suurstof species (ROS), mitokondriale funksie, endoplasmiese retikulum (ER) stress en die ubikwitienproteosoompad te ondersoek. In die finale deel van hierdie studie, is 'n *in vivo* model gebruik om die moontlike voordelige effek van verhoogde outofagie in 'n GFP-LC-3 tumor-draende muismodel met akute DKS-geïnduseerde kardiotoksisiteit, ondersoek.

Materiaal en Metodes: Volwasse rotte is in twee groepe verdeel waar een groep ses intraperitoneale inspuitings van 2 mg/kg DNR op afwissellende dae ontvang het

en die andergroep as ‘n kontrole, ‘n soutoplossing gekry het. Die harte is verwyder en geperfuseer op ‘n werkende hartsisteem een dag na die laaste inspuiting en gevriesklamp vir biochemiese analises.

H_9C_2 selle is vir 6 uurgekweek en behandel met Bafilomisien A1 (10 nM, ‘n autofagie inhibitor), 24 uur met Rapamisien (50 µM, ‘n autofagie induseerder), 24 uur met DKS (3 µM) of ‘n kombinasie van hierdie middels. Na behandeling is selle ge-oes vir analises in seldood, proteolitiese aktiwiteit en oksidatiewe stress deur van westelike kladtegniek, fluoresensie mikroskopie en vloeisitometrie gebruik te maak.

In die finale fase van hierdie studie is vier en twintig, agt weke oue wyfie muise ingespuit met ‘n muisborskankersellyn (E0771) en is tumorgroei waargeneem; die diere is of behandel met een rapamisien inspuiting (i.p) (4 mg/kg), of twee DKS inspuitings (i.p.) (10 mg/kg) of ‘n kombinasie van die twee middels. Na die eksperimentele protokol, is die muise van kant gemaak en hulle harte vinnig verwyder. Die harte is in twee verdeel en gebruik vir biochemiese- en histologiese analises.

Resultate en Bespreking: DNR behandeling het kardiale funksie betekenisvol verswak en apoptose in die hart verhoog. DNR-geïnduseerde kardiotoksisiteit is geassosieer met die opregulering van E_3-ligases, MuRF-1 en MAFbx en het ook ‘n betekenisvolle toename in twee outofagie merkers, beclin-1 en LC-3 veroorsaak. Hierdie veranderinge wat in die hart waargeneem is, is ook geassosieer met ‘n onderdrukking van die PI3-kinase/Akt seinweg.

Die toename in outofagie met rapamisien voor DKS behandeling het seldood in die vorm van apoptose betekenisvol verlaag. Daarmee saam het verhoogde outofagie ‘n noodsaaklike oorlewings meganisme vir akute DKS-geïnduseerde kardiotoksisiteit gedemonstreer. Die rede hiervoor is dat dit ROS produksie verlaag het, mitokondriale funksie verbeter het en DKS translokasie vanuit die sitoplasma tot

binne die nukleus verhoed het. Hierdie veranderinge in kardiomiosiete is ook met ‘n afname in die ubikwitienproteosoomseinweg (EPS) geassosieer.

In die finale deel van hierdie studie, is ‘n nuwe tumor-draende muismodel ontwikkel om die resultate wat in die *in vitro* studie gekry is, te bevestig. Daar is bewys dat akute DKS-geïnduseerde kardiomiotoksisiteit aanleiding gegee het tot verhoogde apoptose, outofagie inhibisie en verhoogde proteolise via die EPS. Hierdie bevindinge is geassosieer met ‘n verlaging in liggaamsgewig en kardiomiosiet dwarssnit area. Die kardiotoksiese effekte van DKS is insiggewend verminder as autofagiege ïnduseer is met rapamisien. Om saam te vat: Ons data bevestig dat dit moontlik is om die kardiotoksiese effekte van DKS in kanker pasiënte te verminder deur outofagie vlakke te monitor en te kontroleer deur middel van rapamisien behandeling as bykomende terapie.

Acknowledgements

My sincerest appreciation to the following people, for without their assistance this study would not have been completed:

Thank you **Heavenly Father** for giving me the strength, ability and endurance to persevere in challenging times

Prof Anna-Mart Engelbrecht (supervisor): who patiently guided and supported me every step of the way. I cannot express my gratitude to you and what you have done for me. Thank you for entrusting me with this mammoth project. Thank you for the opportunity to learn something new and for allowing me to spread my wings. Thank you for having so much faith in me even though at times I didn't have any. You are truly one in a million

Dr Benjamin Loos (co-supervisor): for your advice, expertise and overwhelming support with this project. Thank you for the endless hours you've spent with me trying to explain difficult concepts and in doing so, stimulating my brain with ideas. You are an inspiration to me and many others

Prof Jacques van Rooyen (co-supervisor): for the motivation for this project. Thank you for entrusting me with the huge task of western blots when you needed someone to do them. Most importantly, thank you for a great time spent in Norway

Prof Anne K Jonassen, Lars Breivik, Eva-Katrine Aarnes & Anita Wergeland: for teaching me the art of perfusions. Thank you for welcoming me with open arms and making me feel at home in Norway. Thank you for the many laughs we shared and for teaching me how to ski

Prof Kathy H Myburgh: for seeing something in me way back in 2007. Thank you for considering my application for honours when I didn't even meet the minimum requirements. Thank you for saying "you can do it" and for pushing me in the right direction. And last but not least, thank you for the CRITICAL ANALYSIS lectures, had it not been for those lectures …

Prof Faadiel M Essop: for showing me that the heart is not such a complicated organ to understand. Thank you for your patience and the passion you have for the department. And thank you for always listening to the cries of the students

Dr Theo Nell (my brother from another mother): for your encouraging words and your help in translating my abstract from English to Afrikaans

My friends and colleagues: for their help, encouragement and support, especially the DSG team. Their spirit, enthusiasm, sense of humour and laughter helped insure an uplifting environment everyday

Dr Fillipo Macaluso, Ashwin Issacs & MJ van Vuuren: for your technical assistance with my histological samples

Academic and Technical Staff: for their GREAT leadership

Katrina: Thank for greeting me with a smile every morning without fail and for keeping me company during the weekends. **Johnifer**: for the friendly chats about the weekend's soccer

My parents, brothers and sisters, family members: for their love and support

TandekileLubelwana: for being such a great friend. Thank you for the long “catch-up” sessions via skype and for always telling me to think big

ThandoMakomazi: for his enthusiasm, tolerance and encouragement when it was most needed. Thank you for being such a great audience whenever I needed someone to practice my talks with

National Research Foundation and the **Andrew Mellon Foundation**: for their financial support which allowed me to continue with my studies

BSCR-SASCAR: for the opportunity provided to attend the 1st BSCR-SASCAR Cardiovascular Research Workshop held in London, UK

List of Conference Proceedings

International

- Sishi B & Engelbrecht A-M. Anthracycline-induced cardiotoxicity: the influence of elevated autophagy through amino acid deprivation and rapamycin treatment. Presented at the 1st BSCR-SASCAR Cardiovascular Research Workshop held in London, UK; 6th December-10th December 2010.

National

- Sishi B andEngelbrecht A-M. The effect of obesity-induced insulin resistance on skeletal muscle signalling in a rodent model. 35th meeting of the Physiology Society of Southern Africa (PSSA). 9th-12th September 2007. University of Witwatersrand, South Africa. Abstract accepted for Oral presentation

- Sishi B andEngelbrecht A-M. An investigation into the PI3K/Akt signalling pathway in TNF-α-induced muscle proteolysis in L6 myotubes. 36th meeting of the Physiology Society of Southern Africa (PSSA). 16th-19th September 2008. University of Pretoria, South Africa. Abstract accepted for Oral presentation

- Sishi B and Engelbrecht A-M. Anthracycline-induced cardiac myopathy. 37th meeting of the Physiology Society of Southern Africa (PSSA). 7th-9th September 2009. University of Stellenbosch, South Africa. Abstract accepted

- Sishi B, van Rooyen J and Engelbrecht A-M. Anthracycline-induced cardiotoxicity: Role of proteolytic pathways. 10th Annual Congress of the South African Heart Association (SAHA). 22nd – 25th October 2009. Sun City, South Africa. Abstract accepted for Poster presentation

- Sishi B and Engelbrecht A-M. Diet-induced obesity alters signalling pathways and induces atrophy and apoptosis in skeletal muscle in a prediabetic model. 38th meeting of the Physiology Society of Southern Africa (PSSA). 27th-29th September 2010. Walter Sisulu University (WSU), South Africa. Abstract accepted for Oral presentation

- Sishi B, Loos B, van Rooyen J and Engelbrecht A-M. Anthracycline-induced cardiotoxicity: the role of autophagy. 39th meeting of the Physiology Society of Southern Africa (PSSA). 28th - 31th August 2011. University of the Western Cape (UWC), South Africa. Runner-up in the Wyndham Student Competition

- Sishi B, Loos B, van Rooyen J and Engelbrecht A-M. Anthracycline-induced cardiotoxicity: Role of proteolytic pathways. 11th Annual Congress of the South African Heart Association (SAHA). 23rd – 26th October 2011. East London, South Africa. Best Oral presentation in the Basic Sciences Category

List of Publications

- Sishi, B., Loos, B., Ellis, B., Smith, W., du Toit, E., Engelbrecht, A.-M. 2010. Diet-induced obesity alters signalling pathways and induces atrophy and apoptosis in skeletal muscle in a prediabetic model. *Experimental Physiology*. 96: 179-193

- Sishi, B.J.N., Engelbrecht, A.-M. 2011. Tumor necrosis factor alpha (TNF-α) inactivates the PI3-Kinase/PKB pathway and induces atrophy and apoptosis in L6 myoblasts. *Cytokine*. 54: 173-184

- Sishi, B.J.N., Bester, D.J., Wergeland, A., Loos, B., Jonassen, A.K., van Rooyen, J., Engelbrecht, A.-M. Daunorubin therapy is associated with upregulation of E3 ubiquitin ligases in the heart. Recently (31 October 2011) accepted for publication in *Experimental Biology and Medicine*

List of Collaborative Publications

- Wergeland, A., Bester, D.J., Sishi, B.J.N., Engelbrecht, A.-M., Jonassen, A.K., van Rooyen, J. 2011. Dietary Red Palm Oil protects the heart against the cytotoxic effects of anthracyclines. *Cell Biochemistry and Function*. 29: 356-364

INDEX

Chapter 2–*Ex vivo* Model

Chapter 3–*In vitro* model

Chapter 4 – *In vivo* model

Chapter 5

Appendices

List of Figures

Chapter 1

Chapter 2

Chapter 3

Chapter 4

List of Tables

Chapter 2

Chapter 3

List of Abbreviations

&	and
1º	Primary
2º	Secondary
3MA	3-methyladenine

A

AC/s	Anthracycline/s
ADP	Adenosine phosphate
AMP	Adenosine monophosphate
AMPK	AMP-activated protein kinase
ANOVA	Analysis of variance
AO	Aortic output
AOP	Aortic pressure
Apaf-1	Apoptosis protease activation factor-1
APS	Ammonium persulfate
ASK-1	Apoptosis signal-regulating kinase-1
ATF-2	activating transcription factor 2
ATF-4	activating transcription factor 4
ATP	Adenosine triphosphate
AVO/s	Acidic vesicular organelle/s

B

Bax	Bcl-associated partner containing six exons
Bcl2	B-cell lymphoma 2
BD	Bafilomycin doxorubicin

Bid	Bcl2 -interacting domain
BSA	Bovine serum albumin

C

C	Control
Ca^{2+}	Calcium
CaMKK-β	Ca^{2+}/calmodulin-dependent kinase kinase-β
Caspase	Cysteine aspartate-specific protease
CD	Control doxorubicin
CF	Coronary flow
CH_3	Methyl group
CHF	Chronic Heart Failure
CHOP	CCAAT/enhancer binding protein (C/EBP) homologous protein
CK	Creatine kinase
CM	Control siRNA (mTOR)
CMA	Chaperone mediated autophagy
CO_2	Carbon dioxide
$COOH^-$	Carboxyl terminal
c-PARP	cleaved-poly ADP ribose polymerase
CR	Control rapamycin
CVD/s	Cardiovascular disease/s
Cyto.-c	Cytochrome-c

D

DAPI	4',6-Diamidino-2-phenylindole
dATP	Deoxyadenosine triphosphate
DCF	Dichlorodihydrofluorescein

DMEM	Dulbecco's modified Eagle's medium
DMSO	Dimethyl sulfoxide
DNA	Deoxyribonucleic acid
DNR	Daunorubicin
DTT	Dithiothreitol
DXR	Doxorubicin

E

ECG	Electrocardiogram
EDTA	Ethylenediaminetetraacetic acid
eIF2α	Eukaryotic initiation factor 2α
et al	Et alii
ER	Endoplasmic reticulum
ERAD	Endoplasmic reticulum-associated protein degradation
ERK/s	Extracellular signal-regulated kinase/s

F

FADD	Fas-associated death domain
FAS-L	FAS ligand
FBS	Fetal bovine serum
FITC	Fluorescein isothiocyanate
FKBP-12	FK506-binding protein-12
FLIP	FLICE inhibitory protein
FoxO	Forkhead box
FoxO1	Forkhead box 1
FoxO3	Forkhead box 3

G

GADD34	Growth arrest DNA damage-inducible protein 34
GFP-LC3	Green fluorescent protein -microtubule-associated protein light chain 3
GSK3β	Glycogen synthase kinase 3β
GβL	G-protein β-subunit like protein

H

H&E	Hematoxylin and Eosin
H_2O_2	Hydrogen peroxide
HCl	Hydrogen chloride
HF	Heart Failure
HIF-1	Hypoxia inducible factor-1
Hsp70	Heat shock protein 70

I

i.p.	Intraperitoneal
IGF	Insulin growth factor
IKK	I kappa B kinase
IRE-1	Inositol requiring kinase1
IRS-1	Insulin receptor substrate-1

J

JC-1	5,5',6,6',-tetrachloro-1,1',3,3',-tetraethylbenzimidazolylcarbocyanine
JNK	c-Jun NH_2-terminal kinase

K

KHB	Krebs Henseleit Buffer

L

Lys	Lysine
LC-3	Microtubule-associated protein light chain-3
LDH	Lactate dehydrogenase
LPS	lipopolysaccharide
LV	Left ventricular
LVEF	Left ventricular ejection fraction

M

MADD	MAP kinase-activating death domain protein
MAFbx	Muscle atrophy F-box
MAPK	Mitogen activated protein kinase
MD	siRNA (mTOR) doxorubicin
mRNA	messenger Ribonucleic acid
mTOR	Mammalian target of rapamycin
mTORC1	Mammalian target of rapamycin complex 1
MTT	3-(4,5-dimethylthiazol-2-yl)-2,5-diphenyltetrazolium bromide
MuRF-1	Muscle RING finger-1
MyPB-C	Myosin binding protein-C

N

NaCl	Sodium chloride
NADH	Nicotinamide adenine dinucleotide reduced
NADPH	Nicotinamide adenine dinucleotide phosphate

NaF	Sodium fluoride
NFAT	Nuclear factor of activated T-cells
NF-κB	Nuclear factor- kappa B
NIK	NFkB inducing kinase
Nox1	NADPH oxidase 1

O

O_2^-	Superoxide anion
OD	Optical density
OH	Hydroxyl radical

P

P	phosphate
p70S6-K	p70S6-kinase
PARP	Poly ADP ribose polymerase
PBS	Phosphate buffered saline
PCD	Programmed cell death
Penstrep	Penicillin/Streptomycin
PERK	RNA-dependent protein kinase (PKR)-like ER kinase
PI	Prodium Iodide
PI3-K	Phosphotidylinositol 3-kinase
PKB	Protein kinase B
PMSF	Phenylmethylsulphonyl fluoride
PTEN	Phosphatase and tensin homolog
PUMA	p58-upregulated mediator of apoptosis
PVDF	Polyvinylidene fluoride

R

RAIDD	RIP associated Ich-1/CED homologous protein with death domain
raptor	Regulatory associated protein of mTOR
RD	Rapamycin doxorubicin
RIP	receptor-interacting protein
RIPA	Radio immunoprecipitation assay
ROS	Reactive oxygen species

S

SBTI	Soybean trpysin inhibitor
SDS-PAGE	Sodium dodecyl sulphate polyacrylamide gel electrophoresis
SEM	Standard error of the mean
Ser	Serine
SiRNA	Small interfering ribonucleic acid
SOD	Superoxide dismutase
SQSTM1	Sequestome 1
SRC	Standard rat chow

T

tBid	Truncated Bid
TBS-T	TRIS-buffered saline-Tween
TNF-R	TNF- α receptor
TNF-R1	Tumor necrosis factor receptor type 1
TNF-α	Tumour necrosis factor-α
TnI	Troponin I
TnT	Troponin T
TRADD	Tumor necrosis factor receptor type 1-associated death domain

TRAF-2	TNF receptor-associated factor 2
TRAIL	Tumor necrosis factor-related apoptosis-inducing ligand
TRIS-HCl	Tri-(hydroxyl-methyl)-aminomethane-hydrogen chloride
TUNEL	Terminal nucleotidyltransferase-mediated nick end labelling

U

Ub	Ubiquitin
UPP	Ubiquitin-proteasome pathway
UPR	Unfolded protein response
UV	Ultraviolet

V

vs	versus

Units of measurement

%	percent/percentage
A	ampere
AU	arbitrary units
cm	centimetre
cm^2	centimetres squared
g	gram
hr/s	hour/s
kD	kilodalton
l/L	litre
M	molar
mg	milligram
mg/kg	milligram per kilogram
mg/m^2	milligram per metre squared
min	minutes
ml	millilitres
ml/min	millilitre per minute
mm	millimetre
mM	millimolar
mmol/l	millimoles per litres
mm/Hg	millimetres of mercury
mm^2	millimetre squared
nm	nanometre
nM	nanomolar
ºC	degrees Celsius
RLU	relative light units

rpm	revolutions per minute
sec	seconds
V	volt
µg	microgram
µg/ml	microgram per millilitre
µmol/L	micromoles per litre
µl	microlitre
µm	micrometre
µM	micromolar
μm^2	micrometre squared

Chapter 1

Literature Overview

1.1: Introduction

Heart failure is clinically a complex syndrome with a number of causes. Despite aggressive treatment, heart failure leads to substantial morbidity and mortality, and is increasing in most parts of the world (Hunt *et al*, 2005). The prevention of heart failure is therefore a very important clinical and public health priority. Due to this condition being costly, disabling and potentially lethal, there is a need for novel adjuvant therapies that act in ways unlike those currently established therapies.

Since their introduction in the early 1960s, drugs of the anthracycline (AC) group, in particular doxorubicin (DXR, Adriamycin) and daunorubicin (DNR), have made significant advances in the improvement of cancer treatment (Singal *et al*, 1997; Barrett-Lee *et al*, 2009; Tokarska-Schlattner *et al*, 2006). These drugs are considered the most effective and extensively used potent anti-cancer agents for the treatment of a wide variety of soft and solid human malignancies (Di Marco *et al*, 1969). This optimism however quickly faded when it became evident that their clinical utility is limited by their cumulative, dose-dependent progressive myocardial damage (cardiotoxicity) that may lead to irreversible heart failure (HF), a reduced quality of life or even death (Lefrak *et al*, 1973; Swain *et al*, 2003; O'Shaughnessy *et al*, 2002). Although the methods for detecting and treating cancer have improved, and the survival rate of cancer patients increased, the side effects of cancer adjuvant therapy remains clinically relevant. Cardiotoxicity induced by ACs is dose-related, with the incidence of complications increasing with each subsequent dose (Lefrak *et al*, 1973; Von Huff *et al*, 1977).

Rigorous studies on AC-induced cardiotoxicity have been conducted and literature has provided several mechanisms for their mode of action. However, no consensus currently exists on optimal treatment for adverse cardiac effects in patients with advanced breast cancer. This review discusses current concepts about the

pathophysiology of AC-induced cardiotoxicity, the possible signalling pathways involved and different approaches for its reduction. Although this manuscript revisits an area of research that has been extensively studied, very little attention has been paid to the role of AC-induced cardiotoxicity and proteolytic pathways of the cell, which include autophagy and the ubiquitin proteasome pathway. As both pathways have been implicated to play a role in this context, this may pave the way to identify protective mechanisms that may be exploited for treating or preventing AC-induced cardiotoxicity.

The purpose of this review is therefore to classify AC-induced cardiotoxicity and to discuss the mechanisms involved in its induction. Secondly, it aims to clarify the role of apoptosis and necrosis in the pathogenesis of AC-induced cardiotoxicity. Finally, this review aims to discuss the role of autophagy and the ubiquitin-proteasome pathway, both of which are vital proteolytic systems, in the context of AC-induced cardiotoxicity. It is hoped that this review contributes to a better understanding of the different roles that these pathways play in this context. This may shed new light on the role of the proteolytic systems as a potential avenue to advance current treatment regimens.

1.2: Classification of AC toxicity

The effects of AC toxicity on the cardiovascular system can be categorized as acute, chronic and late-onset (delayed). Many studies have also reported subclinical cardiotoxicity in addition to the observed clinical toxicity which manifests as chronic heart failure (CHF). Studies conducted by Zuppinger *et al* (2007) and Vergely *et al* (2007) have indicated an assortment in the occurrence of both clinical and subclinical cardiotoxicity after AC administration.

1.2.1: Acute cardiotoxicity

Acute and sub-acute cardiotoxicity are rare and independent of the AC dose administered. They are classified by asymptomatic electrocardiographic (ECG) changes, transient arrhythmias, tachycardia, hypotension and myocarditis (Barrett-Lee *et al*, 2009; Singal *et al*, 1997; Tokarska-Schlattner *et al*, 2006). These abnormalities are usually minor and can occur during or immediately after AC

treatment. The acute effects of AC administration are generally not considered a cause for major concern because they are reversible; they resolve unexpectedly and/or are clinically manageable (Steinberg *et al*, 1987). The measurement of plasma concentrations of cardiac tropin I (TnI), a regulatory protein that initiates contractile activity in the myocardium, is a sensitive technique used to detect acute myocardial injury. A powerful and specific biochemical marker of left ventricular damage and inadequate cardiac output is indicated by elevated levels of TnI immediately after a high dose of AC (Cardinale *et al*, 2002; Schimmel *et al*, 2004). This method can also be used as a predictor of the development of ventricular dysfunction (Cardinale *et al*, 2000). Additionally, troponin T (TnT) has also been implicated in the diagnosis and prognosis of cardiomyocyte damage. Evidence supporting this has been found in studies where both children and adults have previously been treated with ACs. Although promising results have been obtained in children, the studies conducted in adults have been contradictory (Lipshultz *et al*, 1997; Sparano *et al*, 2002).

1.2.2: Chronic cardiotoxicity

In contrast, chronic AC-cardiotoxicity, which can manifest months or years after treatment, is clinically the most detrimental type of toxicity, as it is dose-dependent. This type of toxicity ultimately leads to irreversible cardiomyopathic changes with a grim prognosis for affected patients (Horenstein *et al*, 2000; Elliot, 2006). Typical, clinical characteristics of chronic AC cardiotixicity include an excessive decline in blood pressure and ejection fraction, a distinctly increased heart rate and ventricular dilation with subsequent failure (Lefrak *et al*, 1973). Additionally, literature indicates that cardiomyopathy induced by chemotherapeutic agents can be classified by specific ultrastructural pathology. Cardiac biopsies from affected patients feature atrophic cells resulting in smaller diameters (3-6 μ) as well as cytoplasmic vacuolization caused by dilation (Buja *et al*, 1973). The ultrastructural changes can be quantified using the “Billingham scale” in order to determine the severity of heart damage (Bristow, 1982). In a long term prospective study by Von Hoff and colleagues (1979), a total cumulative dose was identified as the major risk factor for the development of CHF, with the risk increasing with each subsequent dose. The total dose was determined to be a cumulative percentage of 3% for patients who received a total cumulative dose

of 400 mg/m^2, 7% for 550 mg/m^2 and 18% for 700 mg/m^2 of ACs (Figure 1). In addition, a similar study has shown that a dose of 850-1000 mg/m^2 induces an increase of CHF over a 5 year period from 11% at 1 year to 14% after 2 years and 20% after 5 years (Jensen *et al*, 2002). These estimations are debatable as the proportion of patients developing AC-induced CHF is said to be approximately 26% (Swain *et al*, 2003).

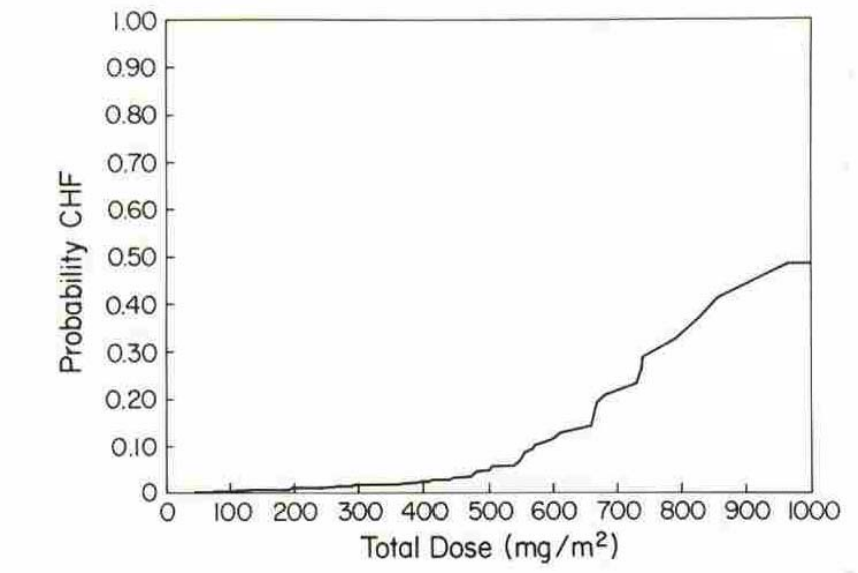

Figure 1: Cumulative probability of developing AC-induced congestive heart failure plotted against total cumulative dose of AC (doxorubicin) in all patients who received the drug. Reproduced from Shan, 1996.

1.2.3: Delayed cardiotoxicity

Late-onset/delayed cardiotoxicity may also be dose related. It occurs years or even decades after AC exposure. It has been suggested to occur in patients who have been exposed to ACs as children, or in patients who present with a thin-walled ventricle that operates against an elevated systolic wall stress (Leandro *et al*, 1994). This stagnant state of compensation over a number of years clinically manifests as late-onset AC-induced cardiac dysfunction. Cardiovascular stressors such as surgery, pregnancy, weight-lifting and acute-viral infection are plausible triggers for late-onset AC-induced cardiotoxicity (Sereno *et al*, 2008; Ali *et al*, 1994).

Various hypotheses highlighting potential mechanisms and/or targets of ACs have been suggested to clarify AC-induced cardiotoxicity, but none of these have been considered fulfilling. This has lead to the definition of AC-induced cardiotoxicity as a

multifactoral process that eventually induces cardiomyocyte death as the terminal downstream event (Minotti *et al*, 2004). Additionally, drug-associated cardiotoxicity, as defined by the cardiac review committee (Cardiac Review and Evaluation Committee - CREC) includes one or more of the following: (i) in terms of cardiomyopathy, a decrease in left ventricular ejection fraction (LVEF), either globally or more severely in the septum; (ii) signs and symptoms of heart failure (HF), such as tachycardia and/or S3 gallop, (iii) a decrease in LVEF that is equal to or greater than 10% but less that 55% without associated signs and symptoms of HF or a decrease in LVEF that is less than or equal to 5% but less that 55% with associated signs and symptoms of HF (Seidman *et al*, 2002).

1.3: Mechanisms of AC-induced cardiotoxicity

Despite its well-documented cardiotoxic effects, the glycosidic AC antibiotics, DXR and DNR (Figure 2), are important antineoplastic agents because of their high anti-tumor efficacy in most types of cancers. The activity of these agents against rapidly dividing cells is mediated by their ability to intercalate into cell DNA base pairs or to form toxic DNA-drug cross-links, thereby interfering with cell division and thus triggering cell death (Gewirtz, 1999). Being chemically unstable in an acidic environment, ACs cannot be taken orally. ACs have a half-life of longer than 24 hours and, after biotransformation in the liver, they are excreted in the bile (Balis *et al*, 1993). The mechanisms by which ACs lead to toxicity include (i) the formation of free reactive oxygen radicals, (ii) direct DNA damage and/or interference with DNA repair and (iii) activation of immune reactions involving antigen-presenting cells in the myocardium (Zhang *et al*, 1993). The cytotoxic action by ACs involves, in addition to its effects on nucleic acids and cellular membranes, the cytoskeleton of tumor cells and cardiomyocytes (Molinari *et al*, 1990). Cytoskeletal changes comprise the decrease in the density of myofibrillar bundles (Jaenke, 1974), modifications on the Z-disc structure of the sarcomere as well as the disorder and depolimerization of actin filaments (Lewis *et al*, 1986; Billingham *et al*, 1978). These detrimental transformations may be induced by the potent inhibitory effect of ACs on cardiac muscle gene expression for myosin light chain 2, troponin, α-actin and the M-isoform of creatine kinase *in vivo* (Ito *et al*, 1990).

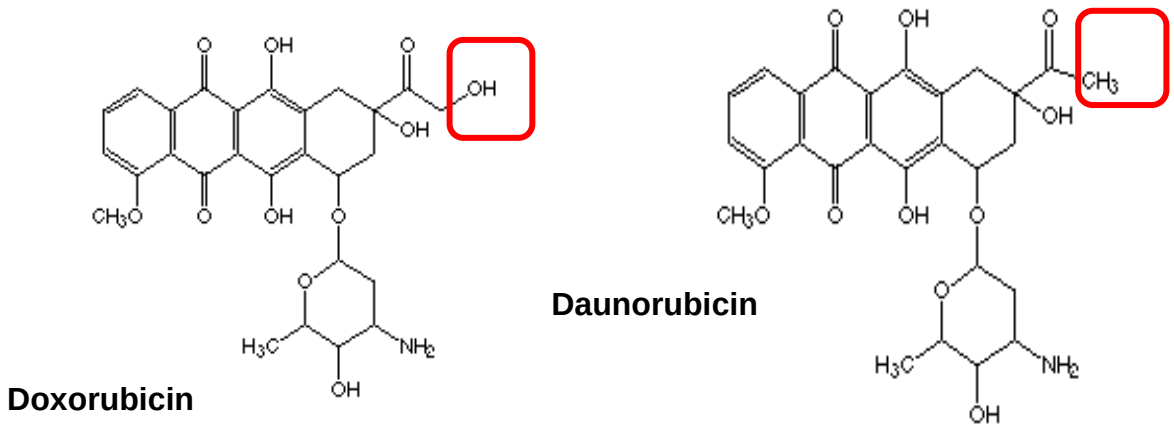

Figure 2: Chemical structures of Doxorubicin (DXR) and Daunorubicin (DNR). Both anthracyclines are identical in structure with the exception that DXR entails a hydroxyl (OH) group whereas DNR entails a methyl (CH_3) group.

The main role player suggested to contribute to AC-induced cardiotoxicity is oxidative stress generated during intracellular metabolism (Vander Heide *et al*, 2007; Schimmel *et al*, 2004; Shan *et al*, 1996). ACs induce the generation of oxygen derived free radicals via two key pathways: a non-enzymatic pathway which makes use of iron (Fe^{2+}) and the enzymatic pathway which operates via the mitochondrial respiratory chain (Figure 3). The non-enzymatic pathway begins with one electron being reduced off an AC molecule to produce an AC semiquion radical by a reduced flavoenzyme such as NADPH-cytochrome-P450 reductase. Reduced AC semiquion radicals bind to iron to form an AC-iron free radical complex. This newly formed complex reduces oxygen to form superoxide and to restore the AC. The superoxide is thus dismutated into hydrogen peroxide (H_2O_2) and oxygen (Rajagopalan *et al*, 1988). Iron is a vital cofactor in the production of many toxic free-radical species that catalyze the Haber-Weiss reaction ($O^{\cdot-}_2 + H_2O_2 \rightarrow HO^{\cdot} + O_2 + HO^{-}$) (Kehrer, 2000). This has led to numerous experimental systems to study iron chelation as an approach to circumvent the generation of free radicals. In this regard, dexrazoxane (Zynecard, Cardioxane) has been found to be a promising agent able to inhibit the production of free radicals due to the iron-chelating effect on intracellular iron (Swain *et al*, 1997; Speyer *et al*, 1988). Even though dexrazoxane can be dispensed intravenously and often in doses 10-fold that of ACs, leukopenia has appeared as a side effect of this drug (Hochster *et al*, 1995), thus rendering it less suitable.

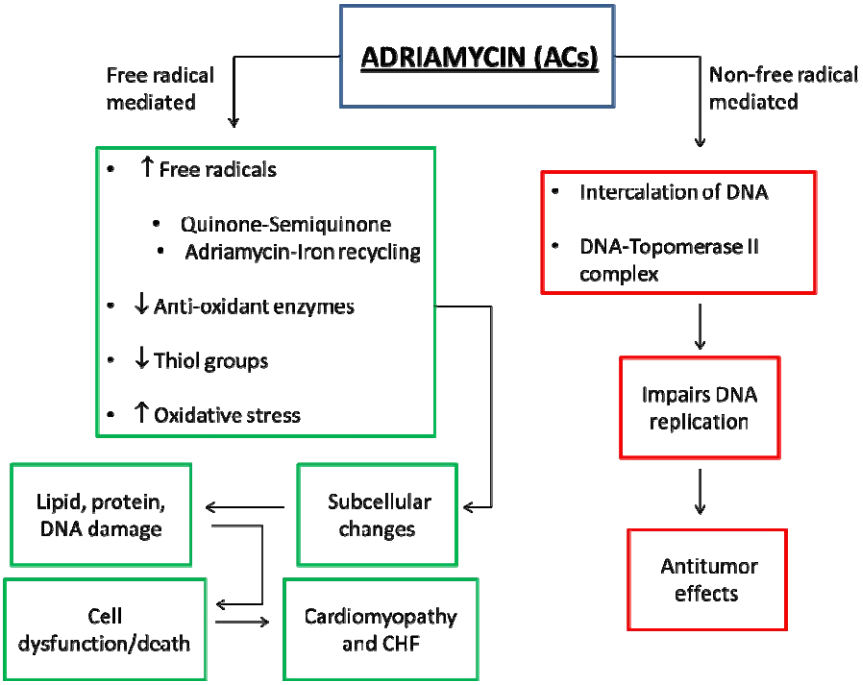

Figure 3: Distinction between the cardiotoxic (green blocks) and antitumor (red blocks) mechanisms of action of anthracyclines (ACs). Abbreviations: CHF – Congestive Heart Failure. Modified from Singal *et al*, 1997.

1.3.1: Role of mitochondria in the mechanism leading to AC-induced cardiotoxicity

Abnormal mitochondria are one of the earliest and most prominent histomorphological features of acute AC-induced cardiomyopathy (Rosenhoff *et al*, 1975). ACs have a high affinity for cardiolipin, a crucial phospholipid first isolated form cardiac tissue, which is enriched in the inner mitochondrial membrane (Nicolay *et al*, 1984; Cheneval *et al*, 1985). This high affinity allows ACs to concentrate within the myocytes (Goormaghtigh *et al*, 1990). A study conducted by Nicolay *et al* (1986) has illustrated that intracellular AC distribution can be monitored through auto-fluorescence microscopy. This technique has produced positive results by demonstrating that ACs accumulate within the mitochondria as well as in the nucleus of the cell. However, the specific mechanism by which this occurs remains to be fully elucidated. Possible explanations for this phenomenon include sustained free radical production due to respiratory chain defects caused by AC-induced mitochondrial damage and the release of cytochrome-c from impaired mitochondria which essentially leads to cardiomyocyte apoptosis (Vander Heide *et al*, 2007). Mitochondria thus play a major role in the action of ACs, predominantly with regard to cardiotoxicity. Another important aspect in AC-induced cardiotoxicity is that

mitochondrial permeability transition provoked by oxidative stress, is thought to trigger several responses depending on the severity of oxidative damage: (i) mild oxidative damage stimulates mitophagy, the selective degradation of mitochondria through autophagy, as a survival or death pathway (Lemasters *et al*, 1998; Kissova *et al*, 2004; Tal *et al*, 2007; Priault *et al*, 2005); (ii) moderate oxidative damage induces apoptosis after mitochondrial membrane permealization and the release of cytochrome-c; and (iii) substantial oxidative damage results in necrotic cell death due to ATP depletion.

The accumulation of ROS within the mitochondria can also initiate additional mitochondrial ROS release which adds to the already elevated oxidative stress in the cell (Suzuki *et al*, 2001). Adult myocytes are terminally differentiated cells which are highly susceptible to oxidative stress due to their high oxidative metabolism and reasonably inferior antioxidant defenses compared to many other organs (Doroshow *et al*, 1980). Indeed, studies in cultured cardiomyocytes suggest that antioxidants such as trolox, 5-aminosalicyclic acid, aminofostine or α-phenyl-tert-butyl nitrone, administered before AC treatment, reduces the incidence of oxidative stress and myocyte injury (DeAtley *et al*, 1999; Dorr *et al*, 1996). Moreover, transgenic mice overexpressing catalase and superoxide dismutase (SOD), which are major antioxidant enzymes in myocytes, have been proven to be cardioprotective against AC-induced cardiotoxicity (Kang *et al*, 1996; Yen *et al*, 1996). Therefore, while the understanding of the mechanism of AC-induced cardiotoxicity continues to advance, the ability to modify myocyte injury awaits development of systems allowing selective but specific delivery of these agents in the heart.

1.4: Cell death associated with AC-induced toxicity

AC-induced toxic insults can trigger a multitude of reactions in cardiomyocytes leading to alterations in myocardial physiology, biochemistry and morphology. Some injuries can be repaired but others cause cell death in the form of apoptosis and necrosis. If the cell survives, structural and functional changes are likely to be present. AC-induced oxidative stress stimulates detrimental modifications to numerous cellular macromolecules including lipids (Myers *et al*, 1977) and proteins (Mihm *et al*, 2002) and DNA (Pacher *et al*, 2002).

1.4.1: Apoptosis

It has long been known that myocardial apoptosis (Figure 4) is a common feature of both acute and chronic myocyte loss (Shan *et al*, 1996; Arola *et al*, 2000), but the mechanism by which ACs induce cardiomyocyte apoptosis remains to be fully elucidated (for comprehensive reviews of the apoptotic pathway see Elmore, 2007; O'Brien *et al*, 2008; Gastman, 2001). Four mechanisms of action have been proposed: (i) ACs stabilize reaction intermediates with DNA and topoisomerase II, consequently resulting in breakage of DNA strands and oncogene (p53)-mediated programmed cell death; (ii) ACs are able to bind to specific allosteric sites on the 20S proteasome causing the accumulation of aggregate prone proteins thus aiding in apoptosis induction; (iii) increased oxygen radical activity generated through semiquione moiety of the AC molecule causes lipid peroxidation and DNA damage. Furthermore, the indirect elicitation of apoptosis by mitochondrial membrane modifications, MAPK signalling molecules, transcription factors, acid sphingomyelinases or apoptotic regulatory proteins, form part of this free radical-mediated myocyte damage; and (iv) iron-mediated free radical production and cell injury by iron release from aconitase of alcohol derivatives of ACs also contribute to myocyte injury (Minotti *et al*, 2004; Shan *et al*, 1996; Laurent *et al*, 2001).

Although ample evidence exists for AC-induced apoptosis in *in vitro* experiments, it is currently unknown whether AC-induced cardiotoxicity induces apoptosis *in vivo*. Although Zhang and co-workers (1996) described DXR-induced apoptosis only in the kidney and intestine but not in the myocardium, Unverferth and others (1983) confirmed morphological characteristics, characteristic of apoptotic cell death in human heart samples (Unverferth *et al*, 1983). In light of this discrepancy, Arola *et al* (2000) described that acute DXR-induced apoptosis in cardiomyocytes was reduced to non-significant levels three days after the cumulative doses were achieved (Arola *et al*, 2000). The induction of apoptosis thus appears to be model and dose-dependent.

Even though most reports employ standard techniques to evaluate apoptotic cell death including Annexin V binding, electron microscopy, caspase-3 activity, DNA fragmentation and terminal nucleotidyl transferase-mediated nick end labeling (TUNEL) positivity, there is still conflicting data on the specificity of the apoptotic

pathway concerned. Findings from Childs and colleagues (2002) revealed elevated cytochrome C release, consistent with the intrinsic mitochondrial pathway of apoptosis (Childs *et al*, 2002). Additionally, Ascensao *et al* (2005) illustrated decreased oxygen consumption at stage 3 of the mitochondrial respiratory chain, elevated malondialdehyde, carbonyl groups, free thiols and suppressed aconitase, all supportive of electron leakage from electron transport complexes (Ascensao *et al*, 2005). In contrast, others have produced evidence of elevated cardiac Fas ligand levels (Nakamura *et al*, 2000; Yamaoka *et al*, 2000), indicating a role for the extrinsic pathway of apoptosis. Furthermore, TNF-α receptor (TNFR) expression levels also appear to be a relevant event in DXR-induced cardiomyocyte death. These studies suggest a role for both the extrinsic and intrinsic pathways of apoptosis, but whether one pathway is dominant over the other or whether both pathways are activated concurrently remains uncertain.

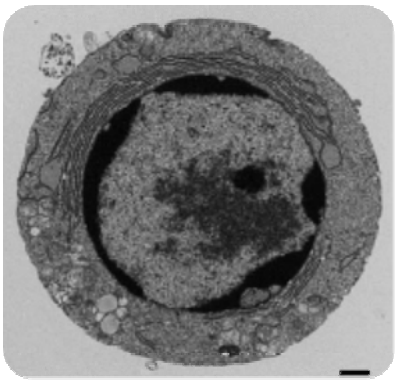

Figure 4: Apoptotic cell death. This type of cell death is morphologically characterized by cell shrinkage combined with pyknosis (chromatin condensation) and karyorrhexis (nuclear fragmentation). Adopted from Edinger & Thompson, 2004.

1.4.2: Necrosis

In contrast to apoptosis, necrosis (Figure 5) has been conventionally viewed as a passive form of cell death and has been widely used to describe myocardial cell death in the past (for comprehensive reviews of the necrotic pathway see Goldstein *et al*, 2006; Chen, 2009; Zong, 2006). The impact of necrosis in myocardial pathogenesis cannot be underestimated. Previously, apoptosis (Type I) and necrosis (Type III) were defined as two distinct forms of programmed cell death (Wyllie, 1994)

of which both can occur simultaneously in cultured cells and tissues (Kajstura *et al*, 1998). However the duration and intensity of the injury potentially decides the eventual outcome (Loos *et al*, 2011). Although apoptosis and necrosis may share a common insult, downstream mediators and the availability of ATP directs cells towards programmed cell death by either apoptosis or necrosis (Leist *et al*, 1997).

Very little attention has been paid to the role of necrosis in the context of AC-induced cardiotoxicity. Lim and co-workers (2004) demonstrated that 1 µM DXR induced necrotic cell death in cardiomyocytes, which was confirmed with an increase in trypan blue uptake and creatine kinase (CK) liberation. This observation appeared to be time-dependent as the percentage of trypan blue positive cells increased from a base-line value of ± 8 to 12% after 48 hrs of DXR treatment. Concomitantly, calpain activity also increased with DXR treatment after 1 hr and remained elevated till 48 hrs. Co-treatment with calpain inhibitors preserved titin degradation, diminished myofibrillar disarray and necrosis declined. These data suggest that a change in calpain activity is an early event occurring in cardiomyocytes after DXR treatment, seemingly to target titin for proteolysis. Degradation of titin conceivably influences cardiomyocytes to contribute to diastolic dysfunction, myofilament instability and necrotic cell death.

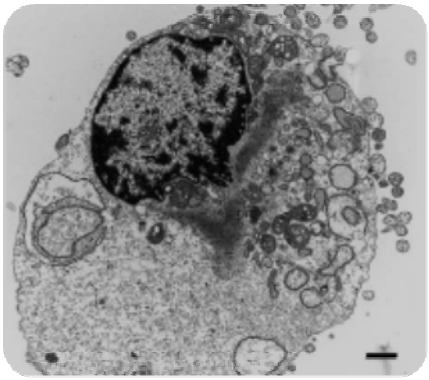

Figure 5: Necrotic cell death. This type of cell death is morphologically characterized by cytoplasmic swelling, irreversible plasma membrane damage and irreversible changes in the nucleus such as pyknosis, karyorrhexis and karyolysis as well as organelle swelling and breakdown. Adopted from Edinger & Thompson, 2004.

1.5: Induction of proteolytic pathways by ACs

Cellular proteins exist in a balance between continuous synthesis and degradation. This drift of synthesis and degradation (i.e. turnover) contributes to the exertion of cell type specific functions and maintenance of cell homeostasis (Mizushima *et al*, 2007; Kuma *et al*, 2010). Environmental stimuli such as UV irradiation and oxygen radicals frequently cause various types of protein damage that alter normal cellular functions as well as homeostasis and may eventually cause cell death. Rapid eradication of damaged or harmful proteins, which are especially significant in terminally differentiated cells such as neurons and cardiomyocytes (Nedelsky *et al*, 2008), are entirely dependent on sufficient performance of the catabolic machinery. Two major protein degradation systems play fundamental roles: autophagy, whereby cells respond to energetic stress by recycling intracellular components; predominantly long-lived proteins, lipids and even entire organelles (Cuervo, 2004; Mizushima *et al*, 2008) and the ubiquitin-proteasome pathway (UPP), which selectively degrades predominantly short-lived regulatory proteins (Herrmann *et al*, 2004; Willis *et al*, 2006; Paul, 2008). Both proteolytic systems have been implicated to play a role in AC-induced cardiotoxicity; however the underlying mechanisms are poorly understood.

1.5.1: Autophagy

Autophagy is a process by which cytoplasmic material, including macromolecules and organelles, are delivered to lysosomes for degradation. Three different types of autophagy have been identified: microautophagy, chaperone-mediated autophagy (CMA) and macroautophagy (Klionsky *et al*, 2000). Microautophagy involves the confining and destruction of small constituents of the cytoplasm by lysosomes via invaginations of the limiting membrane (Marzella *et al*, 1981). In chaperone-mediated autophagy, misfolded proteins are translocated by heat shock 70 (Hsp70) to the lysosomes for degradation (Cuervo, 2004). Macroautophagy (hereafter referred to as autophagy), the predominant type of autophagy, is a dynamic and highly coordinated process of self-digestion (Klionsky *et al*, 2000; Mizushima *et al*, 2008). This highly conserved cellular process is responsible for the elimination or salvaging of long-lived proteins and organelles and thus supplies cells with an alternate source of metabolites (Cuervo *et al*, 2004).

The hallmark of autophagy is the *de novo* synthesis of an isolation membrane or phagophore which elongates around the cytoplasmic contents to be degraded. Cytoplasmic content is hence engulfed by the isolation membrane, resulting in the formation of a double-membrane structure known as the autophagososme. The outer membrane of the autophagososme fuses with the lysosome to form an autophagolysosome. This fusion allows for the degradation of the inner membrane as well as the cytoplasmic content of the autophagosome by digestive enzymes (acid hydrolases) present within the lysosome (Korolchuk *et al*, 2009) (Figure 6) (for comprehensive reviews of the autophagic pathway see Muzishima, 2007; Levine *et al*, 2008; Ravikumar *et al*, 2010).

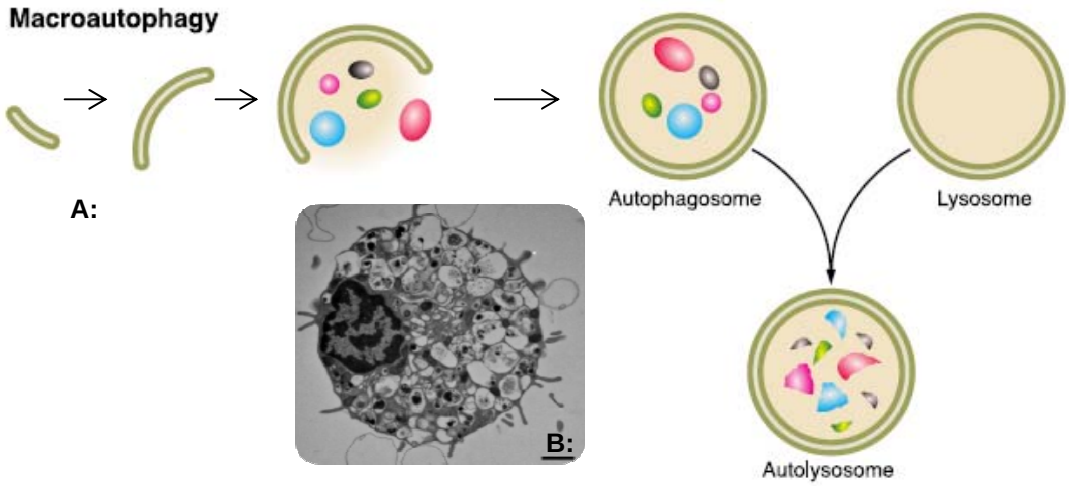

Figure 6: Autophagic degradation. **A**: Degradation of cytoplasmic contents by autophagy (Modified from Ravikumar *et al*, 2010). **B**: Representative cell with extensive accumulation of autophagic vacuoles, indicating cell death with autophagy. Adopted from Edinger & Thompson, 2004.

Autophagy plays a number of physiological roles such as facilitating survival, differentiation, development, aging, immunity and homeostasis (Delgado *et al*, 2008; Winslow *et al*, 2008). In eukaryotic cells, autophagy occurs constitutively at low levels to perform housekeeping functions such as the destruction of dysfunctional organelles (Komatsu *et al*, 2007; Kuma *et al*, 2010). Upregulation of autophagy occurs in the presence of external stressors such as hormonal imbalance, oxidative stress and starvation as well as intracellular stimuli (e.g. removal of protein aggregates), thus signifying autophagy also as an important survival mechanism.

Whilst autophagy is active under baseline conditions, its activity is often altered during disease. Elevated autophagic activity in cardiomyocytes has been previously described following various forms of cardiovascular stress including heart failure (Kostin *et al*, 2003; Yan *et al*, 2005; Saijo *et al*, 2004). However, whether autophagy participates as a pro-survival or pro-death pathway during disease remains to be determined. Literature indicates that autophagy can have both beneficial and detrimental effects in the myocardium depending on the state of autophagic activity at the time. For example, increased levels of autophagy may have beneficial effects by removing damaged or injured organelles and preventing the accumulation of protein aggregates (Tannous *et al*, 2008), thereby recycling proteins in order to generate amino acids and free fatty acids that are required to maintain energy production (Kuma *et al*, 2010). On the other hand, extensive autophagy can also contribute to cellular demise, plausibly via excessive self-digestion or metabolic failure (Loos *et al* 2011; Gozuacik *et al*, 2007). Autophagosomes have also been observed in dying cells, but it is not clear whether autophagy directly contributes to cell death or whether it is upregulated in an effort to prevent it.

1.5.2: The Autophagic Pathway as a therapeutic target

The modulation of autophagy as a therapeutic modality in CVD has several limitations. Firstly, 3-methyladenine (3MA), a class III phosphoinositol-kinase (PI3-K) autophagy inhibitor, commonly used in cell culture experiments, is highly toxic and therefore inappropriate for *in vivo* applications (Mizushima, 2004). Secondly, nutrient starvation, a potent inducer of autophagy in mammalian cells, is often very dangerous from a cardiovascular view point because long-lasting starvation initiates relentless cardiovascular complications and even cell death (Rose *et al*, 1979).

The attenuation of autophagic degradation is accountable for increased myocardial mass in hypertrophy and several other heart defects (Dammrich *et al*, 1983). When autophagy is induced in this scenario as a result of therapy, proteolysis is elevated and hypertrophy declines (Frenzel *et al*, 1987). On the other hand, dilated cardiomyopathy and consequent HF is associated with intensified PCD, yet during ischemic heart disease, autophagy either acts as a repair mechanism or a constituent of PCD, depending on the quantity of myocardial damage (Elsasser *et al*, 2004; Krijnen *et al*, 2002; Decker *et al*, 1980). Myocardial injury caused by

autoimmune disease, intoxication or infection invigorates reparative autophagy which is followed by PCD, if the damage is severe (Akazawa *et al*, 2004; Nepomnyashchikh *et al*, 2000). Some researchers suggest that enhanced autophagy indirectly removes protein aggregates by clearing aggregate precursors, thereby shifting the equilibrium away from aggregate formation (Rubinsztein, 2006; Komatsu *et al*, 2007). Furthermore, it has been suggested that the pathophysiological outcome depends on the severity and/or duration or the nature of the autophagic response (Rothermel *et al*, 2008). Additionally, the context- and dose-dependent role of autophagy possesses specific challenges. For example, it is currently unknown how long autophagy can remain upregulated without harmful consequences for the cellular system. Moreover, there is inconsistency in the literature regarding autophagic cardiomyocyte deaths in patients suffering from heart failure, which is detected in very few cells, whereas the impact on functional parameters is remarkable. To selectively control autophagy and thereby autophagy-mediated survival without provoking cell death specific pathways therefore remains a challenge.

Lambert and co-workers (2008) have demonstrated autophagy as a novel mechanism of enhanced synergistic cytotoxicity between DXR and roscovitine (Cdk-cyclin-dependent kinase inhibitor) in a sarcoma model. In this particular study, the combination of the two drugs increased autophagy above basal levels. In addition, in the three different sarcoma cell lines used, combined treatment lead to prolonged G_2-M arrest. It was thus postulated that this prolonged arrest, caused by the activation of the DNA damage checkpoint by DXR, followed by the inhibition of the Cdk1-cyclin B complex by roscovitine, might be a trigger for autophagy induction and eventual cell death. Despite being a promising treatment regime for sarcomas, cardiotoxicity remains a major threat for cancer survivors and it is for this reason that various studies have attempted to amend autophagic activity. This may represent a potential therapeutic target to treat or prevent many cardiovascular diseases (CVDs), particularly in the context of AC-induced cardiotoxicity.

Taken together these data suggest that autophagy is a plausible survival pathway that may be manipulated in order to produce beneficial effects within the context of heart disease. Although the role of autophagy in AC-induced cardiotoxicity is far from understood, the potential benefit of exploitation of this pathway may unravel new

insight into the mechanisms of autophagy, which will eventually lead to the discovery of novel mediators responsible for controlling autophagic activity.

1.5.3: Ubiquitin-proteasome pathway

The ubiquitin-proteasome pathway (UPP) and autophagy have long been viewed as independent and parallel degradation systems with no point of intersection. This view was challenged by the observation that monoubiquitination operates as a key signal in endocytosis, a vital process for many cell functions including lysosomal biogenesis (Ross *et al*, 2004). Consequently, various studies have suggested that both the UPP and autophagy are functionally interrelated catabolic processes that often share specific substrates and regulatory molecules (Itawa *et al*, 2005; Pandey *et al*, 2007; Rideout *et al*, 2004). Furthermore, these systems show coordination and in some contexts, serve compensatory functions. It is now becoming increasingly clear that a considerable subset of proteins can be degraded by either pathway which is in contrast to the conventional conception of the UPP and autophagy serving unambiguous routes of degradation for short-lived and long-lived proteins respectively (Li, 2006; Fuertes *et al,* 2003; Fuertes *et al*, 2003).

It is now clear that p62/SQSTMI, an adapter molecule linking ubiquitinated proteins to the autophagic machinery, is responsible for the collaboration between the UPP and autophagy during protein quality control (Zheng *et al*, 2009; Bjorkoy *et al*, 2000). P62 directly binds to polyubiquitinated substrates, LC-3 on autophagosomes (Pankiv *et al*, 2007) and is able to polymerize and interact with the proteasome (Seibenhener *et al*, 2004). This interaction between p62 with autophagosomes and the proteasome may aid in the transfer of targeted proteins towards degradation and it is suggested that p62 can be degraded by either proteolytic pathway (Zheng *et al*, 2009). Another important protein involved in the cross-talk between the UPP and autophagy is FoxO3 (Forkhead box), a transcription factor which activates and regulates both proteolytic pathways (Zhao *et al*, 2007). In addition, cardiac FoxO3 can also induce atrophy by stimulating the transcription of E_3 ligases (Skurk *et al*, 2005) (Figure 7**a**, **b**).

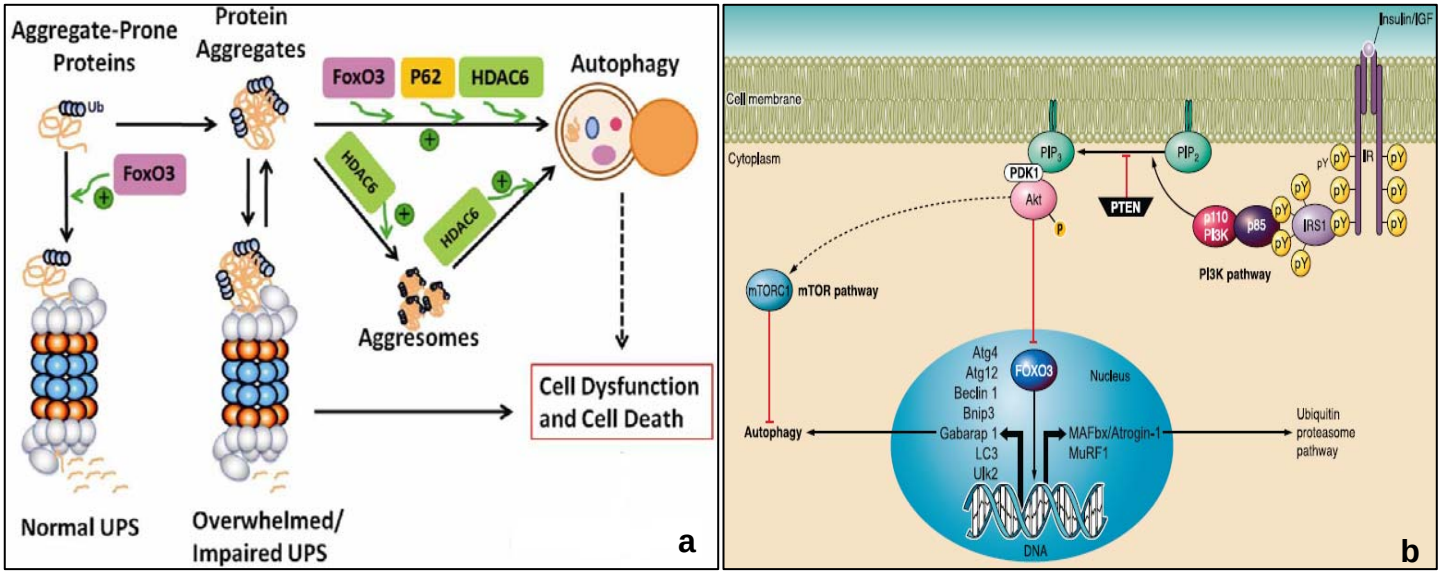

Figure 7 (a): A schematic illustration of the interplay between the UPP and autophagy. Modified from Zheng *et al*, 2009. **(b):** FoxO3 co-ordinately upregulates both autophagy and the ubiquitin proteasome system (UPP) during muscle atrophy. Activation of the IGF/Akt signalling pathway via PI3K during atrophy results in FoxO3 translocation into the nucleus, where it directly binds to promoter regions and upregulates transcription of the atrogenes (MuRF1 and MAFbx/atrogin1) and autophagy-associated genes. Autophagy is also induced by the IGF/Akt signalling pathway via the inhibition of mTOR. Adopted from Ravikumar *et al*, 2010.

Ubiquitination refers to the conjugation of free ubiquitin (Ub) with a substrate protein. Ub is a small, highly conserved compact, globular protein that consists of 76 amino acids. It is ubiquitously expressed in all eukaryotes but only in very few prokaryotes and via a particular enzymatic reaction, it covalently binds to proteins in linear chains (Patterson *et al*, 2007; Powell, 2006). The process for Ub chain assembly requires three enzymatic reactions. The Ub-activating enzyme (E_1) covalently attaches to Ub in an ATP-dependent fashion. The Ub-conjugating enzyme (E_2) consequently transports the Ub molecule from E_1 to itself. The Ub-ligase (E_3) recognizes the specific substrate and thus transfers the Ub molecule from E_2 to a lysine residue (Willis *et al*, 2006) (Figure 8). Specific E_3-ligases, MuRF-1 (Muscle Ring Finger-1) and atrogin1/MAFbx (Muscle Atrophy F-box), are expressed exclusively in the heart and in skeletal muscle tissue (Bodine *et al*, 2001). MuRF-1 demonstrates ubiquitin ligase activity by binding to the sarcomeric protein, titin (Centner *et al*, 2001) and degrades cardiac TnI (Kedar *et al*, 2004). MAFbx binds to calcineurin A, α-actinin-2 (Li *et al*, 2004) and degrades MyoD (Tintignac *et al*, 2005). Whilst the turnover of skeletal muscle proteins involving the ubiquitin ligases MuRF-1 and MAFbx is well established (Glass, 2003), the contribution of these ubiquitin ligases in cardiac remodeling in heart failure remains to be fully elucidated.

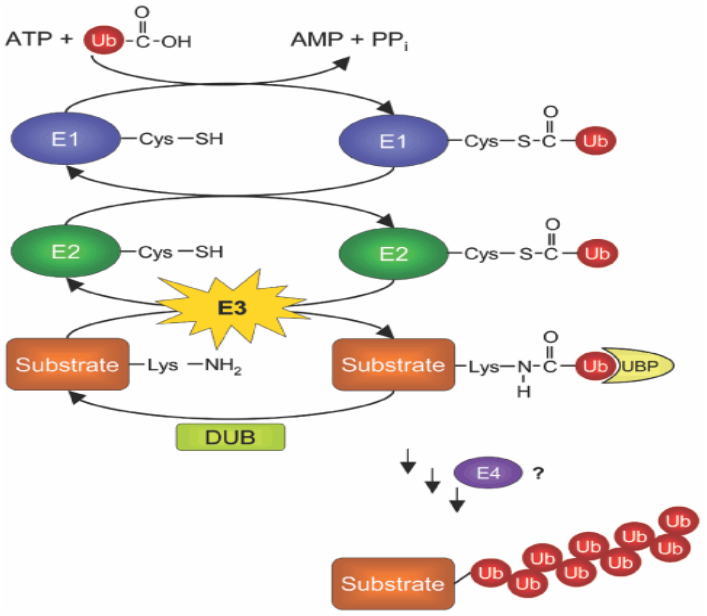

Figure 8: Ubiquitin chain assembly for substrates marked for degradation. Selected abbreviations: E1 - Ubiquitin activating enzyme; E2 - Ubiquitin conjugating enzyme; E3 - Ubiquitin ligase; E4 – Polyubiquitin chain assembly factor. Adopted from Passmore *et al*, 2004

The fate of ubiquitinated proteins depends entirely on the number of Ub molecules as well as the configuration of the Ub-Ub linkages which lead to different cellular outcomes. For example, poly-ubiquitination through lysine 48 (Lys48) linkages (canonical) results in the targeted substrate being degraded by the 26S proteasome (Spence *et al*, 1995; Pickart, 2001). Poly-ubiquitination through another lysine residue (Lys63; non-canonical) does not result in degradation but rather acts as a signal for re-localization, cellular signalling or DNA repair (Habelhah *et al*, 2004). The modification of a substrate with a single Ub molecule (mono-ubiquitination) leads to re-localization or endocytosis of targeted proteins (Bonifacino *et al*, 2003; Haglund *et al*, 2003). Some proteins or receptors cue mono-ubiquitination at multiple sites (multimonoubiquitination) to ensure accurate function or endocytosis (Haglund *et al*, 2003) (Figure 9). A final form of ubiquitination, initially described for the cell cycle regulator p21, is NH_2-terminal ubiquitination. This type of ubiquitination refers to the fusion of Ub to the α-NH_2 group of the NH_2-terminal residue ultimately affecting the stability of the protein and in some cases blocking degradation via an unknown mechanism (Bloom *et al*, 2003; Ciechanover *et al*, 2004). The rationale for assembling Ub in chains is not entirely clear, but it has been suggested that this phenomenon occurs to amplify the signal in order to maximize the efficiency of substrate recognition as well as to distinguish between Ub per se and Ub-like

proteins (Patterson *et al*, 2007).

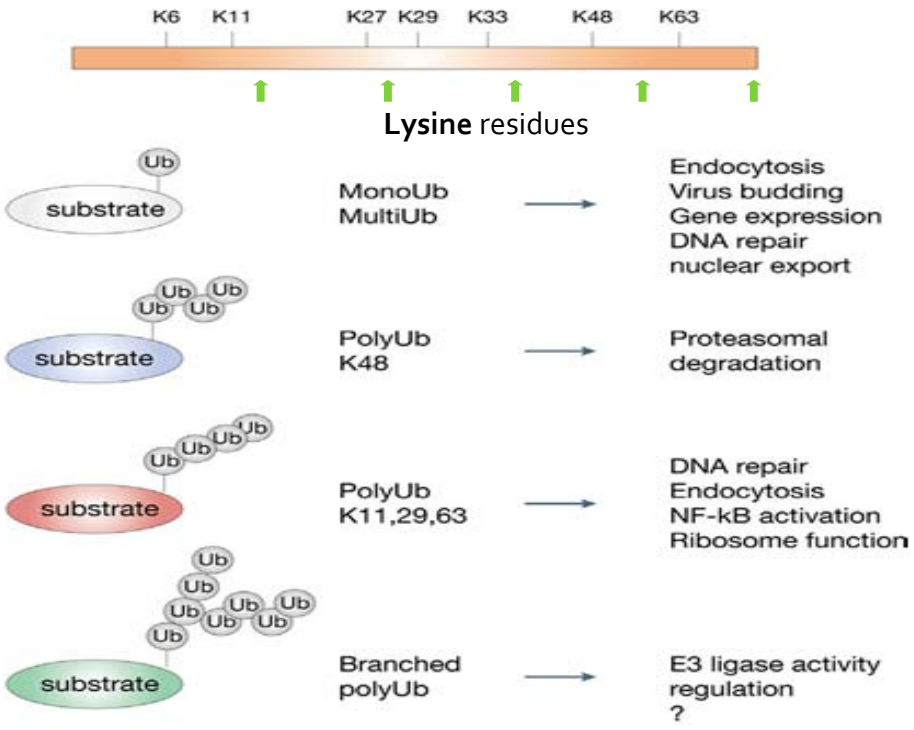

Figure 9: Ubiquitin modification of targeted substrates resulting in different fates for the substrate. Modified from Willis *et al*, 2006

1.5.4: The Ubiquitin-proteasome pathway as a therapeutic target

While the understanding of role of the UPP in regulating cellular processes continues to expand, the elucidation of its role in cardiac disease is becoming increasingly clear. The UPP regulates pivotal processes at all levels of cardiac biology: from membrane-associated ion channels and receptors, to downstream signalling intermediates and transcription factors. Additionally, the UPP also plays a major role in maintaining cardiac protein quality control, as demonstrated by its multiple interactions with the cardiac sarcomere and its crucial role in familial cardiomyopathies (Paul, 2008; Nalepa *et al*, 2006).

In the context of cardiotoxicity, recent studies using a unique reporter system in which the activity of the proteasome can be monitored, indicates that DXR enhances UPP function in both the heart and in cultured cardiomyocytes (Kumarapeli *et al*, 2005). These results suggest that an overactive UPP may be a vital factor in acute or

chronic cardiotoxicity often observed after DXR therapy. More recently, several reports have suggested that DXR activates proteasome-mediated disintegration of particular transcription factors (Poizat *et al*, 2000; Ito *et al*, 2007). Furthermore, the proteasome has been proposed to function as a carrier for the translocation of DXR from the cytoplasm to the nucleus, thus altering its function (Kiyomiya *et al*, 1998, 2002). Kumarapeli *et al* (2005) have illustrated that DXR ameliorates the degradation of a substitute UPP substrate in mice. However the mechanism by which DXR activates the UPP is still unknown.

Liu and colleagues (2008) have shown that: (i) DXR not only increases the proteolysis of an exogenous UPP reporter protein (GFPu), it additionally provokes proteasome inhibitor-induced build-up of endogenous substrates of the UPP such as c-Jun and β-catenin in cultured cardiomyocytes; (ii) DXR facilitates *in vitro* degradation of GFPu and c-Jun by the reconstituted UPP via the elevation of proteasomal function; (iii) DXR stimulates peptidase activities of purified 20S proteasomes at a therapeutically relevant dose and (iv) DXR enhances E_3 ligase COOH-terminus of the heat shock protein cognate 70 in 3T3 cells via a posttranscriptional mechanism. These novel observations propose that DXR stimulates the UPP by directly acting on the ubiquitination machinery and proteasome.

Research indicates defined roles for the UPP in maintaining normal cardiac function through regulation of signalling pathways and maintenance of normal sarcomere structure. It has also been illustrated that downregulation of Ub-ligases may play a pivotal role in the response of the myocardium to hypertrophic stimuli (Oudit *et al*, 2004). Others suggest that dysfunction of the proteasome may be important in cardiac pathologies (Kamikubo *et al*, 1996; Keyvani *et al*, 2000) and even senescent cardiomyocyte loss (Kajstura *et al*, 1996; Higami *et al*, 2000). From a therapeutic point of view, DXR appears to be the only exception in that it can increase the UPP proteolytic function in degrading both substitute and endogenous substrates.

Although the coupling of the UPP's activating effects of DXR and cardiotoxicity remain to be elucidated, DXR is a unique pharmacological agent that embodies an intrinsic activation property. Therefore, DXR-induced stimulation of the UPP is possibly detrimental to the heart. It is thus enticing to examine proteasome inhibition

as an approach to diminish this side effect, especially in light of the fact that proteasome inhibitors have already been used clinically with promising results (Ciolli *et al*, 2008; Voorhees *et al*, 2007). These studies will likely lead to pioneering investigations into whether chemotherapies combining DXR and proteasome inhibitors will improve the parameters of cardiotoxicity compared to those using either one alone.

1.6: ER-stress and Ca^{2+} concentration in cardiotoxicity

Over the past decade, it has become evident that the accumulation of unfolded or misfolded proteins also contributes to numerous neurodegenerative (Kakizuka *et al*, 1998; Niwa *et al*, 1999), immune (Turner *et al*, 2006) and endocrine pathologies (Thameem *et al*, 2006; Araki *et al*, 2003) as their destruction through the proteasome is not always possible (Willis *et al*, 2010). Recent evidence suggests that the build-up of misfolded proteins can contribute to vascular (Forstermann *et al*, 2006) and cardiac diseases (Hamada *et al*, 2004; Okada *et al*, 2004, Willis *et al*, 2010). Cells have acquired intricate protein quality control systems for identifying and eliminating dysfunctional misfolded proteins. As currently understood, protein quality control components involve two main elements: (i) cytosolic and organelle-targeted molecular chaperones, which protect the proteins from misfolding and are necessary for the assembly of particular sarcomere components; and (ii) the UPP (Willis *et al*, 2009). One of the organelle-specific protein quality control systems dwells in the endoplasmic reticulum (ER) and is highly receptive to stresses such as oxidative stress, prompting the accumulation of terminally misfolded proteins in the lumen of the rough ER (Glembotski, 2007).

1.6.1: ER stress and the unfolded protein response

The ER is a vital site for the modifications and folding of proteins destined for the cellular membrane as well as the secretory pathway (Yorimitsu *et al*, 2007). It is extremely sensitive to perturbations in homeostasis from various stimuli such as glucose deprivation, alterations in calcium homeostasis and exposure to free radicals. Under these conditions, changes in the protein folding capacity as well as the conglomeration of malfolded proteins within the ER illicits a phenomenon known as ER stress (Kaufman, 1999). In response to this, the ER stress response,

otherwise known as the unfolded protein response (UPR), is mobilized (Schroder *et al*, 2005; Schroder, 2008; Mandl *et al*, 2009). This response is a highly conserved signalling system that has been studied in multiple cell- and tissue types (McMillan *et al*, 1994; Shamu *et al*, 1994). The UPR is proposed to convey information about the degree of the protein folding capacity from the rough ER to other cellular locations. In doing so, induction of the UPR transiently attenuates the rate of protein synthesis and upregulates genes encoding chaperones, foldases, ER-associated degradation (ERAD) proteins, autophagy regulators and ER membrane biogenesis enzymes (Hetz *et al*, 2008; Wang *et al*, 2008; Yoneda *et al*, 2001). Consequently, UPR signalling reduces the build-up and aggregation of unfolded proteins by augmenting the functional capacity of the ER to promote folding and to abolish abnormal proteins. Accordingly, this facet of the UPR is usually considered the prosurvival phase (Szegezdi *et al*, 2006). However if the ER stress is not resolved, sustained stress leads to the activation of pathways that mediate PCD (Szegezdi *et al*, 2003). Similar to many cellular signalling pathways, the eventual outcome of the UPR is context dependent, thus providing this compex signalling process with the conditional ability to facilitate survival or death.

Despite extensive characterization of the regulatory signalling of the UPR, the morphological changes and determination of the cell fate due to damage caused by ER stress are not well understood. In addition, it also remains unknown whether other signalling pathways are activated in response to ER stress in order for the cell to cope with unfolded or misfolded proteins that gather within the ER. Recent evidence suggests that there is a connection between autophagy, ER stress and the UPR pathway (Yorimitsu *et al*, 2007; Araki *et al*, 2006). Although very little is known as to how autophagy regulates the UPR and vice versa, Li *et al* (2008) have reported that 3-MA, wortmannin and Beclin-1 knockdown inhibits ER stress-induced autophagy but only 3-MA is able to inhibit UPR induction. Moreover, knockdown of the ER molecular chaperone, GRP78, stimulated the UPR pathways and impeded autophagosome formation caused by nutrient starvation and ER stress. It was further discovered that the ER, a feasible membrane source for producing autophagic vacoule membranes (Mijaljica *et al*, 2006; Dunn, 1990), is vastly expanded and is thus unstructured in cells where GRP78 is not present. In order to quantify ER proliferation over time, Bernales and collegues (2006) showed that the ER increases more than 3 fold over a 3 hour time course using electron microscopy. Autophagy

activation in this context may counterbalance ER expansion during the UPR (Ding *et al*, 2007) and may consequently be cytoprotective (Ogata *et al*, 2006; Høyer-Hansen *et al*, 2007).

The ER plays a crucial role in many cellular processes including the facilitation of effective folding of newly synthesized proteins as well as providing the cell with a calcium (Ca^{2+}) reservoir (Mimoi *et al*, 2006; Berridge *et al*, 2002). A high Ca^{2+} concentration exists in the lumen of the ER, similar to that of the extracellular space, and provides the optimum environment for accurate folding of secreted proteins. When a major segment of the Ca^{2+} within the ER is liberated, it could affect Ca^{2+}-dependent processes in- and outside the ER lumen. For example, ER stress causes a release of Ca^{2+} from the ER resulting in an increase in cytosolic free Ca^{2+}. Depending on the condition of the cell as well as the type of ER stress it encounters, the result can be a decline in the amount of proteins entering the ER, elevated removal of proteins from the ER, an enhanced capacity of the ER folding machinery, autophagy or even apoptosis (Bernales *et al*, 2006; Ogata *et al*, 2006; Yorimitsu *et al*, 2006; Rao et al, 2004). The release of Ca^{2+} from the ER into the cytosol can induce various kinases and proteases which participate in autophagy signalling (Yousefi *et al*, 2006; Dermachi *et al*, 2006). A signalling pathway initially described by Høyer-Hansen and co-workers (2007), employing pharmacological inhibitors and RNA interference, showed that Ca^{2+}-mediated autophagy relied on the Ca^{2+}/calmodulin-dependent kinase kinase-β (CaMKK-β)-dependent stimulation of AMPK (AMP activated protein kinase) which eventually leads to the inhibition of mTORC1 (mammalian target of rapamycin complex 1). It is however not clear whether the induction of AMPK is sufficient to initiate autophagy or whether separate independent signals are required. Despite the wealth of knowledge that is now readily available concerning ER stress, the UPR, autophagy and the UPP, the production of free radicals from ACs may possibly also trigger these pathways.

1.7: Oxidative stress and AC-induced cardiotoxicity

The disruptions of Ca^{2+} homeostasis caused by oxidative stress and indirectly by ACs are potent inducers of ER stress, and thus the stimulation of survival pathways remains a significant obstacle and may potentially represent novel therapeutic targets that may reduce cardiotoxicity or lead to better therapeutic regimes for patients with

cancer. Current understanding of AC-induced cardiomyopathy indicates that the primary cause of this condition is elevated oxidative stress (Figure 10), even though the drug's antitumor function in patients may incorporate other mechanisms. Whilst various antioxidants show promise in reducing injury, to date none have been developed that act selectively at the site of toxicity, the heart. Strategies to prevent and manage AC-induced cardiotoxicity are pivotal in order to reduce the mortality of cancer patients. Initiation of these regimens should be conducted before AC exposure in order to minimize the possibility of irreversible cardiac damage. Apart from accurate screening of patients for underlying causes of heart disease, alternative-drug treatment regimens (Healy Bird *et al*, 2008; Chen, 2009) used in combination with ACs have previously been demonstrated. These have been shown to be effective in reducing the prevalence of AC-induced oxidative stress but are also correlated with cardiotoxicity.

As cardiomyocytes are irreplaceable and often experience augmented ROS exposure as a result of intensified oxygen consumption, autophagy in any form is a significant life-sustaining mechanism. In response to stress, autophagy is induced as a compensatory response either for repair or detoxification. This is especially important during oxidative stress where numerous oxidative or impaired macromolecules and organelles, specifically mitochondria, being the active site of ROS production and the principal target of ROS attack, are degraded for essential nutrient supply. It is important to consider however that irreparable damage to cardiac myocytes triggers PCD in the form of apoptosis (PCD-1) or autophagic cell death (PCD-2) (Terman *et al*, 2005; Edinger & Thompson, 2004). In this case autophagy appears to be incapable of completely eliminating all damaged fragments which concentrate extralysosomally and intralysosomally, implying inadequacy of autophagic sequestration and degradation respectively. Despite this, the involvement of autophagy in a wide variety of cardiac pathologies draws consideration to this vital process proposing alternate strategies for the management of cardiovascular diseases as well as the development of cardiotropic drugs.

1.8: Conclusion and Future Recommendations

Cardioprotection can be accomplished by moderating AC cumulative life-time dose by keeping it well below the acclaimed threshold. Besides the cumulative dose of

ACs, it has been postulated that amplifying the therapeutic index of free ACs by liposomal AC formulations, significantly decreases cardiotoxicity. By encapsulating ACs within self-sealing, macromolecular vesicles such as liposomes, the distribution volume of ACs is reduced, diffusion and thus toxicity of viable tissues diminishes while the concentration within neoplastic tissue is enhanced (Giotta *et al*, 2007; Gabizon *et al*, 1992; Mayer *et al*, 1989). Although this treatment regime would particularly benefit patients who have previously been exposed to ACs or those who are known to have attenuated cardiac function, critical modifications may exist amid distinct liposomal preparations as variations in vesicle size, drug-to-lipid ratio as well as lipid composition can have an immense impact on the biodistribution and toxicity of ACs.

Considering the fact that AC-induced oxidative stress cannot be completely abolished, a feasible and practical approach for decreasing AC-induced cardiotoxicity is the acute stimulation of survival via autophagy before AC administration. This can be achieved in two ways: (i) amino acid deprivation or (ii) rapamycin treatment. Both these mechanisms would lead to the demand for fundamental end products of lysosomal degradation and thus supplies the cells' anabolic machinery with new building blocks. Mammalian target of Rapamycin (mTOR), a protein kinase, is believed to play a pivotal role in intracellular control of the autophagic pathway. Furthermore, mTOR is described to act as an ATP sensor (Dennis *et al*, 2001). This notion is favoured by the occurrence of ATP maintenance and sustained cell survival during upregulation of autophagy by rapamycin. However, due to the fact that autophagy is ATP dependent, excessive ATP depletion would nevertheless inhibit autophagic activity (Seglen *et al*, 1990).

This review emphasizes the importance of understanding AC-induced cardiotoxicity in its context. This review also highlights current and new treatment strategies that may focus either on the prevention, inhibition or the delay of AC-induced cardiotoxicity. By proposing autophagy as a potential treatment regime for this condition, it is hoped that this will lead to a better understanding of the beneficial effects of this pathway and thus contribute to improved recovery for cancer patients.

1.9: Motivation for this current study

The motivation for this current study resulted from the fact that the administration of ACs, as the most effective anticancer drugs, leads to the development of HF by a mechanism which is not fully understood. This subsequently lead to a collaboration with researchers in Bergen, Norway and Cape Peninsula University of Technology, South Africa where cardiotoxicity induced by the AC, daunorubicin (DNR), was investigated in an *ex vivo* model (Chapter 2). The **objective** was **(i)** to investigate the effect of DNR treatment on protein and organelle degradation systems in the heart as well as **(ii)** to elucidate some of the signalling mechanisms involved. Although this model was ideal in allowing the characterization of signalling pathways that are affected by DNR, it did not allow for further exploration or manipulation of these signalling mechanisms that may be of potential benefit in this context. This then lead to another (*in vitro*) model where it was **hypothesized** that elevated autophagy alleviates AC-induced toxicity and delays the onset of cardiomyocyte death. The **aims** were: **(i)** to characterize the effect of DXR on the H_9C_2 cell line, **(ii)** to determine whether the induction/inhibition of autophagy in combination with DXR attenuates cytotoxicity and **(iii)** to investigate the influence of induced/inhibited autophagy in combination with DXR on programmed cell death, ROS production and the UPP (Chapter 3). In addition, an *in vivo* model was used to confirm the role of autophagy in DXR-induced cardiotoxicity (Chapter 4).

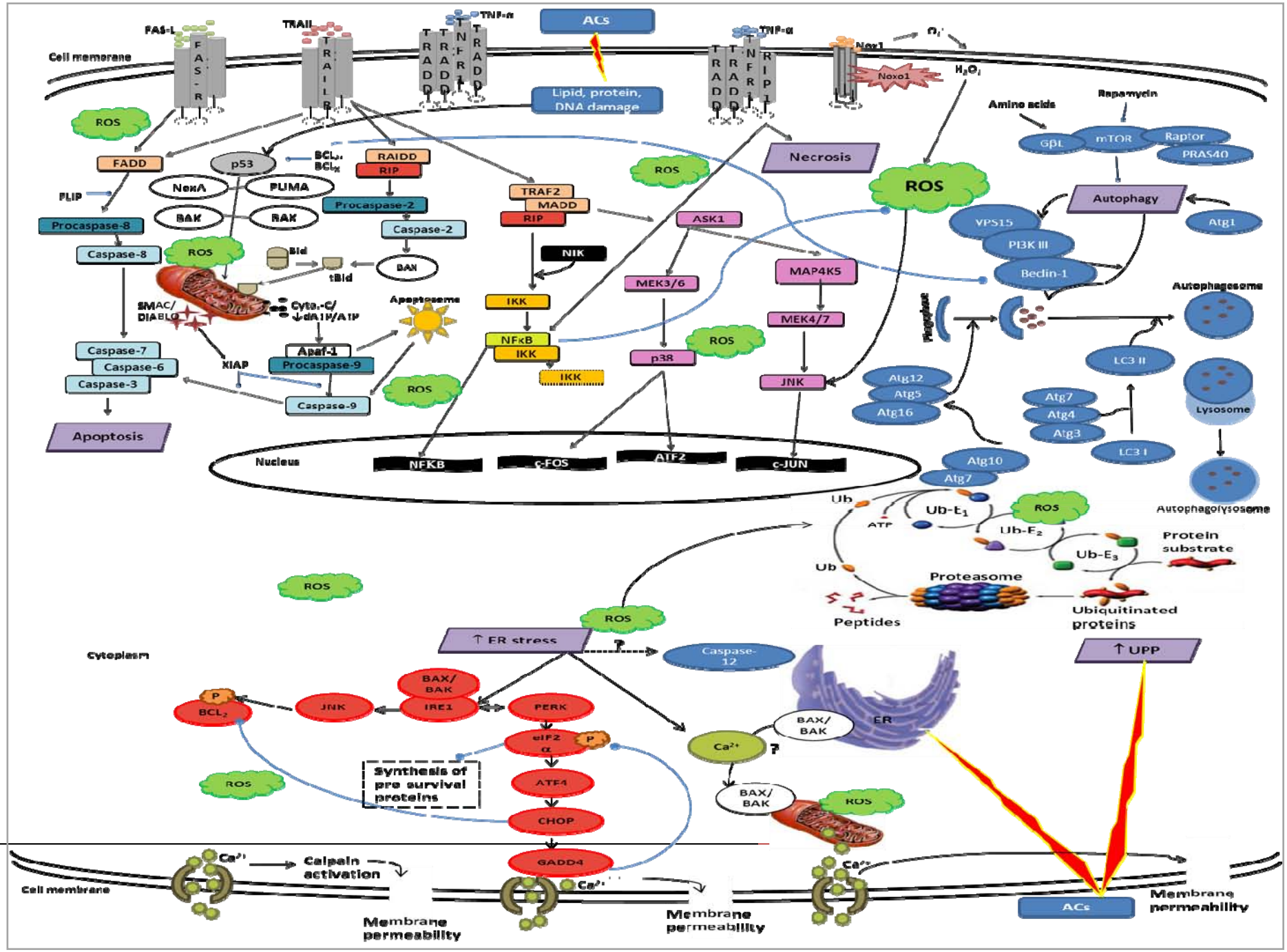
ACs
Cell memerane
FAS-L
TRAIL
TNF-α
Lipid, protein, DNA damage
ROS
FADD
p53
RAIDD
RIP
FLIP
NoxA
PUMA
BAK
BAX
Procaspase-2
Caspase-2
Procaspase-8
Caspase-8
Bid
tBid
BAN
SMAC/ DIABLO
Cyto.-C/ dATP/ATP
Apoptosome
Caspase-7
Caspase-6
Caspase-3
XIAP
Apaf-1
Procaspase-9
Caspase-9
Apoptosis
TRAF2
MADD
RIP
NIK
IKK
NFκB
IKK
IKK
ASK1
MEK3/6
p38
MAP4K5
MEK4/7
JNK
Necrosis
Nox1
Noxo1
Amino acids
Rapamycin
GβL
mTOR
Raptor
PRAS40
Autophagy
Atg1
VPS15
PI3K III
Becdin-1
Phagophore
Autophagosome
LC3 II
LC3 I
Atg12
Atg5
Atg16
Atg7
Atg4
Atg3
Lysosome
Autophagolysosome
Nucleus
NFKB
c-FOS
ATF2
c-JUN
Atg10
Atg7
Ub
ATP
Ub-E1
Ub-E2
Ub-E3
Protein substrate
Proteasome
Peptides
Ubiquitinated proteins
↑ UPP
Cytoplasm
↑ ER stress
Caspase-12
BAX/ BAK
JNK
IRE1
PERK
P
BCL2
eIF2 α
Synthesis of pro survival proteins
ATF4
CHOP
GADD4
ER
Ca2+
Calpain activation
Cell membrane
Membrane permeability
ACs

Figure 10: Scheme demonstrating possible signalling mechanisms affected by AC-induced cardiotoxicity. AC-induced ROS production initiates the activation of cell death pathways including apoptosis, autophagy and necrosis. The disruption of calcium homeostasis as a direct consequence of elevated oxidative stress, results in ER stress, the stimulation of the UPR as well as autophagy. Increased activity of the UPP is also observed in this context. Abbreviations: FAS-L, FAS ligand; TRAIL, Tumor necrosis factor-related apoptosis-inducing ligand; TRADD, Tumor necrosis factor receptor type 1-associated death domain; TNF-R1, Tumor necrosis factor receptor type 1; FADD, FAS-associated death domain; RIP, receptor-interacting protein; RAIDD, RIP associated Ich-1/CED homologous protein with death domain; FLIP, FLICE inhibitory protein; PUMA, p58-upregulated mediator of apoptosis; Bid, Bcl2 -interacting domain; tBid, Truncated Bid; dATP, Deoxyadenosine triphosphate; Cyto.-c, Cytochrome-c; Apaf-1, Apoptotic protease activating factor 1; ACs, Anthracyclines; TRAF-2, TNF receptor-associated factor 2; MADD, MAP kinase-activating death domain protein; NF-KB, Nuclear factor kappa B; NIK, NFkB inducing kinase; IKK, I-kappa-B kinase; ASK-1, Apoptosis signal-regulating kinase1; IKB, I kappa B; JNK, c-Jun NH_2-terminal kinase; Nox1, NADPH oxidase 1; ROS, Reactive oxygen species; O_2^- superoxide anion; H_2O_2, hydrogen peroxide; ATF-2, activating transcription factor 2; ATF-4, activating transcription factor 4; Bcl2, B-cell lymphoma 2; IRE-1, Inositol requiring kinase1; PERK, RNA-dependent protein kinase (PKR)-like ER kinase; Ca^{2+}, Calcium; P, phosphate; CHOP, CCAAT/enhancer binding protein (C/EBP) homologous protein; GADD34, Growth arrest DNA damage-inducible protein 34; ER, Endoplasmic reticulum; eIF2α, Eukaryotic initiation factor 2α; UPP, ubiquitin-proteasome pathway.

References

1. Akazawa, H., Komazaki, S., Shimomura, H., Terasaki, F., Zou, Y., Takano, H., Nagai, T., Komuro, I. 2004. Diphtheria toxin-induced autophagic cardiomyocyte death plays a pathogenic role in mouse model of heart failure. *Journal of Biological Chemistry*. 279: 41095-41103
2. Ali, M.K., Ewer, M.S., Gibbs, H.R., Swafford, J., Graff, K.L. 1994. Late daunorubicin-associated cardiotoxicity in children. The possible role of intercurrent viral infection. *Cancer*. 74: 182-188
3. Araki, E., Oyadomari, S., Mori, M. 2003. Endoplasmic reticulum stress and diabetes mellitus. *Internal Medicine*. 42: 7-14
4. Araki, N., Hamasaki, M., Egami, Y., Hatae, T. 2006. Effect of 3-methyladenine on the fusion process of macropinosomes in EGF-stimulated A431 cells. *Cell Structure and Function*. 31: 145-157
5. Arola, O.J., Saraste, A., Pulkki, K., Kallajoki, M., Parvinan, M., Voipio-Pulkki, L.-M. 2000. Acute doxorubicin cardiotoxicity involves cardiomyocyte apoptosis. *Cancer Research*. 60: 1789-1792
6. Ascensao, A., Magalhaes, J., Soares, J., Ferreira, R., Neuparth, M., Marques, F.M., Oliveira, J., Duarte, J. 2005. Endurance training attenuates doxorubicin-induced cardiac oxidative damage in mice. *International Journal of Cardiology*. 100:451–60
7. Balis, F.M.H., Poplack, J.S., D.G. 1993. General principles of chemotherapy. In: Pizzo PAP, DG (eds) Principles and practice of pediatric oncology. JB Lippincott: Philadelphia. 222-224
8. Barrett-Lee, P.J., Dixon, J.M., Farrell, C., Jones, A., Leonard, R., Murray, N., Palmieri, C., Plummer, C.J., Stanley, A., Verrill, M.W. 2009. Expert opinion on the use of anthracyclines in patients with advance breast cancer at cardiac risk. *Annals of Oncology*. 20: 816-827
9. Bernales, S., McDonald, K.L., Walter, P. 2006. Autophagy counterbalances endoplasmic reticulum stress expansion during the unfolded protein response. *PLoS Biology*. 4: 2311-2324
10. Bernales, S., Papa, F.R., Walter, P. 2006. Intracellular, signaling by the unfolded protein response. *Annual Review of Cell and Developmental Biology*. 22: 487-508

11. Berridge, M.J. 2002. The endoplasmic reticulum: a multifunctional signaling organelle. *Cell Calcium*. 32: 235-249
12. Billingham, M.E., Mason, J.W., Bristow, M.R., and Daniels, J.R. 1978. Anthracycline cardiomyopathy monitored by morphologic changes. *Cancer Treatment Reports*. 62: 865-872
13. Bjorkoy, G., Lamark, T., Brech, A., Outzen, H., Perander, M., Overvatn, A., Stenmark, H., Johansen, T. 2005. p62/SQSTMI forms protein aggregates degraded by autophagy and has a protective effect on Huntingtin-induced cell death. *Journal of Cell Biology*. 171: 603-614
14. Bloom, J., Amador, V., Bartolini, F., De Martino, G., Pagano, M. 2003. Proteasome-mediated degradation of p21 via N-terminal ubiquitinylation. *Cell*. 115: 71-82
15. Bodine, S.C., Latres, E., Baumheuter, S., Lai, V.K.M., Nunez, L., Clarke, B.A., Poueymirou, W.T., Panaro, F.J., Na, E., Dharmarajan, K., Pan, Z.Q., Valenzuela, D.M., DeChiara, T.M., Stitt, T.N., Yancopoulos, G.D., Glass, D.J. 2001. Identification of ubiquitin ligases required for skeletal muscle atrophy. *Science*. 294: 1704-1708
16. Bonifacino, J.S., Traub, L.M. 2003. Signals for sorting of transmembrane proteins to endosomes and lysosomes. *Annual Reviews of Biochemistry*. 72: 395-447
17. Bristow, M.R. 1982. Toxic cardiomyopathy due to doxorubicin. *Hospital Practice*. 17: 101-111
18. Buja, L.M., Ferrans, V.J., Mayer, R.J., Roberts, W.C., Henderson, E.S. 1973. Cardiac ultrastructural changes induced by daunorubicin therapy. *Cancer*. 32: 771-778
19. Cardinale, D., Sandri, M. T., Martinoni A., LabTech, A.T., Civelli, M., Lamantia, G., Cinieri, S., Martinelli, G., Cipolla, C. M., Fiorentini, C. 2000. Left ventricular dysfunction by early troponin I release after high-dose chemotherapy. *Journal of American College of Cardiology*. 36: 517-522.
20. Cardinale, D., Sandri, M. T., Martinoni, A., Borghini, E., Civelli, M., Lamantia, G., Cinieri, S., Martinelli, G., Fiorentini, C., Cipolla, C.M. 2002. Myocardial injury revealed by plasma troponin I in breast cancer treated with high-dose chemotherapy. *Annals of Oncolology*. 13: 710-715

21. Centner, T., Yano, J., Kimura, E., McElhinny, A.S., Pelin, K., Witt, C.C., Bang, M.L., Trambilas, K., Granzier, H., Gregorio, C.C., Sorimachi, H., Labeit, S. 2001. Identification of muscle specific ring finger proteins as potential regulators of the titin kinase domain. *Journal of Molecular Biology*. 306: 717-726
22. Chen, M.H. 2009. Cardiac dysfunction induced by novel targeted anticancer therapy: an emerging issue. *Current Cardiology Reports*. 11: 167-174
23. Chen, Y. 2009. Necrosis: An energy-dependent programmed cell death? *University of Toronto Medical Journal*. 96: 110-112
24. Cheneval, D., Muller, M., Toni, R., Ruetz, S., Carafoli, E. 1985. Adriamycin as a probe for the transversal distribution of cardiolipin in the inner mitochondrial membrane. *Journal of Biological Chemistry.* 260: 13003–13007
25. Childs, A.C., Phaneuf, S.L., Dirks, A.J., Phillips, T., Leeuwenburgh, C. 2002. Doxorubicin treatment in vivo causes cytochrome C release and cardiomyocyte apoptosis, as well as increased mitochondrial efficiency, superoxide dismutase activity, and Bcl-2: Bax ratio. *Cancer Research*. 62:4592–4598
26. Ciechanover, A., Ben Saadan, R. 2004. N-terminal ubiquitination: more protein substrates join in. *Trends in Cell Biology*. 14: 103-106
27. Ciolli, S., Leoni, F., Casini, C., Breschi, C., Santini, V., Bosi, A. 2008. The addition of liposomal doxorubicin to bortezomib, thalidomide and dexamethasone significantly improves clinical outcome of advanced multiple myeloma. *British Journal of Haematology*. 141: 814-819
28. Cuervo, A.M. 2004. Autophagy: Many paths to the same end. *Molecular and Cellular Biochemistry*. 263: 55-72
29. Dammrich, J., Pfeifer, U. 1983. Cardiac hypertrophy in rats after supravalvular aortic constriction: II. Inhibition of cellular autophagy in hypertrophying cardiomyocytes. *Virchows Archive B: Cell Pathology including Molecular Pathology*. 43: 287-307
30. DeAtley, S.M., Adsenov, M.Y., Aksenova, M.V., Harris, B., Hadley, R., Harper, P.C., Carney, J.M., Butterfield, D.A. 1999. Antioxidants protect against reactive oxygen species associated with adriamycin-treated cardiomyocytes. *Cancer Letters*. 136: 41–46.

31. Decker, R.S., Wildenthal, K. 1980. Lysosomal alterations in hypoxic and reoxygenated hearts: I. Ultrastructural and cytochemical changes. *American Journal of Pathology.* 98: 425-444
32. Delgado, M.A., Elmaoued, R.A., Davis, A.S., Kyei, G., Deretic, V. 2008. Toll-like receptors control autophagy. *EMBO Journal*. 27: 1110-1121
33. Dennis, P.B., Jaeschke, A., Saitoh, M., Fowler, B., Kozma, S.C., Thomas, G. 2001. Mammalian TOR: a homeostatic ATP sensor. *Science*. 294: 1102-1105
34. Dermachi F., Bertoli, C., Copetti, T., Tanida, I., Brancolini, C., Eskelinen, E.L., Schneider, C. 2006. Calpain is required for macroautophagy in mammalian cells. *The Journal of Cell Biology*. 175: 595-605
35. Di Marco, A., Gaetani, M., Scarpinato, B. 1969. Adriamycin (NSC-123, 127): A new antibiotic with antitumor activity. *Cancer Chemotherapy Reports.* 53: 33-37
36. Ding, W.-X., Ni, H.-M., Gao, W., Yoshimori, T., Stolz, D.-B., Ron, D., Yin, X.-M. 2007. Lining autophagy to ubiquitin-proteasome system is important for the regulation of endoplasmic reticulum stress and cell viability. *The American Journal of Pathology*. 171: 513-524
37. Doroshow, J.H., Locker, G.Y., Meyers, C.E. 1980. Enzymatic defences of the mouse heart against reactive oxygen metabolites. *Journal of Clinical Investigation*. 65:128–135.
38. Dorr, R.T., Lagel, K., McLean, S. 1996. Cardioprotection of rat heart myocytes with amifostine (Ethyol) and its free thiol, WR-1065, in vitro. *European Journal of Cancer*. 32A:S21–S25.
39. Dunn Jr, W.A. 1990. Studies on the mechanisms of autophagy: formation of the autophagic vacuole. *Journal of Cell Biology*. 110: 1923-1933
40. Edinger, A.L., Thompson, C.B. 2004. Death by design: apoptosis, necrosis and autophagy. *Current Opinion in Cell Biology*. 16: 2445-2462
41. Elliott, P. 2006. Pathogenesis of cardiotoxicity induced by anthracyclines. *Seminars in Oncology*. 33: S2-S7
42. Elmore, S. 2007. Apoptosis: A review of programmed cell death. *Toxicology and Pathology*. 35: 495–516
43. Elsasser, A., Vogt, A.M., Nef, H., Kostin, S., Mollmann, H., Skwara, W., Bode, C., Hamm, C., Schaper, J. 2004. Human hibernating myocardium is

jeopardized by apoptotic and autophagic cell death. *Journal of the American College of Cardiology*. 43: 2191-2199

44. Feurtes, G., Martin De Llano, J.J., Villarroya, A., Rivett, A.J., Knecht, E. 2003. Changes in the proteolytic activities of proteasomes and lysosomes in human fibroblasts produced by serum withdrawal, amino-acid deprivation and confluent conditions. *The Biochemical Journal*. 315: 75-86
45. Feurtes, G., Villarroya, A., Knecht, E. 2003. Role of proteasomes in the degradation of short-lived proteins in human fibroblasts under various growth conditions. *International Journal of Biochemistry: Cell Biology*. 35: 651-664
46. Forstermann, U., Munzel, T. 2006. Endothelial nitric oxide synthase in vascular disease: from marvel to menace. *Circulation*. 113: 1708-1714
47. Frenzel, H., Schwartzkopff, B., Rettig, B., Vogelsang, H. 1987. Morphologic criteria of progression and regression of cardiac hypertrophy. *Journal of Cardiovascular Pharmacology.* 10: S20-S28
48. Gabizon, A., Dagan, A., Goran, D., Barenholz, Y., Fukz, Z. 1992. Liposomes as in vivo carriers of Adriamycin: reduced cardiac uptake and preserved antitumor activity. *Cancer Research*. 42: 4734-4739
49. Gastman, B.R. 2001. Apoptosis and its clinical impact. *Head and Neck*. 23: 409–425
50. Gerwitz, D.A. 1999. A critical evaluation of the mechanisms of action proposed for the antitumor effects of the anthracycline antibiotics adriamycin and daunorubicin. *Biochemical Pharmacology*. 57: 727-741
51. Giotta, F., Lorusso, V., Maiello, E., Filippelli, G., Valerio, M.R., Caruso, M., Verderame, F., Latorre, A., Colucci, G. 2007. Liposomal-encapsulated doxorubicin plus cyclophosphamide as first-line therapy in metastatic breast cancer: a phase II multicentric study. *Annals of Oncology*. 18: vi66-vi69
52. Glass, D.J. 2003. Signalling pathways that mediate skeletal muscle hypertrophy and atrophy. *Nature Cell Biology*. 5: 87-90
53. Glembotski, C.C. 2007. Endoplasmic reticulum stress in the heart. *Circulation*. 101: 975-984
54. Goldstein, P., Kroemer, G. 2006. Cell death by necrosis: towards a molecular definition. *TRENDS in Biochemical Sciences*. 32: 37-43

55. Goormaghtigh, E., Huart, P., Praet, M., Brasseur, R., Ruysschaert, J.M. 1990. Structure of the doxorubicin-cardiolopin complex role in mitochondrial toxicity. *Biophysical Chemistry*. 35: 247-257
56. Gozuacik, D., Komchi, A. 2007. Autophagy and cell death. *Current Topic in Development Biology*. 78: 217-245
57. Habelhah, H., Takahashi, S., Cho, S.G., Kadoya, T., Watanabe, T., Ronai, Z. 2004. Ubiquitination and translocation of TRAF2 is required for activation of JNK but not of p38 or NF-κB. *EMBO Journal*. 23: 322-332
58. Haglund, K., Di Fiore, P.P., Dikic, I. 2003. Distinct monoubiquitination signals in receptor endocytosis. *Trends in Biochemical Sciences*. 28: 598-603
59. Hamada, H., Suzuki, M., Yuasa, S., Mimura, N., Shinozuki, N., Takada, Y., Nishino, T., Nakaya, H., Koseki, H., Aoe, T. 2004. Dilated cardiomyopathy caused by aberrant endoplasmic reticulum quality control in mutant KDEL receptor. *Molecular and Cellular Biology*. 24: 8007-8017
60. Healy Bird, B.R.J., Swain, S.M. 2008. Cardiac toxicity in breast cancer survivors: Review of potential cardiac problems. *Clinical Cancer Research*. 14: 14-24
61. Herrmann, J., Ciechanover, A., Lerman, L.O., Lerman, A. 2004. The ubiquitin-proteasome system in cardiovascular diseases - a hypothesis extended. *Cardiovascular Research*. 61: 11-21
62. Hetz, C., Glincher, L.H. 2008. XBP-1 and the UPRosome: mastering secretory cell functions. *Current Immunology Reviews*. 4: 1-10
63. Higami, Y., Shimokawa, I. 2000. Apoptosis in the aging process. *Cell and Tissue Research*. 301: 125-132
64. Hochster, H., Wasserheit, C., Speyer, J. 1995. Cardiotoxicity and cardioprotection during chemotherapy. *Current Opinion in Oncology*. 7: 304-309
65. Horenstein, M.S., Vander Heide, R.S., L'Ecuyer, T.J. 2000. Molecular basis of anthracycline-induced cardiotoxicity and its prevention. *Molecular Genetics and Metabolism*. 71: 436-444
66. Høyer-Hansen, M., Bastholm, L., Szyniarowski, P., Campanella, M., Szabadkai, G., Farkas, T., Bianchi, K., Fehrenbacher, N., Elling, F., Rizzuto, R., Mathiasen, I.S., Jäättelä, M. 2007. Control of macroautophagy by calcium, calmodulin-dependent kinase kinase-β and Bcl-2. *Molecular Cell*. 25: 193-205

67. Høyer-Hansen, M., Jäättlela, M. 2007. Connecting endoplasmic reticulum stress to autophagy by unfolded protein response and calcium. *Cell Death and Differentiation*. 14: 1576-1582
68. Hunt, S.A., Abraham, W.T., Chin, M.H., Feldman, A.M., Francis, G.S., Ganiats, T.G., Jessup, M., Konstam, M.A., Mancini, D.M., Michl, K., Oates, J.A., Rahko, P.S., Silver, M.A., Stevenson, L.W., Yancy, C.W. 2005. ACC/AHA 2005 guideline update for the diagnosis and management of chronic heart failure in the adult: A report of the American College of Cardiology/American Heart Association task force on Practice Guidelines (Writing Committee to update the 2001 Guidelines for the Evaluation and Management of Heart Failure). *Journal of American College of Cardiology*. 46: e1-e82
69. Ito, H., Miller, S.C., Billingham, M.E., Akinoto, H., Torti, S.V., Wade, R. 1990. Doxorubicin selectively inhibits muscle gene expression in cardiac muscle cells in vivo and in vitro. *Proceedings of the National Academy of Sciences USA*. 87: 4275-4279
70. Ito, T., Fujio, Y., Takahashi, K., Azuma, J. 2007. Degradation of NFAT5, a transcription regulator of osmotic stress-related genes, is a critical event for doxorubicin-induced cytotoxicity in cardiac myocytes. *Journal of Biological Chemistry*. 282: 1152-1160
71. Iwata, A., Riley, B.E., Johnston, J.A., Kopito, R.R. 2005. HDAC6 and microtubules are required for autophagic degradation of aggregated Huntington. *Journal of Biological Chemistry*. 208: 40282-40292
72. Jaenke, R. S. 1974. An anthracycline antibiotic-induced cardiomyopathy in rabbits. *Laboratory Investigation.* 30*:* 292–304
73. Jensen, B.V., Skovsgaard, T., Nielsen, S.L. 2002. Functional monitoring of anthracycline cardiotoxicity: a prospective, blinded, long-term observational study of outcome in 120 patients. *Annals of Oncology*. 13: 699-709
74. Kajustra, J., Cheng, W., Sarangarajan, R., Li, P., Li, B., Nitahara, J.A., Chapnick, S., Reiss, K., Olivetti, G., Anversa, P. 1996. Necrotic and apoptotic myocyte cell death in the aging heart of Fischer 344 rats. *American Journal of Physiology-Heart and Circulatory Physiology*. 271: H1215-H1228
75. Kajstura, J., Liu, Y., Baldini, A., Li, B., Olivetti, G., Leri, A., Ansersa, P. 1998. Coronary artery constriction in rats: necrotic and apoptotic myocyte death. *American Journal of Cardiology*. 82: 30K-41K

76. Kakizuka, A. 1998. A protein precipitation: a common etiology in neurodegenerative disorders? *Trends in Genetics*. 14: 396-402
77. Kamikubi, T., Hayashi, T. 1996. Changes in proteasome activity following transient ischemia. *Neurochemistry International*. 28: 209-212
78. Kang, Y.J., Chen, Y., Epstein, P.N. 1996. Suppression of doxorubicin cardiotoxicity by overexpression of catalase in the heart of transgenic mice. *Journal of Biological Chemistry*. 1996. 271:12610–12616.
79. Kaufman, R.J. 1999. Stress signaling from the lumen of the endoplasmic reticulum: coordination of gene transcriptional and translational controls. *Genes and Development*. 13: 1211-1233
80. Kedar, V., McDonough, H., Arya, R., Li, H.H., Rockman, H.A., Patterson, C. 2004. Muscle-specific RING finger 1 is a bona fide ubiquitin ligase that degrades cardiac troponin I. *Proceedings of the National Academy Sciences USA*. 101: 18135-18140
81. Kehrer, J.P. 2000. The Haber-Weiss reaction and mechanisms of toxicity. *Toxicology*. 149: 43-50
82. Keyvani, K., Reinecke, S., Abts, H.F., Paulus, W., Witte, O.W. 2000. Suppression of proteasome C2 contralateral to ischemic lesions in rat brain. *Brain Research*. 858: 386-392
83. Kissova, I., Deffieu, M., Manon, S., Camougrand, N. 2004. Uth1p is involved in the autophagic degradation of mitochondria. *The Journal of Biological Chemistry*. 279: 39068-39074
84. Kiyomiya, K., Matsuo, S., Kurebe, M. 1998. Proteasome is a carrier to translocate doxorubicin from cytoplasm to nucleus. *Life Sciences*. 62: 1853-1860
85. Kiyomiya, K., Satoh, J., Horie, H., Kurebe, M., Nakagawa, H., Matsuo, S. 2002. Correlation between nuclear action of anthracycline anticancer agents and their binding affinity to the proteasome. *International Journal of Oncology*. 21: 1081-1085
86. Klionsky, D.J., Emr, S.D. 2000. Autophagy as a regulated pathway of cellular degradation. *Science*. 290: 1717-1721
87. Kobayashi, S., Volden, P., Timm, D., Mao, K., Xu, X., Liang, Q. 2010. Transcription factor GATA4 inhibits doxorubicin-induced autophagy and cardiomyocyte death. *Journal of Biological Chemistry*. 285: 793-804

88. Komatsu, M., Ueno, T., Waguri, S., Uchiyama, Y., Komanami, E., Tanaka, K. 2007. Constitutive autophagy: vital role in clearance of unfavorable proteins in neurons. *Cell death and Differentiation*. 14: 887-894
89. Korolchuk, V.I., Mansilla, A., Menzies, F.M., Rubinsztein, D.C. 2009. Autophagy inhibition compromises degradation of ubiquitin-proteasome pathway substrates. *Molecular Press*. 33: 517-527
90. Kostin, S., Pool, L., Elsasser, A., Hein, S., Drexler, H.C., Arnon, E., Hayakawa, Y., Zimmermann, R., Bauer, E., Klovekorn, W.P., Schaper, J. 2003. Myocytes die by multiple mechanisms in failing human hearts. *Circulation Research*. 92: 715-724
91. Krijnen, P.A., Nijmeijer, R., Meijer, C.J., Visser, C.A., Hack, C.E., Niessen, H.W. 2002. Apoptosis in myocardial ischaemia and infarction. *Journal of Clinical Pathology*. 55: 801-811
92. Kuma, A., Mizushima, N. 2010. Physiological role of autophagy as an intracellular recycling system: with an emphasis on nutrient metabolism. *Seminars in Cell and Developmental Biology*. 21: 683-690
93. Kumarapeli, A.R., Horak, K.M., Glasford, J.W., Li, J., Chen, Q., Liu, J., Zheng, H., Wang, X. 2005. A novel transgenic mouse model reveals deregulation of the ubiquitin-proteasome system in the heart by doxorubicin. *FASEB Journal*. 19: 2051-2053
94. Lambert, L.A., Qiao, N., Hunt, K.K., Lambert, D.H., Mills, G.B., Meijer, L., Keyomarsi, K. 2008. Autophagy: A novel mechanism of synergistic cytotoxicity between doxorubicin and roscovitine in a sarcoma model. *Cancer Research*. 68: 7966-7974
95. Laurent, G., Jaffre´zou, J.-P. 2001. Signaling pathways activated by daunorubicin. *Blood*. 98: 913-924
96. Leandro, J., Dyck, J., Poppe, D., Shore, R., Airhart, C., Greenberg, M. Gilday, D., Smallhorn, J., Benson, L. 1994. Cardiac dysfunction late after cardiotoxic therapy for childhood cancer. *American Journal of Cardiology*. 74: 1152-1156
97. Lefrak, E. A., Pitha, J., Rosenheim, S., Gottleib, J. A. 1973. A clinicopathologic analysis of adriamycin cardiotoxicity. *Cancer*. 32: 302-314
98. Leist, M., Nicotera, P. 1997. The shape of cell death. *Biochemical and Biophysical Research Communications*. 236: 1-9

99. Leist, M., Single, B., castoldi, A.F., Kunhle, S., Nicotera, P. 1997. Intracellular adenosine triphosphate (ATP) concentration: a switch in the decision between apoptosis and necrosis. *The Journal of Experimental Medicine*. 185: 1481-1486

100. Lemasters, J.J. 1998. The mitochondrial permeability transition in cell death: a common mechanism in necrosis, apoptosis and autophagy. *Biochimica et Biophysica Acta.* 1366: 177-196

101. Levine, B., Kroemer, G. 2008. Autophagy in the pathogenesis of disease. *Cell*. 132: 27-42

102. Lewis, W., and Gonzales, B. 1986. Anthracycline effects on actin and actin-containing thin filaments in cultured neonatal rat myocardial cells. *Laboratory Investigation*. 54: 416–423

103. Li, D. 2006. Selective degradation of the IKappaB kinase (IKK) by autophagy. *Cell Research*. 16: 855-856

104. Li, J., Ni, M., Lee, B., Barron, E., Hinton, D.R., Lee, A.S. 2008. The unfolded protein response regulator GRP78/BiP is required for endoplasmic reticulum integrity and stress-induced autophagy in mammalian cells. *Cell Death and Differentiation*. 15: 1460-1471

105. Li, H.H., Kedar, V., Zhang, C., McDonough, H., Arya, R., Wang, D.Z., Patterson, C. 2004. Atrogin1/muscle atrophy F-box inhibits calcineurin-dependent cardiac hypertrophy by participating in an SCF ubiquitin ligase complex. *Journal of Clinical Investigation*. 114: 1058-1071

106. Lim, C.C., Zuppinger, C., Guo, X., Kuster, G.M., Helmes, M., Eppenger, H.M., Suter, T.M., Liao, R., Sawyer, D.B. 2004. Anthracyclines induce calpain-dependent titin proteolysis and necrosis in cardiomyocytes. *The Journal of Biological Chemistry*. 279: 8290-8299

107. Lipshultz, S.E., Rifai, N., Sallan, S.E., Lipsitz, S.R., Dalton, V., Sacks, D.B. 1997. Predictive value of cardiac troponin-T in paediatric patients at risk for myocardial injury. *Circulation*. 96: 2641-2648

108. Liu, J., Zheng, H., Tang, M., Ryu, Y.-C., Wang, X. 2008. A therapeutic dose of doxorubicin activates ubiquitin-proteasome system-mediated proteolysis by acting on both the ubiquitination apparatus and proteasome. *American Journal of Physiology-Heart and Circulatory Physiology*. 295: H2541-H2550

109. Loos, B., Genade, S., Ellis, B., Lochner, A., Engelbrecht, A.-M. 2011. At the core of survival: Autophagy delays the onset of both apoptotic and necrotic cell death in a model of ischemic cell injury. *Experimental Cell Research*. 317: 1437-1453

110. Loos, B., Lochner, A., Engelbrecht, A.-M. 2011. Autophagy in heart disease: A strong hypothesis for an untouched metabolic reserve. Medical Hypotheses. 77: 52-57

111. Majaljica, D., Prescott, M., Devenish, R.J. 2006. Endoplasmic reticulum and golgi complex: contributions to, and turnover by autophagy. *Traffic*. 7: 1590-1595

112. Mandl, J. Mèszáros, T., Bánhegyi, G., Hunyady, L., Csala, M. 2009. Endoplasmic reticulum: nutrient sensor in physiology and pathology. *Trends in Endocrinology and Metabolism*. 20: 194-201

113. Marzella, L., Ahlberg, J., Glaumann, H. 1981. Autophagy, heterophagy, microautophagy and crinophagy as the means for intracellular degradation. *Virchows Archives B: Cell Pathology including Molecular Pathology*. 36: 219-234

114. Mayer, L.D., Tai, L.C.L., Ko, D.S.C., Masin, D., Ginsberg, R.S., Cullis, P.R., Bally, M.B. 1989. Influence of vesicle size, lipid composition, and drug-to-lipid ratio on the biological activity of liposomal doxorubicin in mice. *Cancer Research*. 49: 5922-5930

115. McMillan, D.R., Gething, M.J., Sambrook, J. 1994. The cellular response to unfolded proteins: intercompartmental signalling. *Current Opinion in Biotechnology*. 5: 540-545

116. Mihm, M.J., Yu, F., Weistein, D.M., Reiser, P.J., Bauer, J.A. 2002. Intracellular distribution of peroynitrite during doxorubicin cardiomyopathy: evidence for selective impairment of myofibrillar creatine kinase. *British Journal of Pharmacology*. 135: 581-588

117. Minotti, G., Menna, P., Salvatorelli, E., Cairo, G., Gianni, L. 2004. Anthracyclines: molecular advances and pharmacologic developments in antitumor activity and cardiotoxicity. *Pharmacological Reviews*. 56: 185-229

118. Mizushima, N. 2004. Methods for monitoring autophagy. *International Journal of Biochemistry: Cell Biology*. 36: 2491-2502

119. Mizushima, N. 2007. Autophagy: process and function. *Genes and Development*. 21: 2861-2873

120. Mizushima, N., Klionsky, D.J. 2007. Protein turnover via autophagy: implications for metabolism. *Annual Reviews of Nutrition*. 27: 19-40

121. Mizushima, N., Levine, B., Cuervo, A.M., Klionsky, D.J. 2008. Autophagy fights disease through cellular self-digestion. *Nature*. 451: 1069-1075

122. Molinari, A., Calcabrini, A., Crateri, P., Arancia, G. 1990. Interaction of anthracycline antibiotics with cytoskeletal components of cultured carcinoma cells (CG5). *Experimental and Molecular Pathol*ogy. 53: 11–33

123. Momoi, T. 2206. Conformational diseases and ER stress-mediated cell death: apoptotic cell death and autophagic cell death. *Current Molecular Medicine*. 6: 111-118

124. Myers, C.E., McGuire, W.P., Liss, R.H., Ifrim, I., Grotzinger, K., Young, R.C. 1977. Adriamycin: the role of lipid peroxidation n cardiac toxicity and tumor response. *Science*. 197: 165-167

125. Nakamura, T., Ueda, Y., Juan, Y., Katsuda, S., Takahashi, H., Koh, E. 2000. Fas-mediated apoptosis in adriamycin-induced cardiomyopathy in rats: In vivo study. *Circulation*. 102:572–578.

126. Nalepa, G., Rolfe, M., Harper, J.W. 2006. Drug discovery in the ubiquitin-proteasome system. *Nature Reviews*. 5: 596-613

127. Nedelsky, N.B., Todd, P.K., Taylor, J.P. 2008. Autophagy and the ubiquitin-proteasome system: Collaborators in neuroprotection. *Biochimica et Biochemistry Acta*. 1782: 691-699

128. Nepomnyashchikh, L.M., Lushnikova, E.L., Semenov, D.E. 2000. Focal degradation of cytoplasmic organelles in cardiomyocytes during regenerative and plastic myocardial insufficiency. *Bulletin of Experimental Biology and Medicine*. 130: 1190-1195

129. Nicolay, K., Fok, J.J., Voorhout, W., Post, J.A., de Kruijff, B. 1986. Cytofluorescence detection of adriamycin-mitochondria interactions in isolated perfused rat heart. *Biochimica et Biophysica Acta.* 887: 35–41

130. Nicolay, K., Timmers, R.J., Spoelstra, E., Van der Neut, R., Fok, J.J., Huigen, Y.M., Verkleij, A.J., De Kruijff, B. 1984. The interaction of adriamycin

with cardiolipin in model and rat liver mitochondrial membranes. *Biochimica et. Biophysica Acta* 778: 359–371.

131. Niwa, M., Sidrauski, C., Kaufman, R.J., Walter, P. 1999. A role for preselin-1 in nuclear accumulation of IRE1 fragments and induction of the mammalian unfolded protein response. *Cell*. 99: 691-702

132. O'Brien, M.A., Kirby, R. 2008. Apoptosis: A review of pro-apoptotic and anti-apoptotic pathways and dysregulation in disease. *Journal of Veterinary Emergency and Critical Care*. 18: 572–585

133. Ogata, M., Hino, S., Saito, A., Morikawa, T., Kondo, S., Kanemoto, S., Murakami, T., Taniguchi, M., Tanii, I., Yoshinaga, K., Shiosaka, S., Hammarback, J.A., Urano, F., Imaizumi, K. 2006. Autophagy is activated for cell survival after endoplasmic reticulum stress. *Molecular and Cellular Biology*. 26: 9220-9231

134. Okada, K., Minamino, T., Tsukamoto, Y., Liao, Y., Tsukamoto, O., takashima, S., Hirata, A., Fujita, M., Nagamachi, Y., Nakatani, T., Yutani, C., Ozawa, K., Ogawa, S., Tomoike, H., Hori, M., Kitakaze, M. 2004. Prolonged endoplasmic reticulum stress in hypertrophic and failing heart after aortic constriction: possible contribution of endoplasmic reticulum stress to cardiac myocyte apoptosis. *Circulation*. 110: 705-712

135. O'Shaughnessy, J., Twelves, C., Aapro, M. 2002. Treatment for anthracycline-pretreated metastatic breast cancer. *Oncologist*. 7: 4-12.

136. Oudit, G.Y., Sun, H, Kerfant, B.G., Crackower, M.A., Penninger, J.M., Backx, P.H. 2004. The role of phosphoinositide-3 kinase and PTEN in cardiovascular physiology and disease. *Journal of Molecular and Cellular Cardiology*. 37: 449-471

137. Pacher, P., Liaudet, L., Bai, P., Virag, L., Mabley, J.G., Hasko, G., Szabo, C. 2002. Activation of poly (ADP-ribose) polymerase contributes to development of doxorubicin-induced heart failure. *Journal of Pharmacology and Experimental Therapeutics*. 300: 862-867

138. Pandey, U.B., Nie, Z., Batlevi, Y., McCray, B.A., Ritson, G.P., Nedelsky, N.B., Schwartz, S.L., DiProspero, N.A., Knight, M.A., Schuldiner, O., Padmanabhan, R., Hild, M., Berry, D.L., Garza, D., Hubbert, C.C., Yao, T.P., Baehrecke, E.H., Taylor, G.P. 2007. HDAC6 rescues neurodegeneration and

provides an essential link between autophagy and the UPS. *Nature*. 447: 859-863

139. Pankiv, S., Hoyvarde Clausen, T., Lanmark, T., Brech, A., Bruun, J.A., Outzen, H., Overvattn, A., Bjorkoy, G., Johansen, T. 2007. p62/SQSTMI1 binds directly to Atg8/LC3 to facilitate degradation of ubiquitinated protein aggregates by autophagy. *Journal of Biological Chemistry*. 282: 24131-24145

140. Passmore, L.A., Barford, D. 2004. Getting into position: the catalytic mechanism of protein ubiquitylation. *The Journal of Biochemistry*. 379: 513-525

141. Patterson, C., Ike, C., Willis (IV), P.W., Stouffer, G.A., Willis, M.S. 2007. The ubiquitin-proteasome system and cardiac dysfunction. *Circulation*. 115: 1456-1463

142. Paul, S. 2008. Dysfunction of the ubiquitin-proteasome system in multiple disease conditions: therapeutic conditions. *BioEssays*. 30: 1172-1184

143. Pickart, C.M. 2001. Mechanisms underlying ubiquitination. *Annual Reviews of Biochemistry*. 70: 503-533

144. Poizat, C., Sortorelli, V., Chung, G., Kloner, R.A., Kedes, L. 2000. Proteasome-mediated degradation of the coactivator p300 impairs cardiac transcription. *Molecular and Cellular Biology*. 20: 8643-8654

145. Powell, S.R. 2006. The ubiquitin-proteasome system in cardiac physiology and pathology. *American Journal of Physiology: Heart and Circulatory Physiology*. 291: H1-H19

146. Priault, M., Salin, B., Schaeffer, J., Vallette, F.M., di Rago, J.P., Martinou, J.C. 2005. Impairing the bioenergetic status and the biogenesis of mitochondria triggers mitophagy in yeast. *Cell Death & Differe*ntiation. 12: 1613-1621

147. Rajagopalan, S., Politi, P.M., Sinha, B.K., Myers, C.E. 1988. Adriamycin-induced free radical formation in the perfused rat heart: implications for cardiotoxicity. *Cancer Research*. 48: 4766-4769

148. Rao, R.V., Ellerby, H.M., Bredesen, D.E. 2004. Coupling endoplasmic reticulum stress to the cell death program. *Cell Death and Differentiation*. 11: 372-380

149. Ravikumar, B., Sarkar, S., Davies, J.E., Futter, M., Garcia-Arencibia, M., Green-Thompson, Z.W., Jimenez-Sanchez, M., Korolchuk, V.I.,

Lichtenberg, M., Luo, S., Massey, D.C.O., Menzies, F.M., Moreau, K., Narayanan, U., Renna, M., Siddiqi, F.H., Underwood, B.R., Winslow, A.R., Rubensztein, D.C. 2010. Regulation of mammalian autophagy in physiology and pathophysiology. *Physiology Reviews*. 90: 1383-1435

150. Rideout, H.J., Lang-Rollin, I., Stefanis, L. 2004. Involvement of macroautophagy in the dissolution of neuronal inclusions. *International Journal of Biochemistry: Cell Biology*. 36: 2551-2562

151. Rose, M., Greene, R.M. 1979. Cardiovascular complications during prolonged starvation. *Western Journal of Medicine*. 30: 170-177

152. Rosenoff, S.H., Olson, H.M., Young, D.M., Bostick, F., Young, R.C. 1975. Adriamycin-induced cardiac damage in the mouse: a small-animal model of cardiotoxicity. *Journal of the National Cancer Institute.* 55: 191–194

153. Ross, C.A., Pickart, C.M. 2004. The ubiquitin-proteasome pathway in Parkinson's disease and other neurodegenerative diseases. *Trends in Cell Biology*. 14: 703-711

154. Rothermel, B.A., Hill, J.A. 2008. Autophagy in load-induced heart disease. *Circulation Research*. 103: 1363-1369

155. Rubinstein, D.C. 2006. The roles of intracellular protein degradation pathways in neurodegeneration. *Nature*. 443: 780-786

156. Saijo, M., Takemura, G., Koda, M., Okada, H., Miyata, S., Ohno, Y., Kawasaki, M., Tsuchiya, K., Nishigaki, K., Minatoguchi, S., Goto, K., Fujiwara, H. 2004. Cardiomyopathy with prominent autophagic degeneration, accompanied by an elevated plasma brain natriuretic peptide level despite the lack of overt heart failure. *Internal Medicine*. 43: 700-703

157. Schimmel, K.J.M., Richel, D.J., van den Brink, R.B.A., Guchelaar, H.-J. 2004. Cardiotoxicity of cytotoxic drugs. *Cancer Treatment Reviews*. 30: 181-191

158. Schröder, M. 2008. Endoplasmic reticulum stress responses. *Cellular and Molecular Life Sciences*. 65: 862-894

159. Schröder, M., Kaufman, R.J. 2005. ER stress and the unfolded protein response. *Mutation Research*. 569: 29-63

160. Seglen, P.O., Gordon, P.B., Holen, I. 1990. Non-selective autophagy. *Seminars in Cell Biology*. 1: 441-448

161. Seibenhener, M.L., Babu, J.R., Geetha, T., Wong, H.C., Krishna, N.R., Wooten, M.W. 2004. Sequestrome 1/p62 is a polyubiquitin chain binding protein involved in ubiquitin proteasome degradation. *Molecular Cell Biology*. 24: 8055-8068

162. Seidman, A., Hudis, C., Pierri, M.K., Shak, S., Paton, V., Ashby, M., Murphy, M., Stewart, S.J., Keefe, D. 2002. Cardiac dysfunction in the trastuzumab clinical trials experience. *Journal of Clinical Oncology*. 20: 1215-1221

163. Sereno, M., Brunello, A., Chiappori, A., Barriuso, J., Belda. E.C.C., de Castro, J., Feliu, J., González-Barón, M. 2008. Cardiac toxicity: old and new issues in anti-cancer drugs. *Clinical and Translational Oncology*. 10: 35-46

164. Shamu, C.E., Cox, J.S., Walter, P. 1994. The unfolded protein response pathway in yeast. *Trends in Cell Biology*. 4: 56-60

165. Shan, K., Lincoff, M., Young, J.B. 1996. Anthracycline-induced cardiotoxicity. *Annals of Internal Medicine*. 125: 47-58

166. Singal, P.K., Iliskovic, N., Li, T., Kumar, D. 1997. Adriamycin cardiomyopathy: pathophysiology and prevention. *FASEB Journal*. 11: 931-936

167. Singal, P.K., Iliskovic, N. 1998. Doxorubicin-induced cardiomyopathy. *New England Journal of Mecidine*. 339: 900-905

168. Skurk, C., Izumiya, Y., Maatz, H., Razeghi, P., Shiojima, I., Sandri, M., Sato, K., Zeng, L., Schiekofer, S., Pimentel, D., Lecker, S., Taegtmeyer, H., Goldberg, A.L., Walsh, K. 2005. The FOXO3a transcription factor regulates cardiac myocyte size downstream of AKT signaling. *Journal of Biological Chemistry*. 280: 20814-20823

169. Sparano, J.A., Brown, D.L., Wolff, A.C. 2002. Predicting cancer therapy-induced cardiotoxicity. The role of troponins and other markers. *Drug Safety*. 25: 301-311

170. Spence, J., Sadis, S., Haas, A.L., Finley, D. 1995. A ubiquitin mutant with specific defects in DNA repair and multiubiquitination. *Molecular and Cellular Biology*. 15: 1265-1273

171. Speyer, J.L., Green, M.D., Kramer, E., Rey, M., Sanger, J., Ward, C., Dubin, N., Ferrans, V., Stecy, P., Zeleniuch-Jacquotte, A., Wernz, J., Feit, F., Slater, W., Blum, R., Muggia, F. 1988. Protective effect of the

bispiperazinedione ICRF-187 against doxorubicin-induced cardiac toxicity in women with advanced breast cancer. *New England Journal of Medicine*. 319: 745-752

172. Steinberg, J. S., Cohen, A. J., Wasserman, A. G., Cohen, P., Ross, A. M. 1987. Acute arrhythmogenicity of doxorubicin administration. *Cancer.* 60: 1213-1218

173. Suzuki, K., Imai, Y., Nakayama, H., Takahashi, K., Takio, K., Takahashi, R. 2001. A serine protease, HtrA2, is released from the mitochondria and interacts with XIAP, inducing cell death. *Molecular Cell*. 8: 613-621

174. Swain, S.M., Whaley, F.S., Ewer, M.S. 2003. Congestive heart failure in patients treated with doxorubicin: a retrospective analysis of three trials. *Cancer*. 97: 2869-2879.

175. Swain, W.M., Whaley, F.S., Gerber, M.C., Weisberg, S., York, M., Spicer, D., Jones, S.E., Wadler, S., Desai, A., Vogel, C., Speyer, J., Mittelman, A., Reddy, S., Pendergrass, K., Velez-Garcia, E., Ewer, M.S., Bianchine, J.R., Gams, R.A. 1997. Cardioprotection with dexrazoxane for doxorubicin-containing therapy in advanced breast cancer. *Journal of Clinical Oncology*. 15: 1318-1332

176. Szegezdi, E., Fitzgerald, U., Samali, A. 2003. Caspase-12 and ER-stress-mediated apoptosis: the story so far. *Annals of the New York Academy of Science*. 1010: 186-194

177. Szegezdi, E., Logue, S.E., Gorman, A.M., Samali, A. 2006. Mediators of endoplasmic reticulum stress-induced apoptosis. *EMBO Reports*. 7: 880-885

178. Tannous, P., Zhu, H., Nemchenjo, A., Berry, J.M., Johnstone, J.L., Shelton, J.M., Miller (Jr), F.J., Rothermal, B.A., Hill, J.A. 2008. Intracellular protein aggregation in a proximal trigger of cardiomyocyte autophagy. *Circulation*. 117: 3070-3078

179. Tal, R., Winter, G., Ecker, N., Klionsky, D.J., Abeliovich, H. 2007. Aup1p, a yeast mitochondrial protein phosphatase homolog, is required for efficient stationary phase mitophagy and cell survival. *The Journal of Biological Chemistry*. 282: 5617-5624

180. Terman, A., Brunk, U.T. 2005. Autophagy in cardiac myocyte homeostasis, aging, and pathology. *Cardiovascular Research*. 68: 355-365

181. Thameem, F., Farook, V.S., Bogaidus, C., Prochazka, M. 2006. Association of amino acid variants in the activating transcription factor 6 gene (ATF6) on 1q21-q23 with type 2 diabetes in Prima Indians. *Diabetes*. 55: 839-842

182. Tintignac, L.A., Lagirand, J., Botonnet, S., Sirri, V., Leibovitch, M.P., Leibovitch, S.A. 2005. Degradation of MyoD mediated by the SCF (MAFbx) ubiquitin ligase. *Journal of Biological Chemistry*. 280: 2847-2856

183. Tokarska-Schlattner, M., Wallimann, T., Schlattner, U. 2006. Alterations in myocardial energy metabolism induced by the anti-cancer drug doxorubicin. *Comptes Rendus Biologies*. 329: 657-668

184. Turner, B.J., Atkin, J.D. 2006. ER stress and UPR in familial amyotrophic lateral sclerosis. *Current Molecular Medicine*. 6: 79-86

185. Unverferth, B.J., Magorien, R.D., Balcerzak, S.P., Leier, C.V., Unverferth, D. V. 1983. Early changes in human myocardial nuclei after doxorubicin. *Cancer (Phila.)*. 52: 215–221

186. Vander Heide, R.S., L'Ecuyer, T.J. 2007. Molecular basis of anthracycline-induced cardiotoxicity. *Heart and Metabolism*. 35: 1-4

187. Vergely, C., Delemasure, S., Cottin, Y., Rochette, L. 2007. Preventing the cardiotoxic effects of anthracyclines: from basic concepts to clinical data. *Heart and Metabolism.* 35: 1-7.

188. Von Hoff, D.D., Layard, M.W., Basa, P., Davis, H.L. Jr, Von Hoff, A.L., Rozencweig, M., Muggia, F.M. 1979. Risk factors for doxorubicin-induced congestive heart failure. *Annals of Internal Medicine*. 91: 710-717

189. Von Huff, D.D., Rozencweig, M., Layar, M., Slavik, M., Muggia, F.M. 1977. Daunomycin-induced cardiotoxicity in children and adults: a review of 110 cases. *American Journal of Medicine*. 62: 200-208

190. Voorhees, P.M., Orlowski, R.Z. 2007. Emerging data on the use of anthracyclines in combination with bortezomib in myeloma. *Clinical Lymphoma and Myeloma.* 7: S156-S162

191. Wang, X., Su, H., Ranek, M.J. 2008. Protein quality control and degradation in cardiomyocytes. *Journal of Molecular and Cellular Cardiology*. 45: 11-27

192. Willis, M.S., Patterson, C. 2006. Into the heart: The emerging role of the ubiquitin-proteasome system. *Journal of Molecular and Cellular Cardiology*. 41: 567-579

193. Willis, M.S., Schisler, J.C., Portbury, A.L., Patterson, C. 2009. Build it up - Tear it down: protein quality control in the cardiac sarcomere. *Cardiovascular Research*. 81: 439-448

194. Willis, M.S., Townley-Tilson, W.H.D., Kang, E.Y., Homeister, J.W., Patterson, C. 2010. Sent to destroy. The ubiquitin proteasome system regulates cell signaling and protein quality control in cardiovascular development and disease. *Circulation Research*. 106: 463-478

195. Winslow, A.R., Rubinsztein, D.C. 2008. Autophagy in neurodegeneration and development. *Biochimica et Biophysica Acta.* 1782: 723-729

196. Wyllie, A.H. 1994. Death from inside out: an overview. *Philosophical Transactions of the Royal Society of London. Series B: Biological Sciences*. 345: 237-247

197. Yamaoka, M., Yamaguchi, S., Suzuki, T., Okuyama, M., Nitobe, J., Nakamura, N., Mitsui, Y., Tomoike, H. 2000. Apoptosis in rat cardiac myocytes induced by Fas ligand: priming for Fas-mediated apoptosis with doxorubicin. *Journal of Molecular and Cellular Cardiology*. 32:881–889.

198. Yan, L., Vatner, D.E., Kim, S.J., Ge, H., Masurekar, M., Massaover, W.H., Yang, G., Matsui, Y., Sadoshima, J., Vatner, S.F. 2005. Autophagy in chronically ischemic myocardium. *Proceedings of the National Academy Sciences USA*. 102: 13807-13812

199. Yen, H.C., Oberley, T.D., Vichitbandha, S., Ho, Y.S., St Clair, D.K. 1996. The protective role of manganese superoxide dismutase against adriamycin-induced acute cardiac toxicity in transgenic mice. *Journal of Clinical Investigation*. 98:1253–1260

200. Yoneda, T., Imaizuma, K., Oono, K., Yui, D., Gomi, F., Katayama, T., Tohyoma, M. 2001. Activation of caspase-12, an endoplasmic reticulum (ER) resident caspase, through tumor necrosis factor receptor-associated factor 2-dependent mechanism in response to the ER stress. *The Journal of Biological Chemistry*. 276: 13935-13940

201. Yorimitsu, T., Klionsky, D.J. 2007. Endoplasmic reticulum stress: a new pathway to induce autophagy. *Autophagy*. 3: 160-162

202. Yorimitsu, T., Nair, U., Yang, Z., Klionsky, D.J. 2006. Endoplasmic reticulum stress triggers autophagy. *The Journal of Biological Chemistry*. 281: 30299-30304

203. Yousefi, S., Perozzo, R., Schimid, I., Ziemiecki, A., Schaffner, T., Scapozza, L., Brunner, T., Simon, H.-W. 2006. Calpain-mediated cleavage of Atg5 switches autophagy to apoptosis. *Nature Cell Biology*. 8: 1124-1132

204. Zhang, J., Clark, J. R., Herman, E. H., and Ferrans, V. J. 1996. Doxorubicin-induced apoptosis in spontaneously hypertensive rats: differential effects in heart, kidney and intestine, and inhibition by ICRF-187. *Journal of Molecular and Cellular Cardiology*. 28: 1931–1943

205. Zhang, J., Clark, J.R., Herman, E.H., and Ferrans, V.J. 1993. Dendritic cells in the hearts of spontaneously hypertensive rats treated with doxorubicin with or without ICRF-187. *American Journal of Pathology*. 142: 1916–1926

206. Zhao, J., Brault, J.J., Schild, A., Cao, P., Sandri, M., Schiaffino, S., Lecker, S.H., Goldberg, A.L. 2007. Fox-O3 coordinately activates protein degradation by the autophagic/lysosomal and proteasomal pathways in atrophying muscle cells. *Cell Metabolism*. 6: 472-483

207. Zheng, Q., Li, J., Wang, X. 2010. Interplay between the ubiquitin-proteasome system and autophagy in proteinopathies. *International Journal of Physiology, Pathophysiology and Pharmacology*.1: 127-142

208. Zong, W.-X., Thompson, C.B. 2006. Necrotic death as a cell fate. *Genes and Development*. 20: 1-15

209. Zuppinger, C., Timolati, F., Suter, T. M. 2007. Pathophysiology and diagnosis of cancer drug induced cardiomyopathy. *Cardiovascular Toxicology.* 7: 61-66

Chapter 2

Ex vivo model

2.1: Introduction

Anthracyclines such as daunorubicin (DNR), doxorubicin (DXR), epirubicin and idarubicin are widely used for treatment of various haematological and solid tumor malignancies including breast cancer, leukemia and sarcomas (Fisher *et al*, 2005) Although these anthracyclines are very effective, its clinical use is limited due to cardiotoxicity which leads to congestive heart failure, reduced quality of life, or death (Von Hoff *et al*, 1977; Fajardo *et al*, 2006) On molecular level, anthracyclines induce apoptosis, alterations in iron homeostasis, deregulation of calcium homeostasis, and mitochondrial dysfunction (Vergely *et al*, 2007).

Antracycline cardiotoxicity can be classified as acute or chronic. Acute cardiotoxicity is independent of the anthracycline dose and is characterized by hypotension, tachycardia, arrhythmias, and depression of left ventricular function (Fumoleau *et al*, 2006). Chronic or delayed cardiotoxicity is dose-related, typically irreversible and usually presents within one year after the end of treatment.

Since the early detection and treatment of cardiotoxicity can reduce its clinical outcome, it is particularly important to understand the molecular events leading to these adverse effects in order to develop new treatment strategies to manage the side-effects appropriately. Several mechanisms have been proposed for anthracycline-mediated cardiac toxicity such as the formation of reactive oxygen species (Liu *et al*, 2004) and the formation of secondary alcohol metabolites within cardiac tissue (Minotti *et al*, 2000). Furthermore, it was also shown that the ubiquitin-

proteasome pathway (UPP) is deregulated by DXR in the heart (Poizat *et al*, 2000; Kumarapeli *et al*, 2005). The UPP is one of two major pathways which are responsible for the clearance of proteins and organelles in the eukaryotic cell. The UPP predominantly degrades short-lived normal protein molecules after they have fulfilled their duty in the cell, such as proteins involved in regulation of cell division, gene transcription, signal transduction and endocytosis (Hochstrasser *et al*, 1995). The UPP also degrades abnormal proteins such as misfolded, oxidised, and mutant proteins, thereby serving as a critical step of post-translational protein quality control in the cell (Gomes *et al*, 2006). Targeted proteolysis by the UPP includes two main steps: 1) the attachment of a series of Ub molecules to the target protein molecule via a process known as ubiquitination and 2) degradation of the ubiquitinated proteins by the proteasome (Patterson *et al*, 2007; Young *et al*, 2008). A series of energy-consuming reactions, involving ubiquitin-activating enzymes (E_1), ubiquitin-conjugating enzymes (E_2) and ubiquitin ligases (E_3) are required to tag targeted proteins. Two E_3 ligases, muscle RING finger-1 (MuR-1) and muscle atrophy F-box (MAFbx) are expressed specifically in striated (cardiac and skeletal) muscle and are central players in the UPP regulated turnover of sarcomeric proteins (Li *et al*, 2004; Li *et al*, 2007).

The other major pathway responsible for degradation of cytoplasmic proteins, organelles and long-lived proteins is the autophagy-lysosomal pathway (Yoshimori *et al*, 2004). Although there is a constant low level of autophagic activity under normal conditions in the heart (Levine *et al*, 2004), autophagy is upregulated in response to stressors such as ischaemia/reperfusion injury, cardiac hypertrophy, heart failure and nutrient deprivation (Gustafsson *et al*, 2008). Autophagy requires a cascade of evolutionarily conserved proteins (Atg proteins) that comprise two conjugation pathways: 1) the Atg12-Atg5 pathway; and 2) the light chain 3-phosphatidylethanolamine (LC3 or Atg8-PE) pathway (Gustafsson *et al*, 2009). Beclin 1 (Atg6) is part of a phosphoinositide 3-kinase (PI3-K) complex and seems to play an important role during the initial steps of autophagosome formation by mediating the localization of other Atg proteins to the isolation membrane (Fuertes *et al*, 2003).

The distinction of substrate preference between these two proteolytic systems are relative as recent studies indicate the UPP can participate in the degradation of long-lived proteins while autophagy can also be involved in the degradation of short-lived proteins (Fuertes *et al*, 2003; Li *et al*, 2006). Together, these systems play an essential role in the maintenance of sarcomeric function in the face of physiological and pathophysiological stimuli. Therefore, the aim of this study was to characterize these proteolytic systems after DNR-induced cardiotoxicity in a rat model.

2.2: Materials and Methods

2.2.1: Animal model and treatment

Male Wistar rats (180 – 200 g, n=14) were fed a standard rat chow diet (SRC) with free access to water. All experiments were approved by the ethics committee at the Faculty of Health and Wellness Sciences, Cape Peninsula University of Technology, South Africa (Ref: CPUT/HW-REC 2008/009) and conforms with the European Communities Council Directive of 1986 (86/609/EEC) and the United States National Institute of Health guidelines.

2.2.2: Experimental protocol

Adult rats were divided into two groups where one group received DNR treatment and the other saline injections as control. Animals of the DNR group received six intraperitoneal injections of 2 mg/kg on alternate days resulting in a 12 mg/kg cumulative dose. The evaluation of heart function was performed the day after the last injection.

2.2.3: Working heart perfusions

After the experimental protocol, rats were injected with sodium pentobarbitone solution (Euthenase, 50 mg/kg), and their hearts rapidly excised and placed in cooled Krebs Henseleit buffer [(KHB) - 121.5 mmol/l NaCl; 3.8 mmol/l KCl; 1.2 mmol/l MgCl 6 H_2O; 2.5 mmol/l $CaCl_2$; 15.5 mmol/l $NaHCO_3$; 1.2 mmol/l KH_2PO_4; 11.0 mmol/l glucose] , before being mounted on a working heart perfusion apparatus by canulating the aorta and pulmonary vein. Retrograde aortic perfusion was initiated and sustained for 10 min (stabilization period) at a constant perfusion pressure of 100 cm KHB. After the stabilization period, the hearts were switched to the working heart mode for 35 min, during which aortic output (AO), coronary flow (CF) and aortic pressure (AOP) was measured every 5 min. At the end of the perfusion protocol hearts were freeze clamped for biochemical analysis.

2.2.4: Western-blot Analysis

Tissue protein were extracted with a lysis buffer containing (in mM): Tris 20, p-nitrophenylphosphate 20, EGTA 1, sodium fluoride (NaF) 50, sodium orthovanadate 0.1, phenylmethyl sulphonyl fluoride (PMSF) 1, dithiothreitol (DTT) 1, aprotinin 10 µg/ml, leupeptin 10 µg/ml. The tissue lysates were diluted in Laemmli sample buffer, boiled for 5 minutes and 10 µg (for kinases, E_3 ligases and LC-3 and beclin) or 50 µg protein (for caspase-3 and PARP) were subjected to electrophoresis. The lysate protein content was determined using the Bradford technique (Bradford, 1976). The separated proteins were transferred to a PVDF membrane (ImmobilonTM P, Millipore). These membranes were routinely stained with Ponceau Red for visualization of proteins and stripped and reprobed with anti-actin antibody to ensure equal loading. Non-specific binding sites on the membranes were blocked with 5% fat-free milk powder dissolved in Tris-buffered saline-0.1% Tween 20 (TBST) and then incubated with the primary antibodies that recognize phospho-specific and total PKB Ser473 and FoxO1, caspase-3 (p17 fragment pAb) and PARP (p89 fragment pAb), Bcl-2, Bax, LC-3 and beclin-1 (all from Cell Signalling Technology) and MAFbx, MuRF-1 and ubiquitin from Santa Cruz. Membranes were subsequently washed with large volumes of TBST (5 x 5 min) and the immobilized antibody

conjugated with a diluted horseradish peroxidase-labeled secondary antibody (Amersham LIFE SCIENCE). After thorough washing with TBS-T, membranes were covered with ECLTM detection reagents and quickly exposed to an autoradiography film (Hyperfilm ECL, RPN 2103) to detect light emission through a non-radioactive method (ECL^{TM} Western blotting). Films were densitometrically analyzed (UN-SCAN-IT, Silkscience) and phosphorylated protein values were corrected for minor differences in protein loading, if required. All blots were scanned at a resolution of 150 dpi. The exact outline of each band was demarcated in the UN-SCAN-IT programme, which takes all aspects of density and distribution into account. The full experimental range was analyzed on a particular blot. These analyses were performed under conditions where autoradiographic detection was in the linear response range.

2.2.5: Statistics

Values are presented as mean ± standard error of the mean (S.E.M). Western blot data are presented as means ± S.E.M. of triplicate analysis of the protein samples from seven rats per group. The student's unpaired t test was used to determine statistical significance. A value of $p \leq 0.05$ was considered statistically significant.

2.3: Results

2.3.1: DNR suppresses cardiac function (Table 1)

We have previously demonstrated that the anti-cancer treatment regimen with the anthracycline, DNR, significantly attenuated cardiac function in the isolated rat heart (Wergeland *et al*, 2011). DNR significantly decreased aortic pressure [(93.98 ± 8.53 mmHg vs 117.80 ± 2.99 mmHg ($p < 0.05$)] aortic output [(31.73 ± 2.20 ml/min vs 38.25 ± 1.25 ml/min ($p < 0.05$)] and coronary flow rate [(17.07 ± 1.41 ml/min vs 21.88 ± 1.21 ml/min ($p < 0.05$)] compared to their respective control groups.

Functional characteristics of animal hearts		
	Control	**DNR**
Aortic Pressure	117.80 ± 2.99 mmHg	93.98 ± 8.53 mmHg*
Aortic Output	38.25 ± 1.25 ml/min	31.73 ± 2.20 ml/min*
Coronary Flow Rate	21.88 ± 1.21 ml/min	17.07 ± 1.41 ml/min*
***p<0.05 vs. Control**		

Table 1: Functional characteristics of animal hearts. During the perfusion protocol, aortic pressure, output and coronary flow rate were measured. All values are reported as a mean ± SEM. Statistical significance at $^{*}p \leq 0.05$, n = 7

2.3.2: DNR induces apoptosis in the rat heart (Figure 2.3.1 - 3)

DNR significantly increased caspase-3 [(215.00 ± 8.88 vs 182.70 ± 4.05 avg pixels (p = 0.029)] as well as PARP cleavage [(221.00 ± 3.78 vs 185.30 ± 7.79 avg pixels (p = 0.014)] in the rat heart. In animals treated with DNR, Bcl-2 protein expression in the hearts decreased, but Bax protein expression increased compared to control. More importantly, the ratio of Bcl-2/Bax increased during DNR treatment, indicating that DNR down-regulated Bcl-2 expression and up-regulated Bax expression [(0.48 ± 0.09 vs control (p = 0.009)].

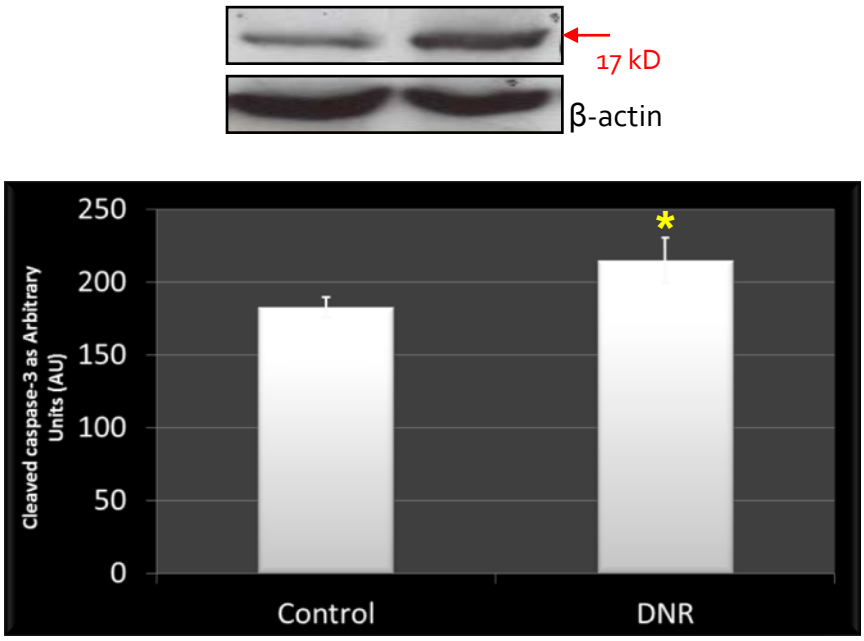

Figure 2.3.1: The effect of DNR treatment on apoptosis in the heart. After the perfusion protocol, the heart tissue was freeze clamped and analyzed for apoptotic marker cleaved caspase-3. All values are reported as a mean ± SEM. Statistical significance at $^{*}p = 0.029$, n = 7

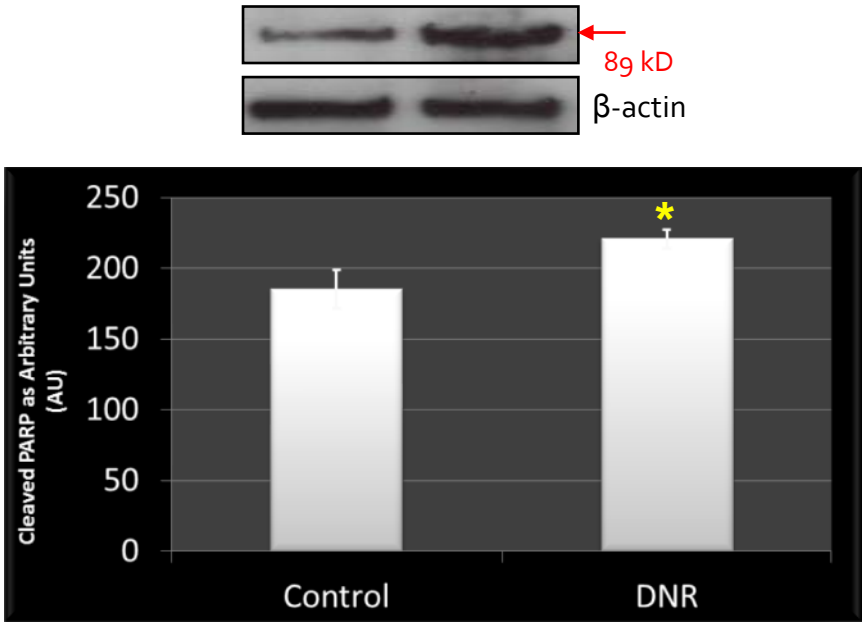

Figure 2.3.2: The effect of DNR treatment on apoptosis in the heart. After the perfusion protocol, the heart tissue was freeze clamped and analyzed for apoptotic marker cleaved-PARP. All values are reported as a mean ± SEM. Statistical significance at $^{*}p = 0.014$, n = 7

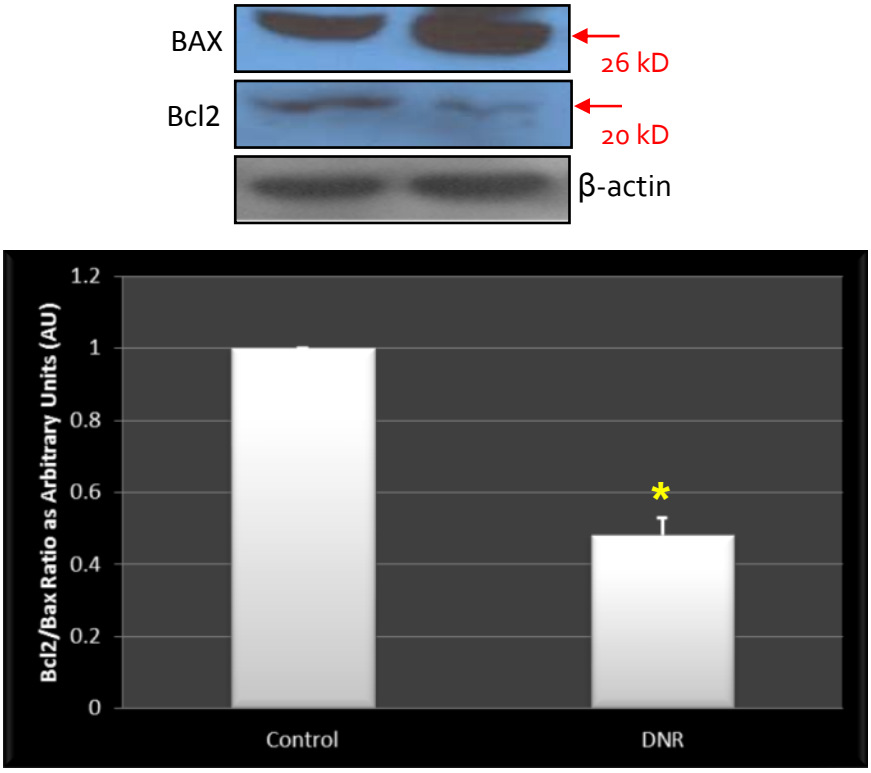

Figure 2.3.3: The effect of DNR treatment on apoptosis in the heart. After the perfusion protocol, the heart tissue was freeze clamped and analyzed for apoptotic markers Bcl-2 and Bax. All values are reported as a mean ± SEM. Statistical significance at $^{*}p = 0.009$, n = 7

2.3.3: DNR induces autophagy in the rat heart (Figure 2.3.4 - 6)

DNR caused significant increases in two markers of autophagy. A 24% increase in beclin-1 [(206.10 ± 2.51 vs 156.60 ± 6.40 avg pixels (p = 0.0002)] as well as a 46% increase in LC-3 lipidation [(210.60 ± 2.58 vs 114.10 ± 4.85 avg pixels (p = 0.0002)] was observed after DNR treatment. DNR also caused a significant attenuation of p62/SQSTM1 [(152.70 ± 5.81 vs 174.50 ± 2.45 avg pixels (p = 0.008)].

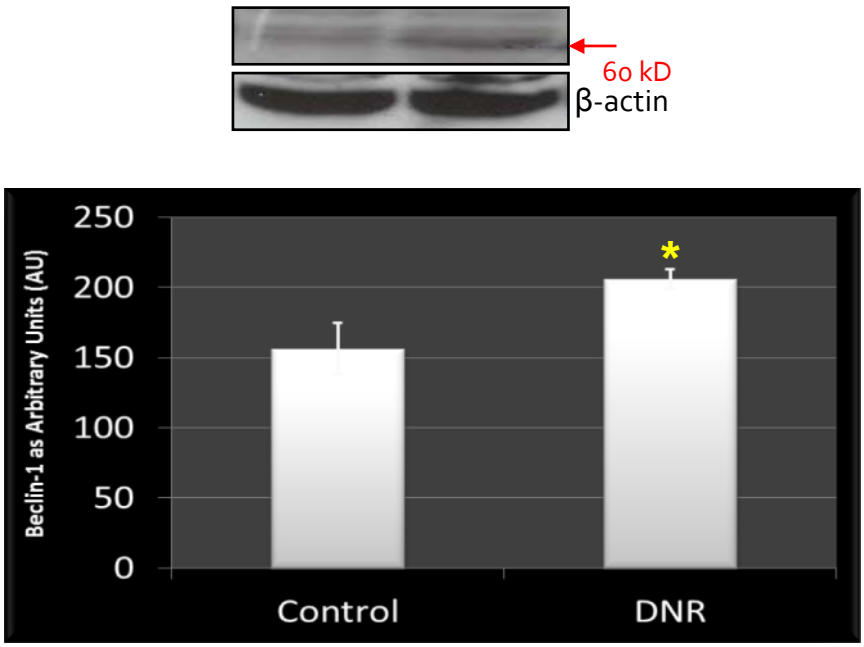

Figure 2.3.4: The effect of DNR treatment on autophagy in the heart. After the perfusion protocol, the heart tissue was freeze clamped and analyzed for the autophagic marker Beclin-1. All values are reported as a mean ± SEM. Statistical significance at $^{*}p = 0.0002$, n = 7

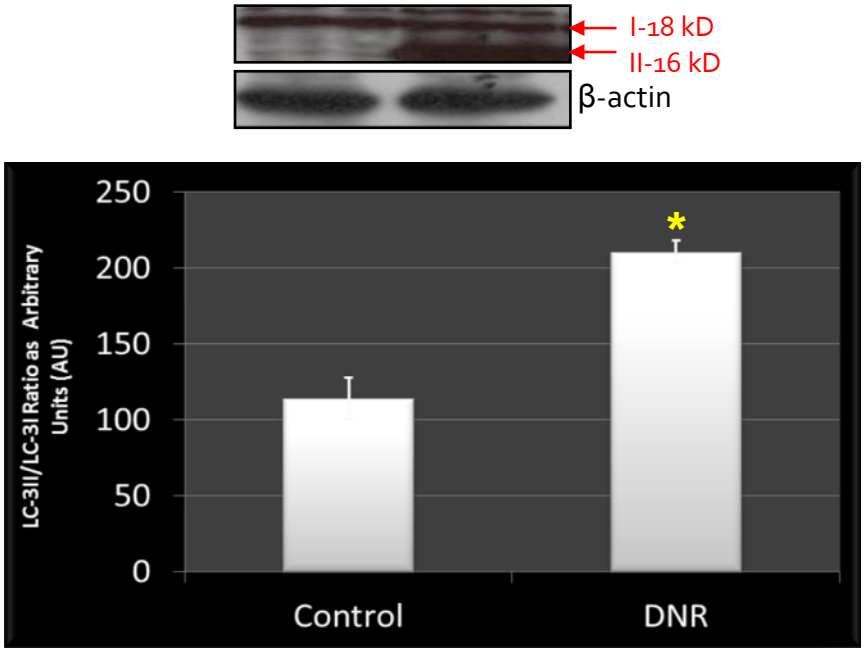

Figure 2.3.5: The effect of DNR treatment on autophagy in the heart. After the perfusion protocol, the heart tissue was freeze clamped and analyzed for the autophagic marker LC-3. All values are reported as a mean ± SEM. Statistical significance at $^{*}p = 0.0002$, n = 7

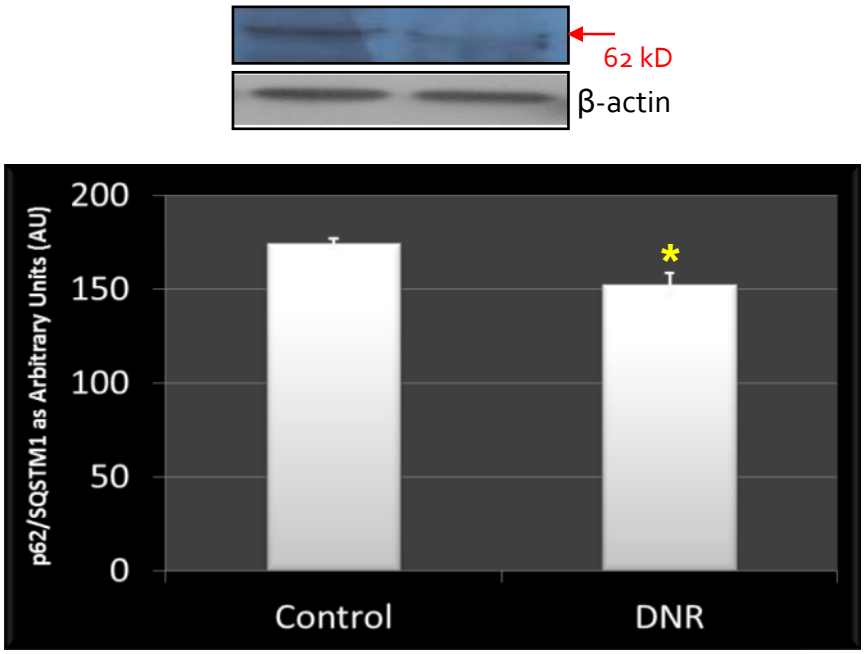

Figure 2.3.6: The effect of DNR treatment on autophagy in the heart. After the perfusion protocol, the heart tissue was freeze clamped and analyzed for the autophagic marker p62/SQSTM1. All values are reported as a mean ± SEM. Statistical significance at $^{*}p = 0.008$, n = 7

2.3.4: DNR attenuates the PI3-Kinase/Akt signalling pathway (Figure 2.3.7 - 8)

Akt (Ser^{473}) phosphorylation was significantly inhibited after DNR treatment [(90.00 ± 0.58% (p = 0.001)]. One substrate of Akt, FoxO1, was also significantly dephosphorylated after DNR treatment [(95.60 ± 1.20% (p = 0056)].

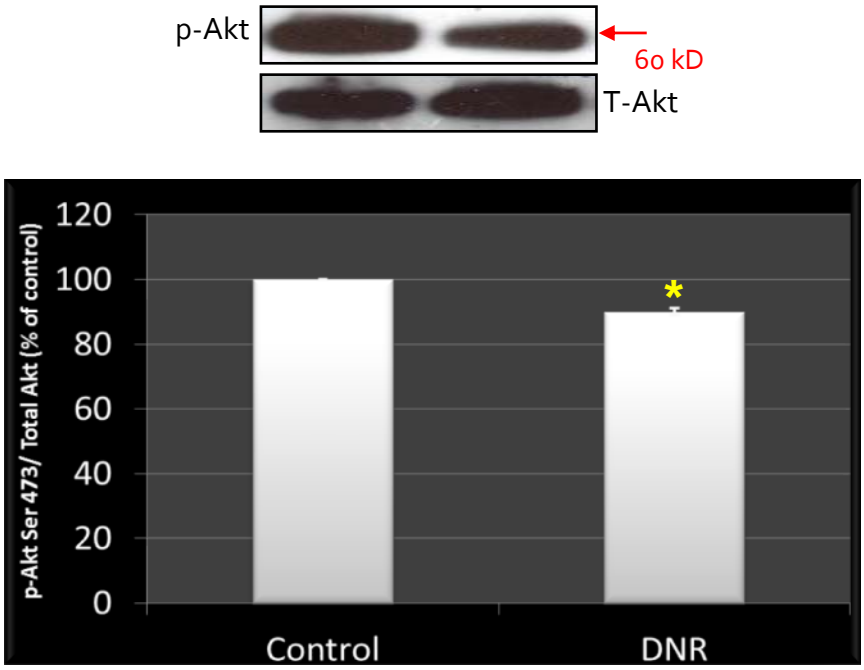

Figure 2.3.7: The effect of DNR treatment on the PI3-kinase/Akt signalling pathway**.** After the perfusion protocol, the heart tissue was freeze clamped and analyzed for phosphorylated and total Akt (Ser^{473}). All values are reported as a mean ± SEM. Statistical significance at $^{*}p = 0.001$, n = 7

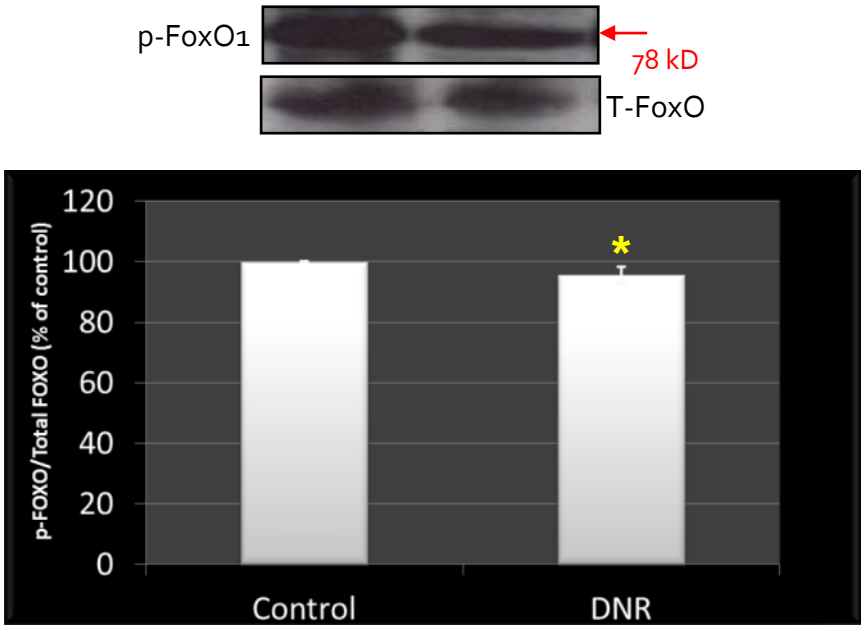

Figure 2.3.8: The effect of DNR treatment on the PI3-kinase/Akt signalling pathway**.** After the perfusion protocol, the heart tissue was freeze clamped and analyzed for phosphorylated and total FoxO1. All values are reported as a mean ± SEM. Statistical significance at $^{*}p = 0.0056$, n = 7

2.3.5: DNR activates the ubiquitin ligases, MuRF-1 and MAFbx (Figure 2.3.9 - 11)

DNR caused a significant increase (44%) in the induction of MuRF-1 [(137.90 ± 10.15 vs 77.22 ± 9.45 avg pixels (p = 0.001)], as well as a 40% increase in MAFbx [(172.90 ± 4.82 vs 103.90 ± 10.94 avg pixels (p < 0.0001)]. DNR treatment also caused a significant increase in the accumulation of ubiquitinated proteins [(153.20 ± 4.09 vs 141.40 ± 4.66 avg pixels (p = 0.049)].

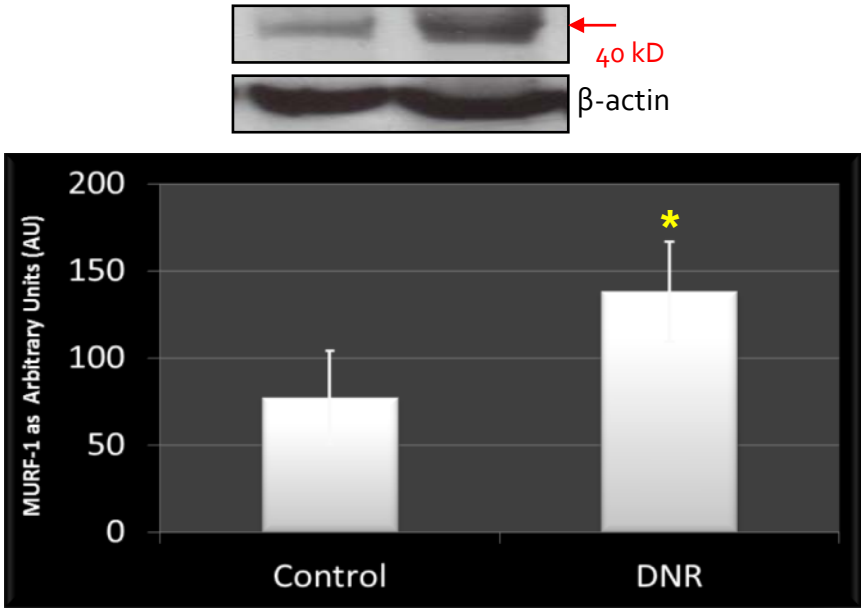

Figure 2.3.9: The effect of DNR treatment on the UPP in the heart. After the perfusion protocol, the heart tissue was freeze clamped and analyzed for the E_3 ligase MuRF-1. All values are reported as a mean ± SEM. Statistical significance at $^{*}p = 0.0011$, n = 7

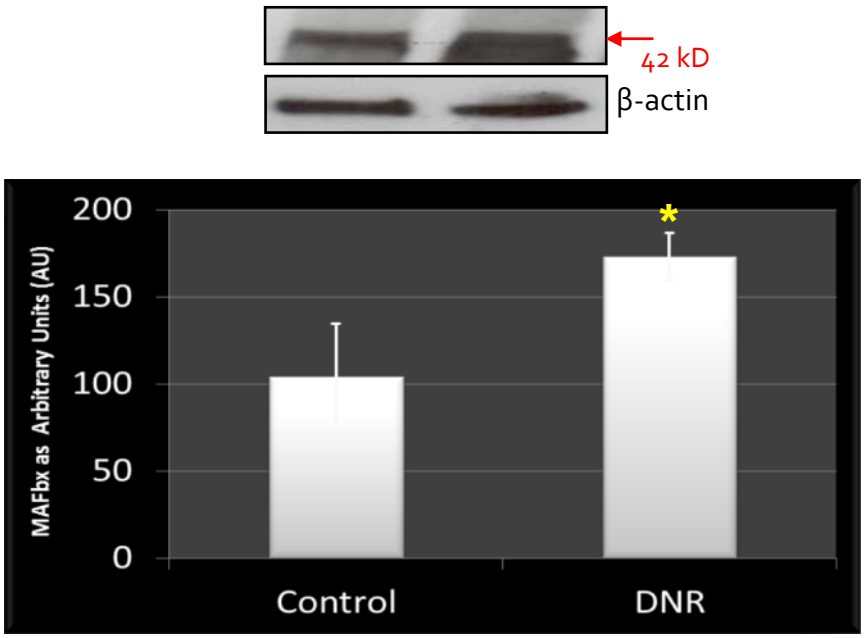

Figure 2.3.10: The effect of DNR treatment on the UPP in the heart. After the perfusion protocol, the heart tissue was freeze clamped and analyzed for the E_3 ligase MAFbx. All values are reported as a mean ± SEM. Statistical significance at $^{*}p = 0.0001$, n = 7

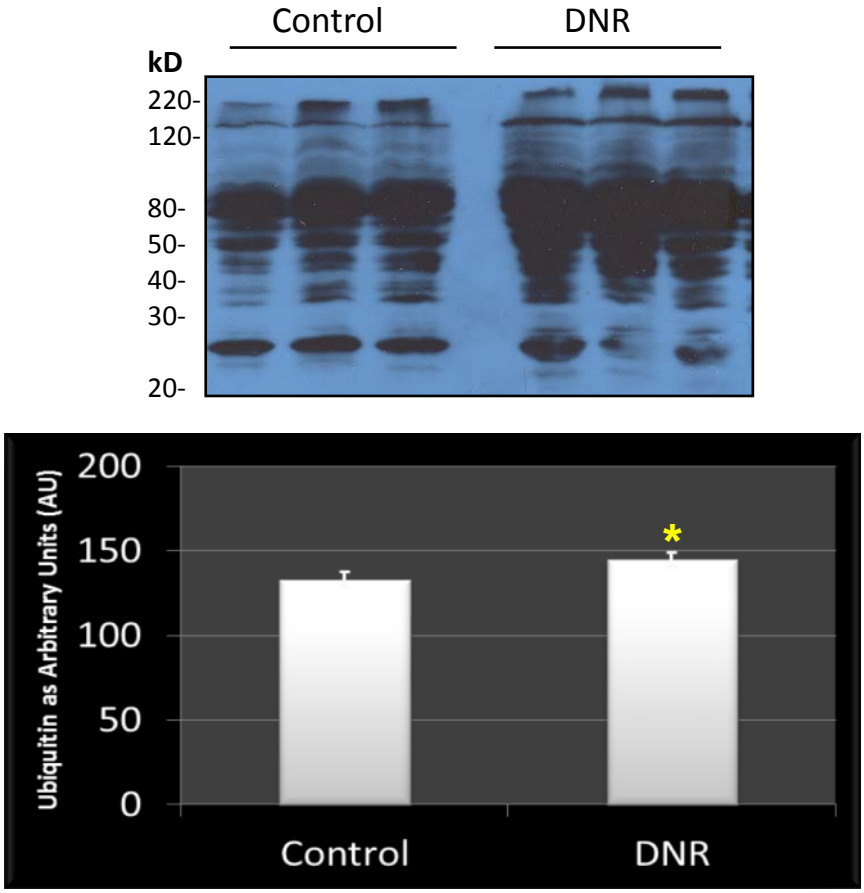

Figure 2.3.11: The effect of DNR treatment on the UPP in the heart. After the perfusion protocol, the heart tissue was freeze clamped and analyzed for Ubiquitin conjugates. All values are reported as a mean ± SEM. Statistical significance at $^{*}p = 0.049$, n = 7

2.4: Discussion

The data presented in this part of the study supports a model where acute DNR-induced cardiac dysfunction is associated with the upregulation of the UPP and autophagy. DNR-induced cardiac dysfunction is reflected in significant decreases in aortic pressure, aortic output and coronary flow rate (Wergelend *et al*, 2011). The attenuation of heart function induced by DNR was also associated with increased apoptosis in our model (Figures 2.3.1, 2.3.2, 2.3.3). It is well accepted that apoptosis of cardiomyocytes could be one of the fundamental mechanisms that initiates and/or aggravates heart failure after acute anthracycline therapy (Zhu *et al*, 2009). It has also been previously demonstrated that very low levels of myocyte apoptosis are sufficient to cause lethal, dilated cardiomyopathy (Wencker *et al*, 2003). In the present study, we used a clinically relevant dose of DNR, similar to that of Gausdal, *et al*, 2008.

Although the involvement of the UPP and the E_3 ligases, MuRF-1 and MAFbx, in the turnover of skeletal muscle proteins is clearly established (Acharryya *et al*, 2004; Costelli *et al*, 2001), no evidence exists for the potential role of these two E_3 ligases following acute DNR therapy. We have demonstrated for the first time that acute DNR therapy is associated with upregulation of MuRF-1 and MAFbx (Figures 2.3.9, 2.3.10) and concomitant accumulation of ubiquitin proteins (Figure 2.3.11). Although it was previously shown that a therapeutic dose of DXR activates the UPP by acting directly on both the ubiquitination apparatus and the proteasome, these researchers explore the mechanisms involved rather than investigating the role of these two ligases (Liu *et al*, 2008). Although the pathophysiological role of MuRF-1 and MAFbx has been largely confined to diseases that involve peripheral skeletal muscle wasting (Adams *et al*, 2008; Centner *et al*, 2001), only recent evidence exists for a possible role for these ligases in ventricular remodelling. Several investigators have demonstrated that the UPP is activated during cardiac hypertrophy (Fielitz *et al*, 2007; Fielits *et al*, 2007). Upregulation of MuRF-1 and MAFbx are also associated with increased protein degradation via the UPP during myocardial remodelling in chronic heart failure (Adams *et al*, 2007). Molecular targets ubiquitinylated by MAFbx

and MuRF-1 include myofibrillar proteins like troponin-1, titin, nebulin, myosin light chain 2, as well as metabolic enzymes involved in energy production (Kedar *et al*, 2004; Witt *et al*, 2005). MuRF-1-mediated degradation of troponin-1 appears to be very specific as demonstrated by Van der Velden *et al* (2004), who have shown that structural proteins such as myosin, actin or MyBP-C are not down-regulated. This study was however conducted on pigs with myocardial infarction (Van der Velden *et al*, 2004).

Although autophagy has long been depicted as a survival pathway which allow cells to maintain energy production under various stress and starvation conditions (Mizushima, 2005), it has also been shown to contribute to cell death in other contexts, suggesting autophagy could either be protective or detrimental, depending on the cellular environment (Matsui *et al*, 2007; Eisenberg-Lerner *et al*, 2009). Therefore, the functional significance of autophagy induction has to be determined individually within the specific context of each study. In our model, DNR-induced cardiotoxicity is associated with an up-regulation of the autophagy markers, beclin-1 and LC-3 and down-regulation of p62 (Figures 2.3.4, 2.3.5, 2.3.6). Beclin-1 is part of the PI (3)-kinase class III lipid kinase complex which plays a central role in the induction of autophagy (Levine *et al*, 2008). When autophagy is induced, microtubule-associated protein light-chain 3 (LC3), encoded by autophagy-related gene ATG8, is processed from LC3-I (18 kDa) to LC3-II (16 kDa) and incorporated into autophagic vacuoles (Tanida *et al*, 2004). p62 (also known as SQSTM1/sequestome 1) is an adaptor protein which targets protein aggregates and damaged organelles for autophagic degradation; in so functioning, p62 is selectively incorporated into autophagosomes through binding to LC3-II, degraded by autophagy and a good marker for efficient autophagic activity (Bjorkoy *et al*, 2005). Autophagy is often also associated with apoptosis, which make it even more difficult to determine the role of autophagy in cell death and cell survival. The interaction between autophagy and apoptosis has been characterized as follows: (1) autophagy and apoptosis can act as partners to co-ordinately induce cell death; (2) autophagy can act as an agonist to block cell death and (3) autophagy can act as an enabler of apoptosis (Eisenberg-Lerner *et al*, 2009). In accordance with our results, Kobayashi

and co-workers (2010) also demonstrated that DXR dramatically increased autophagy flux in cardiomyocytes which was associated with elevated apoptosis (Kobayashi *et al*, 2010). These researchers also demonstrated that inhibition of autophagy resulted in significant attenuation of cell death while the activation of autophagy with rapamycin exacerbated DXR-induced cardiomyocyte death, suggesting that autophagy is linked to apoptosis and act as partners to promote cell death.

The induction of the UPP and autophagy is tightly controlled by many positive and negative regulators (Eisenberg-Lerner *et al*, 2009; Klionsky *et al*, 2007). The PI3-Kinase/Akt signalling pathway, which is activated by insulin, growth factors and metabolic signals are well known to inhibit autophagy and the UPP. The activation of Akt results in the phosphorylation of both cytoplasmic and nuclear target proteins which include FoxO proteins, a subgroup of the Forkhead transcription factors and mTOR. Phosphorylation of FoxO proteins by Akt promotes FoxO sequestration by 14-3-3 proteins in the cytoplasm leading to inhibition of their transcriptional functions. On the other hand, dephosphorylation of FoxO leads to nuclear entry and transcription of ubiquitin ligases (Huang *et al*, 2007). In the present study, we observed a significant attenuation in Akt and Foxo1 phosphorylation (Figures 2.3.7, 2.3.8), which might be responsible for the increased induction of MuRF-1 and MAFbx in the DNR group. Furthermore, the attenuation of Akt phosphorylation by DNR might also be responsible for increased autophagy observed in our model through inhibition of mTOR, another downstream target of Akt. Our findings are indirectly supported by Zhu and co-workers (2009) who observed that DXR treatment decreased mTOR activity in non-transgenic mice (Zhu *et al*, 2009).

In summary, the results reported here suggests that acute DNR-induced cardiotoxicity, which is reflected in attenuation of cardiac function and increased apoptosis, is associated with an increased induction of the ubiquitin proteasome pathway and autophagy as well as blunted Akt/FoxO signalling. Although a molecular link between the UPP-activating effects of DNR and its cardiotoxicity

remains to be established, the present study is the first to demonstrate that DNR activates the E_3 ubiquitin ligases, MuRF-1 and MAFbx. This might implicate that the modulation of MuRF-1/MAFbx might represent a novel strategy to attenuate cardiotoxicity after DNR treatment.

References

1. Acharryya, S., Ladner, K.J., Nelsen, L.L., Damrauer, J., Reiser, P.J., Swoap, S. 2004. Cancer cachexia is regulated by selective targeting of skeletal muscle gene products. *Journal of Clinical Investigation*. 114: 370-378

2. Adams, V., Linke, A., Gielen, S., Erbs, S., Hambrecht, R., Schuler, G. 2008. Modulation of MURF-1 and MAFbx expression in the myocardium by physical exercise training. *European Journal of Cardiovascular Prevention and Rehabilitation.* 15: 293-299

3. Adams, V., Linke, A., Wisloff, U., Döring, C., Erbs, S., Kränkel, N., Witt, C.C., Labeit, S., Müller-Werdan, U., Schuler, G., Hambrecht, R. 2007. Myocardial expression of Murf-1 and MAFbx after induction of chronic heart failure: Effect on myocardial contractility. *Cardiovascular Research*. 73: 120-129

4. Bjorkoy, G., Lamark, T., Brech, A., Outzen, H., Perander, M., Overvatn, A., Stenmark, H., Johansen, T. 2005. p62/SQSTM1 forms protein aggregates degraded by autophagy and has a protective effect on huntingtin-induced cell death. *Journal of Cell Biology*. 171: 603-614

5. Bradford, M.M. 1976. A rapid and sensitive method for quantitation of microgram quantities of protein utilizing the principle of protein-dye binding. *Annals of Biochemistry*. 71: 248-254

6. Centner, T., Yano, J., Kimura, E., McElhinny, A.S., Pelin, K., Witt, C.C., Bang, M.L., Trombitas, K., Granzier, H., Gregorio, C.C., Sorimachi, H., Labeit, S. 2001. Indentification of muscle specific ring finger proteins as potential regulators of the titin kinase domain. *Journal of Molecular Biology*. 306: 717-726

7. Costelli, P., Tullio, R.D., Baccino, F.M., Melloni, E. 2001. Activation of Ca (2+)-dependent proteolysis in skeletal muscle and heart in cancer cachexia. *British Journal of Cancer*. 84: 946-950

8. Eisenberg-Lerner, A., Bialik, S., Simon, H.U., Kimchi, A. 2009. Life and death partners: apoptosis, autophagy and cross-talk between them. *Cell Death and Differentiation*. 16: 966-974

9. Fajardo, G., Zhao, M., Powers, J., Bernstein, D. 2006. Differential cardiotoxic/cardioprotective effects of □-adrenergic receptor subtypes in myocytes and fibroblasts in doxorubicin cardiomyopathy. *Journal of Molecular and Cellular Cardiolology*. 40: 375-383

10. Fielits, J., van Rooij, E., Spencer, J.A., Shelton, J.M., Latif, S., van der Nagel, R., Bezprozvannaya, S., de Windt, L., Richardson, J.A., Bassel-Duby, R., Olsen, E.N. 2007. Loss of muscle-spesific RING-finger 3 predisposes the heart to cardiac rupture after myocardial infarction. *Proceedings of the National Academy of Sciences of the USA*. 104: 4377-4382

11. Fielitz, J., Kim, M.S., Shelton, J.M., Latif, S., Spencer, J.A., Glass, D.J., Richardson, J.A., Bassel-Duby, R., Olsen, E.N. 2007. Myosin accumulation and striated muscle myopathy result from the loss of muscle RING finger 1 and 3. *Journal of Clinical Investigation*. 117: 2486-2495

12. Fisher, P.W., Salloum, F., Das, A., Hyder, H., Kukreja, R.C. 2005. Phosphodiesterase-5 inhibition with sildenafil attenuates cardiomycyte apoptosis and left ventricular dysfunction in a chronic model of doxorubicin cardiotoxicity. *American Heart Association.* 111: 1601-1610

13. Fuertes, G., Martin De Llano, J.J., Villarroya, A., Rivett, A.J., Knecht, E. 2003. Changes in the proteolytic activities of proteasomes and lysosomes in human fibroblasts produced by serum withdrawal, amino-acid deprivation and confluent conditions. *Biochemistry Journal*. 375: 75-86

14. Fuertes, G., Villaroya, A., Knecht, E. 2003. Role of proteasomes in the degradation of short-lived proteins in human fibroblasts under various growth conditions. *International Journal of Biochemistry & Cell Biology*. 35: 651-664

15. Fumoleau, P., Roche, H., Kerbrat, P., Bonneterre, J., Romestaing, P., Fargeot, P., Namer, M., Monnier, A., Montcuque, A. 2006. Long-term cardiac

toxicity after adjuvant epirubicin-based chemotherapy in early breast cancer: French Adjuvant study group results. *Annals of Oncology*. 17: 85-92

16. Gausdal, G., Gjerstsen, B.T., McCormack, E., Van Damme, E., Hovland, R., Krakstad, C., Bruserad, Ø., Gevaerd, K., Vandekerckhove, J., Døskeland, S.O. 2008. Abolition of stress-induced protein synthesis sensitizes leukaemia cells to anthracycline-induced death. *Blood*. 111: 2866-2877

17. Gomes, A.V., Zong, C., Ping, P. 2006. Protein degradation by the 26S proteasome system in the normal and stressed myocardium. *Antioxidant & Redox Signaling*. 8: 1677-1691

18. Gustafsson, A.B., Gottlieb, R.A. 2008. Recycle or die: the role of autophagy in cardioprotection. *Journal of Molecular and Cellular Cardiololgy*. 44: 654-661

19. Gustafsson, A.B., Gottlieb, R.A. 2009. Autophagy in ischemic heart disease. *Circulation Research*. 104: 150-158

20. Hochstrasser, M. 1995 Ubiquitin, proteasomes, and the regulation of intracellular protein degradation. *Current Opinion in Cell Biology*. 7: 215-223

21. Huang, H., Tindall, D.J. 2007. Dynamic FoxO transcription factors. *Jounal of Cell Science*. 120: 2479-2487

22. Kedar, V., McDonough, H., Arya, R., Li, H.H., Rockman, H.A., Patterson, C. 2004. Muscle-specific RING finger 1 is a bona fide ubiquitin ligase that degrades cardiac troponin 1. *Proceedings of the National Academy of Sciences of the USA.* 101: 18135-18140

23. Klionsky, D.J. 2007. Autophagy: from phenomenology to molecular understanding in less than a decade. *Nature Reviews Molecular Cell Biology*. 8: 931-937

24. Kobayashi, S., Volden, P., Timm, D., Mao, K., Xu, X., Liang, Q. 2010. Transcription factor GATA4 inhibits doxorubicin-induced autophagy and cardiomyocyte death. *Journal of Biological Chemistry*. 285(1): 793-804

25. Kumarapeli, R.K.A., Horak, K.M., Glasford, J.W., Li, J., Chen, Q., Liu, J., Zheng, H., Wang X. 2005. A novel transgenic mouse model reveals deregulation of the ubiquitin-proteasome system in the heart by doxorubicin. *FASEB Journal*. 19: 2051-2053

26. Levine, B., Klionsky, D.J. 2004. Development by self-digestion: molecular mechanisms and biological functions of autophagy. *Developmental Cell*. 6: 463-477

27. Levine, B., Sinha, S., Kroemer G. 2008. Bcl-2 family members: dual regulators of apoptosis and autphagy. *Autophagy*. 4: 600-606

28. Li, D. 2006. Selective degradation of the IkappaB kinase (IKK) by autophagy. *Cell Research*. 16: 855-856

29. Li, H.H., Kedar, V., Zhang, C., McDonough, H., Arya, R., Wang, D.Z., Patterson, C. 2004. Atrogin-1/muscle atrophy F-box inhibits calcineurin-dependent cardiac hyperthrophy by participating in an SCF ubiquitin ligase complex. *Journal of Clinical Investigation*. 114: 1058-1071

30. Li, H.H., Willis, M.S., Lockyer, P., Miller, N., McDonough, H., Glass, D.J., Patterson, C. 2007. Atrogin-1 inhibits Akt-dependent cardiac hyperthrophy in mice via ubiquitin-dependent coactivation of forkhead proteins. Journal of Clinical Investigation. 117: 3211-3233

31. Liu, J., Zheng, H., Tang, M., Ryu, Y.-C., Wang, X. 2008. A therapeutic dose of doxorubicin activated ubiquitin proteasome system-mediated proteolysis by acting on both the ubiquitination apparatus and proteasome. *American Journal of Physiology: Heart and Circulatory Physiology*. 295: H2541-H2550

32. Liu, X., Chua, C.C., Gao, J., Chen, Z., Landy, C.L., Hamdy, R., Chua, B.H. 2004. Pifithrin-α protects against doxorubicin-induced apoptosis and acute cardiotoxicity in mice. *American Journal of Physiology: Heart and Circulatory Physiology*. 286: H933-H939

33. Matsui, Y., Takagi, H., Qu, X., Abdellatif, M., Sakado, H., Asano, T., Levine, B., Sadoshima, J. 2007. Distinct roles of autophagy in the heart during

ischemia and reperfusion: roles of AMP-activated protein kinase mediating autophagy. *Circulation Research*. 100: 914-922

34. Minotti, G., Licata, S., Saponiero, A., Menna, P., Calafiore, A.M., Di Giammarco, G., Liberi, G., Animati, F., Cipollone, A., Manzini, S., Maggi, C.A. 2000. Anthracycline metabolism and toxicity in human myocardium: comparison between doxorubicin, epirubicin, and a novel disaccharide analogue with a reduced level of formation and reactivity of its secondary alcohol metabolite. *Chemical Research in Toxicology*. 13: 1336-1341

35. Mizushima, N. 2005. The pleiotropic role of autophagy: from protein metabolism to bactericide. *Cell Death and Differentiation*. 12: 1535-1541

36. Patterson, C., Ike, C., Willis, P.W., Stouffer, G.A., Willis, M.S. 2007. The bitter end: the ubiquitin-proteasome system and cardiac dysfunction. *Circulation*. 115: 1456-1463

37. Poizat, C., Sartorelli, V., Chung, G., Kloner, R.A., Kedes, L. 2000. Proteasome-mediated degradation of the coactivator p300 impairs cardiac transcription. *Molecular and Cellular Biology*. 20: 8643-8654

38. Tanida, I., Ueno, T., Kominami, E. 2004. Human light chain 3/MAP1LC3B is cleaved at its carboxyl-terminal Met121 to expose Gly 120 for lipidation and targeting to autophagosomal membranes. *Journal of Biological Chemistry*. 36: 2503-2518

39. Van der Velden, J., Merkus, D., Klarenbeek, B.R., James, A.T., Boontje, N.M., Dekkers, D.H.W. 2004. Alteration in myofilament function contributes to left ventricular dysfunction in pigs early after myocardial infarction. *Circulation Research*. 95: e85-95

40. Vergely, C., Delemasure, S., Cottin, Y., Rochette, L. 2007. Preventing the cardiotoxic effects of anthracyclines: from basic concepts to clinical data. *Heart Metabolism*. 35: 1-7

41. Von Hoff, D.D., Rozencweig, M., Layard, M., Slavik, M., Muggia, F.M. 1977. Daunomycin-induced cardiotoxicity in children and adults. A review of 100 cases. *American Journal of Medicine*. 62: 200-208

42. Wencker, D., Chandra, M., Nguyen, K., Miao, W., Garantziotis, S., Factor, S.M., Shirani, J., Armstrong, R.C., Kitsis, R.N. 2003. A mechanistic role for cardiomyocyte apoptosis in heart failure. *Journal of Clinical Investigation*. 111: 1497-1504

43. Wergeland, A., Bester, D.J., Sishi, B.J.N., Engelbrecht, A.-M., Jonassen, A.K., van Rooyen, J. 2011. Dietary Red Palm Oil protects the heart against the cytotoxic effects of anthracyclines. *Cell Biochemistry and Function*. 29: 356-364

44. Witt, S.H., Granzier, H., Witt, C.C., Labeit, S. 2005. Murf-1 and Murf-2 target a specific subset of myofibrillar proteins redundantly: towards understanding Murf-dependent ubiquitination. *Journal of Molecular Biology*. 350: 713-722

45. Yoshimori, T. 2004. Autophagy: a regulated bulk degradation process inside cells. *Biochemistry and Biophysical Research Communications*. 313: 453-458

46. Young, G.W., Wang, Y., Ping, P. 2008. Understanding proteasome assembly and regulation: importance to cardiovascular medicine. *Trends in Cardiovascular Medicine*. 18: 93-98

47. Zhu, W., Soonpa, M.H., Chen, H., Shen, W., Payne, R.M., Liechty, E.A., Caldwell, R.L., Shou, W., Field, L.J. 2009. Acute doxorubicin cardiotoxicity is associated with p53-induced inhibition of the mammalian target of rapamycin pathway. *Circulation*. 119: 99-106

Chapter 3

In vitro model

3.1: Introduction

The use of doxorubicin (DXR, Adriamycin), a broad spectrum chemotherapeutic agent in oncologic practice, has been limited by its dose-dependent cumulative cardiotoxicity, which leads to irreversible and often fatal drug-induced congestive heart failure (Petit, 2004; Minow *et al*, 1975; Minow *et al*, 1977; Cortez *et al*, 1975; Lefrak *et al*, 1975). The prevailing mechanism by which DXR induces cardiotoxicity is oxidative stress associated with mitochondrial dysfunction (Singal *et al*, 1987; Singal *et al*, 1995). Although the "oxidative stress hypothesis" is supported by the ability of several antioxidants to reduce DXR cardiotoxicity in animal models (Kang *et al*, 1996; Kumar *et al*, 2001; Sun *et al*, 2001), these results could not be reproduced in clinical trials (Ladas *et al*, 2004). It is therefore suggested that other mechanisms than oxidative stress might also contribute to DXR-induced heart failure.

Maintenance of the structure and function of the sarcomere is essential for the protection against cytotoxicity. Ensuring sufficient function of the sarcomere requires precise control of protein synthesis, processing and degradation. Two important protein degradation systems within the heart include autophagy and the ubiquitin-proteasome pathway (UPP). Autophagy is the major pathway for degradation and recycling of long-lived proteins and organelles that are sequestered in double-membrane vesicles known as autophagosomes (Gottlieb *et al*, 2009). After fusing with lysosomes to form autophagolysosomes, the inner membrane and its contents is degraded and recycled. The UPP on the other hand, functions by targeting specific proteins, labelling them with multiple ubiquitin molecules which then allow for recognition and subsequent degradation by the 26S proteasome (Passmore *et al*,

2004; Willis *et al*, 2010). Together, these pathways play an essential role in the maintenance of sarcomeric function in the face of DXR-induced cytotoxic stimuli.

Autophagy functions as a cytoplasmic quality control mechanism to remove protein aggregates and damaged organelles. In this respect, autophagy has been shown to play a vital role in cardiac homeostasis as the inactivation of an autophagy associated gene, ATG5, resulted in myocardial dysfunction (Nakai *et al*, 2007). Autophagy induction during ischemia has also been shown to be cardioprotective (Loos *et al*, 2011; Yan *et al*, 2005; Matsui *et al*, 2007). However, increased autophagic activity can also be detrimental to the heart under certain conditions (Levine *et al*, 2005) such as pressure overload (Rothermel *et al*, 2008).

A number of cellular stresses such as nutrient deprivation, alterations in glycosylation status, and disturbances in calcium flux lead to the accumulation of misfolded and unfolded proteins in the endoplasmic reticulum (ER) lumen which ultimately results in the induction of ER stress (Austin, 2009; Rasheva *et al*, 2009). ER stress triggers a signalling cascade which couples the ER protein folding load with the ER folding capacity and is referred to as the unfolded protein response (UPR). Under normal circumstances, the UPR is a cytoprotective response, however excessive UPR results in apoptosis.

Rapamycin is a very versatile drug with well-documented effects in reducing growth in numerous cancers (Wu *et al*, 2007; Namba *et al*, 2006). It is also being utilized as undercoats for drug-eluting stents to prevent the progression of restenosis after coronary angioplasty (Hausleiter *et al*, 2004) and has been shown to be a potent inhibitor of left ventricular (LV) hypertrophy *in vivo* (McMullen *et al*, 2004; Shioi *et al*, 2003). Furthermore, as a potent mTOR (mammalian target of rapamycin) inhibitor, rapamycin has also been widely used to activate autophagy. Although rapamycin treatment is known to be beneficial in many contexts, its potential cardioprotective effects in DXR-induced cardiotoxicity has not been investigated.

Therefore, we hypothesized that elevated autophagy through rapamycin treatment, alleviates AC-induced toxicity and attenuates cardiomyocyte death. We aimed to (i) characterize the effect of DXR on H_9C_2 cells, (ii) to determine whether the induction/inhibition of autophagy in combination with DXR alleviates cytotoxicity and (iii) to investigate the influence of elevated/reduced autophagy in combination with DXR on apoptosis, ROS production, mitochondrial function, the ubiquitin-proteasome pathway (UPP) and ER stress.

3.2: Materials and Methods

3.2.1: Cell Culture Preparation

H_9C_2 rat heart myoblasts (European Collection of Cell Cultures – ECACC), were seeded at 12 000/cm^2, and cultured in Dulbecco's modified Eagle's medium (DMEM) supplemented with 10% heat-inactivated fetal bovine serum (FBS), 4% L-glutamine and 1% penicillin/streptomycin in a humidified atmosphere, 37 °C, in the presence of 5% CO_2. In brief, cells were washed with 0.01 M sterile phosphate-buffered saline, (PBS), trypsinized (0.25% Trypsin – EDTA), centrifuged for 3 min at 6000 x g and seeded as follows: $1x10^6$ myoblasts per 75 cm^2 tissue culture flask, $3x10^5$ myoblasts per 25 cm^2 tissue culture flask, $1x10^5$ myoblasts per culture dish in six-well plates and $2x10^4$ myoblasts per 8-chamber slide. Growth medium was replenished every 48 hrs.

3.2.2: Passaging Protocol

Cells were passaged at 70-80% confluency. Growth medium was discarded and cells rinsed with warm (37°C) sterile PBS. Warm 0.25% trypsin-EDTA (3/5 ml) was added and cells were incubated until cells detached from the surface (2-3 min). Culture medium (double the volume of trypsin used; 6/10 ml) was added to the cell suspension, which was then transferred to a 15/50 ml falcon tube, centrifuged for 3 min at 6000 x g. Medium was decanted and cells resuspended in fresh medium. Aliquots for new flasks were made as required according to the desired seeding density.

3.2.3: Treatment of H_9C_2 cells with decreasing amino acid concentrations

In order to assess the influence of amino acids on autophagic activity, H_9C_2 cells were subjected for 24 and 48 hrs to decreasing concentrations of amino acids (see table below) using two different types of growth media: normal growth medium containing the necessary growth factors and antibiotics and growth medium containing the necessary growth factors and antibiotics, excluding all amino acids.

Normal Growth Medium	Growth Medium without amino acids
100%	0%
90%	10%
70%	30%
50%	50%
30%	70%
10%	90%
0%	100%

Table 2: Amino acid concentrations. Normal growth media were combined with growth media without amino acids to achieve different amino acid concentrations.

3.2.4: Treatment of cells with Rapamycin or Bafilomycin

Cells were treated with either 50 nM rapamycin (Sigma, R8781) or 10 nM bafilomycin A1 (Sigma, 1793) for 24 and 6 hrs respectively (dose response data in appendix B and C).

3.2.5: Silencing of mammalian target of rapamycin (mTOR)

In order to mimic the effects of rapamycin, mTOR was silenced using siRNA. H_9C_2 cells were grown and maintained as previously described in 24-well plates. After reaching a confluency of 50%, cells were transfected with siRNA-mTOR (Cell

Signalling, 6381) using the FuGENE transfection reagent (Roche, 11814443001) following the manufacturer's instructions.

3.2.6: Treatment of cells with DXR

At 70 – 80% confluency, H_9C_2 cells were treated with different concentrations of DXR (Sigma, D1515) (1 – 10 µM) at various time points (1, 6, 12, 24 and 48 hrs) in order to establish an appropriate dose and time point to be employed.

3.3: Assessment of Cell Viability

3.3.1: Determination of H_9C_2 myoblast viability (MTT Assay)

H_9C_2 myoblast viability was analysed at all above mentioned points post treatment with the MTT [3-(4,5-dimethylthylyhiazol-2-yl)-2,5-Diphenyltertrazolium Bromide] assay described by Gomez and colleagues (1997). This assay is based upon the principal of reducing MTT into blue formazan pigments by viable mitochondria in healthy cells. At the end of the experimental procedure, medium was removed from the cells, 1.5 ml PBS and 500 µl MTT (0.01 g/ml) solution was carefully added to each 6-well and incubated at 37ºC for 2 hrs at an atmosphere of 5% CO_2. This time period was found to be optimal for the development of colour that is associated with formazan product formation. If there were cells that had detached, the content was transferred to eppendorf tubes and centrifuged for 2 min at 1000 rpm. The supernant was decanted; 2 ml HCl (hydrogen chloride)-isopropanol/Triton (1% HCl in isopropanol; 0.1% Triton X-100; 50:1) solution was added to each pellet and resuspended. Resuspended cells were then added back to the original plates where some cells remained attached. Next, 2 ml HCl-isopropanol/Triton solution was added to each well, which was then covered with foil and placed on a belly dancer for 5 min. This solution causes lysis of cell membranes and the release of formazan pigments. The cell suspension was transferred to 2 ml eppendorf tubes and centrifuged for 2 min at 1400 rpm. The optical density (OD) was determined spectrophotometrically (Cecil-CE 2021-2000 Series, Lasec) at a wavelength of 540 nm, using HCl-isopropanol/Triton solution as the blank. The values obtained are expressed as percentages of the control values.

3.4: Morphological Analysis of Cell Death

3.4.1: Nuclear condensation

Nuclear condensation (pyknosis) as well as fragmentation (karyorrhexis) have previously been demonstrated as morphological characteristics for apoptosis (Kajustra *et al*, 1996). Using the DNA intercalating dye, Hoechst 33342 (in a 1:200 dilution in PBS) (Sigma, B2261), differentiation between normal nuclear morphology and apoptotic morphology is possible. After subjecting H_9C_2 myoblasts to the various treatment regimens, Hoechst was added onto the cells at a final concentration of 50 µg/ml, and incubated for 10 min. Using the Olympus Cell^R Soft Imaging Systems, images of random fields of view were acquired immediately thereafter. Cells were classified according to their nuclear signal: (i) normal nuclei with blue chromatin, showing organization with a distribution of heterochromatin and euchromatin and (ii) cells displaying bright blue and substantially condensed or fragmented nuclei indicative of apoptosis. For each experimental condition, images of four random fields of view were acquired. Data are represented as the number of apoptotic cells/total number of cells x 100 as demonstrated by Lacerda *et al* (2006) and Engelbrecht *et al* (2007).

3.4.2: Propidium Iodide (PI) exclusion

The loss of membrane integrity has previously been described as an indicator for necrosis (Festjens *et al*., 2006). The DNA intercalating dye, Propidium Iodide (PI), is not able to penetrate the membrane of viable cells and is thus omitted from binding to the cell's nucleus. If the membrane integrity of the cell is lost, PI penetrates the cell membrane and intercalates with the DNA with specificity for double-stranded nucleic acids, absorbing in blue-green (493 nm), fluorescing red (630 nm). The PI exclusion technique therefore allows for distinct differentiation between viable cells (PI-negative), and cells which have lost their membrane integrity (PI-positive). Following the experimental protocol, Hoechst and PI (in a 1:200 dilution with PBS) (Sigma, P4170) were added onto the cells at a final concentration of 50 µg/ml and 1 µg/ml respectively. Cells were incubated for 10 min and images were acquired immediately thereafter. Using the Olympus Cell^R Soft Imaging Systems, four

random fields of view were acquired for each experimental condition. Using a Xenon-Arc burner (Olympus Biosystems GMBH) as light source, images were acquired with the 360 nm and 572 nm excitation filter; emission was collected using a UBG triple band pass emission filter cube (Chroma). Necrotic cells showed bright red nuclei. The percentage (%) PI-positive cells was calculated as number of PI-positive cells/total cells x 100.

3.4.3: Trypan Blue exclusion

Following the various treatment regimens, H_9C_2 myoblasts were washed with warm PBS; trypsinized and neutralized using growth medium. Cell solutions from each well were centrifuged, the supernant decanted and the pellet resuspended in 500 µl PBS and 500 µl 0.4% trypan blue solution and incubated for 2 min at room temperature. This technique analyses the incorporation of trypan blue into cells with a damaged membrane (Kitakaze *et al*, 1997). The number of blue cells/total cells was counted. To avoid false positives, the count was performed within 5 min after exposure of cells to the trypan blue stain. Results are expressed as the percentage (%) of viable cells utilizing the Countess^{TM} Automated cell counter (Invitrogen).

3.4.4: Caspase-Glo Assay

This assay (Promega, G8091) is a luminescent cell based technique that measures caspase-3 and -7 activities. Following caspase cleavage, a substrate for luciferase (amino-luceferin) is released, resulting in the luciferase reaction and the production of light. H_9C_2 cells were grown and treated as previously stated in white-walled 96-well luminometer plates after which 100 µl of caspase-3/7 reagent was added to each well and incubated for 30 min at room temperature. This was followed by measuring the luminescence using a luminometer (GLOMAX 96 microplate Luminometer, Promega).

3.5: Flow Cytometry

3.5.1: Acidic vacuole accumulation

In order to assess autophagic activity, flow cytometry utilizing lysotracker was employed. Lysotracker (Molecular Probes, L7528) is a fluorescent probe that accumulates within intracellular acidic compartments such as lysosomes. It is thus being used as an indicator for the relative amount of acidic compartments. As autophagy is characterized by the development of acidic vesicular organelles (AVOs), lysotracker has been employed to detect and quantify AVOs (Azad *et al*., 2008). H_9C_2 cells were grown and treated as previously described in 25 cm^2 tissue culture flasks. Growth medium was discarded and cells rinsed with warm (37°C), sterile PBS. Warm 0.25% trypsin-EDTA (3 ml) was then added and cells were incubated until cells detached from the surface (2-3 min). Culture medium (double the volume of trypsin used; 6 ml) was added to the cell suspension, which was then transferred to a 15 ml falcon tube and centrifuged for 3 min at 6000 x g. Medium was decanted and cells resuspended in 500 µl warm PBS. Lysotracker was directly added onto the unfixed cells at a final concentration of 50 nM, incubated for 10 min, and analysed on the flow cytometer (BD FACSAria I) immediately thereafter. A minimum of 10 000 events (cells) were collected, and using the 488 nm laser and 590 nm (Abs. = 577 nm) emission filter, fluorescence was measured. Fluorescence intensity signal was measured using the geometric mean on the intensity histogram. It should be noted that due to the autofluorescence of DXR in the red channel, which is similar to the emission of the fluorescent probe used for lysosomal production, the values presented in the results have been subtracted with the DXR-induced autofluorescence signal.

3.5.2: Generic and mitochondrial ROS production

Generic and mitochondrial ROS generation was evaluated with the aid of 6-carboxy-2'7'-dichlorodihydrofluoresce in diacetate, diacetoxymethyl ester (DCF, Molecular Probes, D399) and MitoSOX (Molecular probes, M7514) respectively. H_9C_2 cells were grown and treated as previously described in 25 cm^2 tissue culture flasks. Growth medium was discarded and cells rinsed with warm (37°C) sterile PBS. Warm

0.25% trypsin-EDTA (3 ml) was added and cells were incubated until cells detached from the surface (2-3 min). Culture medium (double the volume of trypsin used; 6 ml) was added to the cell suspension, which was then transferred to a 15 ml falcon tube and centrifuged for 3 min at 6000 x g. Medium was decanted and cells resuspended in 500 µl warm PBS. DCF and MitoSOX were directly added onto the unfixed cells at a final concentration of 50 µmol/L and 5 µM respectively and incubated for 15 min, and analysed on the flow cytometer (BD FACSAria I) immediately thereafter. A minimum of 10 000 events (cells) were collected, and using the 488 nm laser and 510/580 nm emission filters, fluorescence intensity signal was measured. In addition, a concentration of 100 µmol/L H_2O_2 was used as a positive control. Fluorescence intensity signal was measured using the geometric mean on the intensity histogram. It should be noted that due to the autofluorescence of DXR in the red channel, which is similar to the emission of the fluorescent probe used for mitochondrial ROS production, the values presented in the results have been subtracted with the DXR-induced autofluorescence signal.

3.5.3: Assessment of Mitochondrial Load

In order to determine the mitochondrial load, the cell-permeant, Mitotracker (Molecular Probes, M7514) was utilized. This fluorescent probe contains a mildly thiol-reactive chloromethyl moiety specific for mitochondrial labelling. H_9C_2 cells were grown and treated as previously described in 25 cm^2 tissue culture flasks. Growth medium was discarded and cells rinsed with warm (37°C) sterile PBS. Warm 0.25% trypsin-EDTA (3 ml) was added and cells were incubated until cells detached from the surface (2-3 min). Culture medium (double the volume of trypsin used; 6 ml) was added to the cell suspension, which was then transferred to a 15 ml falcon tube and centrifuged for 3 min at 6000 x g. Medium was decanted and cells resuspended in 500 µl warm PBS. Mitotracker was directly added onto the unfixed cells at a final concentration of 25 nM, incubated for 15 min, and analysed on the flow cytometer (BD FACSAria I) immediately thereafter. A minimum of 10 000 events (cells) were collected, and using the 490/516 nm excitation/emission filters, fluorescence intensity signal was measured using the geometric mean on the intensity histogram.

3.5.4: Assessment of Mitochondrial function

In order to determine mitochondrial function, the ratiometric 5, 5', 6, 6',-tetrachloro-1, 1', 3, 3',-tetraethylbenzimidazolylcarbocyanine (JC-1) (Invitrogen, T3168) was utilized. This fluorescent probe is a cationic dye specific for mitochondrial labelling. In live cells, the dye exists either as a monomer and yields a green fluorescence at depolarized membrane potentials, or the dye forms red/orange fluorescent J-aggregates at hyperpolarized membrane potentials, that exhibit a broad excitation spectrum and an emission maximum at 590 nm. The red/green ratio can thus be utilized as a sensitive marker for mitochondrial membrane potential. H_9C_2 cells were grown and treated as previously described in 25 cm^2 tissue culture flasks. Growth medium was discarded and cells rinsed with warm (37°C) sterile PBS. Warm 0.25% trypsin-EDTA (3 ml) was added and cells were incubated until cells detached from the surface (2-3 min). Culture medium (double the volume of trypsin used; 6 ml) was added to the cell suspension, which was then transferred to a 15 ml falcon tube and centrifuged for 3 min at 6000 x g. Medium was decanted and cells resuspended in 500 µl warm PBS. JC-1 was directly added onto the unfixed cells at a final concentration of 5 µM, incubated for 20 min, and analysed on the flow cytometer (BD FACSAria I) immediately thereafter. A minimum of 10 000 events (cells) were collected using the 488 nm laser and emission was collected between 515-545 nm and 575-625 nm. Fluorescence intensity signal was measured using the geometric mean on the intensity histogram.

3.5.5: Assessment of Endoplasmic Reticulum (ER) Load

In order to determine ER load, the cell-permeant ER-tracker (Molecular Probes, E12353) was utilized. This fluorescent probe is highly selective for ER labelling. H_9C_2 cells were grown and treated as previously described in 25 cm^2 tissue culture flasks. Growth medium was discarded and cells rinsed with warm (37°C) sterile PBS. Warm 0.25% trypsin-EDTA (3 ml) was added and cells were incubated until cells detached from the surface (2-3 min). Culture medium (double the volume of trypsin used; 6 ml) was added to the cell suspension, which was then transferred to a 15 ml falcon tube and centrifuged for 3 min at 6000 x g. Medium was decanted and cells resuspended in 500 µl warm PBS. ER-tracker was directly added onto the unfixed cells, using a

final concentration of 100 nM, incubated for 10 min, and analysed on the flow cytometer (BD FACSAria I) immediately thereafter. A minimum of 10 000 events (cells) were collected. Utilizing the 407 nm laser and the 430-640 nm emission filters, fluorescence intensity signal was measured using the geometric mean on the intensity histogram.

3.6: Fluorescence Microscopy

Image acquisition was performed on an Olympus Cell^R system attached to an IX 81 inverted fluorescence microscope equipped with a F-view-II cooled CCD camera (Soft Imaging Systems). Using a Xenon-Arc burner (Olympus Biosystems GMBH) as a light source, images were acquired using the 360, 497 or 572 nm excitation filters. Emission was collected using a UBG triple-bandpass emission filter cube (Chroma). Images were acquired through z-stacks where appropriate, using an Olympus Plan Apo N60x/1.4 oil objective, or a 10x objective. The top and bottom focus position parameter were selected, indicating the upper and lower dimensions of the sample to be acquired with a step width of 0.26 µm between the single image frames. Images were processed and background-subtracted using the Cell^R software, and presented in a maximum intensity projection. In setting up a defined experiment in the Experiment Manager facet of the Cell^R software, image acquisition parameters such as exposure time, illumination settings and emission filter cube selection were kept constant for all groups and ensured appropriate selection of parameters. The DAPI 360 nm excitation wave length was used for setting the focal plane, avoiding unnecessary photo-bleaching.

3.6.1: Live Cell Imaging

In order to establish a dynamic approach of monitoring various changes within the cell and its organelles after treatment, live cell imaging was performed. For that purpose, H_9C_2 cells were maintained at 37 °C in growth medium and seeded in 8-chamber dishes with a density of $2x10^4$ cells. After reaching confluency, cells were

treated as previously described and stained accordingly. For the staining procedure, the cell death (Sections 3.4.1 - 5) and flow cytometry (Sections 3.5.1 - 5) protocol including the different fluorescent probes and concentrations were used. Image acquisition was performed on an Olympus Cell^R system attached to an IX 81 inverted fluorescence microscope equipped with a F-view-II cooled CCD camera (Soft Imaging Systems). Using a Xenon-Arc burner (Olympus Biosystems GMBH) as light source, images were acquired.

3.6.2: Nuclear condensation

Hoechst 33342 (50 µg/ml)

- Pyknotic cells are indicated with arrows

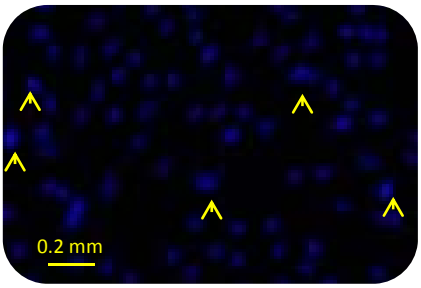

Representative image
Mag. → 10X
Scale → 0.2 mm

3.6.3: PI Exclusion

PI (1 µg/ml)

- PI positive cells are indicated with arrows

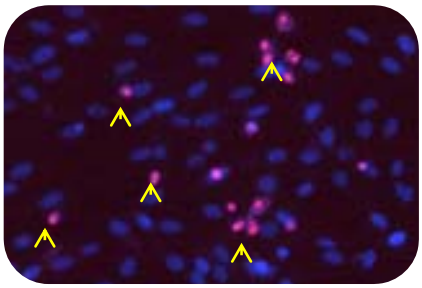

Representative image
Mag. → 10X
Scale → 0.2 mm

3.6.4: Acidic Vacuole accumulation

Lysotracker (50 nM)

- Accumulation of acidic vacuoles indicated in red

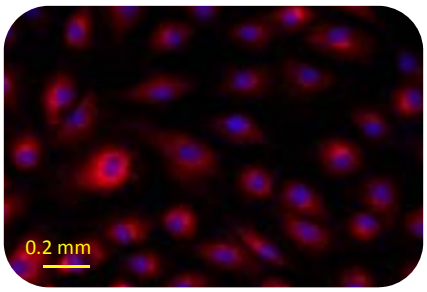

Representative image
Mag. → 10X
Scale → 0.2 mm

3.6.5: ROS assessment

DCF and MitoSOX (50 µmol/L and 5 µM)

- Generic ROS indicated in green and mitochondrial ROS in red

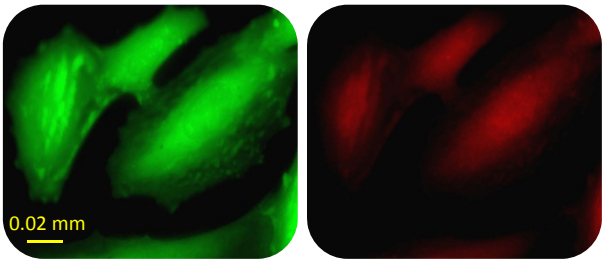

Representative image
Mag. → 60X
Scale → 0.02 mm

3.6.6: Mitochondrial Morphology

MitoTracker (25 nM)

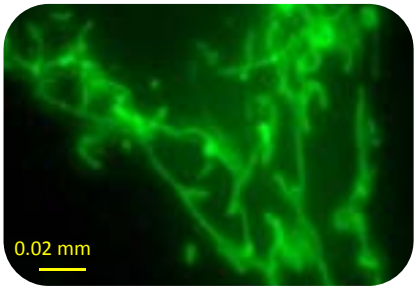

Representative image
Mag. → 60X
Scale → 0.02 mm

3.6.7: Mitochondrial Function

JC-1 (5 µM)

- Depolarized membrane potentials indicated in green and hyperpolarized membrane potentials indicated in red/orange

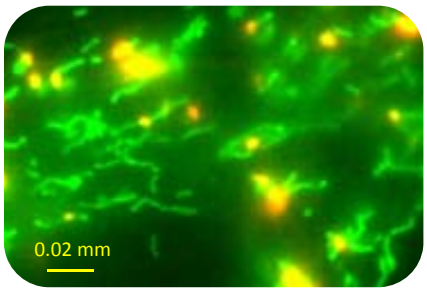

Representative image
Mag. → 60X
Scale → 0.02 mm

3.6.8: DXR Localization

DXR (3 µM)

- DXR indicated in red

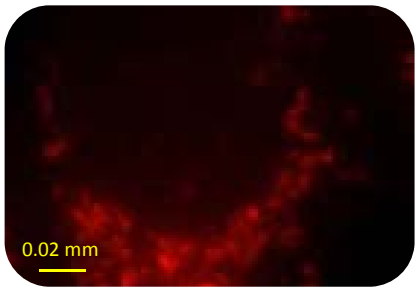

Representative image
Mag. → 60X
Scale → 0.02 mm

3.6.9: ER Load

ER-tracker (100 nM)

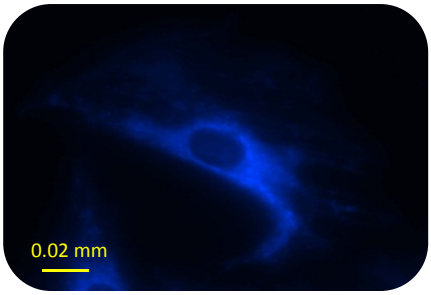

Representative image
Mag. → 60X
Scale → 0.02 mm

3.7: Proteasome Activity Analysis

3.7.1: Chymotrypsin-like Cell-based Assay

To investigate the activity of the proteasome after treatment, the Proteasome-Glo chymotrypsin-like cell-based assay (Promega, G8661) was employed. This assay is a luminescent cell based technique that measures the chymotrypsin-like protease activity associated with the proteasome complex in cultured cells. H_9C_2 cells were grown and treated as previously described in white-walled 96-well luminometer plates where after 100 µl of the Proteasome-Glo cell-based reagent was added to each well. The contents of the wells were mixed at 700 rpm using a plate shaker for 2 min and incubated for 10 min at room temperature. This was followed by measuring the luminescence signal using a luminometer (GLOMAX 96 microplate Luminometer, Promega).

3.8: Western Blotting Analysis

3.8.1: Protein extraction

H_9C_2 myoblasts were washed thoroughly with PBS where after 250 µl ice cold RIPA (Radio immunoprecipitation assay)/lysis buffer containing (in mM): tri-(hydroxylmethyl)-aminomethane (TRIS)-HCl 50, NP-40 1%, Na-Deoxycholate 0.25%, EDTA (Ethylenediaminetetraacetic acid) 1, sodium fluoride (NaF) 1, soybean trypsin inhibitor (SBTI) 4 µg/ml, phenylmethyl sulphonyl fluoride (PMSF) 1, Benzamidine 1, leupeptin 1µg/ml and Triton X-100 was added to each well for 5 min. The cells were scraped free from the wells and transferred into eppendorf tubes

maintained on ice. Cells were then sonicated (Ultrasonic Liquid Processor, Qsonica) for approximately 15 sec in order to allow the release of proteins. Centrifugation commenced (8000 rpm at 4ºC for 10 min) to remove nuclei and cellular debris.

3.8.2: Protein quantification using the Bradford technique

The rapid and sensitive Bradford method for the quantitation of microgram quantities of protein utilizing the principle of protein-dye binding was employed (Bradford, 1976). This technique involves the binding of Coomassie Brilliant Blue G-250 to protein which causes a shift in the absorption maximum of the reagent from 465 nm to 595 nm. The increase in absorption at 595 nm is monitored spectrophotometrically (Cecil – CE 2021-2000 Series, Lasec). Cell lysates were thawed while kept on ice and sonicated for 10 sec at power level 3 (Vir Sonic 300, Virtis Gardiner) followed by centrifugation for 10 min at 4 °C at 5000 x g (ALC-PK121R) in order to pellet cell debris and to expose the whole cellular protein fraction. For the establishment of a standard curve, a protein dilution series was set up, pipetting 2 µg, 4 µg, 8 µg, 12 µg, 16 µg and 20 µg bovine serum albumin dissolved in PBS (BSA, 200 µg/ml) and 900 µl Bradford reagent into test tubes, adjusted to 1000 µl with deionized water. Sample protein concentrations were determined through pipetting 5 µl of the sample supernatant with 900 µl Bradford reagent and adjusted to 1000 µl with 95 µl deionized water. Samples were vortexed, incubated for 5 min at room temperature where after the absorbance was measured at a wavelength of 595 nm against a reagent blank. The weight of protein in µg/ml was plotted against the absorbance and the protein concentration was determined.

3.8.3: Sodium-dodecyl-sulfate-polyacrylamide gel electrophoresis (SDS-PAGE)

Laemmli sample buffer was prepared, using (in M): 33.3 ml TRIS 0.5, pH 6.8, 10% SDS, 2.5 ml glycerol, 0.2 ml 0.5% bromophenol blue in deionized water. A volume of 150 µl mercaptoethanol was added to 850 µl sample buffer. Cell lysates were boiled for 5 min and shortly spun in a microcentrifuge. Total protein (20 µg) was separated by 8%, 10% or 15% sodium-dodecyl sulfatepolyacrylamide- gel-electrophoresis (SDS-PAGE) and a 4% stacking gel.

3.8.4: Transfer, Incubation and Visualization

After completion of protein separation, proteins were transferred to PVDF membranes (ImmobilonTM P, Millipore). Membranes were routinely stained with Ponceau Red for visualisation of proteins. Non-specific binding sites were blocked with 5% fat-free milk in TRIS-buffered saline-Tween (TBS-T) and membranes were incubated with the primary antibodies that recognise cleaved-caspase-3, cleaved-PARP, Beclin-1, p62/SQSTM1, LC-3, phospho-specific and total FoxO, MAFbx, MuRF-1, phospho-specific and total mTOR, ubiquitin and β-Actin. Membranes were subsequently washed with large volumes of TBS-T (3 x 5 min) and the immobilized antibody was conjugated with a diluted horseradish peroxidase-labelled secondary antibody (Amersham LIFE SCIENCE). After thorough washing with TBS-T, membranes were incubated with ECL^{TM} detection reagents and quickly exposed to an autoradiography film (Hyperfilm ECL, RPN 2103) to allow the detection of light emission through a non-radioactive method (ECL^{TM} Western blotting). Films were densitometrically analysed (UN-SCAN-IT, Silkscience version 5.1) and phosphorylated protein values were corrected for minor differences in protein loading, if required.

3.9: Statistical Analysis

All data are presented as mean ± SEM. Comparisons between the groups were performed by the one-way analysis of variance (ANOVA) followed by Bonferroni's post hoc test conducted with the statistical program GraphPad Prism, version 5.0 (GraphPad Inc.). A value of $p \leq 0.05$ was considered statistically significant. All experiments were repeated three times for accuracy.

3.10: Results

3.10.1: DXR concentrations (Figure 3.10.1)

In order to determine an appropriate concentration and time point for treatment, a concentration- and time-response curve was established. The incubation of cells with 3 µM of DXR for a duration of 24 hrs was chosen as most appropriate as viability decreased significantly when compared to the control.

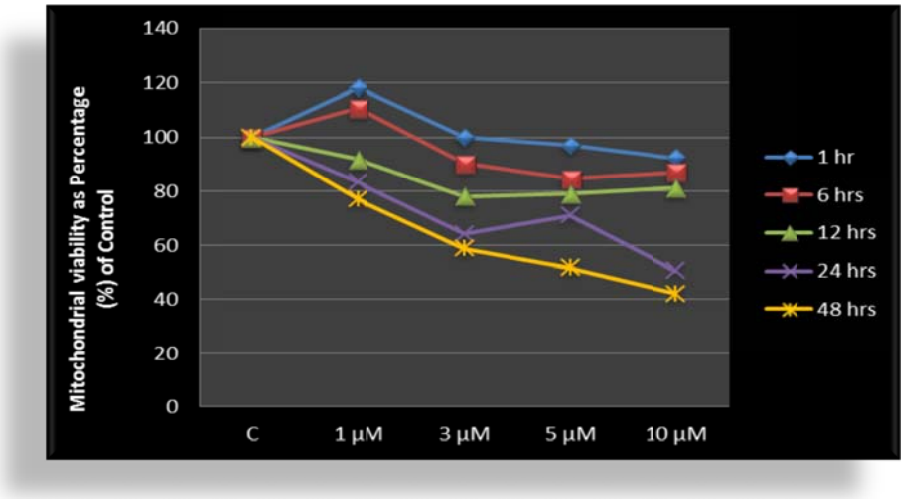

Figure 3.10.1: The effect of various DXR concentrations on mitochondrial viability. H_9C_2 myoblasts were incubated with increasing concentrations of DXR for 1, 6, 12, 24 and 48 hrs.

3.10.2: Morphological Assessment of H_9C_2 cells (Figure 3.10.2)

Evaluation of the morphology of H_9C_2 cells after treatment with DXR showed very distinct and enlarged nuclei when compared to the control. In fact, all groups treated with DXR displayed enlarged nuclei (indicated with arrows).

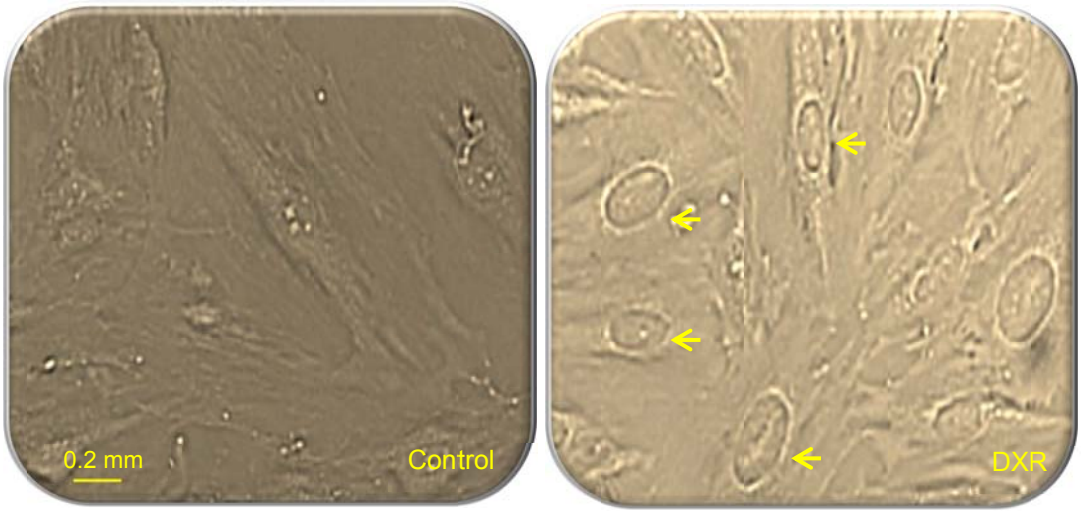

Figure 3.10.2: The effect of DXR treatment on cell morphology of H_9C_2 cells. H_9C_2 myoblasts were incubated with 3 µM DXR for 24 hrs. Magnification = 10X. Scale bar = 0.2 mm.

3.10.3: Assessment of metabolically viable cells (Figure 3.10.3)

Analysis of the MTT assay results showed that the upregulation of autophagy using the 10% amino acid concentration and rapamycin was not detrimental to the cells when compared to the control (see Appendix A, Fig 5.1.1 for preliminary studies). The inhibition of autophagy with bafilomycin A1, on the other hand, significantly reduced mitochondrial viability [76.74 ± 2.39% ($p < 0.05$)] when compared to the control (100%). Significance was also obtained in the DXR treated group where viability decreased to 65.58 ± 2.25% ($p < 0.01$) when compared to the control. Upregulating autophagy using amino acid deprivation in conjunction with DXR (10D) [55.87 ± 1.88% ($p < 0.05$)] and amino acid deprivation with rapamycin treatment in conjunction with DXR (10RD) [42.95 ± 8.45% ($p < 0.01$)] were unable to salvage cells when compared to DXR treatment alone. However, rapamycin combined with DXR significantly improved viability [78.93 ± 10.85% ($p < 0.05$)] when compared to DXR treatment alone. Inhibiting autophagy in conjunction with DXR treatment significantly decreased cell viability [46.55 ± 4.44% ($p < 0.01$)] when compared to DXR treatment alone. Based on these results, all amino acid groups were excluded from further experiments as they appeared to have detrimental effects in the presence of DXR.

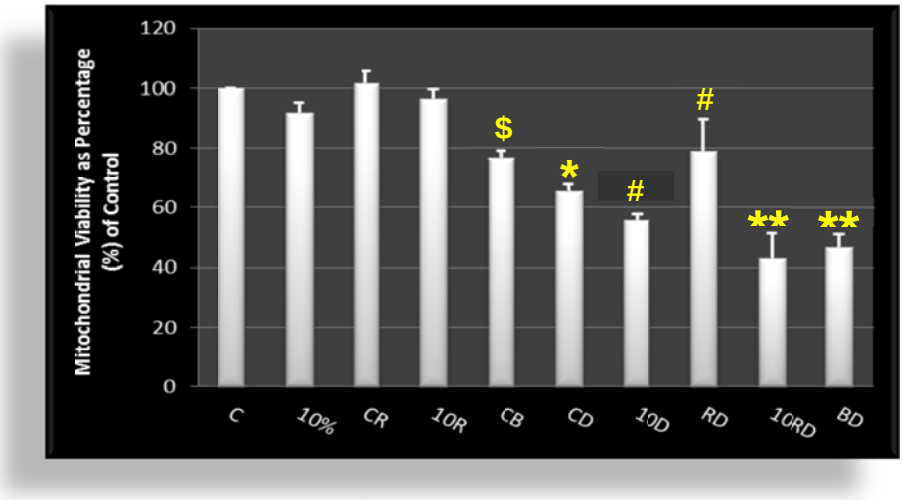

Figure 3.10.3: Effect of various treatment regimens on mitochondrial viability in H_9C_2 cells. H_9C_2 myoblasts were incubated with a 10% amino acid concentration, 50 nM rapamycin and 3 µM DXR for 24 hrs as well as 10 nM Bafilomycin A1 for 6 hrs. Results are presented as mean ± SEM ($n \geq 3$). $^{\$}P < 0.05$, $^{*}P < 0.01$ versus control; $^{\#}P < 0.05$, $^{**}P < 0.01$ versus DXR. Abbreviations - **C**: control; **10%**: 10% amino acid; **CR**: rapamycin; **10R**: 10% amino acids and rapamycin; **CB**: bafilomycin A1; **CD**: DXR; **10D**: 10% and DXR; **RD**: rapamycin and DXR; **10RD**: 10% amino acids, rapamycin and DXR; **BD**: bafilomycin A1 and DXR.

3.10.4: Assessment of Apoptosis during combination treatment (Figure 3.10.4)

Apoptosis was evaluated using the Caspase-Glo assay. Results showed a significant upregulation in caspase activity in DXR group (CD) [216.10 ± 33.15% ($p < 0.05$)] when compared to the control (100%). On the other hand, a significant reduction in caspase activity was observed in the RD group [31.97 ± 13.92% ($p < 0.05$)] when compared to group CD. Although group BD showed no significant differences when compared to DXR treatment alone, the elevated activity of caspase-3/7 in this combination demonstrates that inhibiting autophagy with DXR treatment is detrimental.

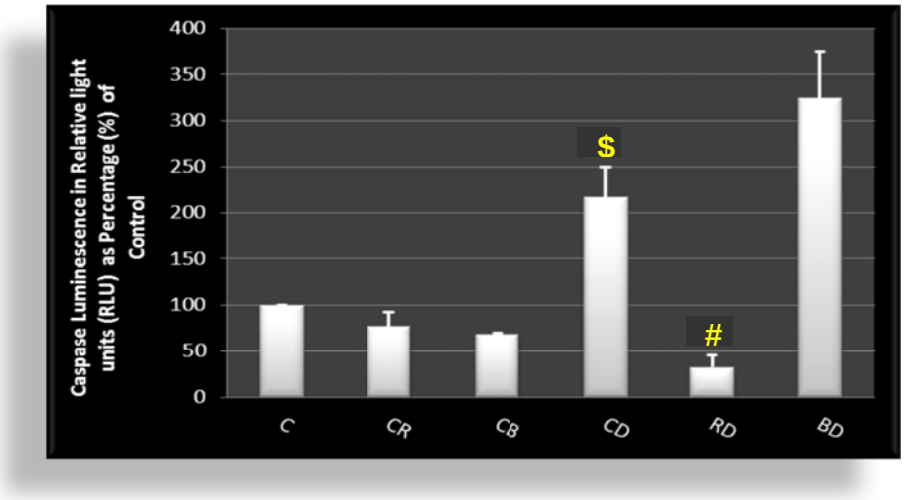

Figure 3.10.4: Effect of various treatment regimens on apoptotic activity in H_9C_2 cells. H_9C_2 myoblasts were incubated with a 50 nM rapamycin, 3 µM DXR for 24 hrs as well as 10 nM Bafilomycin A1 for 6 hrs. Results are presented as mean ± SEM (n = 3). $^{\$}P < 0.05$ versus control, $^{\#}P < 0.05$ versus DXR . Abbreviations - **C**: control; **CR**: rapamycin, **CB**: bafilomycin A1, **CD**: DXR, **RD**: rapamycin and DXR, **BD**: bafilomycin A1 and DXR.

3.10.5: Assessment of Necrosis during combination treatment (Figure 3.10.5)

In order to evaluate necrotic cell death, the trypan blue exclusion stain was employed. The incorporation of the dye through the membrane indicates loss of membrane integrity and thus necrosis. Significance was observed in group CD [12.29 ± 0.80% ($p < 0.001$)] when compared to the control (5.72 ± 0.61%) and group BD [26.00 ± 4.15% ($p < 0.05$)] when compared to CD.

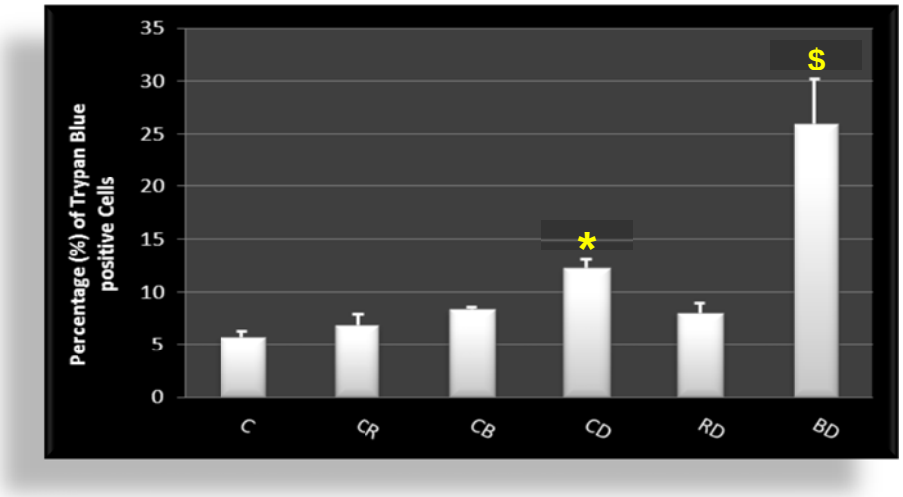

Figure 3.10.5: Effect of various treatment regimens on necrotic cell death in H_9C_2 cells. H_9C_2 myoblasts were incubated with a 50 nM rapamycin, 3 µM DXR for 24 hrs as well as 10 nM Bafilomycin A1 for 6 hrs. Results are presented as mean ± SEM ($n \geq 3$). $^{*}P < 0.001$ versus control, $^{\$}P < 0.05$ versus DXR. Abbreviations - **C**: control; **CR**: rapamycin, **CB**: bafilomycin A1, **CD**: DXR, **RD**: rapamycin and DXR, **BD**: bafilomycin A1 and DXR.

3.10.6: Assessment of Autophagy during combination treatment (Figure 3.10.6 - 9)

LC-3, p62/SQSTM1 and beclin-1 as markers of autophagic activity were assessed by western blotting. LC-3 examination was significantly higher in group CR [134.00 ± 1.92% ($p < 0.01$)] when compared to the control (100%) and RD [122.10 ± 1.05% ($p < 0.05$)] when compared to group CD (109.77 ± 5.83%). Analysis of the LC-3 immunoblot (image) demonstrated increased LC-3 (I) and LC-3 (II) accumulation in groups CB, CD and BD suggesting hindrance in the lipidation process required for autophagy execution. This phenomenon was expected in groups CB and BD as autophagy was inhibited with bafilomycin. Groups CR and RD showed decreased LC-3 (I) and increased LC-3 (II) suggesting that LC-3 (I) is being lipidated faster than LC-3 (II) is being degraded, indicative of autophagy execution. P62, a poly-ubiquitin protein degraded by autophagy or the ubiquitin-proteasome pathway (UPP); is inversely proportional to the extent of autophagic activity. Inhibition of autophagy, caused a signification accumulation in p62 protein levels in groups CB [141.60 ± 1.05% ($p < 0.001$)] when compared to the control (100%) and BD [144.80 ± 0.53% ($p < 0.001$)] when compared to group CD. The presence of DXR (group CD) also resulted in significant accumulation [131.10 ± 0.43% ($p < 0.01$)] of p62 when compared to the control. In the combination where autophagy was stimulated (group

RD), a significant decrease in p62 accumulation [104.80 ± 1.33% ($p < 0.001$)] was observed when compared to group CD thus confirming autophagic activity. No significant differences were observed with regards to beclin-1 expression levels in any of the groups.

Autophagic activity was also assessed by flow cytometry using Lysotracker red. A significant increase in mean fluorescence intensity was observed in group BD [213.50 ± 14.03% ($p < 0.001$)] when compared to DXR treatment (group CD) alone (113.10 ± 5.43%).

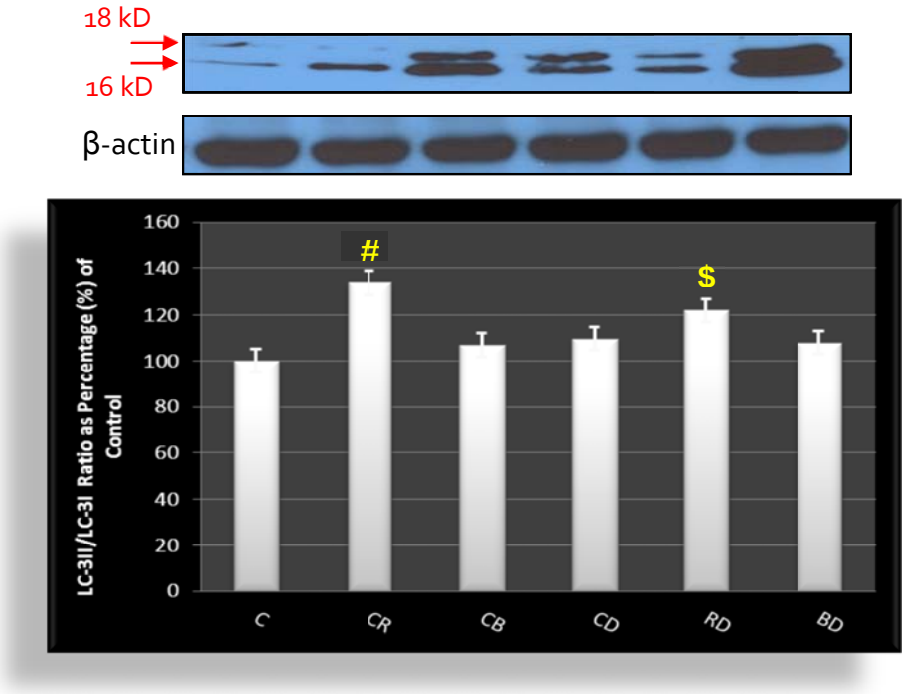

Figure 3.10.6: Immunoblot analysis and the relative quantification of LC-3 in the H_9C_2 cell line supplemented with 50 nM rapamycin, 3 µM DXR for 24 hrs as well as 10 nM Bafilomycin A1 for 6 hrs. Results are presented as mean ± SEM ($n \geq 3$). $^{\#}P < 0.001$ versus control, $^{\$}P < 0.05$ versus DXR. Abbreviations - **C**: control; **CR**: rapamycin, **CB**: bafilomycin A1, **CD**: DXR, **RD**: rapamycin and DXR, **BD**: bafilomycin A1 and DXR.

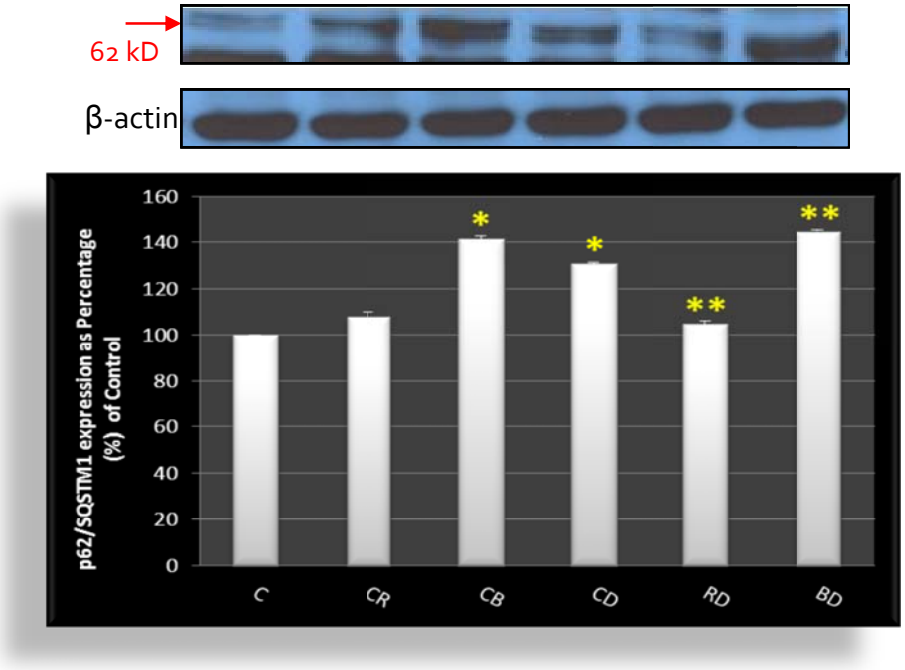

Figure 3.10.7: Immunoblot analysis and the relative quantification of p62 in the H_9C_2 cell line supplemented with 50 nM rapamycin, 3 µM DXR for 24 hrs as well as 10 nM Bafilomycin A1 for 6 hrs. Results are presented as mean ± SEM (n = 3). $^{*}P < 0.001$ versus control, $^{**}P < 0.001$ versus DXR. Abbreviations - **C**: control; **CR**: rapamycin, **CB**: bafilomycin A1, **CD**: DXR, **RD**: rapamycin and DXR, **BD**: bafilomycin A1 and DXR.

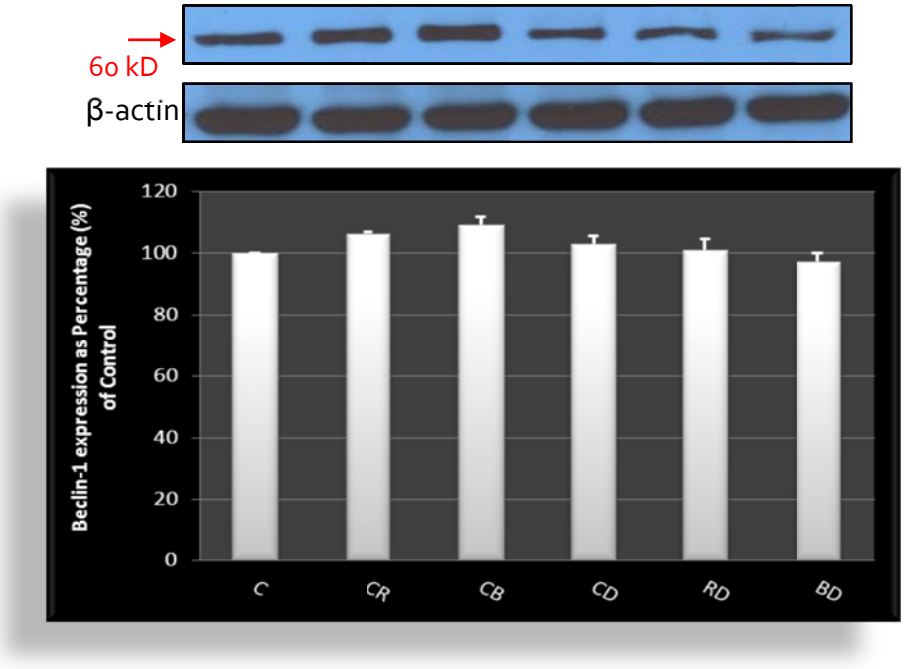

Figure 3.10.8: Immunoblot analysis and the relative quantification of Beclin-1 in the H_9C_2 cell line supplemented with 50 nM rapamycin, 3 µM DXR for 24 hrs as well as 10 nM Bafilomycin A1 for 6 hrs. Results are presented as mean ± SEM (n = 3). Abbreviations - **C**: control; **CR**: rapamycin, **CB**: bafilomycin A1, **CD**: DXR, **RD**: rapamycin and DXR, **BD**: bafilomycin A1 and DXR.

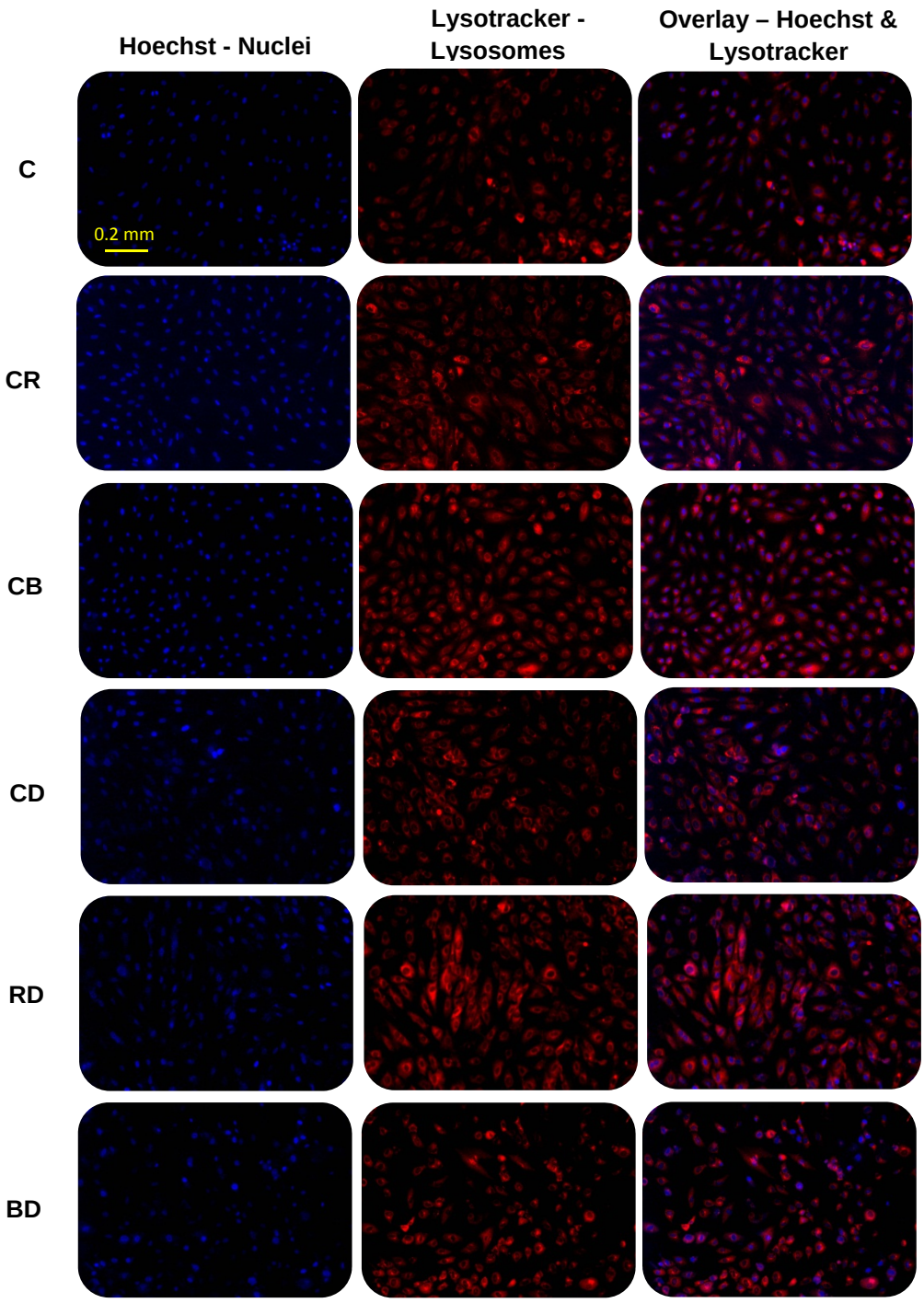

Figure 3.10.9 (a): Effect of various treatment regimens on acidic vacuole (lysosomes) accumulation in H_9C_2 cells. H_9C_2 myoblasts were stained with both Hoechst 33342 (blue) and Lysotracker (red) and assessed for lysosomal activity using fluorescence microscopy. Abbreviations - **C**: control; **CR**: rapamycin, **CB**: bafilomycin A1, **CD**: DXR, **RD**: rapamycin and DXR, **BD**: bafilomycin A1 and DXR. Magnification = 10X. Scale bar = 0.2 mm.

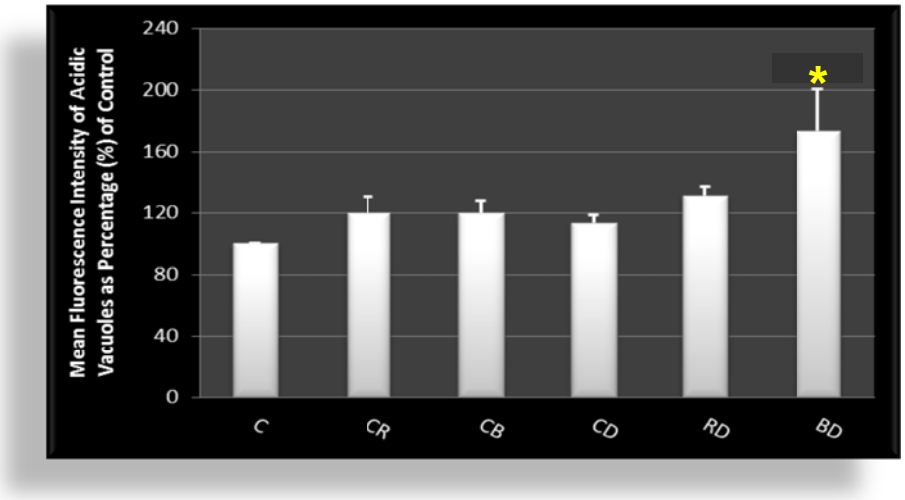

Figure 3.10.9 (b): Effect of various treatment regimens on acidic vacuole (lysosomes) accumulation in H_9C_2 cells. H_9C_2 myoblasts were incubated with a 50 nM rapamycin, 3 µM DXR for 24 hrs as well as 10 nM Bafilomycin A1 for 6 hrs. Results are presented as mean ± SEM ($n \geq 3$). *$P < 0.001$ versus DXR. Abbreviations - **C**: control; **CR**: rapamycin, **CB**: bafilomycin A1, **CD**: DXR, **RD**: rapamycin and DXR, **BD**: bafilomycin A1 and DXR.

3.10.7: Assessment of ROS production and mitochondrial load during combination treatment (Figure 3.10.10 - 12)

As oxidative stress has been implicated in AC-induced cardiotoxicity, ROS production was measured. This study differentiated between generic and mitochondrial ROS using specific fluorescent probes. A significant increase in generic ROS was observed in Group CB [134.10 ± 9.47% ($p < 0.05$)] when compared to the control (100%). Interestingly, in the presence of DXR alone (group CD), a significant reduction [59.89 ± 4.37% ($p < 0.05$)] in generic ROS was observed when compared to the control.

Results obtained from mitochondrial ROS production demonstrated that the source of ROS in the presence of DXR is likely to be mitochondria. A significant increase was observed in group CD [1068.00 ± 52.75% ($p < 0.001$)] when compared to the control (100%). In group BD, ROS significantly decreased [749.20 ± 19.86% ($p < 0.05$)] when compared to CD.

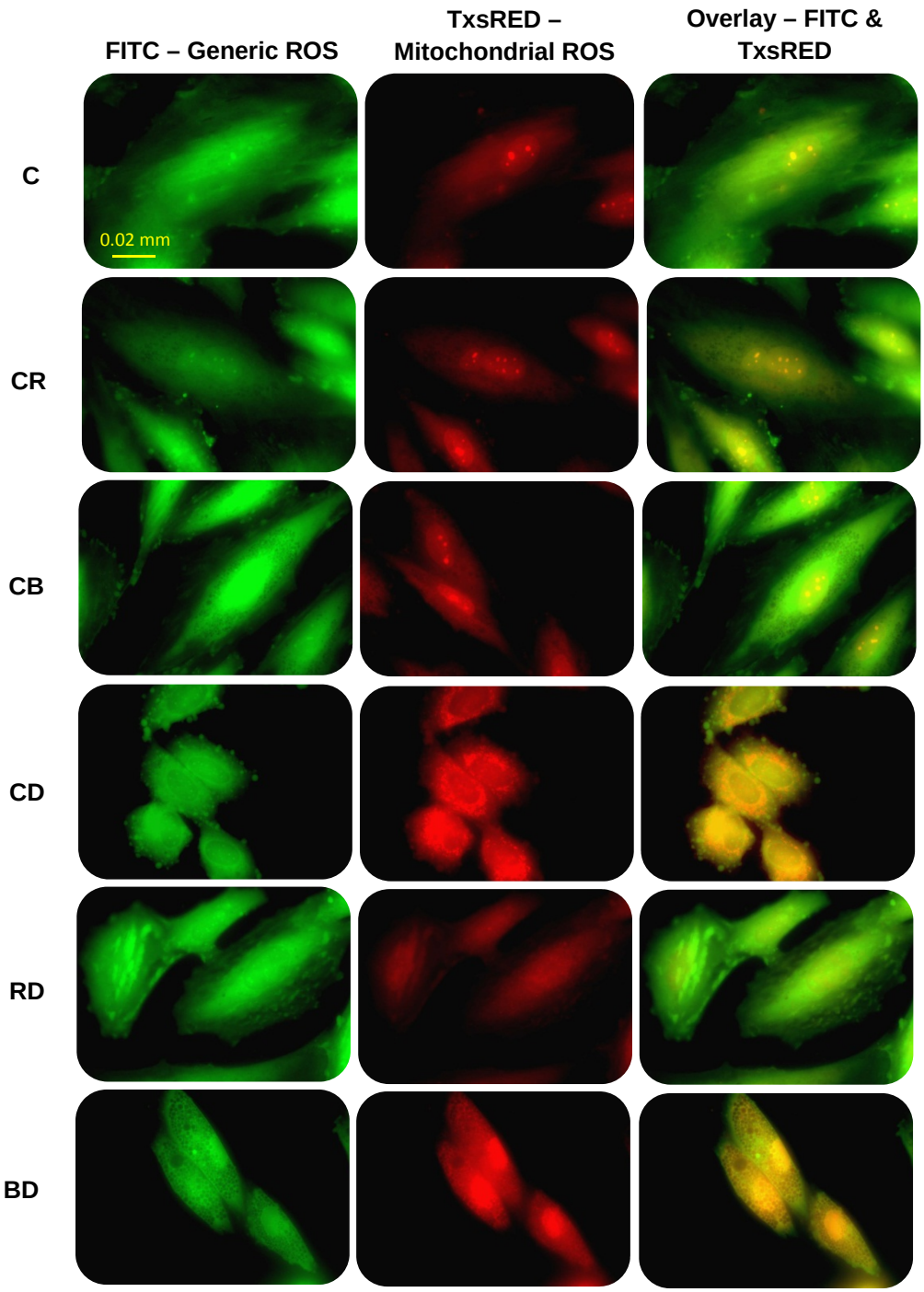

Figure 3.10.10 (a): Effect of various treatment regimens on generic and mitochondrial ROS production in H_9C_2 cells. H_9C_2 myoblasts were stained with both DCF (green) and MitoSOX (red) and assessed for generic and mitochondrial ROS using fluorescence microscopy. Abbreviations - **C**: control; **CR**: rapamycin, **CB**: bafilomycin A1, **CD**: DXR, **RD**: rapamycin and DXR, **BD**: bafilomycin A1 and DXR. Magnification = 60X. Scale bar = 0.02 mm.

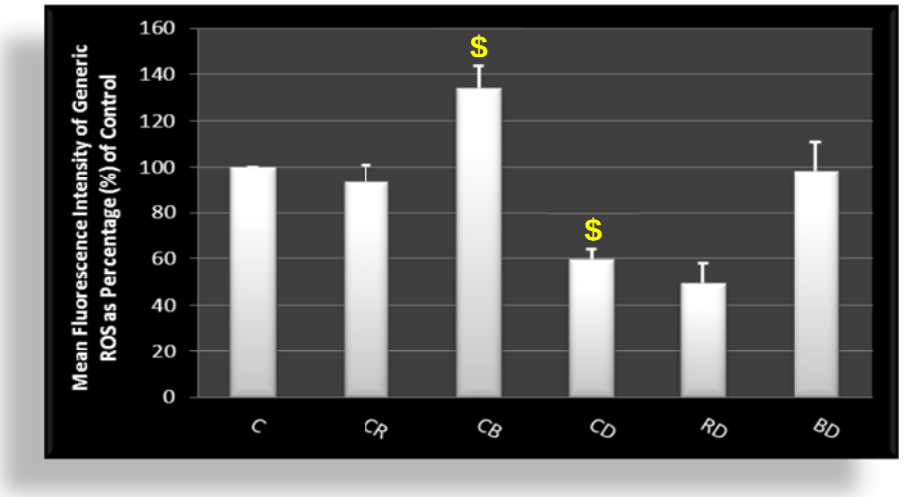

Figure 3.10.10 (b): Effect of various treatment regimens on intracellular (generic) ROS production in H_9C_2 cells. H_9C_2 myoblasts were incubated with a 50 nM rapamycin, 3 µM DXR for 24 hrs as well as 10 nM Bafilomycin A1 for 6 hrs. This was followed by fluorescent staining with DCF where the mean fluorescence was assessed. Results are presented as mean ± SEM ($n \geq 3$). $^{\$}P < 0.05$ versus control. Abbreviations - **C**: control; **CR**: rapamycin, **CB**: bafilomycin A1, **CD**: DXR, **RD**: rapamycin and DXR, **BD**: bafilomycin A1 and DXR.

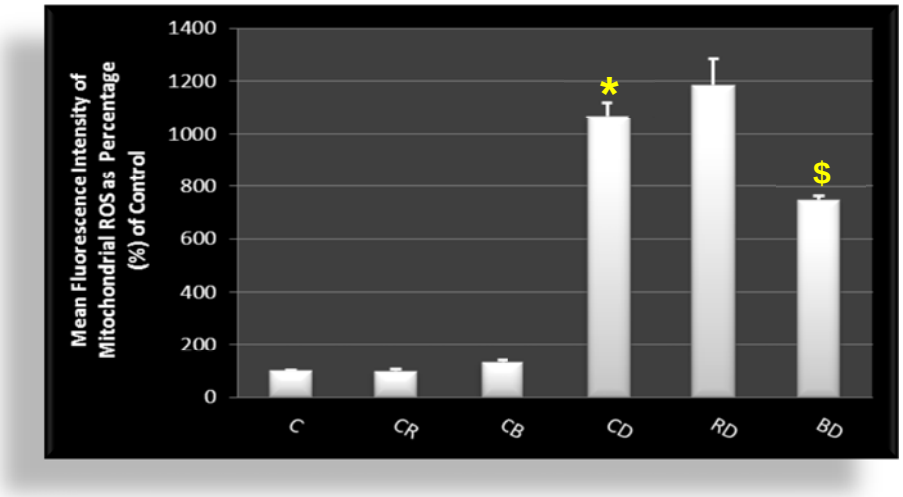

Figure 3.10.10 (c): Effect of various treatment regimens on mitochondrial ROS production in H_9C_2 cells. H_9C_2 myoblasts were incubated with a 50 nM rapamycin, 3 µM DXR for 24 hrs as well as 10 nM Bafilomycin A1 for 6 hrs. This was followed by fluorescent staining with MitoSOX where the mean fluorescence was assessed. Results are presented as mean ± SEM ($n \geq 3$). $^{*}P < 0.001$ versus control, $^{\$}P < 0.05$ versus DXR. Abbreviations - **C**: control; **CR**: rapamycin, **CB**: bafilomycin A1, **CD**: DXR, **RD**: rapamycin and DXR, **BD**: bafilomycin A1 and DXR.

In addition to the mitochondrial ROS, the mitochondrial load was assessed. A significant increase in mitochondrial load was observed in group CD [257.30 ± 9.29%

(p < 0.001)] when compared to the control (100%) as well as group RD [420.40 ± 14.25% (p < 0.001]) when compared to group CD. A significant reduction in mitochondrial load was observed in group BD [144.40 ± 5.17% (p < 0.01)] when compared to group CD.

To obtain a more accurate reflection of ROS production in the cell, mitochondrial ROS generation relative to the mitochondrial load was calculated (Figure 3.10.12). In presence of DXR alone (group CD), ROS production increased over 4-fold [4.15 ± 0.11 (p < 0.001)] when compared to the control. The combination where autophagy was inhibited (group BD) also resulted in a significant increase in ROS production [5.19 ± 0.12 (p < 0.001)], significantly higher than that observed in group CD. In the combination where autophagy was stimulated (group RD), mitochondrial ROS production was significantly reduced [2.81 ± 0.14 (p < 0.001)] when compared to group CD.

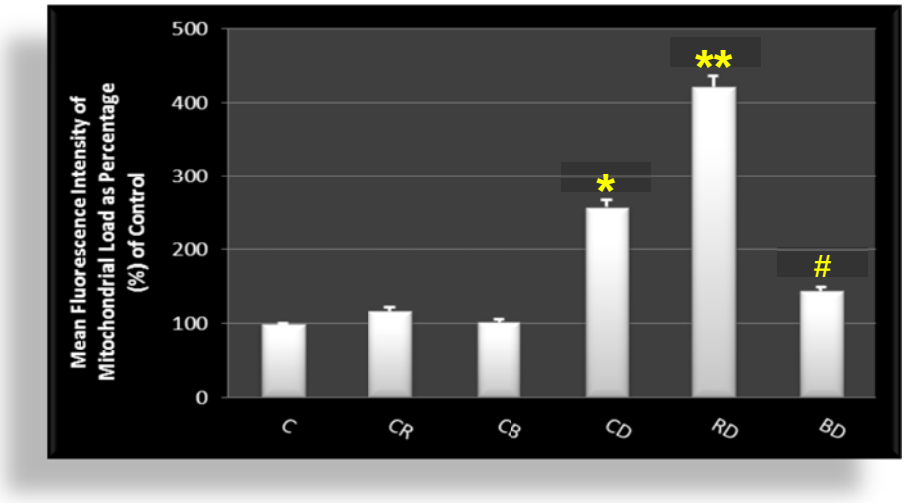

Figure 3.10.11: Effect of various treatment regimens on mitochondrial load in H_9C_2 cells. H_9C_2 myoblasts were incubated with a 50 nM rapamycin, 3 µM DXR for 24 hrs as well as 10 nM Bafilomycin A1 for 6 hrs. This was followed by fluorescent staining with Mitotracker green where the mean fluorescence was assessed. Results are presented as mean ± SEM ($n \geq 3$). $^{*}P < 0.001$ versus control; $^{\#}P < 0.01$, $^{**}P < 0.001$ versus DXR. Abbreviations - **C**: control; **CR**: rapamycin, **CB**: bafilomycin A1, **CD**: DXR, **RD**: rapamycin and DXR, **BD**: bafilomycin A1 and DXR.

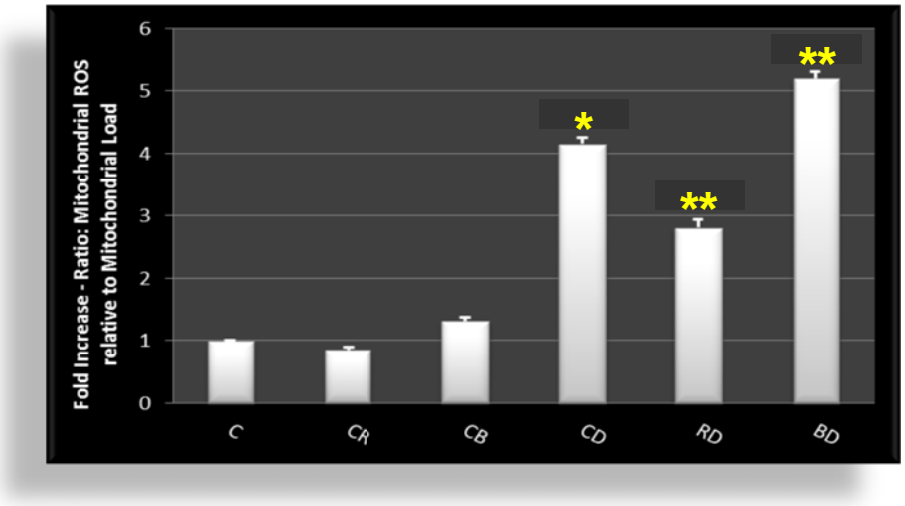

Figure 3.10.12: Effect of various treatment regimens on mitochondrial ROS relative to mitochondrial load in H_9C_2 cells. H_9C_2 myoblasts were incubated with a 50 nM rapamycin, 3 µM DXR for 24 hrs as well as 10 nM Bafilomycin A1 for 6 hrs. This was followed by fluorescent staining with Mitotracker green where the mean fluorescence was assessed. Results are presented as mean ± SEM ($n \geq 3$). $^{*}P < 0.001$ versus control; $^{**}P < 0.001$ versus DXR. Abbreviations - **C**: control; **CR**: rapamycin, **CB**: bafilomycin A1, **CD**: DXR, **RD**: rapamycin and DXR, **BD**: bafilomycin A1 and DXR.

3.10.8: Assessment of mitochondrial morphology and intracellular doxorubicin localization during combination treatment (Figure 3.10.13)

To establish whether AC-induced cardiotoxicity affects mitochondrial morphology, fluorescence microscopy was employed. Our data indicate that mitochondria in the control and CR groups appeared to be elongated, tubular in structure and displayed an interconnected network. However, in the groups where autophagy was inhibited (CB and BD) mitochondria appeared to be short, disintegrated and irregular, displaying a punctate pattern. A similar morphology was observed in group CD, whereas in group RD, normal mitochondrial shape was maintained.

In addition, the intracellular localization of DXR was assessed. The fluorescent images indicate that in group CD, DXR appears to be located in the perinuclear region. A reduced amount of DXR was also present within the nuclear region. In group BD however, DXR strongly localized within the nuclear region. In group RD, a seemingly smaller amount of DXR was present in the nuclear region while the majority of the DXR appeared in the perinuclear region. DXR also appeared to localize strongly within mitochondria as confirmed by colocalization analysis. Groups

RD [0.45 ± 0.06 ($p < 0.05$)] and BD [0.37 ± 0.04($p < 0.01$)] both showed a significant decrease in the area of colocalization when compared to group CD (0.68 ± 0.06).

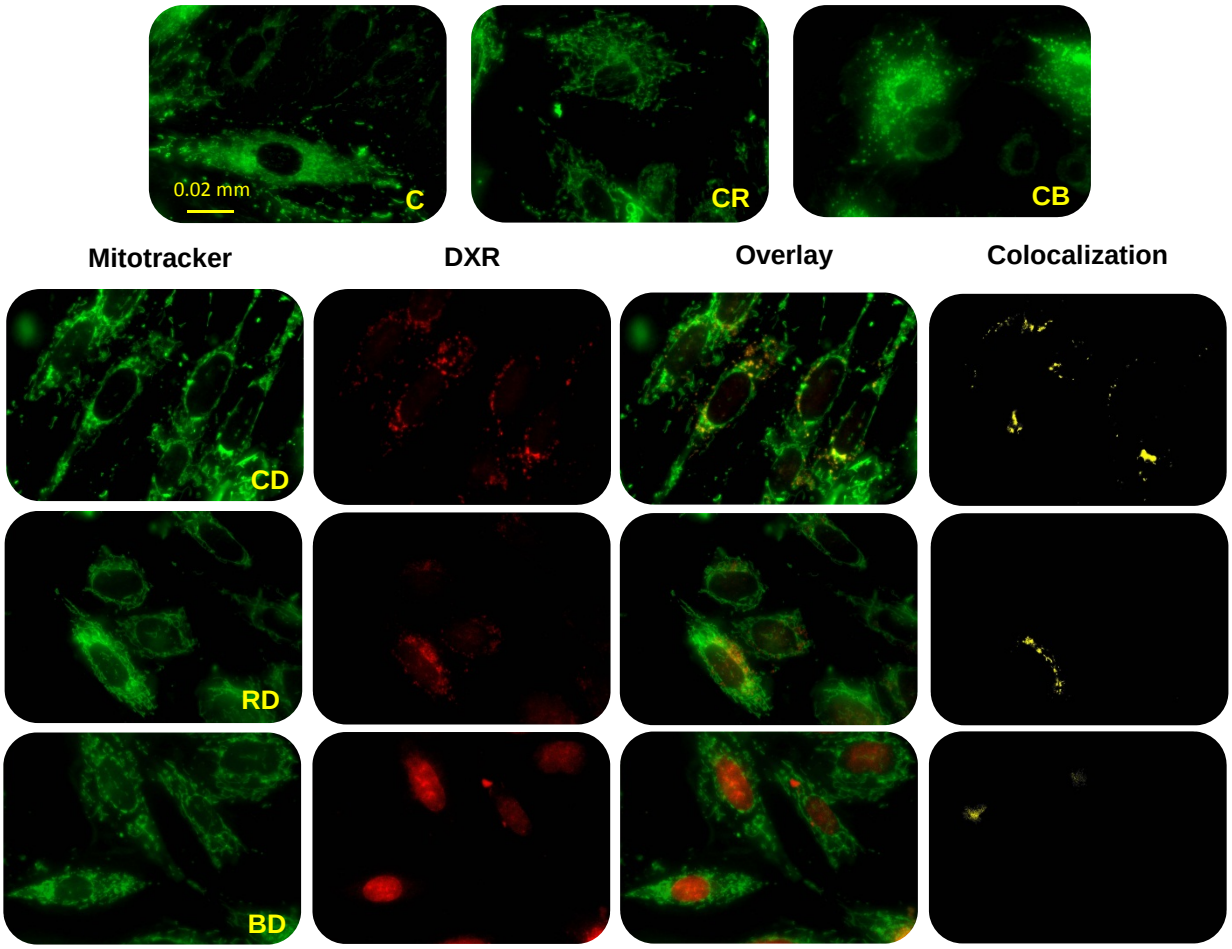

Figure 3.10.13 (a): Effect of various treatment regimens on mitochondrial morphology and DXR localization in H_9C_2 myoblasts. H_9C_2 cells were stained with MitoTracker green (green) and DXR (red) and assessed using fluorescence microscopy (n = 3). Abbreviations - **C**: control; **CR**: rapamycin, **CB**: bafilomycin A1, **CD**: DXR, **RD**: rapamycin and DXR, **BD**: bafilomycin A1 and DXR. Magnification = 60X. Scale bar = 0.02 mm.

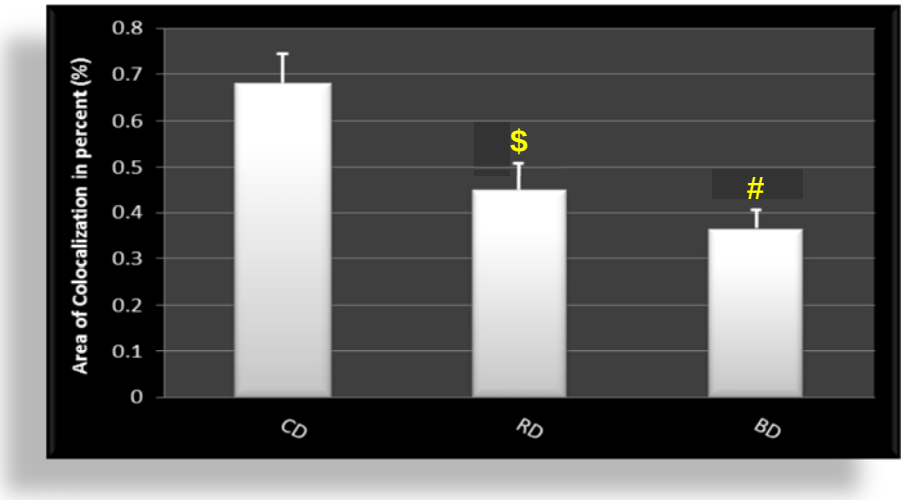

Figure 3.10.13 (b): Area of colocalization (%) of DXR with mitochondria using fluorescence microscopy (n ≥ 3). Results are presented as mean ± SEM (n ≥ 3). $^{\$}P < 0.05$, $^{\#}P < 0.01$ versus DXR. Abbreviations - **CD**: DXR, **RD**: rapamycin and DXR, **BD**: bafilomycin A1 and DXR.

3.10.9: Assessment of mitochondrial function during combination treatment (Figure 3.10.14)

Mitochondrial membrane potential was assessed as an indicator of mitochondrial function utilizing JC-1. Regions of high mitochondrial potential are indicated by red fluorescence due to J-aggregate formation by the concentrated dye. Depolarized mitochondrial regions are indicated by green fluorescence of the JC-1 monomer. Analysis of the results with flow cytometry demonstrated that the inhibition of autophagy (groups CB and BD) decreased mitochondrial function significantly [0.92 ± 0.01 ($p < 0.001$) and 0.75 ± 0.01 ($p < 0.001$)] when compared to either the control or group CD respectively. On the other hand, elevated autophagy (groups CR and RD) increased mitochondrial function significantly [1.26 ± 0.01 ($p < 0.001$) and 1.64 ± 0.02 ($p < 0.01$)] when compared to either the control or group CD. In the presence of DXR (group CD) alone, mitochondrial function was significantly augmented [1.14 ± 0.02 ($p < 0.001$)] when compared to the control.

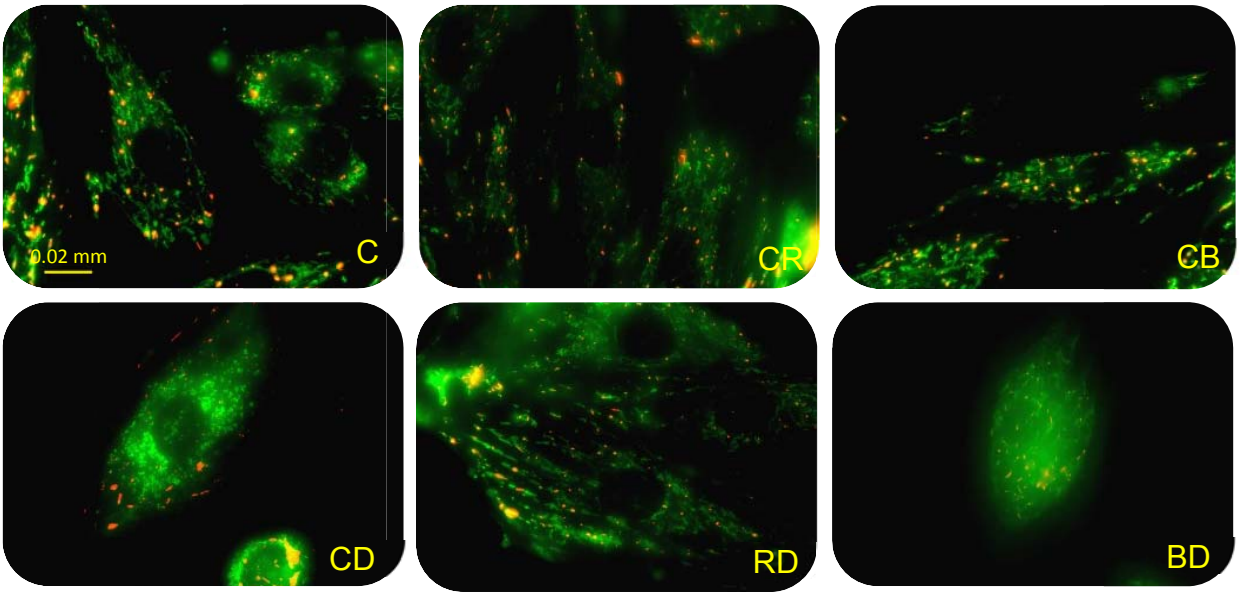

Figure 3.10.14 (a): Effect of various treatment regimens on mitochondrial function in H_9C_2 myoblasts. H_9C_2 cells were stained with JC-1 and visualized using fluorescence microscopy ($n \geq 3$). Abbreviations - **C**: control; **CR**: rapamycin, **CB**: bafilomycin A1, **CD**: DXR, **RD**: rapamycin and DXR, **BD**: bafilomycin A1 and DXR. Magnification = 60X. Scale bar = 0.02 mm.

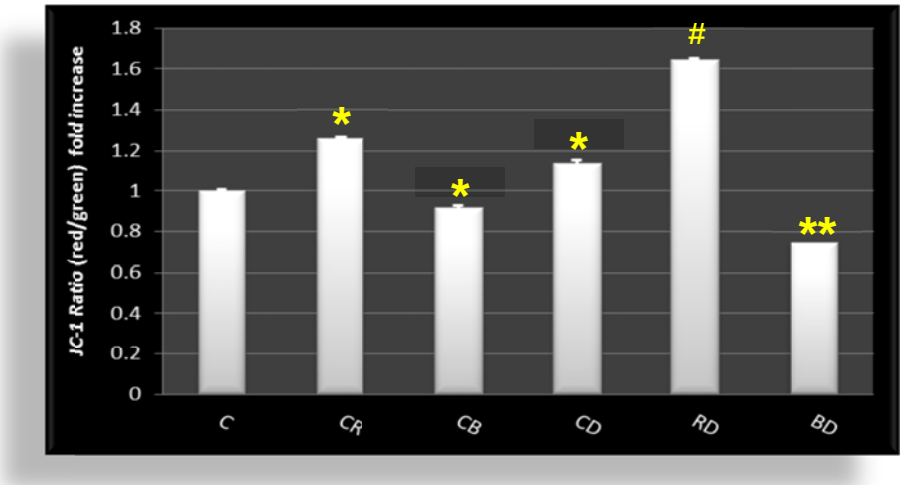

Figure 3.10.14 (b): Effect of various treatment regimens on mitochondrial function in H_9C_2 cells. H_9C_2 myoblasts were incubated with a 50 nM rapamycin, 3 µM DXR for 24 hrs as well as 10 nM Bafilomycin A1 for 6 hrs. This was followed by fluorescent staining with JC-1 where the change in mean fluorescence was assessed. Results are presented as mean ± SEM ($n \geq 3$). $^{*}P < 0.001$ versus control; $^{\#}P < 0.01$, $^{**}P < 0.001$ versus DXR. Abbreviations - **C**: control; **CR**: rapamycin, **CB**: bafilomycin A1, **CD**: DXR, **RD**: rapamycin and DXR, **BD**: bafilomycin A1 and DXR.

3.10.10: Assessment of the ubiquitin-proteasome pathway (UPP) during combination treatment (Figure 3.10.15 - 19)

The phosphorylation of FoxO (specifically FoxO3), a transcription factor involved in the simultaneous activation and regulation of both the autophagic pathway and the UPP (Zhao *et al*, 2007) was significantly decreased in group CD [90.24 ± 3.70% ($p < 0.05$)] when compared to the control (100%). A significant upregulation of both ubiquitin ligases MuRF-1 [119.00 ± 3.12% ($p < 0.05$]) and MAFbx [121.70 ± 3.82% ($p < 0.05$) in group CD was observed when compared to the control (100%). The evaluation of ubiquitinated proteins by means of western blotting corresponded with the results obtained above. A significant increase in ubiquitination was observed in groups CB [130.20 ± 6.24% ($p < 0.05$)] and CD [127.80 ± 5.82% ($p < 0.05$)] when compared to the control (100%).

There was a significant decrease in proteasome activity in the presence of DXR alone (group CD) [75.43 ± 4.54% ($p < 0.05$)] when compared to the control (100%). The upregulation (group RD) as well as the inhibition (group BD) of autophagy in the presence of DXR both appeared to exacerbate the situation causing an even greater decrease [32.88 ± 4.94% ($p < 0.01$) and 41.31 ± 6.78% ($p < 0.05$)] in the chymotrypsin-like activity of the proteasome when compared group CD.

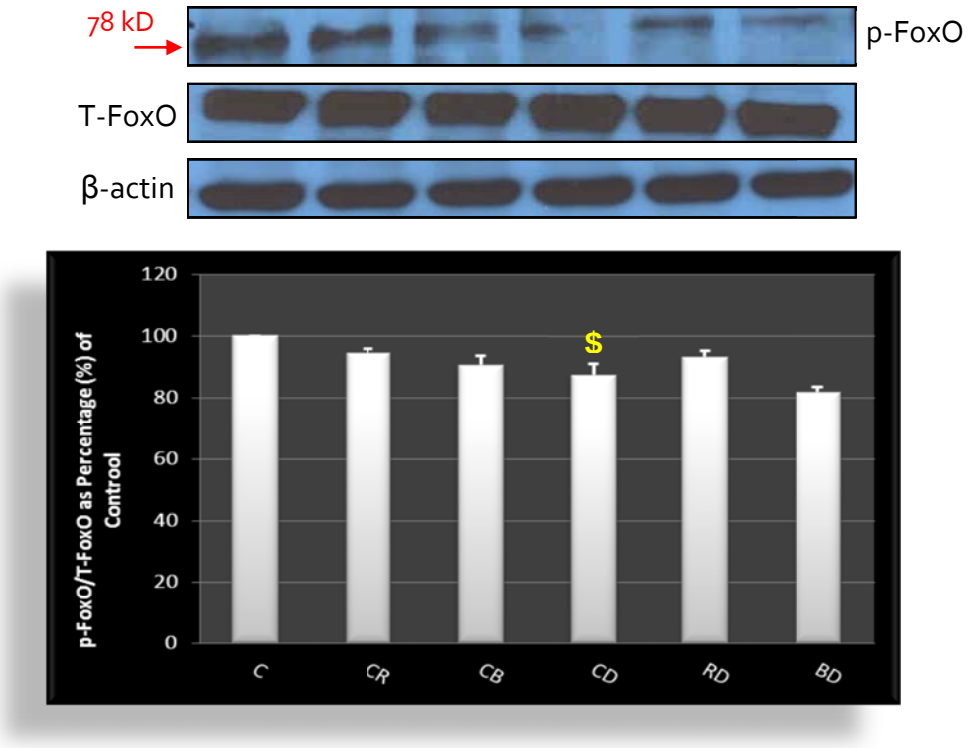

Figure 3.10.15: Immunoblot analysis and the relative quantification of the ratio between p-FoxO3 and T-FoxO in the H_9C_2 cell line supplemented with 50 nM rapamycin, 3 µM DXR for 24 hrs as well as 10 nM Bafilomycin A1 for 6 hrs. Results are presented as mean ± SEM (n = 3). $^{\$}P < 0.05$ versus control. Abbreviations - **C**: control; **CR**: rapamycin, **CB**: bafilomycin A1, **CD**: DXR, **RD**: rapamycin and DXR, **BD**: bafilomycin A1 and DXR.

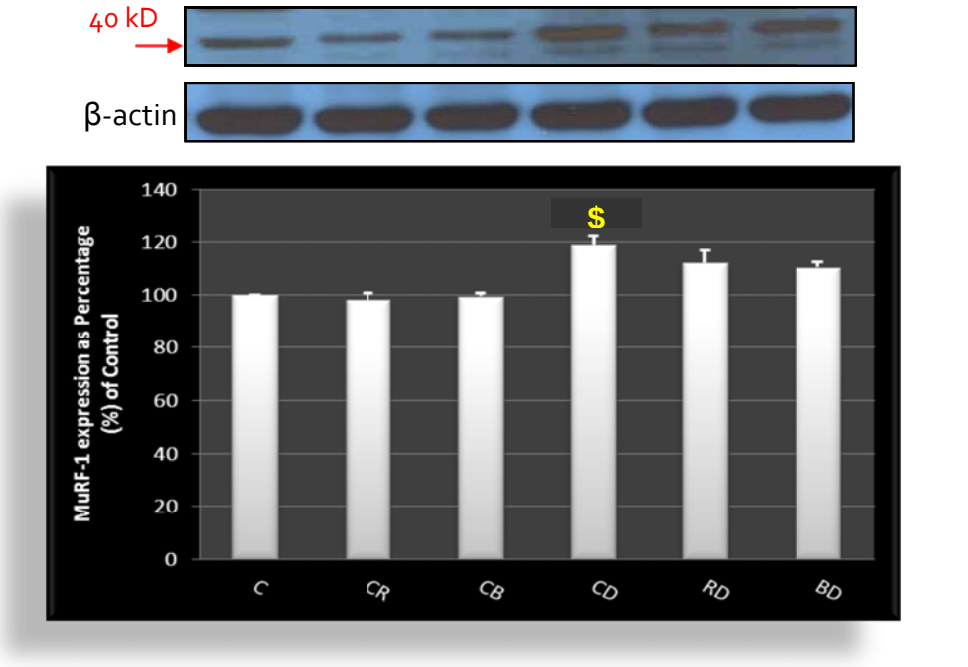

Figure 3.10.16: Immunoblot analysis and the relative quantification of MuRF-1 in the H_9C_2 cell line supplemented with 50 nM rapamycin, 3 µM DXR for 24 hrs as well as 10 nM Bafilomycin A1 for 6 hrs. Results

are presented as mean ± SEM (n = 3). $^{\$}P < 0.05$ versus control. Abbreviations - **C**: control; **CR**: rapamycin, **CB**: bafilomycin A1, **CD**: DXR, **RD**: rapamycin and DXR, **BD**: bafilomycin A1 and DXR.

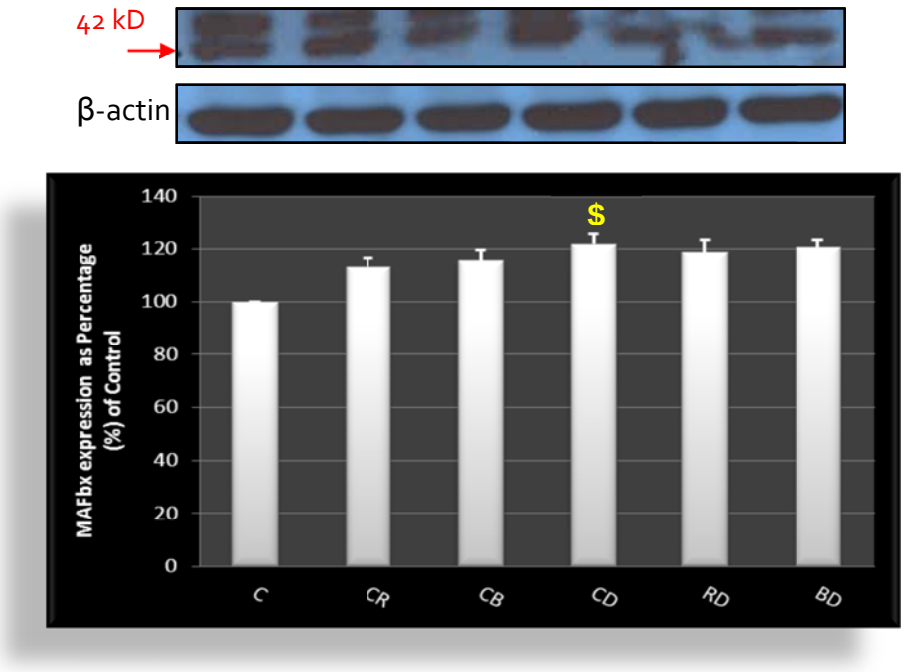

Figure 3.10.17: Immunoblot analysis and the relative quantification of MAFbx in the H_9C_2 cell line supplemented with 50 nM rapamycin, 3 µM DXR for 24 hrs as well as 10 nM Bafilomycin A1 for 6 hrs. Results are presented as mean ± SEM (n = 3). $^{\$}P < 0.05$ versus control. Abbreviations - **C**: control; **CR**: rapamycin, **CB**: bafilomycin A1, **CD**: DXR, **RD**: rapamycin and DXR, **BD**: bafilomycin A1 and DXR.

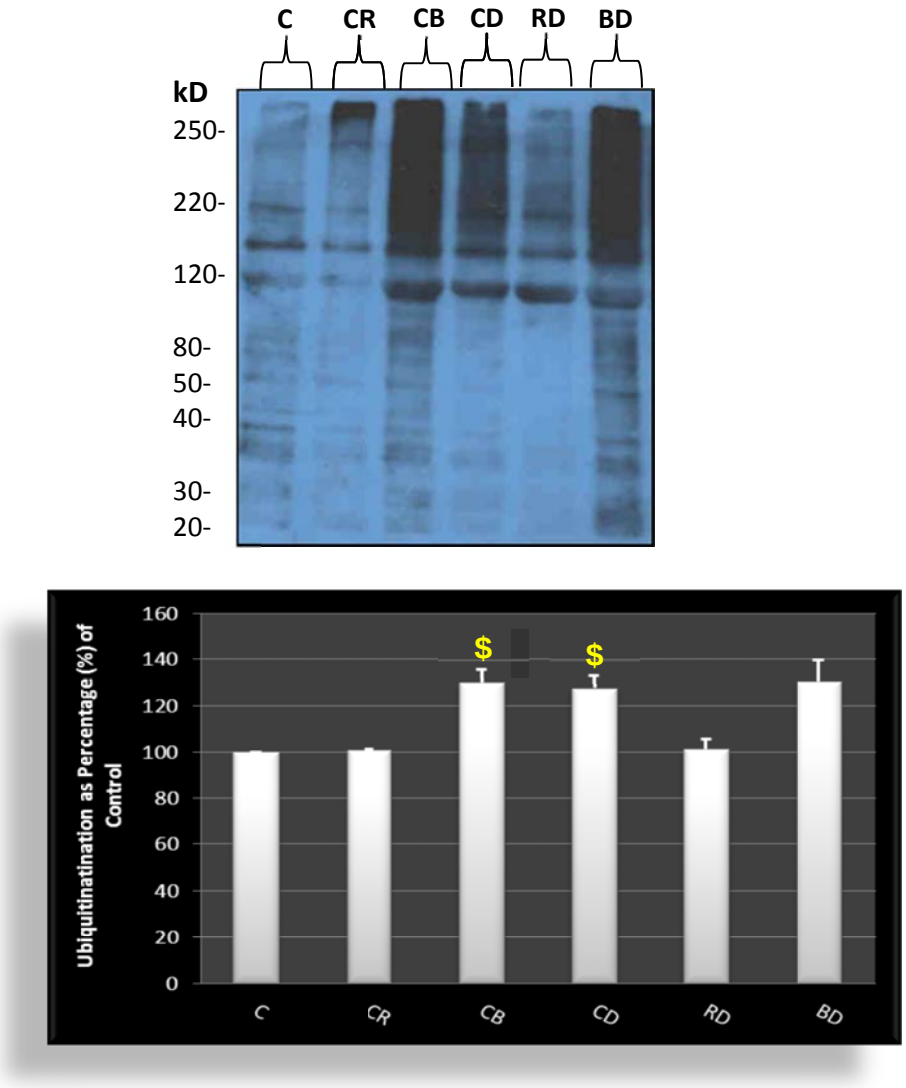

Figure 3.10.18: Immunoblot analysis and the relative quantification of ubiquitinated proteins in the H_9C_2 cell line supplemented with 50 nM rapamycin, 3 µM DXR for 24 hrs as well as 10 nM Bafilomycin A1 for 6 hrs. Results are presented as mean ± SEM (n = 3). $^{\$}P < 0.05$ versus control. Abbreviations - **C**: control; **CR**: rapamycin, **CB**: bafilomycin A1, **CD**: DXR, **RD**: rapamycin and DXR, **BD**: bafilomycin A1 and DXR.

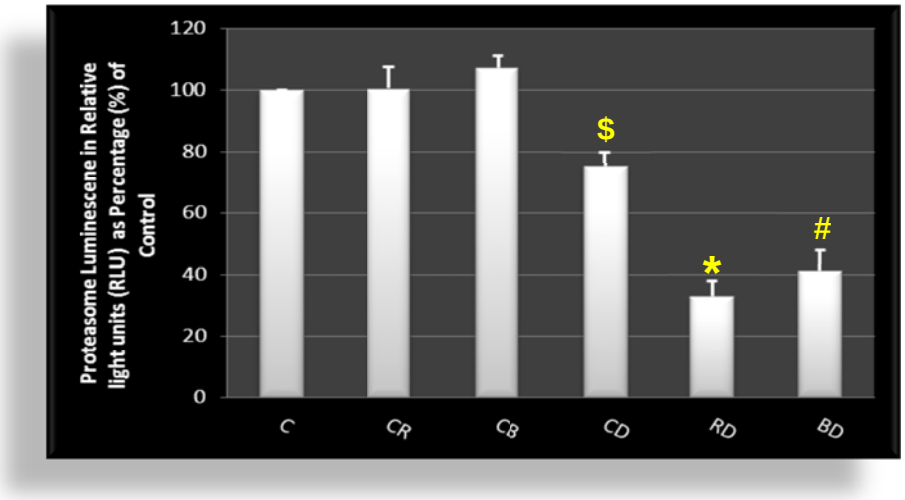

Figure 3.10.19: Effect of various treatment regimens on proteasome (chymotrypsin-like) activity in H_9C_2 cells supplemented with 50 nM rapamycin, 3 µM DXR for 24 hrs as well as 10 nM Bafilomycin A1 for 6 hrs. Results are presented as mean ± SEM (n = 3). $^{\$}P < 0.05$ versus control; $^{\#}P < 0.05$, $^{*}P < 0.01$ versus DXR. Abbreviations - **C**: control; **CR**: rapamycin, **CB**: bafilomycin A1, **CD**: DXR, **RD**: rapamycin and DXR, **BD**: bafilomycin A1 and DXR.

3.10.11: Assessment of ER load during combination treatment (Figure 3.10.20)

To determine whether ER stress is induced in the context of cardiotoxicity, the ER load was assessed. Groups CR [143.10 ± 2.79% ($p < 0.01$)] and CD [141.30 ± 6.22% ($p < 0.01$)] both displayed significantly increased ER load when compared to the control (100%). The combination groups RD [105.10 ± 9.86% ($p < 0.05$)] and BD [100.30 ± 4.35% ($p < 0.05$)] showed a significant decrease in ER load when compared to group CD. A modest amount of colocalization between DXR and the ER was observed, however no significance was revealed when comparing the different groups with regard to the area of colocalization.

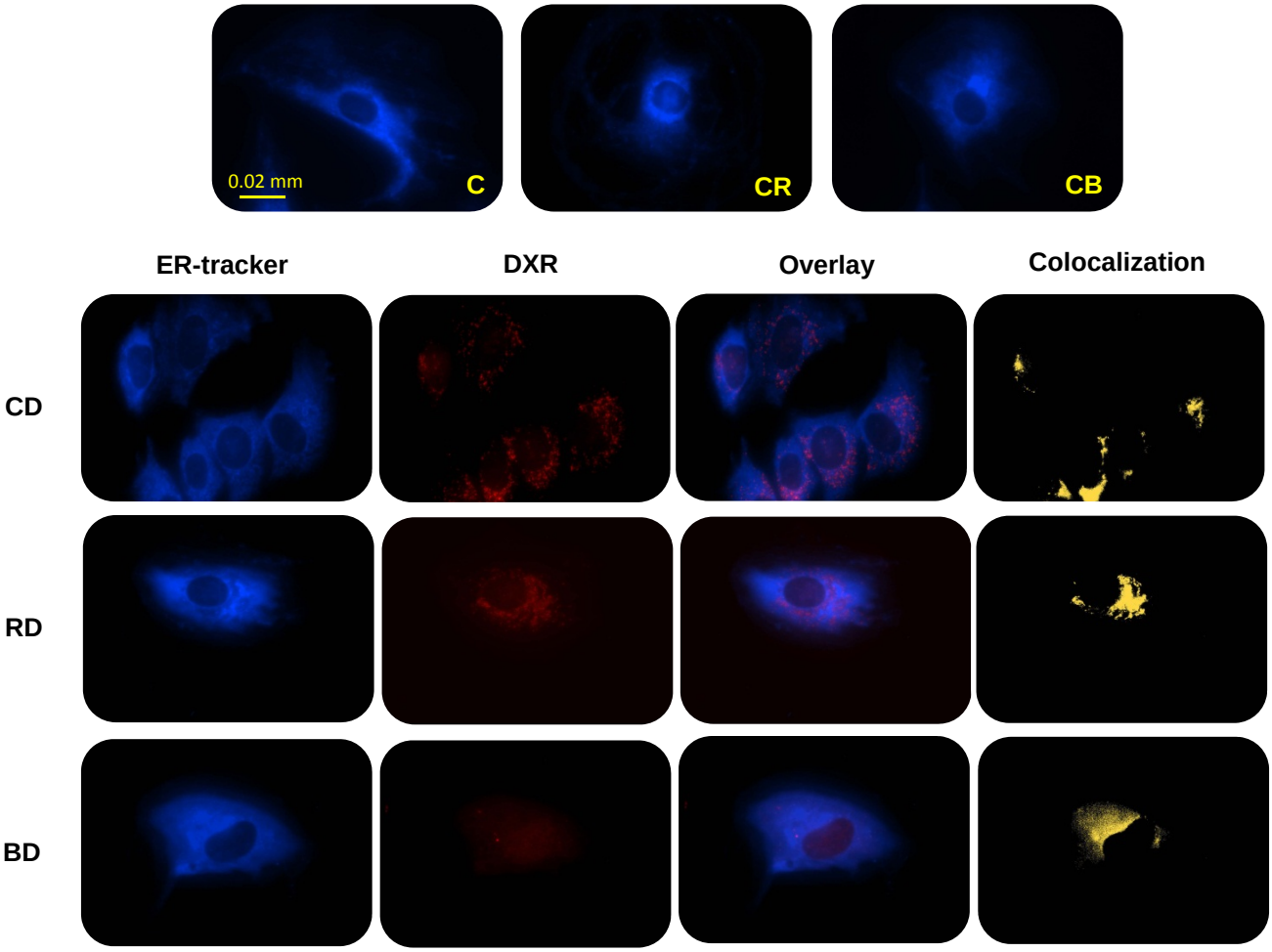

Figure 3.10.20 (a): The effect of various treatment regimens on ER load and DXR localization in H_9C_2 myoblasts. H_9C_2 cells were incubated with ER tracker and visualized using fluorescence microscopy ($n \geq 3$). Abbreviations - **C**: control; **CR**: rapamycin, **CB**: bafilomycin A1, **CD**: DXR, **RD**: rapamycin and DXR, **BD**: bafilomycin A1 and DXR. Magnification = 60X. Scale bar = 0.02 mm.

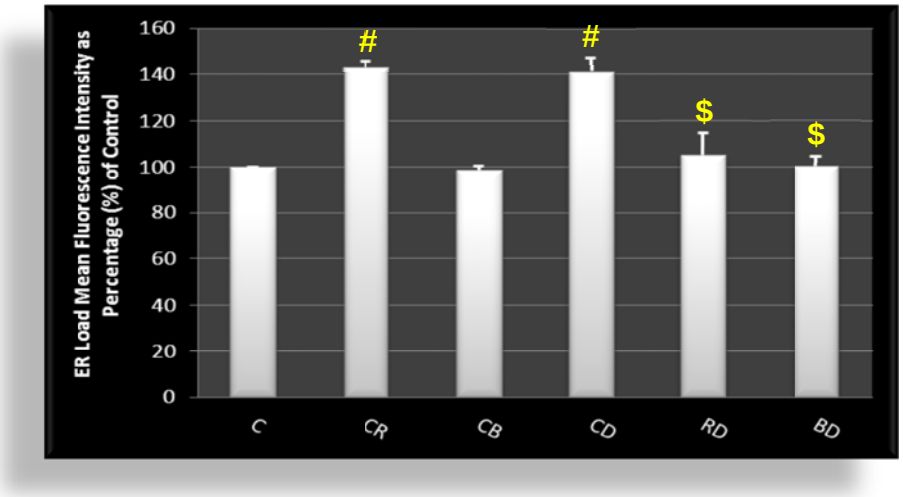

Figure 3.10.20 (b): The effect of various treatment regimens on ER load in H_9C_2 cells. H_9C_2 myoblasts were treated with 50 nM rapamycin, 3 µM DXR for 24 hrs as well as 10 nM Bafilomycin A1 for 6 hrs. This was followed by fluorescent staining with ER-Tracker where the mean fluorescence was assessed. Results are presented as mean ± SEM (n = 3). $^{\#}P < 0.01$ versus control; $^{\$}P < 0.05$ versus DXR. Abbreviations - **C**: control; **CR**: rapamycin, **CB**: bafilomycin A1, **CD**: DXR, **RD**: rapamycin and DXR, **BD**: bafilomycin A1 and DXR.

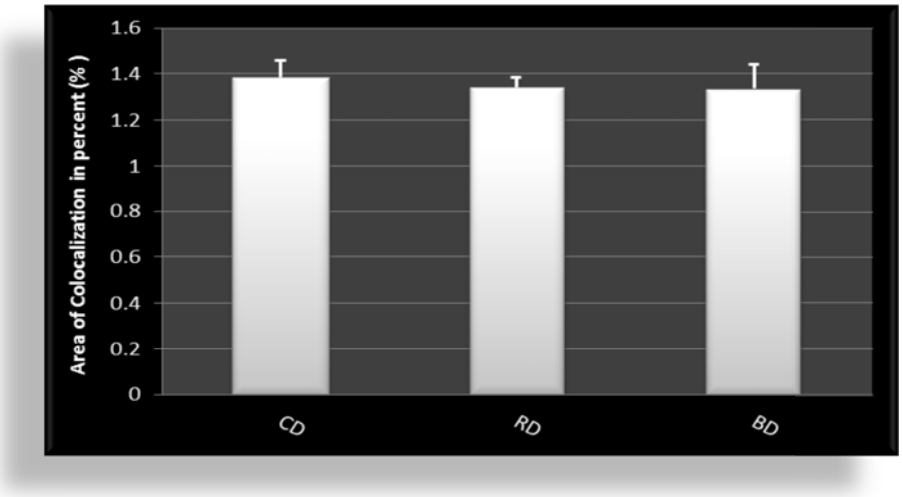

Figure 3.10.20 (c): Area of colocalization (%) of DXR with the ER using fluorescence microscopy (n ≥ 3). Results are presented as mean ± SEM (n = 3). Abbreviations - **CD**: DXR, **RD**: rapamycin and DXR, **BD**: bafilomycin A1 and DXR.

3.10.12: Assessment of the effects of mTOR silencing, as an alternative autophagy inducer, vs rapamycin (Figure 3.10.21- 24)

To confirm the observed effects of rapamycin treatment, mTOR was silenced. Results indicate almost total mTOR inhibition with the silencing vs a significant reduction in p-mTOR with rapamycin. Furthermore, LC-3 upregulation, indicative of

an increase in autophagy, was also much more pronounced in the group where mTOR was silenced compared to the rapamycin group.

Results produced from the assessment of mitochondrial viability indicated that the silencing of mTOR (group CM) for 24 hrs significantly reduced viability [75.48 ± 1.81% ($p < 0.001$)] when compared to the control (100%). Group RD significantly improved viability whereas the combination of silencing mTOR with DXR (group MD) significantly decreased viability when compared to group CD (55.70 ± 3.35%).

Caspase activity was assessed as a marker of apoptosis in these groups; it was demonstrated that caspase activity was significantly increased in group CD [444.60 ± 29.33% ($p < 0.001$)] compared to the control (100%). When comparing group CD with group RD, a significant reduction (78.86 ± 7.14%) in caspase activity was observed.

Mitochondrial morphology and DXR localization revealed the following: Groups C (control), CR (control rapamycin) and CM (control si-mTOR) displayed normal, elongated mitochondria whereas groups CD (control doxorubicin) and MD (mTOR silencing+doxorubicin) displayed shorter mitochondria, similar to that observed as previously described when utilizing bafilomycin. Group RD (rapamycin+doxorubicin), on the other hand, also showed signs of abnormal mitochondria although the majority of the mitochondria preserved their normal elongated morphology. When DXR localization was assessed, groups RD (rapamycin+doxorubicin) and MD (mTOR silencing+doxorubicin) displayed less DXR in the nuclear region whilst the majority of the DXR localized in the perinuclear region when compared to group CD (control doxorubicin).

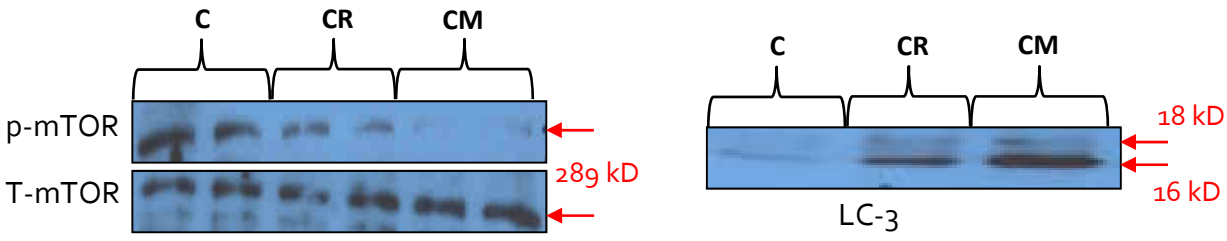

Figure 3.10.21: Immunoblot showing inhibition of mTOR by rapamycin and siRNA, resulting in increased autophagy as demonstrated by LC-3 lipidation. Abbreviations - **C**: control; **CR**: rapamycin; **CM**: siRNA (mTOR)

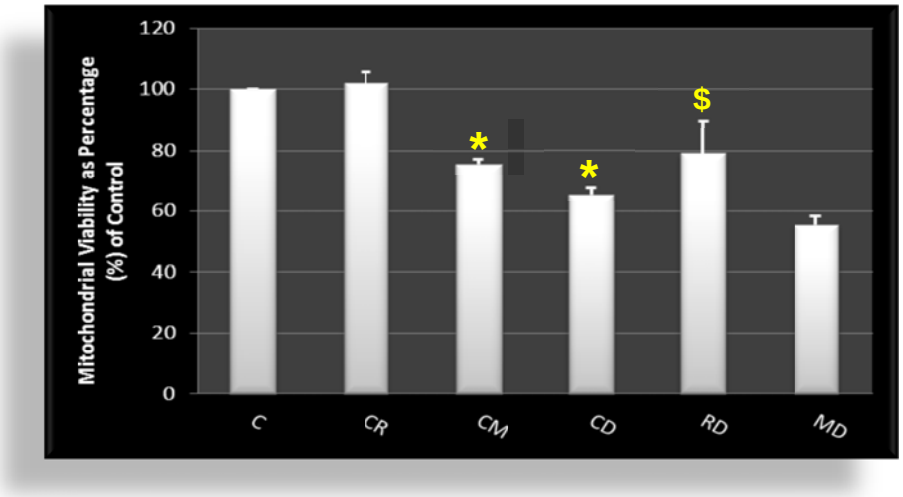

Figure 3.10.22: The effect of various treatment regimens on mitochondrial viability in H_9C_2 cells. H_9C_2 myoblasts were treated with 100 nM SiRNA (mTOR), 50 nM rapamycin and 3 µM DXR for 24 hrs. Results are presented as mean ± SEM ($n \geq 3$). $^{*}P < 0.001$ versus control; $^{\$}P < 0.05$ versus DXR. Abbreviations - **C**: control; **CR**: rapamycin, **CM:** siRNA (mTOR), **CD**: DXR, **RD**: rapamycin and DXR, **MD:** siRNA (mTOR) and DXR

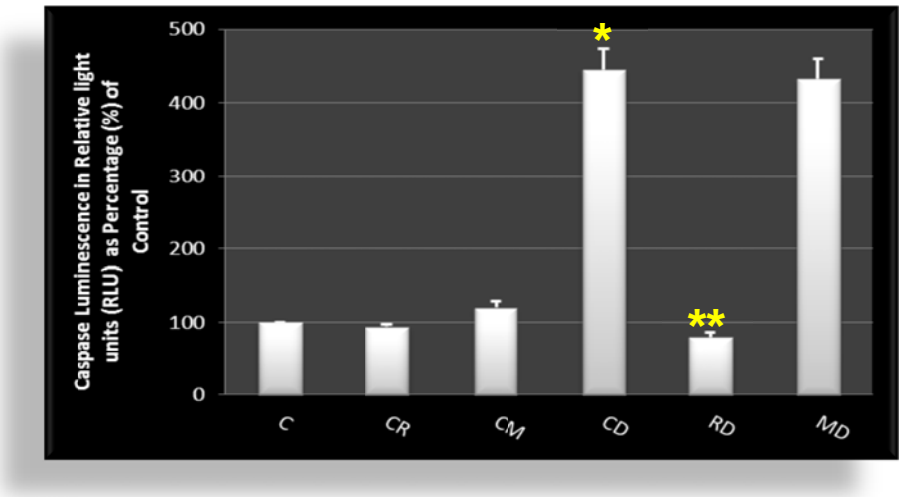

Figure 3.10.23: The effect of various treatment regimens on caspase activity in H_9C_2 cells. H_9C_2 myoblasts were treated with 50 nM rapamycin, 3 µM DXR for 24 hrs as well as 10 nM Bafilomycin A1 for 6 hrs. Results are presented as mean ± SEM ($n = 3$). $^{*}P < 0.001$ versus control; $^{**}P < 0.001$ versus DXR. Abbreviations - **C**: control; **CR**: rapamycin, **CM:** SiRNA (mTOR), **CD**: DXR, **RD**: rapamycin and DXR, **MD:** SiRNA (mTOR) and DXR

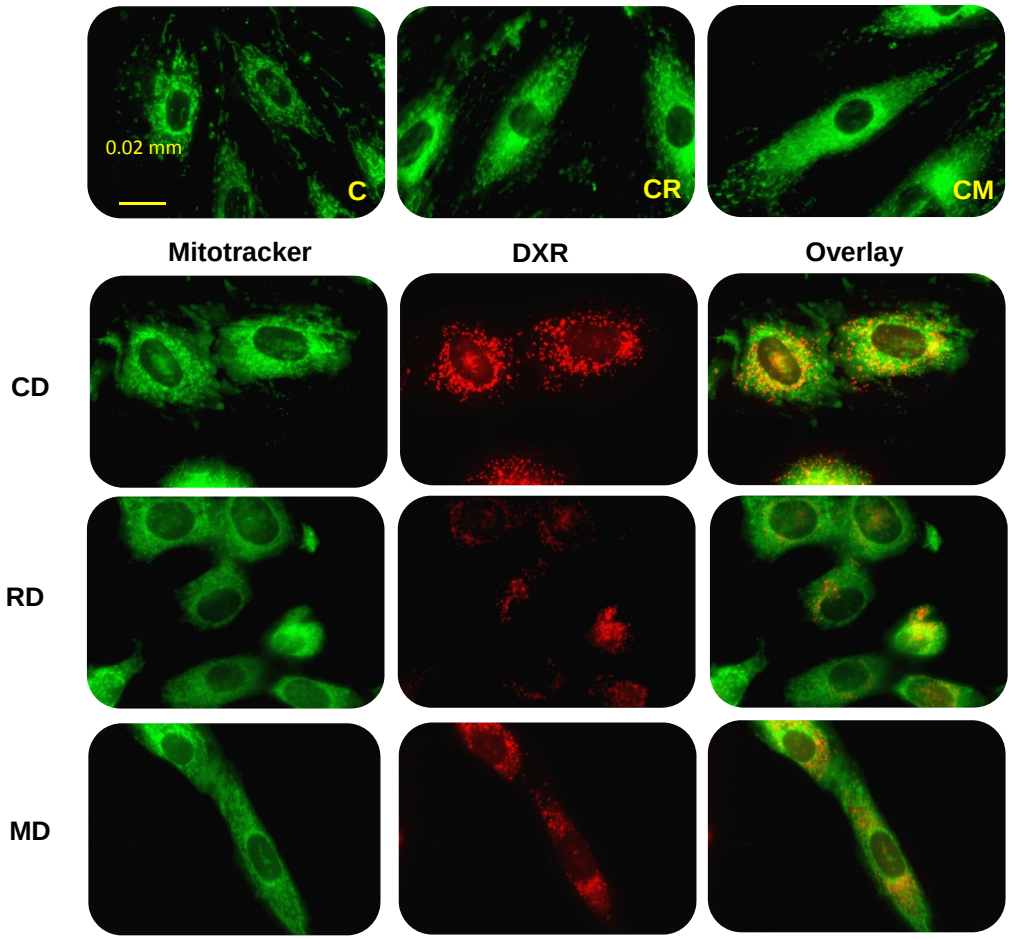

Figure 3.10.24: The effect of various treatment regimens on mitochondrial morphology and DXR localization in H_9C_2 myoblasts. H_9C_2 cells were stained with MitoTracker green (green) and DXR (red) and assessed using fluorescence microscopy ($n \geq 3$). Abbreviations - **C**: control; **CR**: rapamycin, **CM**: SiRNA (mTOR), **CD**: DXR, **RD**: rapamycin and DXR, **MD**: SiRNA (mTOR) and DXR. Magnification = 60X. Scale bar = 0.02 mm.

3.11: Discussion

This study attempted to explore a possible treatment strategy for controlling the overwhelming and harmful effects of DXR on myocardial cells. We have demonstrated that DXR-induced cell death as well as oxidative stress, mitochondrial dysfunction and ER stress could be ameliorated with rapamycin pre-treatment. These results thus indicate a prospective role for rapamycin against DXR-induced cardiotoxicity and highlights rapamycin as a plausible adjuvant therapy to counteract and improve the life-threatening impediment of DXR's actions in clinical practice.

DXR treatment induces cardiomyocyte death

The contribution of apoptosis in cardiotoxicity has previously been established. We have also shown that DXR is a potent inducer of apoptotic cell death (Figure 3.10.4). This is supported by various other researchers who have demonstrated that DXR-induced apoptosis can occur via various mechanisms which include oxidative stress, the dysregulation of apoptosis-related proteins [i.e.: p53, Akt/PKB (protein kinase B), ERKs (extracellular signal-regulated kinases), Bcl-2 (B-cell lymphoma 2 family)] and the dysregulation of transcription and co-activators [i.e.: GATA-4, NF-κB (nuclear factor-kappa B), NFAT (nuclear factor of activated T-cells), p300] (Kawamura *et al*, 2004; Kotamraju *et al*, 2000; Wang *et al*, 2001). Our results also demonstrated that apoptotic cell death could be attenuated by rapamycin treatment, indicating that increased autophagy plays a role in this model of acute DXR-induced cardiotoxicity. Apoptosis is not the only mechanism by which cardiomyocytes die, as we have also demonstrated that necrosis is induced in our model (Figure 3.10.5). Necrosis is typically characterized by the rupture of the cellular membrane, swelling of cytoplasmic organelles and ATP depletion (Zhang *et al*, 2009). This is in agreement with numerous other studies who have observed a similar phenomenon (Ikegami *et al*, 2007; Li *et al*, 2006; Riad *et al*, 2009). The pre-treatment strategy with rapamycin in this model also showed beneficial effects towards a decrease in necrotic cell death.

DXR inhibits autophagic activity

The available literature portrays autophagy as a process with a dual function, either being protective or detrimental depending on the particular cell type, the subcellular environment, the nature and intensity of the stimulus, as well as the levels of autophagy induced (Loos *et al*, 2011; Matsui *et al*, 2007; Kang *et al*, 2008; Eisenberg-Lerner *et al*, 2009). Therefore, the functional significance of autophagy was determined within this specific context. The clinically relevant dose of DXR (3 μM) (Liu *et al*, 2008) used in this study demonstrated a decrease in the activity of the autophagic pathway and autophagic flux as shown in the attenuation of LC-3 II (Figure 3.10.6) and p62 (Figure 3.10.7) accumulation respectively. In contrast, Kobayashi and co-workers (2010) demonstrated that DXR treatment is associated with elevated autophagy. This discrepancy can be due to three major differences in the studies: (i) neonatal cardiac myocytes were used versus our model of cardiac myoblasts; (ii) they have used a concentration of 1 μM DXR, we employed a concentration of 3 μM DXR; (iii) the duration of DXR treatment also differed: their treatment was for 18 hrs versus our treatment duration of 24 hrs. Our current results are also in conflict with the results obtained in the *ex vivo* study (Chapter 2) where we have demonstrated that DNR (daunorubicin)-induced cardiotoxicity is associated with an upregulation of autophagic activity. Interestingly, no changes in beclin-1 were observed in our model between the different groups (Figure 3.10.8) – this is supported by Matsui and co-workers who suggested that increased beclin-1 expression can be indicative of maladaptive autophagic activity (Matsui *et al*, 2007). It is thus clear that the type of model, duration of treatment as well the concentration of DXR used, play an important role in the cellular response of autophagy.

In order to further evaluate the role of autophagy in acute DXR-induced cardiotoxicity, we manipulated autophagic activity using both pharmacological and genetic methodologies. Our data indicates that the inhibition of autophagy by bafilomycin (10 nM) alone or in combination with DXR resulted in significant amplification of apoptosis (Figure 3.10.4) and necrosis (Figure 3.10.5). Conversely, initiation of autophagy by rapamycin (50 nM) treatment in combination with DXR significantly attenuated cell death. However, autophagy stimulation through siRNA

(mTOR) exacerbated cell death (Figure 3.10.22 and 3.10.23). These results demonstrate that the sensitization of H_9C_2 cells to upregulated autophagy via rapamycin treatment (and not by mTOR silencing) before DXR treatment promotes cardiomyocyte survival. Although it remains to be determined how rapamycin-induced autophagy attenuates DXR-induced cell death, our data suggests that this particular stimulus represents a feasible approach for diminishing acute DXR-induced cell death and thereby alleviating DXR-induced cardiotoxicity. These beneficial effects of rapamycin are also supported by Demidenko *et al*, 2008 who have shown that reduced mTOR signalling may prolong lifespan in different species.

Rapamycin counteracts DXR-induced oxidative stress

Oxidative stress due to uncontrolled ROS production is one the mechanisms responsible for DXR-induced cardiotoxicity. We have shown that the main source of DXR-induced ROS production in our model is predominantly the mitochondria (Figure 3.10.10**b**, **c**), which was also confirmed by several other researchers (Vander Heide *et al*, 2007; Schimmel *et al*, 2004 and Shan *et al*, 1996). Furthermore, the co-treatment of DXR with rapamycin effectively reduced mitochondrial ROS production, whereas the co-treatment of DXR with bafilomycin significantly enhanced mitochondrial ROS production, when compared to the group treated with DXR only (Figure 3.10.12). Our results are supported by Yuan and co-workers (2009) who have reported that the induction of autophagy protects myocytes against bacterial endotoxin lipopolysaccharide (LPS) toxicity through the amelioration of ROS production. The mechanism by which autophagy might suppress ROS production remains to be elucidated.

Numerous attempts have been made to augment myocardial antioxidant capacity in order to reduce DXR-induced cardiotoxicity (Kang *et al*, 2002; DeAtley *et al*, 1999; Dorr *et al*, 1996; Yen *et al*, 1996). Though these studies have successfully been able to reduce myocardial oxidative stress *in vitro* and *in vivo*, clinical trials have however demonstrated inadequate efficiency of antioxidant therapy (Ladas *et al*, 2004; Olson *et al*, 1990). For example, the study conducted by Kang *et al* (2002) illustrated that

the overexpression of catalase, a major antioxidant in the heart, prevents chronic DXR-induced cardiotoxicity. It was found that the applicable activities of catalase in the heart were ~60-100 fold higher, which is unlikely to be attained in the heart using pharmaceutical approaches. In addition, suitable methods to constantly maintain elevated activities of catalase in the heart are at present non-existent.

Mitochondrial morphology and function is preserved with rapamycin pre-treatment

Changes in mitochondrial morphology are believed to affect a variety of biological processes including respiration and apoptosis (Dimmer *et al*, 2006, Hausenloy *et al*, 2007). We have shown that mitochondria in the control and CR (control rapamycin) groups appeared to be elongated, tubular in structure and displayed an interconnected network. These characteristics are frequently identified in mitochondria undergoing fusion (Ong *et al*, 2010). In the presence of DXR (group CD), mitochondria also showed signs of abnormality indicative of mitochondrial fission whereas in group RD (rapamycin+doxorubicin), normal mitochondrial shape was maintained (Figure 3.10.13**a**). This characteristic morphology of the mitochondria described above in the rapamycin groups were also associated with improved cell viability (Figure 3.10.3) and mitochondrial function (Figure 3.10.14**b**). In the groups where autophagy was inhibited (CB and BD), mitochondria appeared to be shorter, fragmented and discontinuous, probably indicating mitochondrial fission (Ong *et al*, 2010).

Rapamycin prevents DXR nuclear entry

In terms of DXR localization, we showed that DXR is confined inside the nucleus (Figure 3.10.2) as well as within the mitochondria in the DXR treated group (Figure 3.10.13**a**, **b**). This phenomenon is also supported by Nicolay *et al* (1986) who indicated that mitochondria play a fundamental role in the action of AC-induced cardiotoxicity. We thus propose that DXR induces alterations to create mitochondria with abnormal morphology and function. Markers of autophagy in the DXR group also revealed a blockage of the autophagic flux, thus promoting “autophagic stress”. These cells are thus unable to remove dysfunctional mitochondria through

mitophagy (the removal of impaired mitochondria by a specialised section of the autophagic pathway which delivers mitochondria to the lysosome for degradation). Pharmaceutical inhibition of autophagy thus exacerbates the deleterious effects of DXR on cell viability, thereby promoting apoptosis and necrosis. On the other hand, pharmaceutical induction of autophagy with rapamycin triggered a rescue mechanism where dysfunctional DXR-containing mitochondria can be removed via mitophagy, enabling cell survival. Our results are further supported by the fact that co-treatment of DXR with rapamycin, prevented DXR nuclear entry, implicating that DXR in the mitochondria and the cytosol can be removed through mitophagy and autophagy. Bafilomycin treatment, however, allowed DXR nuclear entry, thereby promoting apoptosis.

Interestingly, genetic manipulation of the autophagic pathway with siRNA (mTOR) in the presence of DXR also appeared to preserve typical mitochondrial morphology and prevented DXR entry into the nucleus, similar to that observed with rapamycin treatment (Figure 3.10.24). However, this phenomenon did not result in protection of cells against DXR-induced cardiotoxicity (Figure 3.10.22 - 23), as was the case with rapamycin. This observation was unexpected since mTOR silencing also resulted in increased autophagy (Figure 3.10.21). We thus propose that the dynamic behaviour is an important parameter in the functional outcome, since rapamycin did not completely inhibit mTOR, while the silencing of mTOR completely abolished the mTOR signal. This might indicate that the residual mTOR activity is still required to limit over activation of the autophagic pathway which can induce autophagic cell death.

DXR-induced activation of the UPP in cardiac myoblasts

The activation of some components of the UPP, a major proteolytic pathway often associated with autophagy in proteinopathies (Zheng *et al*, 2009), have been shown to be elevated in a model of DNR-induced cardiotoxicity (Chapter 2). It is known that both these proteolytic pathways (autophagy and the UPP) are downregulated by the PI3-Kinase/Akt signalling pathway. Phosphorylation of FoxO proteins by Atk

promotes FoxO sequestration by 14-3-3 proteins in the cytoplasm leading to inhibition of their transcriptional functions (Tran *et al*, 2003). Dephosphorylation of FoxO leads to nuclear entry where it induces the expression of E_3 ubiquitin ligases, MuRF-1 (Figure 3.10.16) and MAFbx (Figure 3.10.17). The overall magnitude of ubiquitinated proteins were also elevated in this model of acute DXR-induced cardiotoxicity (Figure 3.10.18), thus suggesting that though different models were employed, increased activity of the UPP is a relevant event during AC-induced cardiotoxicity.

The activity of the proteasome on the other hand has previously been shown to be inhibited at higher concentrations (e.g. ≤ 5 μM) and upregulated at lower concentrations (0.1 – 5 μM) of DXR (Liu *et al*, 2008). We have shown that a concentration as low as 3 μM, is a potent inhibitor of the chymotrypsin-like activity of the proteasome (Figure 3.10.19). The mechanism by which DXR alters proteasome activity appears to be regulated by the amount of DXR molecules binding onto the proteasome (Fekete *et al*, 2005; Kiyomiya *et al*, 2002) which is also believed to be used as a transporter for nuclear translocation (Kiyomiya *et al*, 1998; Kiyomiya *et al*, 2002). This observed inhibition of the proteasome does not imply that proteolysis does not take place; it is likely that these proteins intended for degradation by the UPP are degraded by another pathway such as autophagy. Although rapamycin treatment is known to augment both protein ubiquitination and Akt signalling in pressure-overload hypertrophy (Harston *et al*, 2011), its use in this model (*in vitro*), in combination with DXR, decreased the already elevated protein ubiquitination status induced by DXR treatment.

ER stress acts as a survival mechanism during cardiotoxicity

ER stress induced by misfolded protein accumulation due to proteasome inhibition, overload and ERAD (Endoplasmic reticulum-associated protein degradation) failure has previously been implicated in ischemic and pressure overload cardiac diseases (Schroeder *et al*, 2005; Harding *et al*, 2002; Ogata *et al*, 2006). Our results indicate that ER stress, characterized by ER expansion in our model (Figure 3.10.20**a**) is a

phenomenon that occurs during DXR-induced cardiotoxicity. Although this phenomenon is often accompanied by the UPR (Unfolded protein response) and consequently autophagy upregulation (Ding *et al*, 2007), the UPR in this context was not measured. The upregulation of autophagy is believed to counteract ER expansion during the UPR. We also observed ER expansion in the cardiomyocytes treated with rapamycin alone, however this was attenuated to baseline levels with co-treatment of rapamycin and DXR. While the inhibition of autophagy with bafilomycin alone or in combination with DXR did not induce ER expansion, the inhibition of autophagy in this setting has been demonstrated to be detrimental. The ER is sensitive to changes in oxidative stress and the disruption of Ca^{2+} homeostasis, resulting in the liberation of Ca^{2+} from the ER and ultimately increasing cytosolic free Ca^{2+}. This was, however, not observed in our model of acute DXR-induced cardiotoxicity at the time-point we have investigated (see Appendix D).

In summary, this study clearly demonstrated the beneficial effects of rapamycin treatment in counteracting the detrimental effects of DXR-induced cardiotoxicity. This seemingly advantageous property is especially important as it has shown to be cardioprotective by reducing ROS production, preventing DXR nuclear translocation, maintaining typical mitochondrial morphology and improving mitochondrial function. Although these effects were not able to decrease protein degradation, it was not exacerbated by increased autophagy with rapamycin treatment either. This study also showed that DXR-induced ER stress could be attenuated by pre-treatment with rapamycin. Furthermore, our data support the notion that the clinical use of rapamycin possesses a high therapeutic index. Our findings warrant further investigations into this valuable phenomenon, and indicate the importance of future work focussing on cardiac specific control of autophagic flux in order to minimize DXR-induced cardiotoxicity.

References

1. Austin, R.C. 2009. The unfolded protein response in health and disease. *Antioxidant & Redox Signaling*. 11: 2279-2287
2. Azad, M.B., Chen, Y., Henson, E.S., Cizeau, J., McMillan-Ward, E., Israels, S.J., Gibson, S.B. 2008. Hypoxia induces autophagic cell death in apoptosis-competent cells through a mechanism involving BNIP3. *Autophagy*. 4: 195-204
3. Bradford, M.M. 1976. A rapid and sensitive method for quantitation of microgram quantities of protein utilizing the principle of protein-dye binding. *Annals of Biochemistry*. 71: 248-254
4. Cortes, E.P., Lutman, G., Wanka, J. et al. 1975. Adriamycin (NSC-123127) cardiotoxicity: a clinicopathologic correlation. *Cancer Chemotherapy Reports*. 6: 215-225
5. DeAtley, S.M., Adsenov, M.Y., Aksenova, M.V., Harris, B., Hadley, R., Harper, P.C., Carney, J.M., Butterfield, D.A. 1999. Antioxidants protect against reactive oxygen species associated with adriamycin-treated cardiomyocytes. *Cancer Letters*. 136: 41–46
6. Demidenko, Z.N., Blagosklonny, M.V. 2008. Growth stimulation leads to cellular senescence when the cell cycle is blocked. *Cell Cycle*. 7: 3355-3361
7. Dimmer, K.S., Scorrano, L. 2006. (De)constructing mitochondria: what for? *Physiology (Bathesda)*. 21: 233-241
8. Ding, W.-X., Ni, H.-M., Gao, W., Yoshimori, T., Stolz, D.-B., Ron, D., Yin, X.-M. 2007. Lining autophagy to ubiquitin-proteasome system is important for the regulation of endoplasmic reticulum stress and cell viability. *The American Journal of Pathology*. 171: 513-524
9. Dorr, R.T., Lagel, K., McLean, S. 1996. Cardioprotection of rat heart myocytes with amifostine (Ethyol) and its free thiol, WR-1065, in vitro. *European Journal of Cancer*. 32A:S21–S25
10. Eisenberg-Lerner, A., Bialik, S., Simon, H.U., Kimchi, A. 2009. *Cell Death & Differentiation*. 16: 966-957
11. Engelbrecht, A.-M., Mattheyse, M., Ellis, B., Loos, B., Thomas, M., Smith, R.M., Peters, S., Smith, C., Myburgh, K. 2007. Proanthocyanidin from grape

seeds inactivates the PI3-kinase/PKB pathway and induces apoptosis in a colon cancer cell line. *Cancer Letters*. 258: 144-153

12. Fekete, M.R., McBride, W.H., Pajonk, F. 2005. Anthracyclines, proteasome activity and multi-drug-resistance. *BioMed Central Cancer*. 5: 114
13. Festjens, N., Vanden Berghe, T., Vandenabeele, P. 2006. Necrosis, a well-orchestrated form of cell demise: Signalling cascades, important mediators and concominant immune response. *Biochimica et Biophysica Acta*. 1757:1371-1387
14. Gomez, L.A, Alekseev, A.E., Aleksandrova, L.A., Brady, P.A., Terzic, A. 1997. Use of MTT assay in adult ventricular cardiomyocytes to assess viability. Effects of adenosine and potassium on cellular survival. *Journal of Molecular and Cellular Cardiology*. 29: 1255-1266
15. Gottlieb, R.A., Finley, K.D., Mentzer Jr, R.M. 2009. Cardioprotection requires taking out the trash. *Basic Research in Cardiology*. 104: 1699-180
16. Harding, H.P., Calfon, M., Urano, F., Novoa, I., Ron, D. 2002. Transcriptional and translational control in the mammalian unfolded protein response. *Annual Review of Cell and Developmental Biology*. 18: 575-599
17. Harston, R.K., McKillop, J.C., Moschella, P.C., Van Laer, A., Quinones, L.S., Baicu, C.F., Balasubramanian, S., Zile, M.R., Kuppuswamy, D. 2011. Rapamycin treatment augments both protein ubiquitination and Akt activation in pressure-overload rat myocardium. *American Journal of Physiology – Heart and Circulatory Physiology*. 300: H1696-H1706
18. Hausenloy, D.J., Scorrano, L. 2007. Targeting cell death. *Clinical Pharmacology & Therapeutics*. 82: 370-373
19. Hausleiter, J., Kastrsti, A., Mehilli, J., Vogesser, M., Zohlnhöfer, D., Schühlen, H., Goos, C., Pache, J., Dotzer, F., Pogatsa-Murray, G., Dirschinger, J., Heemann, U., Schömig, A. 2004. Randomized, double-blind, placebo-controlled trial of oral sirolimus for restenosis in patients with in-stent restenosis: the Oral Sirolimus to Inhibit Recurrent In-stent Stenosis (OSIRIS) trial. *Circulation*. 110: 790-795
20. Ikegami, F., Fukazawa, R., Kanbe, M., Watanabe, M., Abe, M., Watanabe, M., Kamisago, M., Hajikano, M., Katsube, Y., Ogawa, S. 2007. Edaravone, a potent free radical scavenger, prevents anthracycline-induced myocardial cell death. *Circulation Journal*. 71: 1815-1820

21. Kajustra, J.W., Cheng, W., Reiss, K., Clark, W.A., Sonneblick, E.H., Krajewski, S., Reed, J.C., Olivetti, G., Anversa, P. 1996. Apoptotic and necrotic myocyte cell deaths are independent contributing variables of infarct size in rats. *Laboratory Investigation*. 79: 949-956
22. Kang, Y.J., Chen, Y., Epstein, P.N. 1996. Suppression of doxorubicin cardiotoxicity by overexpression of catalase in the heart of transgenic mice. *Journal of Biological Chemistry. 1996*. 271:12610–12616
23. Kang, C., Avery, L. 2008. To be or not to be, the level of autophagy is the question: Dual roles of autophagy in the survival response to starvation *Autophagy*. 4: 82-84
24. Kang, Y.J., Sun, X., Chen, Y., Zhou, Z. 2002. Inhibition of doxorubicin chronic toxicity in catalase-overexpressing transgenic mouse hearts. *Chemical Research in Toxicology*. 15: 1-6
25. Kawamura, T., Hasegawa, K., Morimoto, T., Iwai-Kanai, E., Miyamoto, S., Kawase, Y., Ono, K., Wada, H., Akao, M., Kita, T. 2004. Expression of p300 protects myocytes from apoptosis in vivo. *Biochemistry and Biophysical Research Communications*. 315: 733-738
26. Kitakaze, M., Fong, M., Yoshitake, M., Minamino, T., Node, K., Okuyama, Y., Terade, N., Kambayashi, T., Hori, M. 1997. Vesnarinone inhibits adenosine uptake in endothelial cells, smooth muscle cells and monocytes, and mediates cytoprotection. *Journal of Molecular and Cellular Cardiology*. 29: 3413-3417
27. Kiyomiya, K., Kurebe, M., Nakagawa, H., Matsuo, S. 2002. The role of the proteasome in apoptosis induced by anthracycline anticancer agents. *International Journal of Oncology*. 20: 1205-1209
28. Kiyomiya, K., Matsuo, S., Kurebe, M. 1998. Proteasome is a carrier to translocate doxorubicin from cytoplasm into nucleus. *Life Science*. 62: 1853-1860
29. Kiyomiya, K., Satoh, J., Horie, H., Kurebe, M., Nakagawa, H., Matsuo, S. 2002. Correlation between nuclear action of anthracycline anticancer agents and their binding affinity to the proteasome. *International Journal of Oncology*. 21: 1081-1085
30. Kobayashi, S., Volden, P., Timm, D., Mao, K., Xu, X., Liang, Q. 2010. Transcription factor GATA4 inhibits doxorubicin-induced autophagy. *Journal of Biological Chemistry*. 285: 793-804

31. Kotamraju, S., Konorev, E.A., Joseph, J., Kalyanaraman, B. 2000. Doxorubicin-induced apoptosis in endothelial cells and cardiomyocytes is ameliorated by nitrone spin traps and ebselen. Role of reactive and nitrogen species. *Journal of Biological Chemistry*. 275: 33585-33592
32. Kumar, D., Kirshenbaum, I.A., Li, T., Danelisen, I., Singal, P.K. 2001. Apoptosis in Adriamycin Cardiomyopathy and Its Modulation by Probucol *Antioxidant & Redox Signaling*. 3: 135-145
33. Lacerda, L., Smith, R.M., Opie, L., Lecour, S. 2006. TNF-α-induced cytoprotection requires the production of free radicals within mitochondria in C2C12 myotubes. *Life Sciences*. 79: 2194-2201
34. Ladas, E.J., Jacobson, J.S., Kennedy, D.D., Teel, K., Fleischauer, A., Kelly, K.M. 2004. Antioxidants and Cancer Therapy: A Systematic Review. *Journal of Clinical Oncology*. 22: 517-528
35. Lefrak, E.A., Pitha, J., Rosenheim, S., O'Bryan, B.M., Burgess, M.A., Gottlieb, J.A. 1975. Adriamycin (NSC 123127) cardiomyopathy. *Cancer Chemotherapy Reports*. 6: 203-208
36. Levine, B., Yuan, J. 2005. Autophagy in cell death: an innocent convict? *Journal of Clinical Investigation*. 115: 2679-2688
37. Li, K., Sung, R.Y., Huang, W.Z., Yang, M., Pong, N.H., Lee, S.M., Chan, W.Y., Zhao, H., To, M.Y., Fok, T.F., Li, C.K., Wong, Y.O., Ng, P.C. 2006. Thrombopoietin protects against in vitro and in vivo cardiotoxicity induced by doxorubicin. *Circulation*. 113: 2211-2220
38. Liu, J., Zheng, H., Tang, M., Ryu, Y.-C., Wang, X. 2008. A therapeutic dose of doxorubicin activates ubiquitin-proteasome system-mediated proteolysis by acting on both the ubiquitination apparatus and proteasome. *American Journal of Physiology-Heart and Circulatory Physiology*. 295: H2541-H2550
39. Loos, B., Lochner, A., Engelbrecht, A.-M. 2011. Autophagy in heart disease: A strong hypothesis for an untouched metabolic reserve. *Medical Hypotheses*. 77: 52-57
40. Loos, B., Genade, S., Ellis, B., Lochner, A., Engelbrecht, A.-M. 2011. At the core of survival: Autophagy delays the onset of both apoptotic and necrotic cell death in a model of ischemic cell injury. *Experimental Cell Research*. 317: 1437-1453

41. Matsui, Y., Takagi, H., Qu, X., Abdellatif, M., Sakoda, H., Asano, T., Levine, B., Sadoshima, J. 2007. Distinct Roles of Autophagy in the Heart During Ischemia and Reperfusion: Roles of AMP-Activated Protein Kinase and Beclin 1 in Mediating Autophagy. *Circulation Research*. 100: 914-922
42. McMullen, J.R., Sherwood, M.C., Tarnavski, O., Zhang, L., Dorfman, A.L., Shioi, T., Izumo, S. 2004. Inhibition of mTOR signaling with rapamycin regresses established cardiac hypertrophy induced by pressure overload. *Circulation*. 109: 3050-3055
43. Minow, R.A., Benjamin, R.S., Gottllieb, J.A. 1975. Adriamycin (NSC-123127) cardiomyopathy – an overview with determination of risk factors. *Cancer Chemotherapy Reports*. 6: 185-201
44. Minow, R.A., Benjamin, R.S., Lee, E.T., Gottllieb, J.A. 1977. Adriamycin cardiomyopathy – risk factors. *Cancer*. 39: 1397-1402
45. Nakai, A., Yamaguchi, O., Takeda, T., Higuchi, Y., Hikoso, S., Taniike, M., Omiya, S., Mizote, I., Matsumura, Y., Asahi, M., Nishida, K., Hori, M., Mizushima, N., Otsu, K. 2007. The role of autophagy in cardiomyocytes in the basal state and in response to hemodynamic stress. *Nature Medicine*. 13: 619-624
46. Namba, R., Young, L.J.T., Abbey, C.A., Kim, L., Damonte, P., Borowsky, A.D., Qi, J., Tepper, C.G., MacLeod, C., Cardiff, R.D., Gregg, J.P. 2006. Rapamycin inhibits growth of premalignant and malignant mammary lesions in a mouse model of ductal carcinoma *in situ*. *Clinical Cancer Research*. 12: 2613-2621
47. Nicolay, K., Fok, J.J., Voorhout, W., Post, J.A., de Kruijff, B. 1986. Cytofluorescence detection of adriamycin-mitochondria interactions in isolated. Perfused rat heart. *Biochimica et Biophysica Acta*. 887: 35–41
48. Ogata, M., Hino, S., Saito, A., Morikawa, K., Kondo, S., Kanemoto, S., Murakami, T., Taniguchi, M., Tanii, I., Yoshinaga, K., Shiosaka, S., Hammarback, J.A., Urano, F., Imaizumi, K. 2006. Autophagy is activated for cell survival after endoplasmic reticulum stress. *Molecular and Cell Biology*. 26: 9220-9231
49. Olson, R.D., Mushlin, P.S. 1990. Doxorubicin cardiotoxicity: analysis of prevailing hypotheses. *FASEB Journal*. 4: 3076-3086

50. Ong, S.-B., Hausenloy, D.J. 2010. Mitochondrial morphology and cardiovascular disease. *Cardiovascular Research*. 88: 16-29
51. Passmore, L.A., Barford, D. 2004. Getting into position: the catalytic mechanisms of protein ubiquitylation. *Biochemical Journal*. 379: 513-525
52. Petit, T. 2004. Anthracycline-induced cardiotoxicity. *Bulletin du Cancer*. 91: 159-165
53. Rasheva, V.I., Domingos, P.M. 2009. Cellular responses to endoplasmic stress and apoptosis. *Apoptosis*. 14: 996-1007
54. Riad, A., Bien, S., Westermann, D., Becher, P.M., Loya, K., Landmesser, U., Kroemer, H.K., Schultheiss, H.P., Tschöpe, C. 2009. Pretreatment with statin attenuates the cardiotoxicity of doxorubicin in mice. *Cancer Research*. 69: 695-699
55. Rothermel, B.A., Hill, J.A. 2008. Autophagy in load-induced heart disease. *Circulation Research*. 103: 1363-1369
56. Schimmel, K.J.M., Richel, D.J., van den Brink, R.B.A., Guchelaar, H.-J. 2004. Cardiotoxicity of cytotoxic drugs. *Cancer Treatment Reviews*. 30: 181-191
57. Schroder, M., Kaufman, R.J. 2005 The mammalian unfolded protein response. *Annual Reviews of Biochemistry*. 74: 739-789
58. Shan, K., Lincoff, M., Young, J.B. 1996. Anthracycline-induced cardiotoxicity. *Annals of Internal Medicine*. 125: 47-58
59. Shioi, T., McMullen, J.R., Tarnavski, O., Converso, K., Sherwood, M.C., Manning, W.J., Izumo, S. 2003. Rapamycin attenuates load-induced cardiac hypertrophy in mice. *Circulation*. 107: 1664-1670
60. Singal, P.K., Derally, C.M.R., Weinberg, L.E. 1987. Subcellular effects of Adriamycin in the heart: a concise review. *Journal of Molecular and Cellular Cardiology*. 19: 817-828
61. Singal, P.K., Siveski-Illiskovic, N., Hill, M., Thomas, T.P., Li, T. 1995. Combination therapy with probucol prevents Adriamycin-induced cardiomyopathy. *Journal of Molecular and Cellular Cardiology*. 27: 1055-1063
62. Sun, X., Zhou, Z., Kang, Y.P. 2001. Attenuation of Doxorubicin Chronic Toxicity in Metallothionein-overexpressing Transgenic Mouse Heart. *Cancer Research*. 61: 3382-3387

63. Tran, H., Brunet, A., Griffith, E.C., Greenberg, M.E. 2003. The many forks in FOXO's road. *Science's STKE: signal transduction knowledge environment*.172: RE5
64. Vander Heide, R.S., L'Ecuyer, T.J. 2007. Molecular basis of anthracycline-induced cardiotoxicity. *Heart and Metabolism*. 35: 1-4
65. Wang, G.W., Klein, J.B., Kang, Y.J. 2001. Metallothionein inhibits doxorubicin-induced mitochondrial cytochrome c release and caspase-3 activation in cardiomyocytes. *Journal of Pharmacology and Experimental Therapeutics*. 298: 461-468, J.W., Patterson, C. 2010. Sent to destroy: The ubiquitin proteasome system regulates cell signalling and protein quality control in cardiovascular development and disease. *Circulation Research*. 106: 643-478
66. Willis, M.S., Townley-Tilson, W.H.D., Kang, E.Y., Homeisterr
67. Wu, Q., Kuguchi, K., Kawanoto, T., Ajiki, T., Traag, J., Carbajal, S., Ruffino, L., Thames, H., Wistuba, I., Thomas, M., Vasquez, K.M., DiGiovanni, J. 2007. Therapeutic effect of rapamycin on gallbladder cancer in a transgenic mouse model. *Cancer Research*. 67: 3794-3800
68. Yan, L., Vatner, D.E., Kim, S.J., Ge, H., Masurekar, M., Massaover, W.H., Yang, G., Matsui, Y., Sadoshima, J., Vatner, S.F. 2005. Autophagy in chronically ischemic myocardium. *Proceedings of the National Academy Sciences USA*. 102: 13807-13812
69. Yen, H.C., Oberley, T.D., Vichitbandha, S., Ho, Y.S., St Clair, D.K. 1996. The protective role of manganese superoxide dismutase against adriamycin-induced acute cardiac toxicity in transgenic mice. *Journal of Clinical Investigation*. 98:1253–1260
70. Yuan, H., Perry, C.N., Huang, C., Ewasi-Kanai, E., Carreira, R.S., Glembotski, C.C., Gottlieb, R.A. 2009. LPS-induced autophagy is mediated by oxidative signaling in cardiomyocytes and is associated with cytoprotection. *American Journal of Physiology: Heart and Circulatory Physiology*. 296: H470-H479
71. Zhang, Y.-W., Shi, J., Li, Y.-J., Wei, L. 2009. Cardiomyocyte death in doxorubicin-induced cardiotoxicity. *Archivum Immunologiae et Therapia Experimentalis*. 57: 435-445
72. Zhao, J., Brault, J.J., Schild, A., Cao, P., Sandri, M., Schiaffino, S., Lecker, S.H., Goldberg, A.L. 2007. Fox-O3 coordinately activates protein degradation

by the autophagic/lysosomal and proteasomal pathways in atrophying muscle cells. *Cell Metabolism*. 6: 472-483

73. Zheng, Q., Li, J., Wang, X. 2009. Interplay between the ubiquitin-proteasome system and autophagy in proteinopathies. *International Journal of Physiology, Pathophysiology and Pharmacology*.1: 127-142

Chapter 4

In vivo model

4.1: Introduction

Animal models have been widely utilized to study the molecular basis underlying doxorubicin-induced cardiotoxicity and to develop strategies to facilitate cardioprotection. However, most of the animal models utilized only evaluated the cardiotoxic effects of doxorubicin, without considering the effects of a growing tumour in the animal. Our aim was thus to establish a novel mammary tumour model in GFP-LC3 transgenic mice in which the effects of doxorubicin with adjuvant rapamycin treatment could be analysed with respect to cardiac toxicity and simultaneously assessing its effects on tumour size.

Doxorubicin is an anthracycline that inhibits topoisomerase II activity, intercalates with DNA base pairs and decreases DNA and RNA polymerase activity. The therapeutic activity of doxorubicin is most effective against highly proliferative tumours (Singal *et al*, 1997). Much evidence indicates that the cardiotoxic effects induced by doxorubicin are complex and eventually lead to increased apoptosis (Kalyanaraman *et al*, 2002).

Rapamycin is a lipophilic, antifungal antibiotic isolated from a strain of *Streptomyces hygroscopicus* indigenous to Easter Island (Vezina *et al*, 1975). Rapamycin is also a well-established inducing agent of autophagy (Noda & Ohsumi, 1998) through its ability to inhibit mTOR (mammalian target of rapamycin). The mTOR pathway involves two functional complexes: mTORC1 consisting of mTOR, raptor (regulatory associated protein of mTOR) and G*β*L (G-protein *β*-subunit like protein); and mTOR2 comprising mTOR, rictor and G*β*L (Sarbassov et al., 2005). Rapamycin forms a complex with the immunophilin FK506-binding protein-12 (FKBP-12), which then stabilizes the raptor-mTOR association and inhibits the kinase activity of mTORC1 (Kim *et al*, 2002). This selective inhibitory effect of rapamycin on mTORC1 signalling

events likely contributes to the variations in cellular sensitivity to rapamycin and the differential effects observed in clinical settings.

In this study a murine mammary adenocarcinoma cell line (E0771), originally isolated from an immune-competent C57BL6 mouse, was utilized. This cell line is well established and shows a well characterized metastatic potential. In order to establish a model where autophagy could be assessed in the heart during doxorubicin treatment with adjuvant rapamycin treatment, a transgenic mouse strain systemically expressing GFP fused to LC3 (GFP-LC3 mouse) was used as a recipient in conjunction with E0771 murine mammary adenocarcinoma cells. The GFP-LC3 mice were originally generated to assess autophagosomes *in vivo* (Mizushima *et al*, 2004). Using these mice, autophagy can be monitored as GFP-LC3 becomes incorporated into the autophagosomal membrane. Xenographs of cancer cell lines usually require the use of immune compromised animals (Medina, 2007). As GFP-LC3 mice are crossed with C57B/6N Crj mice, it was therefore unclear if E0771 cells could be used to successfully establish tumours in a mouse model where the immune system was not compromised.

4.2: Materials and Methods

4.2.1: Animal model and treatment

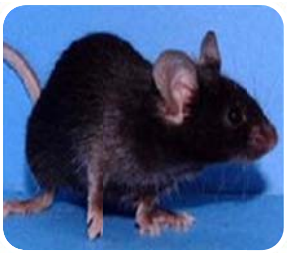

All animal protocols were carried out according to the guidelines for the care and use of laboratory animals implemented at Stellenbosch University (Reference number: 2009B02004). Institutional and international ethical guidelines were applied with respect to the handling of the experimental animals. Eight week old GFP-LC3 female mice (Strain: RBRC00806), kindly donated by Noboru Mizushima, (Department of Cell Biology, National Institute for Basic Biology, Okazaki, Japan) were used in this study. Mice were maintained on a standard rat chow (SRC) diet and tap water *ad libitum* before being submitted to the experimental protocol. Adapted from Ewans *et al* (2006) mice were inoculated on the left pad of the fourth mammary gland with 200 µl of $2.5x10^5$ E0771 cells suspended in Hanks Balanced Salt Solution, using a 23-gauge needle. Mice were injected with cell suspensions on day 0 and small tumours

were evident by days 12-14 post-injection. The tumours grew to reach an approximate volume of 220 mm^3 by day 30. Tumour size was monitored every second day by making measurements in two perpendicular dimensions parallel to the ventral surface of the mice using a digital calliper. The body weight was monitored twice weekly. Tumours grown in GFP-LC3 mice using this protocol generally grew reproducibly. On day 30, mice were divided into four groups which included a Control group, Rapamycin group, DXR group and Rapamycin and DXR group (Figure 4.1.1). The mice received treatment on the days as indicated in Figure 4.1.2. The rapamycin group received 1 injection [4 mg/kg, intraperitoneal (i.p.)] of rapamycin; the DXR group received a total of 2 injections of DXR as described by Zhu *et al* (2009). In brief, 10 mg/kg (i.p.) DXR was administered at 3 day intervals with a cumulative dose of 20 mg/kg. The Rapamycin and DXR group received a combination of 1 dose rapamycin and 2 doses of DXR, at 3 day intervals (Figure 4.1.2). After the completion of the experimental protocol, mice were sacrificed and their hearts rapidly excised. The hearts were sectioned horizontally to allow freeze clamping for biochemical as well as histological analysis.

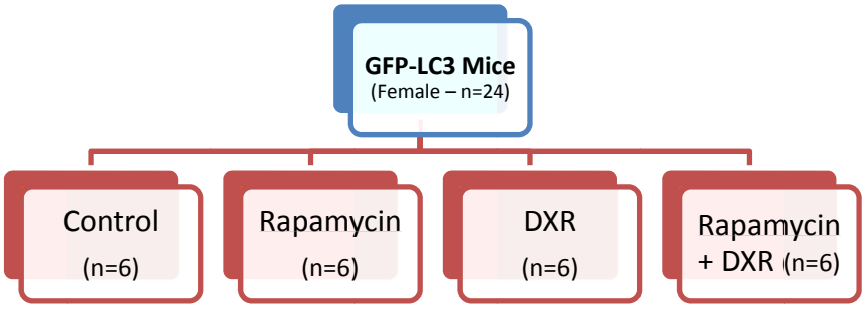

Figure 4.1.1: *In vivo* experimental groups utilized throughout the study

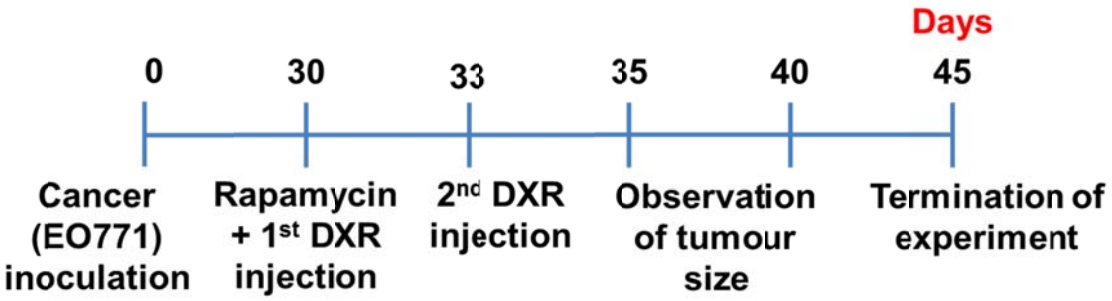

Figure 4.1.2: *In vivo* experimental protocol. All animals displayed visible tumours by days 12-14 and were submitted to the above injection protocol

4.3: Western Blotting Analysis

4.3.1: Protein extraction

Myocardial tissue protein was extracted with 1000 µl ice cold RIPA (Radio immunoprecipitation assay)/lysis buffer containing (in mM): tri-(hydroxylmethyl)-aminomethane (TRIS)-HCl 50, NP-40 1%, Na-Deoxycholate 0.25%, EDTA (Ethylenediaminetetraacetic acid) 1, sodium fluoride (NaF) 1, soybean trypsin inhibitor (SBTI) 4 µg/ml, phenylmethyl sulphonyl fluoride (PMSF) 1, Benzamidine 1, leupeptin 1µg/ml and Triton X-100 1000 µl. Tissues were homogenized and centrifuged at 8000 rpm at 4 ºC for 10 min to remove tissue debris.

4.3.2: Protein quantification using the Bradford technique

The rapid and sensitive Bradford method for the quantitation of microgram quantities of protein utilizing the principle of protein-dye binding was employed (Bradford, 1976). This technique involves the binding of Coomassie Brilliant Blue G-250 to protein which causes a shift in the absorption maximum of the reagent from 465 nm to 595 nm. The increase in absorption at 595 nm was monitored spectrophotometrically (Cecil CE 2021-2000 Series, Lasec). For the establishment of a standard curve, a protein dilution series was set up, pipetting 2 µg, 4 µg, 8 µg, 12 µg, 16 µg and 20 µg albumin bovine serum dissolved in PBS (BSA, 200 µg/ml) and 900 µl Bradford reagent into eppendorf tubes and adjusted to 1000 µl with deionized water. Sample protein concentrations were determined through pipetting 5 µl of the

sample supernatant with 900 µl Bradford reagent and adjusted to 1000 µl with 95 µl deionized water. Samples were vortexed, incubated for 5 min at room temperature and the absorbance was measured at a wavelength of 595 nm against a reagent blank. The weight of protein in µg/ml was plotted against the absorbance and the protein concentration was determined.

4.3.3: Sodium-dodecyl-sulfate-polyacrylamide gel electrophoresis (SDS-PAGE)

Laemmli sample buffer was prepared, using (in M): TRIS 0.5, pH 6.8, 10% SDS, 2.5 ml glycerol, 0.2 ml 0.5% bromophenol blue in deionized water. A volume of 150 µl mercaptoethanol was then added to 850 µl sample buffer. Tissue lysates were boiled for 5 min and shortly spun in a microcentrifuge. Total protein (50 µg) was separated by 8%, 10% or 16% sodium-dodecyl sulfatepolyacrylamide- gel-electrophoresis (SDS-PAGE) and a 4% stacking gel.

4.3.4: Transfer, Incubation and Visualization

After completion of protein separation, proteins were transferred to a PVDF membrane (ImmobilonTM P, Millipore). Membranes were routinely stained with Ponceau Red for visualisation of proteins. Non-specific binding sites were blocked with 5% fat-free milk in TRIS-buffered saline-Tween (TBS-T) and then incubated with the primary antibodies that recognise cleaved-caspase-3, cleaved-PARP, Beclin-1, p62/SQSTM1, LC-3, phospho-specific and total FoxO3, MAFbx, MuRF-1, phospho-specific and total mTOR, ubiquitin and β-Actin. Membranes were subsequently washed with large volumes of TBS-T (3 x 5 min) and the immobilized antibody conjugated with diluted horseradish peroxidase-labelled secondary antibody (Amersham LIFE SCIENCE). After thorough washing with TBS-T, membranes were incubated with ECL^{TM} detection reagents and exposed to autoradiography film (Hyperfilm ECL, RPN 2103) to detect light emission through a non-radioactive method (ECL^{TM} Western blotting). Films were densitometrically analysed (UN-SCAN-IT, Silkscience version 5.1) and phosphorylated protein values were corrected for minor differences in protein loading if required.

4.4: Histology

4.4.1: Fixation and Sectioning

Cardiac tissue for sectioning and staining was placed on a piece of cork, covered in tissue freezing medium (LEICA OCT Compound, SMM instruments, 14020108926), placed in ice cold isopentane (Merck, 1071771000) and frozen in liquid nitrogen. Sectioning was then performed on the RM125 RT microtome (Leica CM 100), generating 8 µm sections which were collected on glass slides.

4.4.2: GFP Fluorescence Microscopy

Image acquisition was performed on an Olympus Cell^R system attached to an IX 81 inverted fluorescence microscope equipped with an F-view-II cooled CCD camera (Soft Imaging Systems). Using a Xenon-Arc burner (Olympus Biosystems GMBH) as light source, images were acquired using the GFP excitation/emission filters.

4.4.3: Haematoxylin Eosin (H & E) stain

In order to assess whether DXR treatment induced any structural damage within the myocardium, the haematoxylin and eosin (H & E) stain was utilized. This technique is a widely used staining method in histology. It involves application of the basic dye haematoxylin, colouring basophilic structures with blue-purple hue, and alcohol-based acidic eosin Y, colouring eosinophilic structures bright pink. The basophilic structures contain nucleic acids, such as ribosomes and the chromatin-rich cell nucleus as well as cytoplasmic regions rich in RNA. The eosinophilic structures are generally composed of intracellular or extracellular proteins.

Sections were hydrated using a xylene and ethanol dilution range as follows: xylene, 100%, 95% and 70% ethanol as well as distilled water (dH_2O). Following this, sections were stained using Harris haematoxylin, acid alcohol, Scott's tap water and eosin. The sections were then rehydrated as follows: 70%, 95%, 100% ethanol and xylene. Sections were mounted onto microscope slides and visualized using a Nikon

Eclipse E 400 microscope fitted with a Nikon DMX 1200 digital camera, using a 40X objective. Ten random areas of interest were acquired for each group in order to determine cellular cross-sectional area and visualisation of structural damage. A minimum of 150 cardiac muscle cells (15 from each image) were measured in μm^2 by means of selecting the sarcolemma as the region of interest and an average was then calculated.

4.5: Statistical Analysis

All data are presented as mean ± SEM. Comparisons between the groups were performed by the one-way analysis of variance (ANOVA) followed by Bonferroni's post hoc test conducted with the statistical program GraphPad Prism, version 5.0 (GraphPad Inc.). A value of $p \leq 0.05$ was considered statistically significant.

4.6: Results

4.6.1: DXR and Rapa-DXR treatment attenuated tumour growth (Figure 4.1.3)

Tumour size was measured every second day as described previously. No significant differences were observed in the volume of E0771 tumours in GFP-LC3 mice between groups prior to treatment interventions. DXR however decreased tumour volume when compared to the control. A similar response was observed in the combination of rapamycin and DXR where tumour volume also decreased (although at a slower rate) when compared to DXR treatment alone. Conversely rapamycin treatment alone did not change tumour volume. These observations were however statistically insignificant.

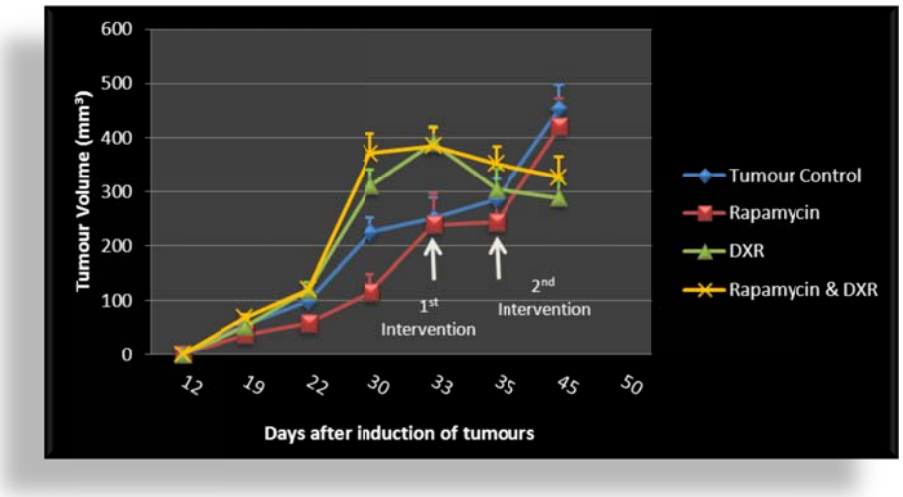

Figure 4.1.3: The effect of different treatment regimens on tumour growth. Tumour size was assessed immediately after occurrence of tumours (± 12 days after tumour injection) and throughout the study. Day 30 represents the last day tumour size was assessed before intervention treatment was initiated. Animals were treated with either rapamycin (4 mg/kg) or DXR (10 mg/kg) or a combination of both drugs. 1st intervention: rapamycin and DXR; 2nd intervention: DXR only. n = 6

4.6.2: Rapa-DXR treatment increased survival of tumour bearing GFP-LC3 mice (Figure 4.1.4)

42% of the animals died before the termination of the experiment. The first death occurred 3 days (Day 30) before treatment began in the rapamycin group as a result of cancer metastasis. All the animals (100%) survived in the tumour control group, 83% in the rapamycin group, 50% in the rapamycin & DXR group and none in the DXR group. As mice presented with 100% survival in the tumour control group, 50% of those animals were treated with DXR to compensate for the animals lost in the DXR group.

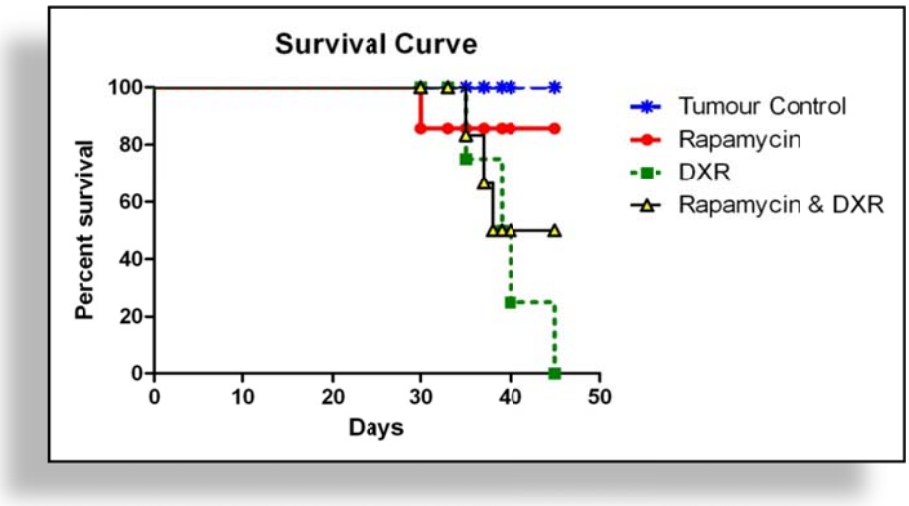

Figure 4.1.4: The effect of different treatment regimens on the survival rate of experimental animals. Day 30 represents the last day tumour size was assessed before intervention treatment was initiated. Animals were treated with either rapamycin (4 mg/kg) on day 33 or DXR (10 mg/kg) on day 33 and day 35 or a combination of both drugs.

4.6.3: DXR treatment reduces body weight of tumour bearing mice (Figure 4.1.5)

In order to determine whether weight loss is associated with acute DXR-induced cardiotoxicity, animals were weighed throughout the duration of the experimental protocol (before and after treatment). Body weight significantly decreased in the DXR group (CD) [19.64 ± 0.40 g ($p < 0.05$)] when compared to the control. Additionally, the heart weights of the animals were also assessed. A trend towards a decrease was observed in group CD, indicating a potential similar scenario to that of the body weight; however no significant differences were observed (Figure 4.1.6).

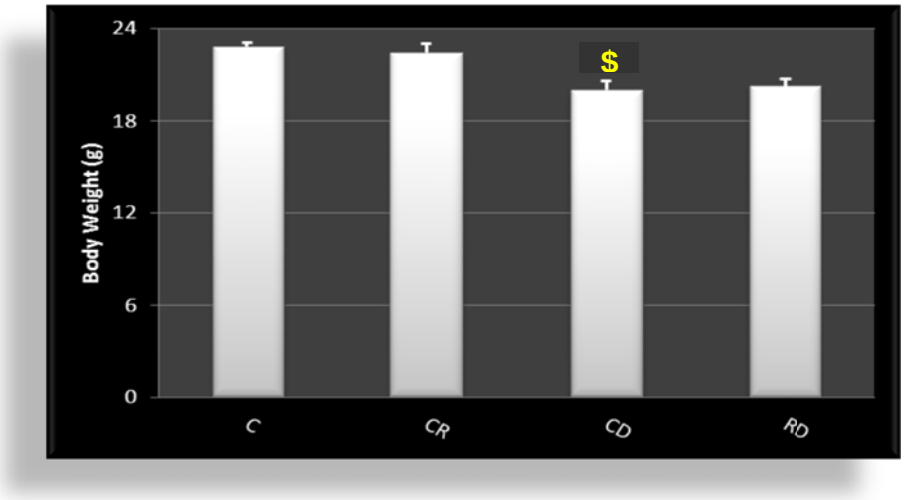

Figure 4.1.5: Effect of different treatment regimens on the weight of experimental animals. Animals were treated with either rapamycin (4 mg/kg) or DXR (10 mg/kg) or a combination of both drugs. A single dose of rapamycin and two doses of DXR were injected into the animals. Results are presented as mean ± SEM (n = 3). $^{\$}P < 0.05$ versus control. Abbreviations - **C**: control, **CR**: rapamycin, **CD**: DXR, **RD**: rapamycin and DXR.

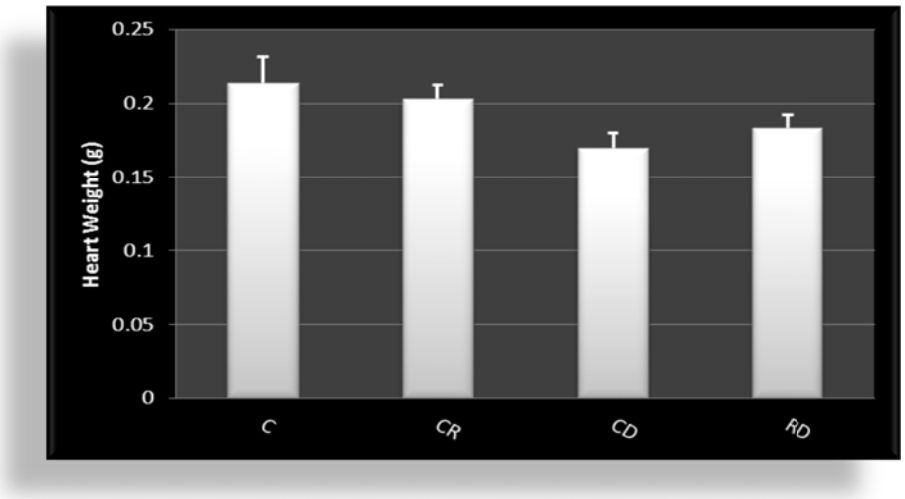

Figure 4.1.6: Effect of different treatment regimens on heart weight of experimental animals. Animals were treated with either rapamycin (4 mg/kg) or DXR (10 mg/kg) or a combination of both drugs. A single dose of rapamycin and two doses of DXR were injected into the animals. Results are presented as mean ± SEM (n = 3). Abbreviations - **C**: control, **CR**: rapamycin, **CD**: DXR, **RD**: rapamycin and DXR.

4.6.4: DXR induces apoptosis in the hearts of tumour bearing mice (Figure 4.1.7 - 8)

Rapamycin treatment (CR) significantly reduced cleaved caspase-3 levels [82.21 ± 3.05% ($p < 0.05$)] when compared to the control (100%). In contrast, treatment with DXR (CD) significantly increased cleaved caspase-3 levels [115.20 ± 2.03% ($p < 0.05$)] when compared to the control whereas treatment with both rapamycin and DXR (RD) reduced caspase-3 activity significantly [92.78 ± 4.27 % ($p < 0.05$)] when compared to DXR treatment alone (115.20 ± 2.03%). Assessment of cleaved-PARP also demonstrated elevated levels in DXR treated animals [111.40 ± 1.03% ($p < 0.05$)] when compared to the control (100%). Although a trend towards a decrease in cleaved-PARP levels was observed in the combination group (RD), no significance was obtained in comparison to DXR treatment alone.

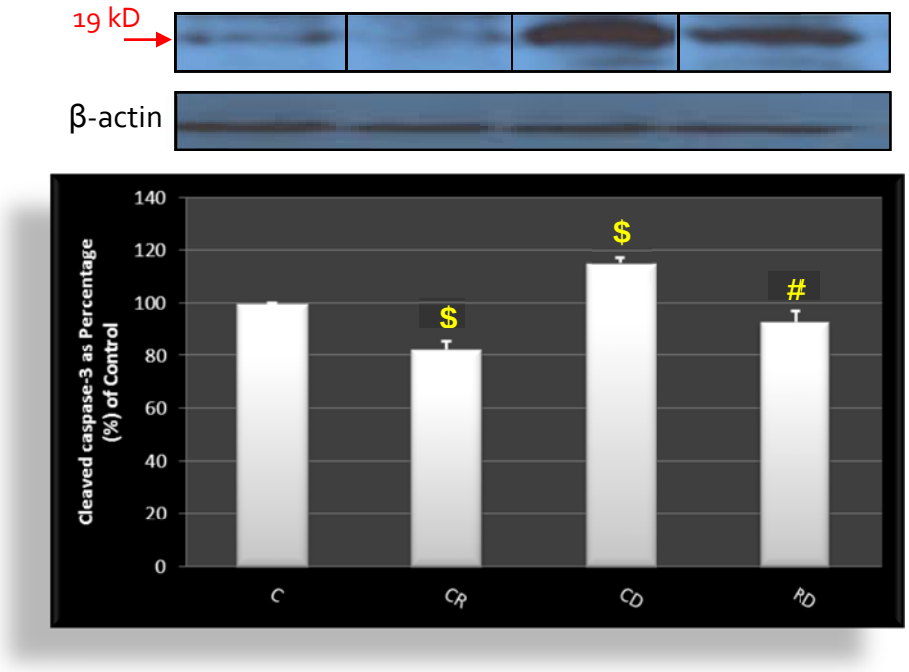

Figure 4.1.7: Immunoblot analysis and the relative quantification of cleaved-caspase-3. Animals were treated with either rapamycin (4 mg/kg) or DXR (10 mg/kg) or a combination of both drugs. A single dose of rapamycin and two doses of DXR was administered intraperitoneally (i.p.) into the animals. Results are presented as mean ± SEM (n = 3). $^{\$}P < 0.05$ versus control; $^{\#}P < 0.05$ versus DXR. Abbreviations - **C**: control, **CR**: rapamycin, **CD**: DXR, **RD**: rapamycin and DXR.

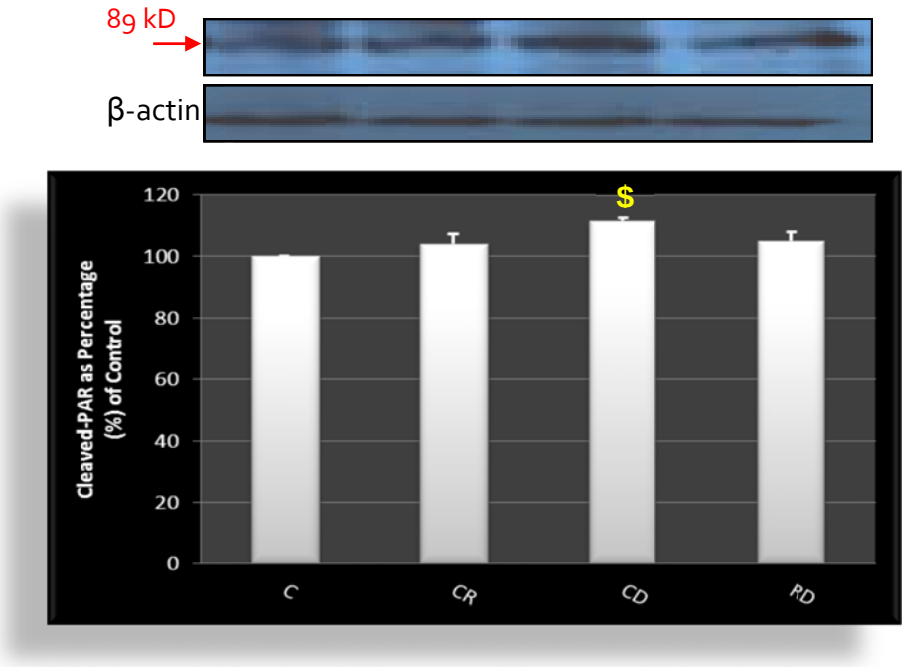

Figure 4.1.8: Immunoblot analysis and the relative quantification of cleaved-PARP. Animals were treated with either rapamycin (4 mg/kg) or DXR (10 mg/kg) or a combination of both drugs. A single dose of rapamycin and two doses of DXR was administered intraperitoneally (i.p.) into the animals. Results are presented as mean ± SEM (n = 3). $^{\$}P < 0.05$ versus control. Abbreviations - **C**: control, **CR**: rapamycin, **CD:** DXR, **RD**: rapamycin and DXR.

4.6.5: DXR stimulates LC-3I and p62 accumulation in the hearts of tumour bearing mice (Figure 4.1.9 – 10)

LC-3 lipidation (conversion of LC-3-I to LC-3-II) data indicate a significant reduction in LC-3 levels with DXR [83.50 ± 3.20%5 ($p < 0.01$)] treatment when compared to the control (100%). In addition, rapamycin treatment reduced autophagic activity significantly [76.26 ± 3.83% ($p < 0.05$)] when compared to control. As demonstrated in Figure 4.1.13, the rapamycin group only received a single injection of rapamycin, which resulted in autophagic activity declining after 48 hrs. LC-3 levels in the combination group (RD) were significantly augmented [117.70 ± 1.17% ($p < 0.001$)] when compared to the DXR treated group. P62/SQSTM1 levels demonstrated that DXR treatment caused a significant increase in p62 accumulation [108.30 ± 0.52% ($p < 0.05$)] when compared to the control (100%). Interestingly, the combination treatment (RD) showed significantly less p62 accumulation [95.32 ± 3.24% ($p < 0.05$)] when compared to DXR treatment alone. No significant differences were observed with Beclin-1 analysis (Figure 4.1.11).

Additionally, the above data were confirmed with GFP-LC-3 histological sections which demonstrated that the GFP signal was reduced with rapamycin (CR) and DXR (CD) treatment confirming a decrease in autophagic activity. In the combination treatment (RD), this effect was lost as shown with increased GFP signal thus indicating elevated autophagic activity (Figure 4.1.12).

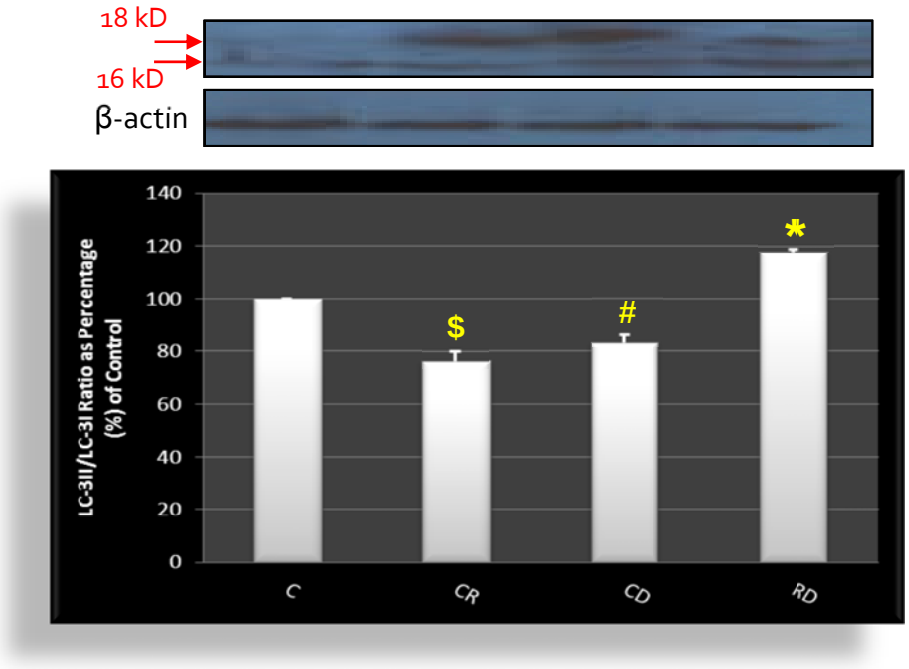

Figure 4.1.9: Immunoblot analysis and the relative quantification of LC-3. Animals were treated with either rapamycin (4 mg/kg) or DXR (10 mg/kg) or a combination of both drugs and LC-3 was assessed. A single dose of rapamycin and two doses of DXR was injected intraperitoneally (i.p.) into the animals. Results are presented as mean ± SEM (n = 3). $^{\$}P < 0.05$, $^{\#}P < 0.01$ versus control; $^{*}P < 0.001$ versus DXR. Abbreviations - **C**: control, **CR**: rapamycin, **CD**: DXR, **RD**: rapamycin and DXR.

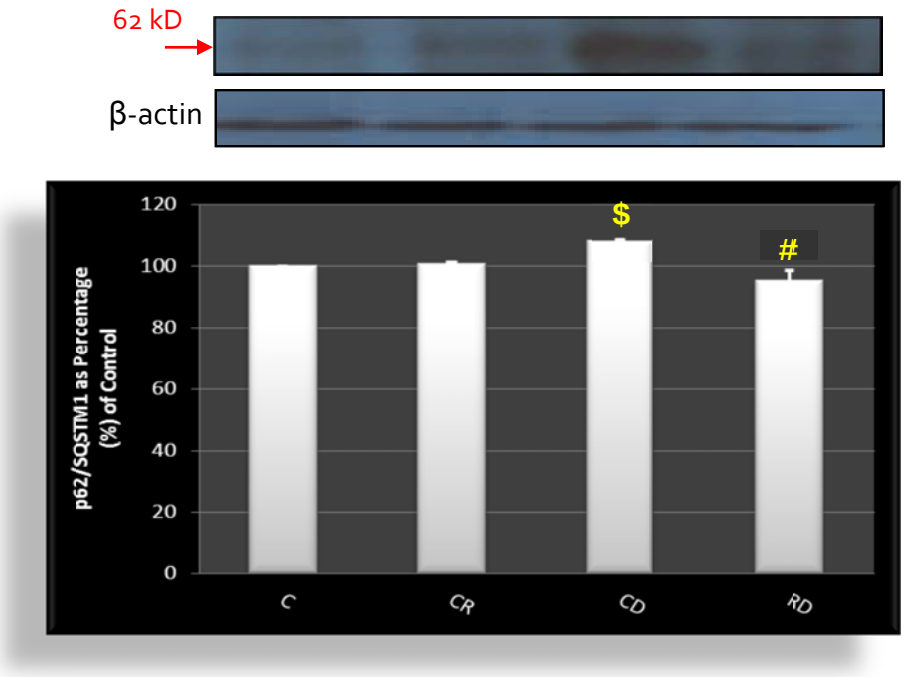

Figure 4.1.10: Immunoblot analysis and the relative quantification of p62. Animals were treated with either rapamycin (4 mg/kg) or DXR (10 mg/kg) or a combination of both drugs. A single dose of rapamycin and two doses of DXR was administered intraperitoneally (i.p.) into the animals. Results are presented as mean ± SEM (n = 3). $^{\$}P < 0.05$ versus control; $^{\#}P < 0.05$ versus DXR. Abbreviations - **C**: control, **CR**: rapamycin, **CD**: DXR, **RD**: rapamycin and DXR.

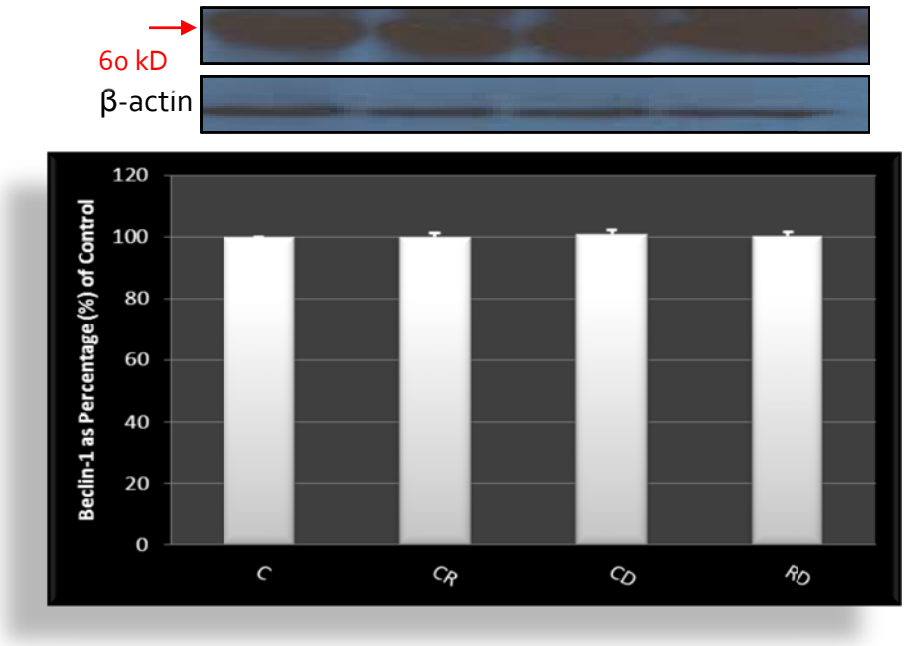

Figure 4.1.11: Immunoblot analysis and the relative quantification of beclin-1. Animals were treated with either rapamycin (4 mg/kg) or DXR (10 mg/kg) or a combination of both drugs. A single dose of rapamycin and two doses of DXR was administered intraperitoneally (i.p.) into the animals. Results are presented as mean ± SEM (n = 3). Abbreviations - **C**: control, **CR**: rapamycin, **CD**: DXR, **RD**: rapamycin and DXR.

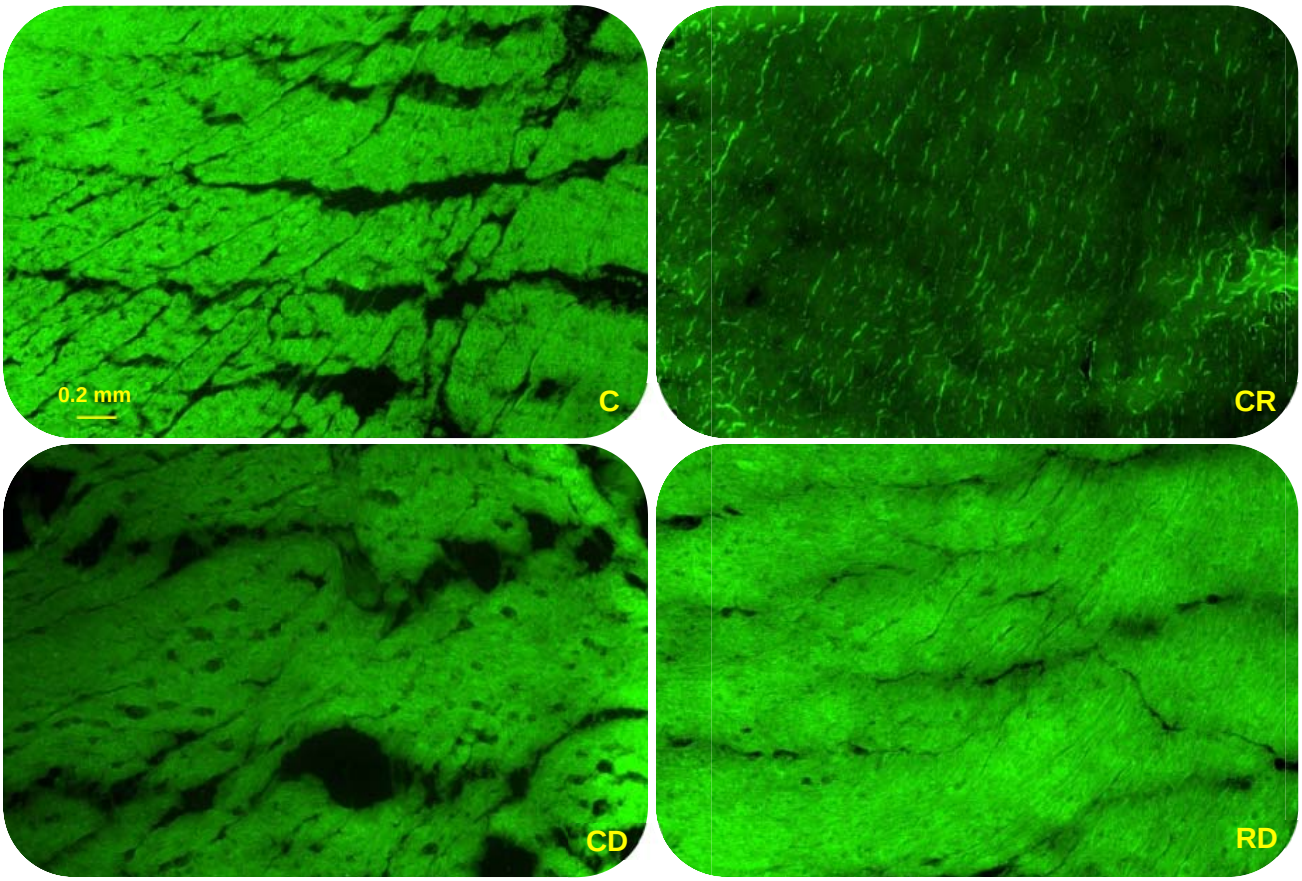

Figure 4.1.12: Fluorescent micrographs indicating GFP-LC-3 expression levels. Abbreviations - **C**: control; **CR**: rapamycin, **CD**: DXR, **RD**: rapamycin and DXR. Magnification = 10X. Scale bar = 0.2 mm.

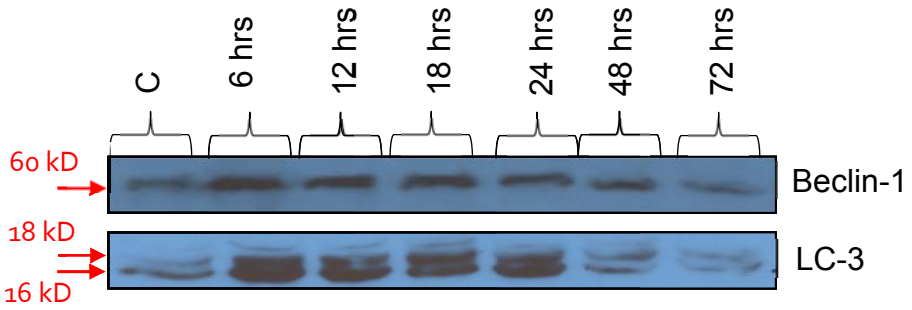

Figure 4.1.13: Autophagy specific markers, beclin-1 and LC-3 protein expression levels following rapamycin (4 mg/kg) treatment. Animals were terminated at the indicated times to show differences in autophagic activity over time. Beclin-1 expression levels were maintained until 18 hrs. At 24, 48 and 72 hrs expression levels began to decrease. LC-3 analysis demonstrated a similar trend; however only after 24 hrs did the expression levels of this protein decrease.

4.6.6: DXR increases MuRF-1 and MAFbx expression (Figure 4.1.14 - 15)

Ubiquitin ligases MuRF-1 [111.50 ± 2.25% ($p < 0.05$)] and MAFbx [112.40 ± 0.13% ($p < 0.01$)] protein expression significantly increased in the presence of DXR when compared to their respective controls (100%). In addition, rapamycin treatment also significantly elevated MAFbx protein expression [112.30 ± 0.68% ($p < 0.01$)] but not MuRF-1 when compared to the control. Moreover, the combination of the two drugs reduced MuRF-1 protein expression significantly [95.16 ± 3.23% ($p < 0.05$)] but not MAFbx. The cytosolic transcription factor FoxO, responsible for the regulation of E_3 ubiquitin ligases as well as various cellular functions, showed no significant difference in phosphorylation in any of the groups when compared to the control (Figure 4.1.16).

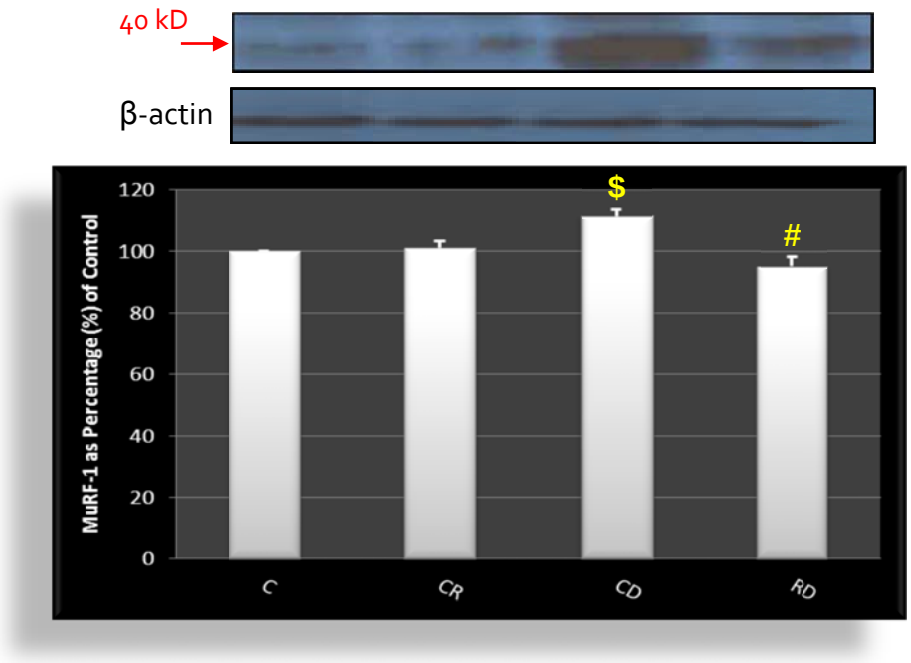

Figure 4.1.14: Immunoblot analysis and the relative quantification of MuRF-1. Animals were treated with either rapamycin (4 mg/kg) or DXR (10 mg/kg) or a combination of both drugs. A single dose of rapamycin and two doses of DXR was injected intraperitoneally (i.p.) into the animals. Results are presented as mean ± SEM (n = 3). $^{\$}P < 0.05$ versus control, $^{\#}P < 0.05$ versus DXR. Abbreviations - **C**: control, **CR**: rapamycin, **CD**: DXR, **RD**: rapamycin and DXR.

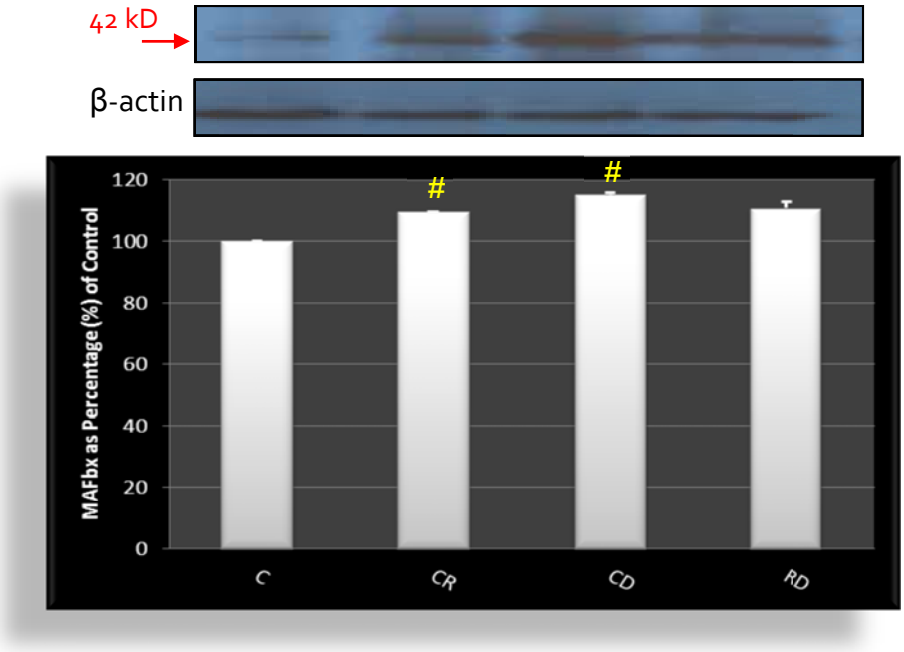

Figure 4.1.15: Immunoblot analysis and the relative quantification of MAFbx. Animals were treated with either rapamycin (4 mg/kg) or DXR (10 mg/kg) or a combination of both drugs and MAFbx was assessed. A single dose of rapamycin and two doses of DXR was injected intraperitoneally (i.p.) into the animals. Results are presented as mean ± SEM (n = 3). $^{\#}P < 0.01$ versus control. Abbreviations - **C**: control, **CR**: rapamycin, **CD**: DXR, **RD**: rapamycin and DXR.

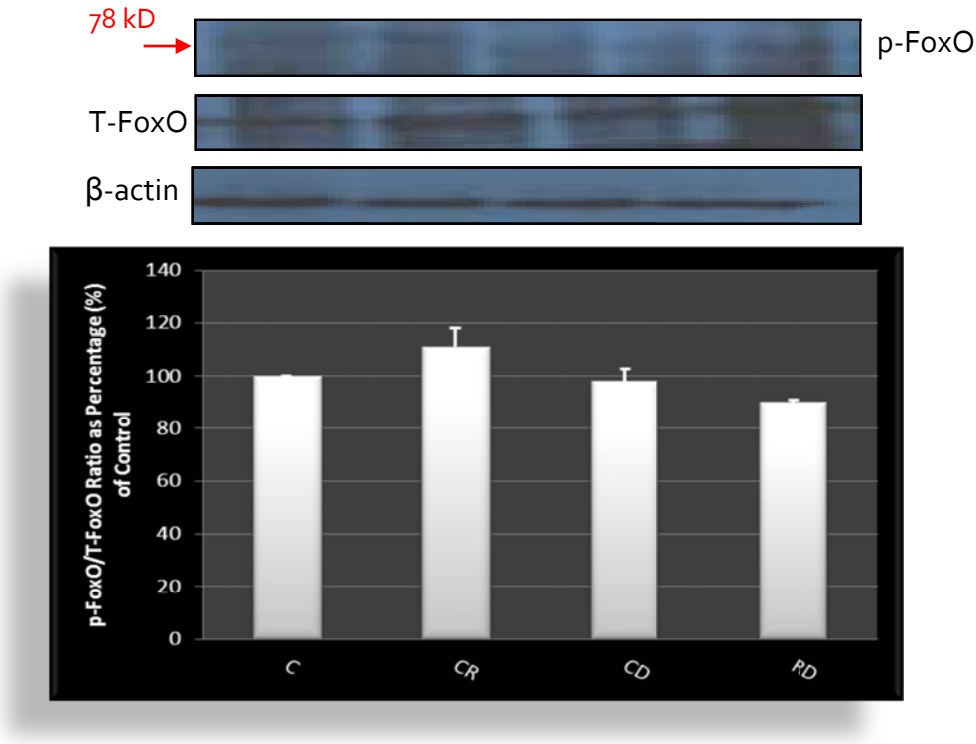

Figure 4.1.16: Immunoblot analysis and the relative quantification of FoxO. Animals were treated with either rapamycin (4 mg/kg) or DXR (10 mg/kg) or a combination of both drugs and FoxO phosphorylation was assessed. A single dose of rapamycin and two doses of DXR was injected intraperitoneally (i.p.) into the animals. Results are presented as mean ± SEM (n = 3). Abbreviations - **C**: control, **CR**: rapamycin, **CD**: DXR, **RD**: rapamycin and DXR.

4.6.7: DXR increases protein ubiquitination (Figure 4.1.17)

A significantly larger amount of ubiquitin tagged proteins was evident in the hearts of animals treated with DXR [108.40 ± 1.97% ($p < 0.05$)] compared to the control (100%). Conversely, rapamycin treatment alone significantly reduced protein ubiquitination [103.02 ± 1.97% ($p < 0.05$)] when compared to the control. The combination treatment produced no significant differences when compared to DXR treatment alone although a trend towards a decrease was observed.

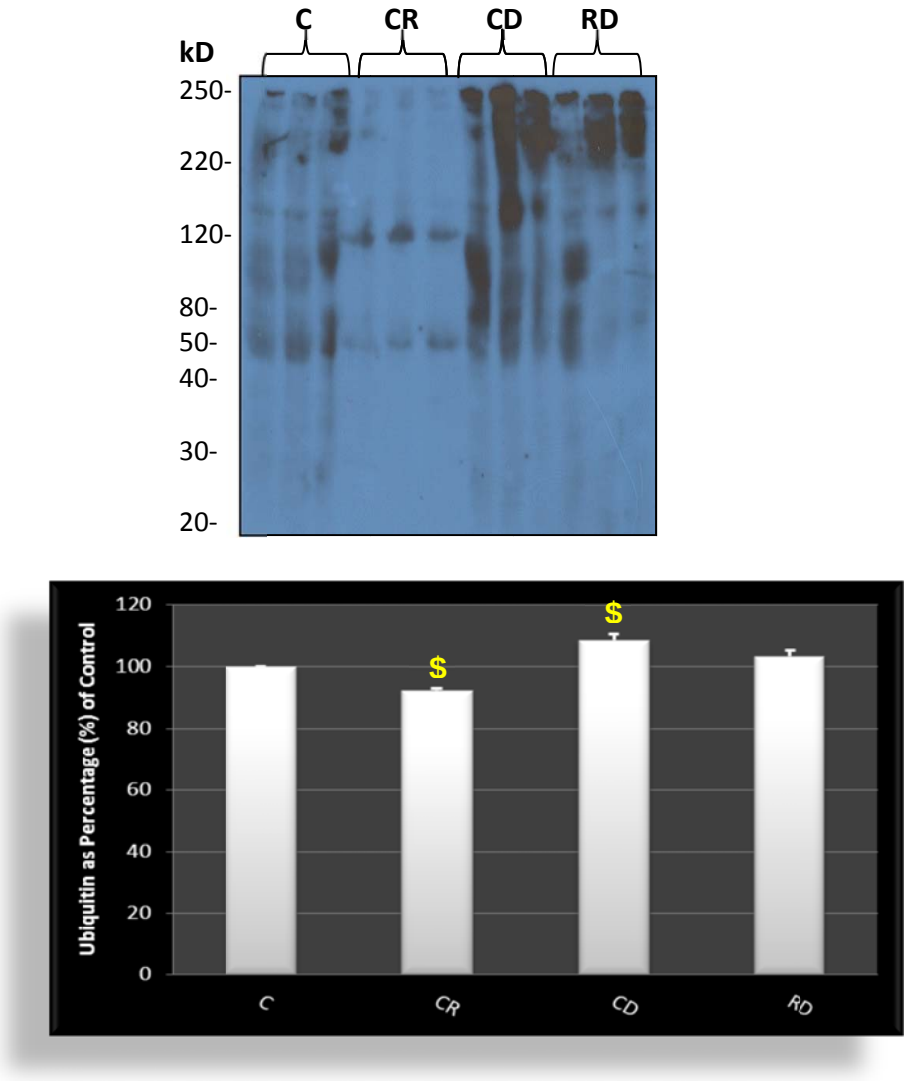

Figure 4.1.17: Immunoblot analysis and the relative quantification of ubiquitinated proteins. Animals were treated with either rapamycin (4 mg/kg) or DXR (10 mg/kg) or a combination of both drugs. A single dose of rapamycin and two doses of DXR was injected intraperitoneally (i.p.) into the animals. Results are presented as their mean ± SEM (n = 3). $^{\$}P < 0.05$ versus control. Abbreviations - **C**: control, **CR**: rapamycin, **CD**: DXR, **RD**: rapamycin and DXR.

4.6.8: DXR reduces cross-sectional myocyte area (Figure 4.1.18 – 19)

The above data were confirmed by analytical histological sections indicating cardiac atrophy in the DXR treated group [130.70 ± 5.17 μm^2 ($p < 0.05$)] when compared to the control (175.50 ± 8.21 μm^2). The combination group preserved cardiomyocyte loss and displayed a significant increase in cross-sectional myocyte area [171.80 ± 11.73 μm^2 ($p < 0.05$)] when compared to DXR treatment alone.

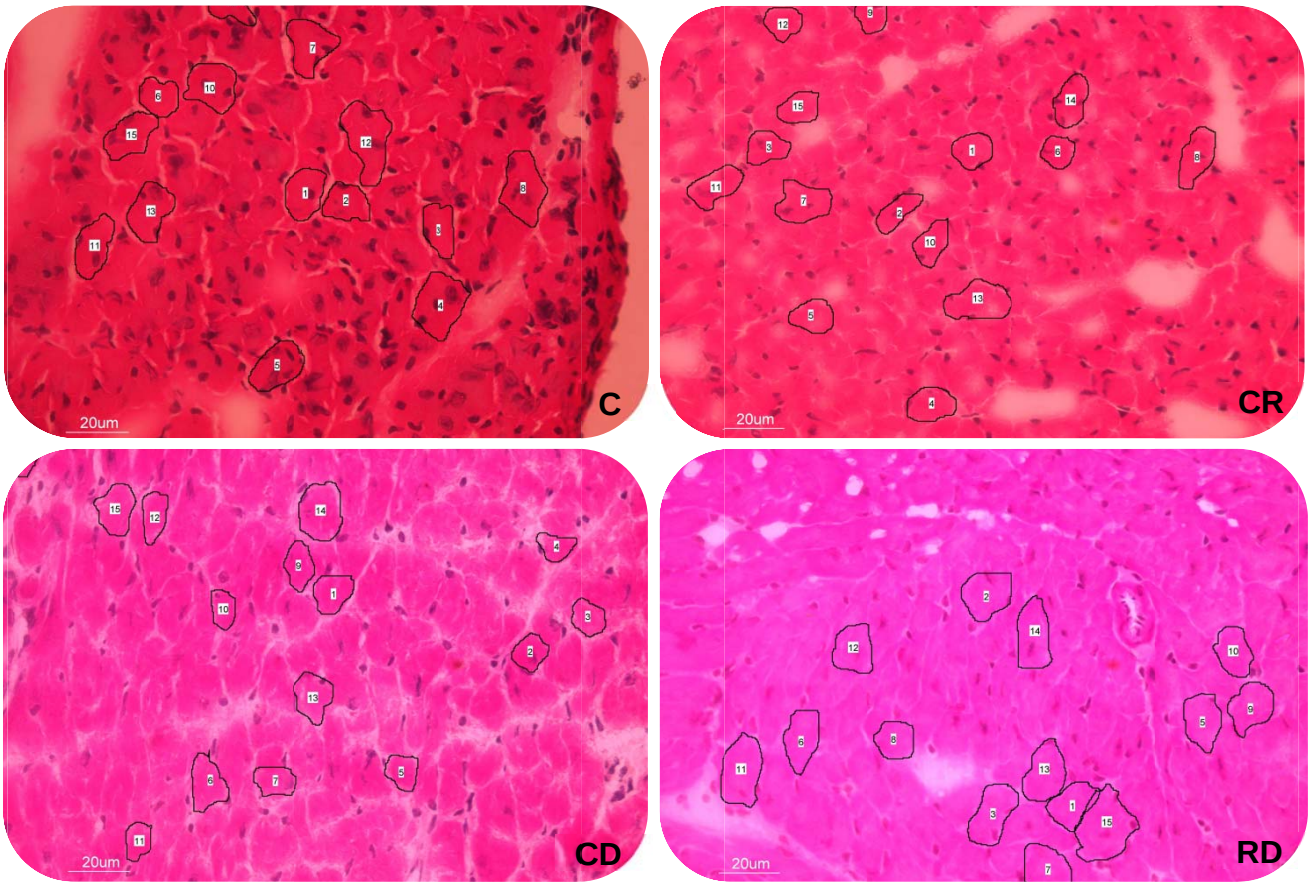

Figure 4.1.18: Representative H & E images indicating myocyte cross-sectional areas**.** Animals were treated with either rapamycin (4 mg/kg) or DXR (10 mg/kg) or a combination of both drugs and myocyte cross-sectional area was assessed. Abbreviations - **C**: control, **CR**: rapamycin, **CD**: DXR, **RD**: rapamycin and DXR. Magnification = 40X. Scale bar = 20 µm.

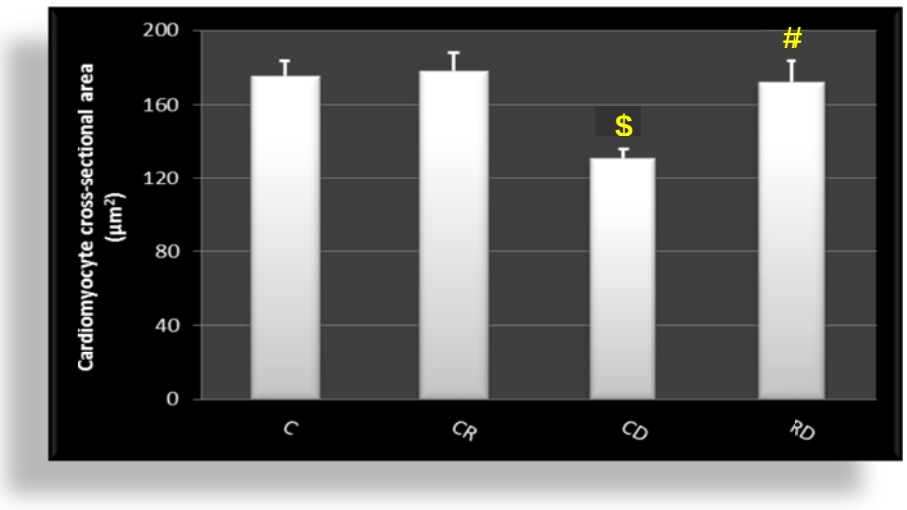

Figure 4.1.19: Quantification of myocyte cross-sectional area. Animal were treated with either rapamycin (4 mg/kg) or DXR (10 mg/kg) or a combination of both drugs. A single dose of rapamycin and two doses of DXR was injected intraperitoneally (i.p.) into the animals. Results are presented as mean ± SEM (n = 3). $^{\$}P < 0.05$ versus control, $^{\#}P < 0.05$ versus DXR. Abbreviations - **C**: control, **CR**: rapamycin, **CD**: DXR, **RD**: rapamycin and DXR.

4.7: Discussion

The data presented support a model of acute doxorubicin-induced cardiotoxicity, characterized by body mass loss, increased apoptosis, attenuated autophagy, elevated E_3 ligase activity as well as protein ubiquitination and decreased muscle fibre cross-sectional area.

Autophagy in the myocardium has long been viewed as a double-edged sword that can be maladaptive in one context and beneficial in another depending on the type (Matsui *et al*, 2007) and duration (Kang *et al*, 2008) of the injury as well as the levels of autophagy stimulated (Eisenberg-Lerner *et al*, 2009). Moreover, autophagy is often accompanied with other forms of cell death such as apoptosis and/or necrosis, thus making it a challenge to assess autophagy as a survival or a death pathway (Kobayashi *et al*, 2010). This complex collaboration has inevitably been portrayed in three different categories: (i) autophagy and apoptosis can act synergistically to induce cell death; (ii) autophagy can act as an antagonist to promote survival by inhibiting apoptosis; or (iii) autophagy facilitates apoptosis by allowing apoptosis to occur without resulting in death by autophagy (Eisenberg-Lerner *et al*, 2009). The present study was thus designed to evaluate the therapeutic potential of elevated autophagy as an adjuvant treatment against DXR-induced myocardial damage.

Rapamycin-doxorubicin co-treatment increased the survival rate of tumour bearing mice

It was demonstrated in this study that treatment with DXR alone and in combination with rapamycin, effectively decreased tumour volume in GFP-LC3 mice after receiving a total cumulative dose of 20 mg/kg DXR (Figure 4.1.3). In the clinical setting, DXR is typically administered in doses between 50-75 mg/m^2 over a brief period of time with a cumulative maximum of 450 mg/m^2, which is equivalent to approximately 12 mg/kg (Yi *et al*, 2005). The condition simulated in this study represents acute DXR-induced cardiotoxicity as the animals received only two doses of DXR. Even though this concentration is relatively greater than that received by

patients, the cardiotoxic dose in mice differs because of factors related to absorption, metabolism and elimination of the drug. The dose in this study was selected for acute exposure on the basis of previous work that verified an inevitably toxic but not rapidly fatal dose indicating myocardial damage (Zhu *et al*, 2008).

The survival curve of the treated groups demonstrated in Figure 4.1.4 showed that all of the DXR treated mice (100%) as well as 50% of the rapamycin and DXR treated mice died after treatment. This may suggest progressive cardiac dysfunction after appropriate exposure to DXR, as observed in human patients suffering from heart failure months or years after DXR treatment has been discontinued. Of note is the better survival rate of mice in the combination group compared to that of the DXR treated group, suggesting a beneficial role for increased autophagy with DXR treatment (Vellai *et al*, 2009; Cuervo, 2008). In support of this notion, mice body weight (Figure 4.1.5) data demonstrate that DXR treated mice lost significantly more weight than their control counterparts whereas in the combination group, although insignificant, rapamycin treatment conserved body weight in relation to the DXR treated group. A comparable trend was also observed with heart weight (Figure 4.1.6). Our observations are in agreement with previous studies despite different doses of DXR being employed (Ewans *et al*, 2006; Zhu *et al*, 2008).

Doxorubicin induces apoptosis in the hearts of tumour bearing mice

Myocardial apoptosis, a common feature of acute DXR-induced cardiotoxicity, was demonstrated in our study (Figures 4.1.7 and 4.1.8). This is supported by various other studies which have shown that multiple pathways are involved in the activation of both intrinsic and extrinsic apoptotic pathways with doxorubicin treatment (Shan *et al*, 1996; Arola *et al*, 2000; Kang, 2001). Furthermore, we have demonstrated that by combining rapamycin with DXR, cleaved caspase-3 is significantly reduced, thus proposing an inhibitory role of autophagy on apoptotic activity. The observed increase in active caspase-3 levels in the DXR treated group was also associated with the loss of myocyte cross-sectional area (Figure 4.1.19) possibly indicating that apoptosis may have partly contributed to this phenomenon. Zhu and co-workers,

however, demonstrate that the main contributor to DXR-induced cardiotoxicity is the loss of myocardial mass rather than cardiomyocyte apoptosis (Zhu *et al*, 2009).

Rapamycin-doxorubicin co-treatment increased autophagy in the hearts of tumour bearing mice

As autophagic activity formed an integral part of this study, its functional significance had to be assessed within this specific context. LC-3 protein levels (Figure 4.1.9) showed down regulation of autophagic activity in both the rapamycin and DXR treated groups as demonstrated by LC-3I accumulation. The extent of p62/SQSTM1 expression, an adapter molecule that is degraded by autophagy (Pankiv *et al*, 2007) or the UPP (Zheng *et al*, 2009), showed significant accumulation in the cardiac samples of the DXR treated mice when compared to the control (Figure 4.1.10). This accumulation of p62 is often considered a sign of autophagic malfunction (Zheng *et al*, 2009) and hence interruption of autophagic flux. By contrast, the combination group (RD) demonstrated reduced levels of p62, suggesting functional autophagic activity. These observations were further confirmed by GFP-LC-3 fluorescent images (Figure 4.9.12) which showed a reduction in autophagic activity in the rapamycin and DXR treated groups, but elevated autophagic activity in the combination group. The observed decline in autophagic activity in the rapamycin group could possibly be explained by the fact that these animals only received one injection of rapamycin for the duration of the study which sustained increased autophagy for ±2 days (Figure 4.1.13) as beclin-1 and LC3 expression levels began to decline. Therefore, these data suggest that at the time of treatment, the levels of autophagy may have already returned to basal levels.

Doxorubicin increased protein ubiquitination and E_3 ubiquitin ligase activity in the hearts of tumour bearing mice

The ubiquitin proteasome pathway (UPP) plays a critical role in protein turnover in the heart and its upregulation is mainly associated with cardiac atrophy. Proteolysis of the sarcomere occurs through the coordinated efforts of the ubiquitin proteasome system, the process of autophagy and the activity of proteases such as calpain and

caspases. A molecular link between autophagy and the proteasome is well-recognized, with studies demonstrating that suppression of autophagy leads to an increase in ubiquitinated proteins (Hara *et al*, 2006; Ding *et al*., 2007). This is confirmed with our results as we have demonstrated that DXR attenuates autophagy and subsequently increases protein ubiquitination (Figure 4.1.17), whereas rapamycin treatment induced autophagy and inhibited protein ubiquitination. Furthermore, we have shown that the E_3 ubiquitin ligases, MuRF-1 and MAFbx were significantly augmented in the cardiac muscle of the DXR treated group (Figures 4.1.14 and 4.1.15). By combining both drugs in the treatment regimen, MuRF-1 expression decreased but not MAFbx. This observation indicates that the transcription of MuRF-1 is prevented during elevated autophagy induced by rapamycin treatment. Additionally, this proposes a regulatory role of rapamycin and/or autophagy on MuRF-1 expression. In muscle undergoing atrophy, FoxO3 activation stimulates and regulates both proteolytic pathways (UPP and autophagy) concurrently (Zhao *et al*, 2007) and induces atrophy by stimulating the transcription of E_3 ligases (Skurk *et al*, 2005). Although our study resulted in no significant differences between the groups in cardiac FoxO3 protein phosphorylation (Figure 4.1.16), an alternate pathway such as the TNF-α/NF-κB signalling pathway often implicated in muscle wasting conditions (Adams *et al*, 2007; Li *et al*, 1998), might be responsible for the observed increases in MuRF-1 and MAFbx. Moreover, a time-dependent effect is also plausible; FoxO3 might have been upregulated early after the administration of DXR and reached baseline levels when the tissue was taken for analysis.

Doxorubicin treatment decreased myocyte cross-sectional area in tumour bearing mice

Histological sections of H & E stained hearts (Figure 4.1.18) revealed heterogeneous myocyte size in the DXR treated group as well as in the combination group. Analysis of the average myocyte cross-sectional area (Figure 4.1.19) demonstrated that DXR treated mice had a significantly reduced myocyte area when compared to the control group. These observations thus confirm muscle wasting in the setting of acute DXR-induced cardiotoxicity and supported the trend observed in heart weight (Figure

4.1.6). Our observations are also corroborated by existing studies that have shown a similar impact on heart weight and cardiomyocyte fiber diameter (Esaki *et al*, 2006; Li *et al*, 2006; Li *et al*, 2006; Li *et al*, 2007) following a single injection of DXR (15 mg/kg) in adult mice.

In summary, this study demonstrates a model of acute DXR-induced cardiotoxicity that resulted in elevated apoptosis, inhibition of autophagy and increased proteolysis by means of the UPP. We have provided substantial evidence that DXR is a potent chemotherapeutic drug that induces cardiomyocyte death. DXR upregulated key molecules involved in apoptosis and proteolysis which ultimately resulted in the gradual loss of body weight and a decrease in myocyte cross-sectional area. Importantly, these detrimental effects of DXR were abolished when treatment included rapamycin. The protective effects provided by combining both drugs in the treatment regimen suggest that it may be possible to mitigate the cardiotoxic effects of DXR in cancer patients by carefully controlling the levels of autophagy with the use of rapamycin.

References

1. Adams, V., Linke, A., Wisloff, U., Döriing, C., Erbs, S., Kränkel, N., Witt, C.C., Labeit, S., Müller-Werdan, U., Schuler, G., Hambrecht, R. 2007. Myocardial expression of Murf-1 and MAFbx after induction of chronic heart failure: Effect on myocardial contractility. *Cardiovascular Research*. 73: 120-129
2. Arola, O.J., Saraste, A., Pulkki, K., Kallajoi, M., Parvinen, M., Voipio-Pulkki, L.-M.. 2000. Acute doxorubicin cardiotoxicity involves cardiomyocyte apoptosis. *Cancer Research*. 60: 1789-1792
3. Benjamin, R.S., Wiernik, P.H., Bachur, N.R. 1974. Adriamycin chemotherapy – efficacy, safety, and pharmacologic basis of an intermittent single high-dose schedule. *Cancer*. 33: 19-27
4. Bradford, M.M. 1976. A rapid and sensitive method for quantitation of microgram quantities of protein utilizing the principle of protein-dye binding. *Annals of Biochemistry*. 71: 248-254
5. Cuervo, A.M. 2008. Autophagy and ageing: keeping that old broom working. *Trends in Genetics*. 24: 604-612
6. Ding, W.X., Ni, H.M., Gao, W., Yoshimori, T., Stolz, D.B., Ron, D., Yin, X.M. 2007. Linking of autophagy to ubiquitin-proteasome system is important for the regulation of endoplasmic reticulum stress and cell viability. *American Journal of Pathology*. 171: 513-524
7. Eisenberg-Lerner, A., Bialik, S., Simon, H.U., Kimchi, A. 2009. Life and death partners: apoptosis, autophagy and the cross-talk between them. *Cell Death & Differentiation*. 16: 966-975
8. Esaki, M., Takemura, G., Kosai, K., Takahashi, T., Miyata, S., Li, L., Goto, K., Maruyama, R., Okada, H., Kanamori, H., Ogino, A., Ushikoshi, H., Minatoguchi, S., Fujiwara, T., Fujiwara, H. 2008. Treatment with an adenoviral vector encoding hepatocyte growth factor mitigates established cardiac dysfunction in doxorubicin-induced cardiomyopathy. *American Journal of Physiology - Heart and Circulatory Physiology*. 294: H1048–H1057
9. Ewens, A., Luo, L., Berleth, E., Alderfer, J., Wollman, R., Hafeez, B.B., Kanter, P., Mihich, E., Ehrke, M.J. 2006. Doxorubicin plus Interleukin-2 chemoimmunotherapy against breast cancer in mice. *Cancer Research*. 66: 5419-5426

10. Hara, T., Nakamura, K., Matsui, M., Yakamoto, A., Nakahara, Y., Suzuki-Migishima, R., Yokoyama, M., Mishima, K., Saito, I., Okano, H., Mizushima, N. 2006. Suppression of basal autophagy in neural cells causes neurodegenerative disease in mice. *Nature*. 441: 885-889
11. Kalyanaraman, B., Joseph, J., Kalivendi, S., Wang, S., Konorev, E., Kotamraju, S. 2002. Doxorubicin-induced apoptosis: implications in cardiotoxicity. *Molecular Cell Biochemistry*. 234-235: 119-124
12. Kang, C., Avery, L. 2008. To be or not to be, the level of autophagy is the question: Dual roles of autophagy in the survival response to starvation *Autophagy*. 4: 82-84
13. Kang, Y.J. 2001. Molecular and cellular mechanisms of cardiotoxicity. *Environmental Health Perspectives*. 109: 27-34
14. Kim, D.H., Sarbassov, D.D., Ali, S.M., King, J.E., Latek, R.R., Erdjument-Bromage, H., Tempst, P., Sabatini, D.M. 2002. mTOR interacts with raptor to form a nutrient-sensitive complex that signals to the cell growth machinery. *Cell*. 110: 163-175
15. Kobayashi, S., Volden, P., Timm, D., Mao, K., Xu, X., Liang, Q. 2010. Transcription factor GATA4 inhibits doxorubicin-induced autophagy. *Journal of Biological Chemistry*. 285: 793-804
16. Ladas, E.J., Jacobson, J.S., Kennedy, D.D., Teel, K., Fleischauer, A., Kelly, K.M. 2004. Antioxidants and Cancer Therapy: A Systematic Review. *Journal of Clinical Oncology*. 22: 517-528
17. Li, K., Sung, R.Y., Huang, W.Z., Yang, M., Pong, N.H., Lee, S.M., Chan, W.Y., Zhao, H., To, M.Y., Fok, T.F., Li, C.K., Wong, Y.O., Ng, P.C. 2006. Thrombopoietin protects against in vitro and in vivo cardiotoxicity induced by doxorubicin. *Circulation.* 113: 2211–2220
18. Li, L., Takemura, G., Li, Y., Miyata, S., Esaki, M., Okada, H., Kanamori, H., Khai, N.C., Maruyama, R., Ogino, A., Minatoguchi, S., Fujiwara, T., Fujiwara, H. 2006. Preventive effect of erythropoietin on cardiac dysfunction in doxorubicin-induced cardiomyopathy. *Circulation*. 113: 535–543
19. Li, L., Takemura, G., Li, Y., Miyata, S., Esaki, M., Okada, H., Kanamori, H., Ogino, A., Maruyama, R., Nakagawa, M., Minatoguchi, S., Fujiwara, T., Fujiwara, H. 2007. Granulocyte colony-stimulating factor improves left

ventricular function of doxorubicin-induced cardiomyopathy. *Laboratory Investigations*. 87: 440–455

20. Li, Y.-P., Schwartz, R.J., Waddell, I.D., Holloway, B.R., Reid, M.B. 1998. Skeletal muscle myocytes undergo protein loss and reaction oxygen-mediated NF-κB activation in response to tumor necrosis factor α. *The FASEB Journal*. 12: 871-880
21. Matsui, Y., Takagi, H., Qu, X., Abdellatif, M., Sakoda, H., Asano, T., Levine, B., Sadoshima, J. 2007. Distinct Roles of Autophagy in the Heart During Ischemia and Reperfusion: Roles of AMP-Activated Protein Kinase and Beclin 1 in Mediating Autophagy. *Circulation Research*. 100: 914-922
22. Medina, D. 2007. Chemical carcinogenesis of rat and mouse mammary glands. *Breast Disease*. 28: 63-68
23. Minotti, G., Menna, P., Salvatorelli, E., Cairo, G., Gianni, L. 2004. Anthracyclines: molecular advances and pharmacologic developments in antitumor activity and cardiotoxicity. *Pharmacological Reviews*. 56: 185-229
24. Mizushima, N., Yamamoto, A., Matsui, M., Yoshimori, T., Ohsumi, Y. 2004. *In vivo* analysis of autophagy in response to nutrient starvation using transgenic mice expressing a fluorescent autophagosome marker. *Molecular Biology of the Cell*. 15: 1101-1111
25. Noda, T., Ohsumi, Y. 1998. Tor, a phosphatidylinositol kinase homologue, controls autophagy in yeast. *Journal of Biological Chemistry*. 273: 3963-3966
26. Pankiv, S., Hoyvarde Clausen, T., Lamerk, T., Brech, A., Bruun, J.A., Outzen, H., Overvatn, A., Bjorkkoy, G., Johansen, T. 2007. p62/SQSTMI1 binds directly to Atg8/LC3 to facilitate degradation of ubiquitinated protein aggregates by autophagy. *Journal of Biological Chemistry*. 282: 24131-24145
27. Sarbassov, D.D., Ali, S.M., Sabatini, D.M. 2005. Growing roles for the mTOR pathway. *Current Opinion in Cell Biology*. 17: 569-603
28. Shan, K., Lincoff, M., Young, J.B. 1996. Anthracycline-induced cardiotoxicity. *Annals of Internal Medicine*. 125: 47-58
29. Singal, P.K., Iliskovic, N. 1998. Doxorubicin-induced cardiomyopathy. *New England Journal of Medicine*. 339: 900-905
30. Singal, P.K., Iliskovic, N., Li, T., Kumar, D. 1997. Adriamycin cardiomyopathy: pathophysiology and prevention. *FASEB Journal*. 11: 931-936

31. Skurk, C., Izumiya, Y., Maatz, H., Razeghi, P., Shiojima, I., Sandri, M., Sato, K., Zeng, L., Schiekofer, S., Pimentel, D., Lecker, S., Taegtmeyer, H., Goldberg, A.L., Walsh, K. 2005. The FOXO3a transcription factor regulates cardiac myocyte size downstream of AKT signaling. *Journal of Biological Chemistry*. 280: 20814-20823
32. Sun, X., Zhou, Z., Kang, Y.P. 2001. Attenuation of Doxorubicin Chronic Toxicity in Metallothionein-overexpressing Transgenic Mouse Heart. *Cancer Research*. 61: 3382-3387
33. Tan, C., Etcubanas, E., Wollner, N. et al. 1973. Adriamycin – an antitumor antibiotic in treatment of neoplastic diseases. *Cancer*. 32: 9-17
34. Tsukamato, O., Minamino, T., Okada, K., Shintani, Y., Takashima, S., Kato, H., Liao, Y., Okazaki, H., Asai, M., Hirata, A., Fujita, M., Asano, Y., Yomazaki, S., Asanuma, H., Hori, M., Kitakazi, M. 2006. Depression of proteasome activities during progression of cardiac dysfunction in pressure-overload heart in mice. *Biochemical and Biophysical Research Communications*. 340: 11255-1133
35. Vellai, T. 2009. Autophagy genes and ageing. *Cell Death & Differentiation*. 16: 94-102
36. Vezina, C., Kudelski, A., Sehgal, S.N. 1975. Rapamycin (AY-22, 989), a new antifungal antibiotic. *The Journal of Antibiotics (Tokyo)*. 28: 721-726
37. Yen, H.C., Oberley, T.D., Vichitbandha, S., Ho, Y.S., St Clair, D.K. 1996. The protective role of manganese superoxide dismutase against adriamycin-induced acute cardiac toxicity in transgenic mice. *Journal of Clinical Investigation*. 98:1253–1260.
38. Yi, X., Bekeredjian, R., DeFilippis, N.J., Siddiquee, Z., Fernandez, E., Shohet, R.V. 2005. Transcriptional analysis of doxorubicin-induced cardiotoxicity. *American Journal of Physiology – Heart and Circulatory Physiology*. 290: H1098-H1102
39. Zhao, J., Brault, J.J., Schild, A., Cao, P., Sandri, M., Schiaffino, S., Lecker, S.H., Goldberg, A.L. 2007. Fox-O3 coordinately activates protein degradation by the autophagic/lysosomal and proteasomal pathways in atrophying muscle cells. *Cell Metabolism*. 6: 472-483

40. Zheng, Q., Li, J., Wang, X. 2009. Interplay between the ubiquitin-proteasome system and autophagy in proteinopathies. *International Journal of Physiology, Pathophysiology and Pharmacology*.1: 127-142
41. Zhu, W., Shou, W., Payne, R.M., Caldwell, R., Field, L.J. 2008. A mouse model for juvenile doxorubicin-induced cardiac dysfunction. *Pediatric Research*. 65: 488-494
42. Zhu, W., Soonpaa, M.H., Chen, H., Shen, W., Patne, R.M., Liechty, E.A., Caldwell, R.L., Shou, W., Field, L.J. 2009. Acute doxorubicin cardiotoxicity is associated with p53-induced inhibition of the mammalian target of rapamycin pathway. *Circulation*. 119: 99-106

Chapter 5

Final Conclusions

Daunorubicin (DNR) and doxorubicin (DXR) are the two most effective drugs known for the treatment of systemic neoplasms and solid tumours. It has become evident however that their therapeutic potential is restricted by their serious side effects (cardiotoxicity) which can lead to congestive heart failure. According to the widely accepted hypothesis, AC therapy, submitted to redox cycling by mitochondria, result in persistent oxidative stress, mitochondrial dysfunction and cell death. Although numerous studies have attempted various methods to reduce AC-induced cardiotoxicity, very few have been able to reproduce their results in a clinical setting. Our study has demonstrated that rapamycin, a potent inhibitor of the mTOR signalling pathway which induces autophagy, possesses cardioprotective effects against AC-induced cardiotoxicity (Figure 5.1.1). We have demonstrated that DXR is a potent inducer of cell death, the ubiquitin-proteasome pathway (UPP), mitochondrial dysfunction and ER stress which are all attenuated by rapamycin treatment. Additionally, the co-treatment of rapamycin and DXR increased cardiomyocyte size in the *in vivo* model and prevented the decrease in body weight induced by DXR treatment. Furthermore, as rapamycin is currently being used in the clinical setting to suppress tumour growth, its characteristics thus make this drug an ideal adjuvant therapy to either treat or prevent cardiotoxicity in order to potentially inhibit or delay heart failure.

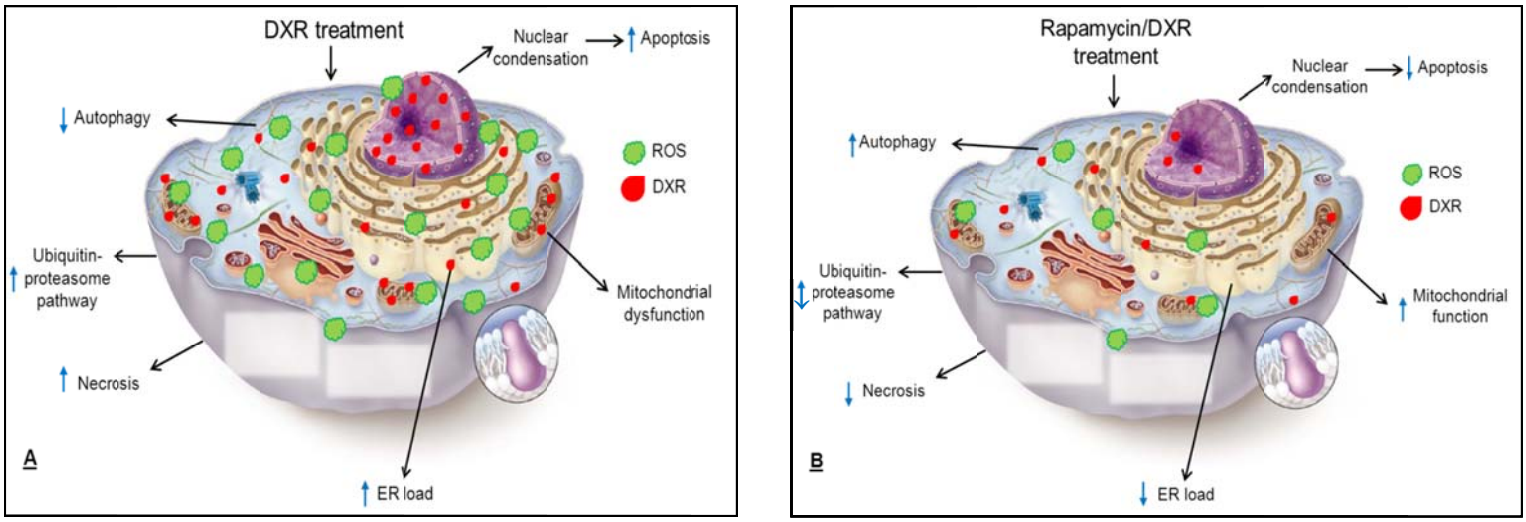

Figure 5.1.1: The effects of DXR and Rapamycin-DXR treatment on cellular function. **A**: DXR treatment induces various detrimental effects including increased ROS (green clouds) production, apoptosis, necrosis, ER load, mitochondrial dysfunction, activation of the ubiquitin-proteasome pathway and inhibition of autophagy. Additionally, DXR (red teardrops) accumulates in the nucleus as well as within the mitochondria. These combined effects constitute DXR-induced cardiotoxicity. **B**: Pre-treatment with rapamycin and DXR alleviates most of these detrimental effects that are induced by DXR ultimately reducing cardiotoxicity.

Appendices

Appendix A – Supplementary Data (Section 1)

Characterizations of H_9C_2s during amino acid deprivation

It is well known that starvation is a potent inducer of autophagy (Scherz-Shouval *et al*, 2007). To simulate this condition *in vitro*, cells were treated with different concentrations of amino acids (see methods) for 24 hrs in order to determine which amino acid concentration is appropriate to upregulate autophagy effectively.

5.1: MTT Assay

Results indicate that all concentrations of amino acid deprivation showed both time and concentration dependent effects. Significant differences were obtained at all concentrations when compared to the control. The lowest concentration of amino acids reduced mitochondrial viability to 51.12 ± 1.27% ($p < 0.001$) versus control (100%) after 24 hrs (Figure 5.1.1).

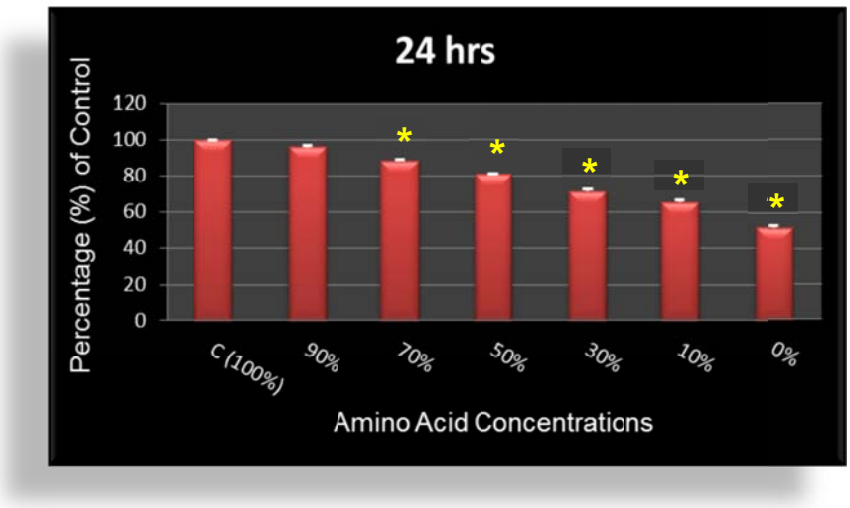

Figure 5.1.1: The effect of different amino acid concentrations on mitochondrial viability. H_9C_2 myoblasts were incubated with 100%, 90%, 70%, 50%, 30%, 10% and 0% amino acid concentrations for 24 hrs. Values are expressed as percentage of control (100%) and presented as mean ± S.E.M (n = 3).*P< 0.001 versus control.

5.2: Assessment of Cell Death during amino acid deprivation

In order to assess apoptotic and late apoptotic/necrotic cell death, cells were stained with Hoechst 33342 and PI respectively. After 24 hrs of amino acid deprivation, the only concentrations to produce significance when compared to the control were the 10% [3.89 ± 0.71% ($p < 0.05$) versus 0.55 ± 0.171%] and the 0% [7.27 ± 1.47% ($p < 0.001$) versus 0.55 ± 0.17%] (Figure 5.2.1 **a**, **b**). Additionally, both these concentrations resulted in significant increases in PI positive cells when compared to the control [10%: 10.45 ± 2.51% ($p < 0.01$) versus 2.70 ± 0.33% and 0%: 9.08 ± 1.57% ($p < 0.05$) versus 2.70 ± 0.33% (Figure 5.2.1 **a**, **c**).

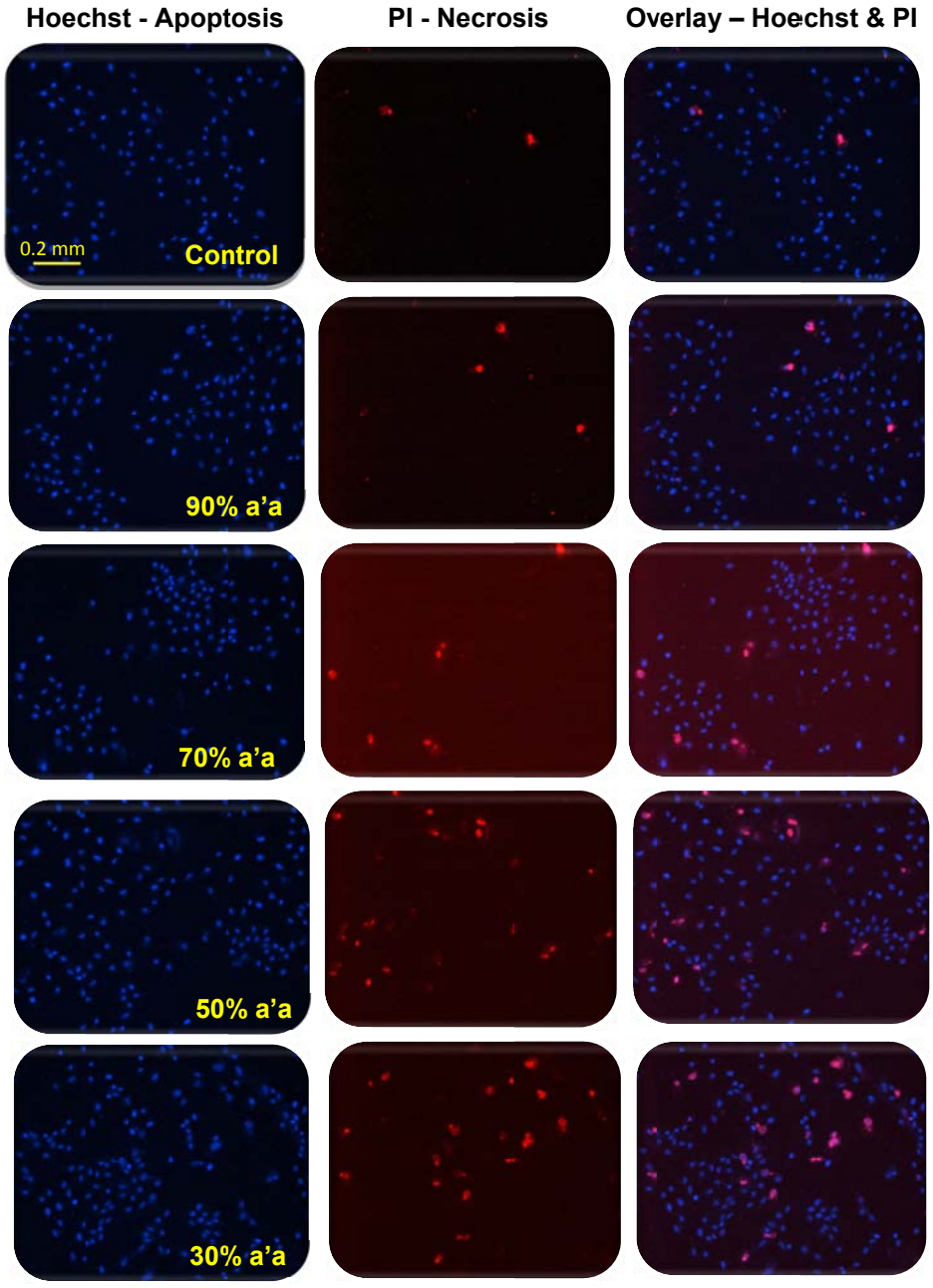

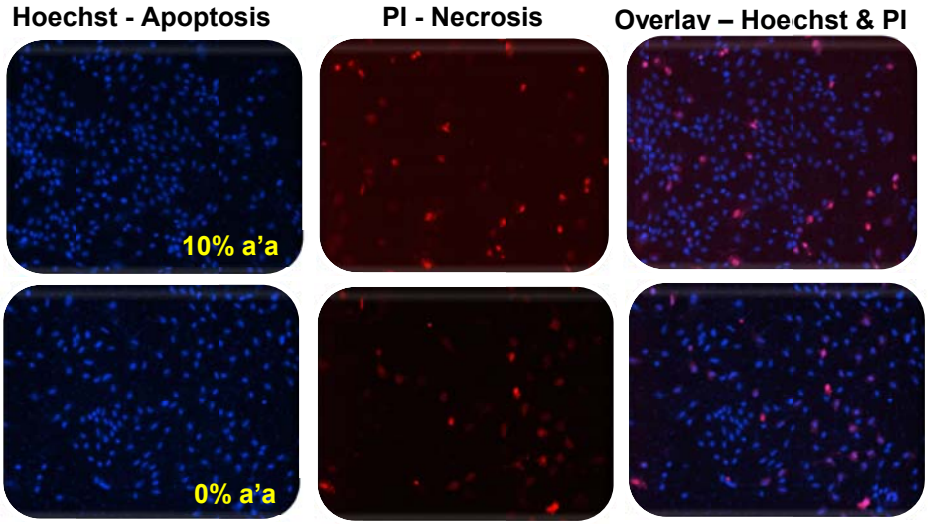

Figure 5.2.1 (a): The effect of decreasing amino acid concentrations on apoptosis and necrosis in H_9C_2 myoblasts after 24 hrs. H_9C_2s were stained with both Hoechst 33342 (blue) and PI (red) and assessed for apoptosis and late apoptosis/necrosis using fluorescence microscopy (n =3). Magnification = 10X. Scale bar = 0.2 mm

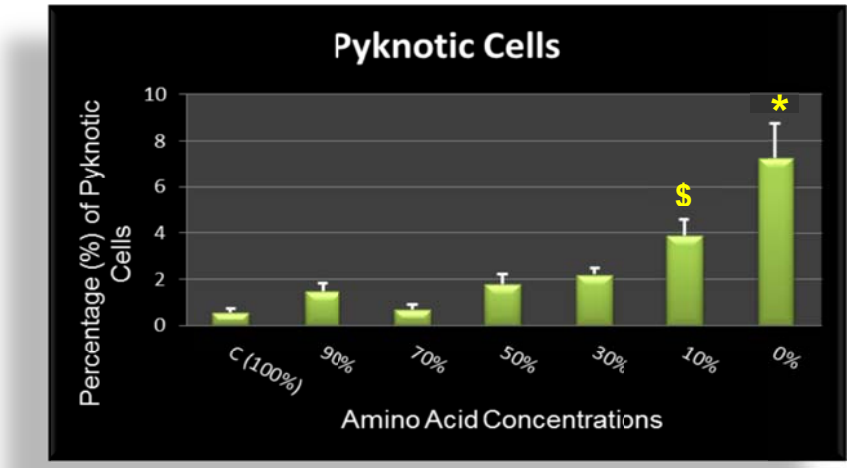

Figure 5.2.1 (b): The effect of decreasing amino acid concentrations on apoptosis in H_9C_2 myoblasts after 24 hrs. H_9C_2s were stained with Hoechst 33342 as an indicator of pyknosis, and thus representing apoptosis, using fluorescence microscopy. At least 300 cells per experiment were assessed for signs of apoptosis. Results are presented as mean ± SEM. $^{\$}P < 0.05$, $^{*}P < 0.001$ versus control ($n \geq 3$).

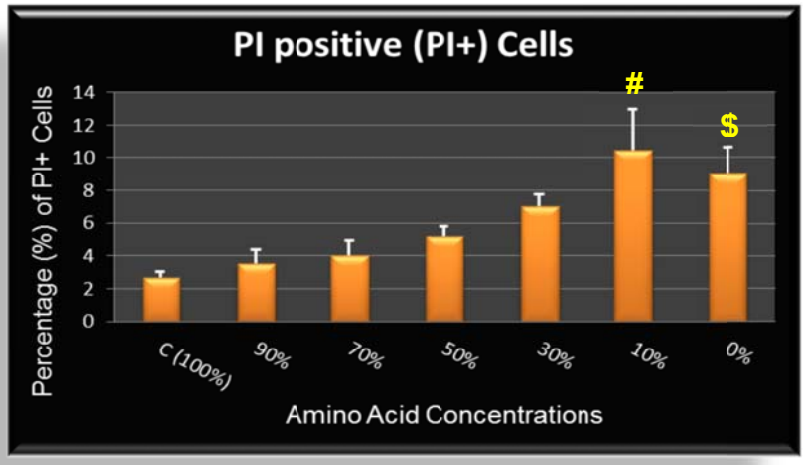

Figure 5.2.1 (c): The effect of decreasing amino acid concentrations on late apoptosis/necrosis in H_9C_2 myoblasts after 24 hrs. H_9C_2s were stained with PI as an indicator of necrosis using fluorescence microscopy. At least 300 cells per experiment were assessed for signs of necrosis. Results are presented as mean ± SEM. $^{\$}P < 0.05$, $^{\#}P < 0.01$ versus control ($n \geq 3$).

5.3: Assessment of autophagy during amino acid deprivation

In order to determine the influence of decreasing amino acid concentrations on the autophagic pathway, LC-3I lipidation to LC-3II during autophagy was evaluated. The ratio of LC-3II/LC-3I is indicated in Figure 5.3.1. After 24 hrs of amino acid deprivation the 50% [118.10 ± 3.78% ($p < 0.05$)], 30% [120.60 ± 4.07% ($p < 0.01$)], 10% [120.90 ± 2.19% ($p < 0.01$)] and 0% [125.80 ± 2.89% ($p < 0.001$)] amino acid groups resulted in a significant increases in LC-3 upregulation when compared to the control (100%).

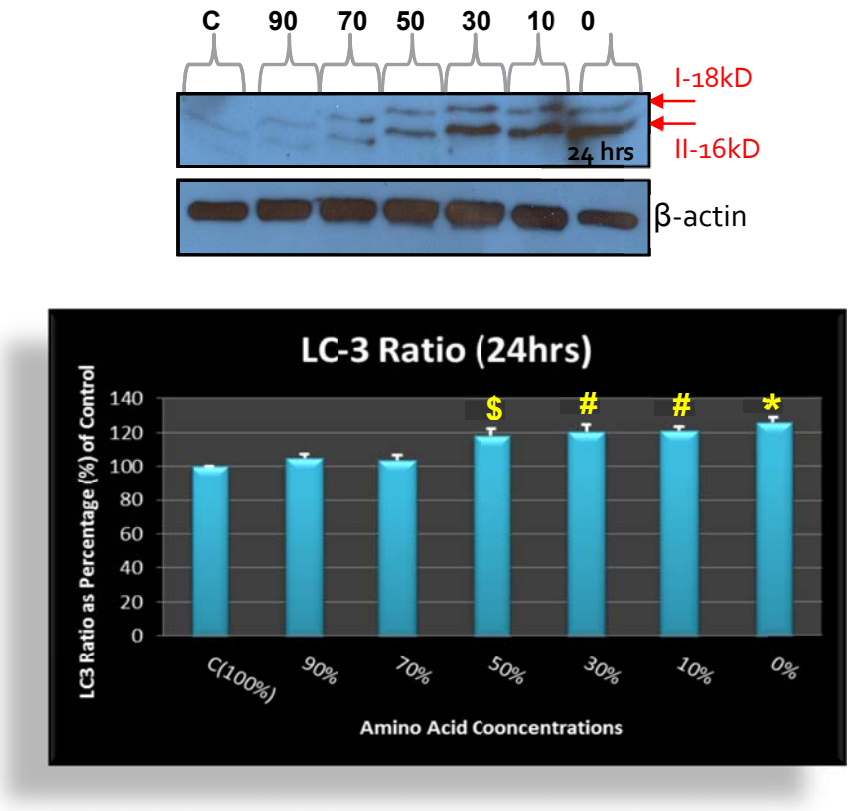

Figure 5.3.1: Immunoblot analysis and the relative quantification of LC-3 in the H_9C_2 cell line supplemented with decreasing amino acid concentrations for 24 hrs. β-actin levels were used as a loading control. All values are reported as a mean of three independent experiments ± SEM. Statistical significance at $^{\$}P < 0.05$, $^{\#}P < 0.01$ and $^{*}P < 0.001$ versus control ($n \geq 3$). Abbreviations - **C**: control; **90%**: 90% amino acids; **70%**: 70% amino acids; **50%**: 50% amino acids; **30%**: 30% amino acids; **10%**: 10% amino acids; **0%**: 0% amino acids.

Appendix B – Supplementary Data (Section 2)

Characterization of H_9C_2s during Rapamycin (autophagy inducer) treatment

Another common mechanism often used to stimulate autophagy is to use a pharmacological agent and in this case, Rapamycin, a well-known stimulant was employed. We needed to determine which dose of Rapamycin was appropriate to upregulate autophagy sufficiently without detrimental effects.

6.1: Dose response

Results obtained from The MTT assay showed that all doses after 24 hrs improved mitochondrial viability when compared to the control. However after 48 hrs, the various doses of Rapamycin appeared to have a detrimental effect and thus decreased viability when compared to the control (Figure. 6.1.1). Additionally, western blotting for beclin-1 and LC-3 was performed using these doses of Rapamycin. Results demonstrate that Beclin-1 after 24 hrs is elevated above basal levels when compared to the control (Figure 6.1.2). After 48 hrs however, the 25 nM and 50 nM concentrations of Rapamycin showed modest decreases in Beclin-1 production when compared to its control. Nevertheless none of the doses used produced significance.

LC-3 on the other hand was increased at all concentrations and at both time points when compared to the control (Figure 6.1.3). From these results, it was concluded that the concentration of 50 nM at 24 hrs of Rapamycin was appropriate and thus will be used throughout the study to assess the autophagic pathway. This concentration has also been previously validated in our laboratory within the same cell line and is therefore applicable for this study (Loos, 2009).

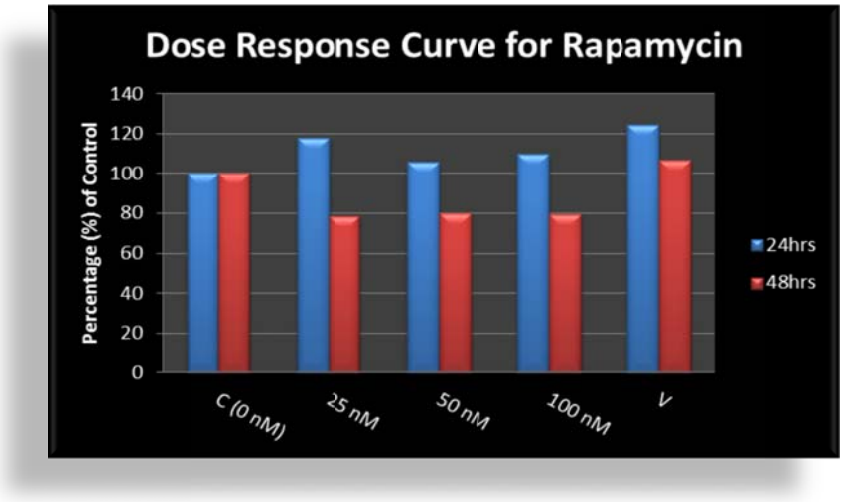

Figure 6.1.1: Effect of various rapamycin concentrations on mitochondrial viability in H_9C_2s. H_9C_2 myoblasts were incubated with increasing concentrations of Rapamycin for 24 and 48 hrs and their cell activities were assessed. Abbreviations - **C**: control; **V**: vehicle (PBS).

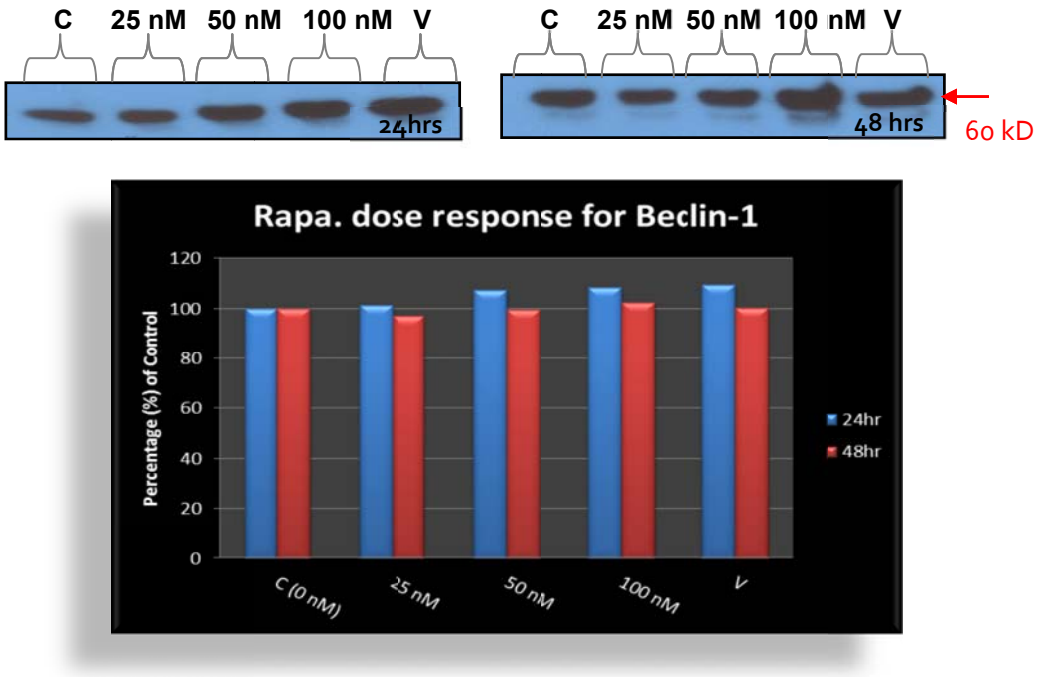

Figure 6.1.2: Immunoblot analysis and the relative quantification of Beclin-1 in the H_9C_2 cell line supplemented with various concentrations of Rapamycin for 24 and 48 hrs. Abbreviations - **C**: control; **V**: vehicle (PBS).

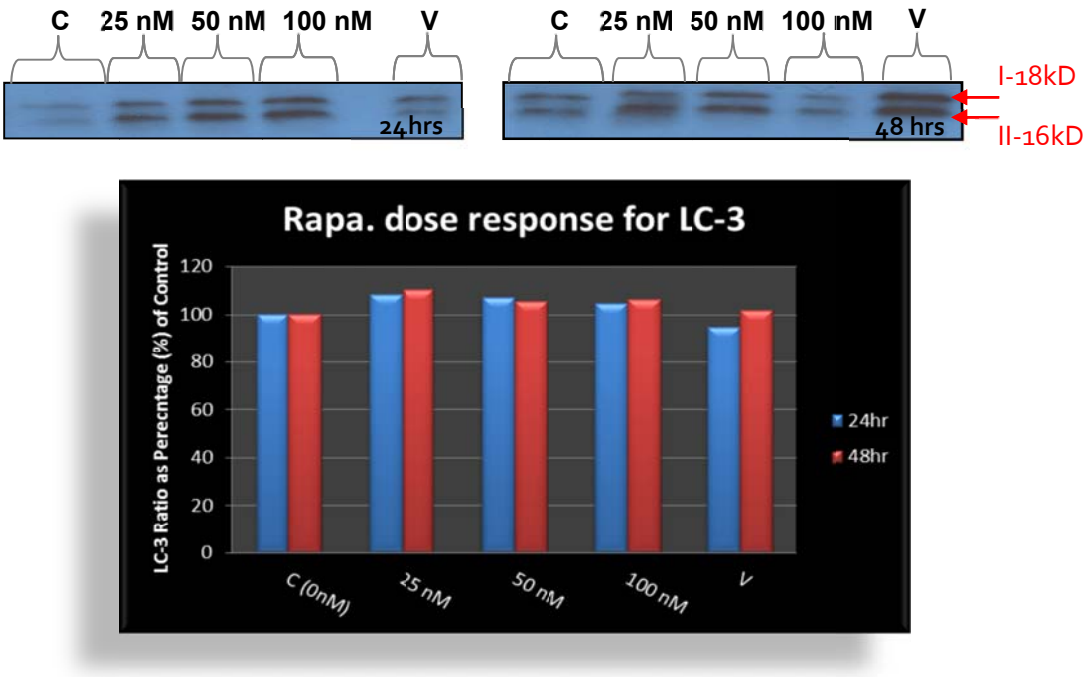

Figure 6.1.3: Immunoblot analysis and the relative quantification of LC-3 in the H_9C_2 cell line supplemented with various concentrations of Rapamycin for 24 and 48 hrs. Abbreviations - **C**: control; **V**: vehicle (PBS).

Appendix C – Supplementary Data (Section 3)

Characterization of H_9C_2s during Bafilomycin A1 (autophagy inhibitor) treatment

In continuation from the previous results obtained (Supplementary Data), autophagy inhibition with Bafilomycin A1 was used. This pharmacological agent blocks the fusion of autophagosomes with lysosomes thereby causing an accumulation of both organelles within the cell. A dose and time response curve was conducted with MTT assays in order to determine the appropriate time and dose to use throughout the study.

7.1: Dose response

A time- and dose-dependent decrease in mitochondrial viability was observed after 6, 24 and 48 hrs when comparing the different doses of bafilomycin A1 to their controls respectively (Figure 7.1.1). Western blot results for Beclin-1 also showed modest increases at all times and doses of bafilomycin A1 when compared to the control (figure 7.1.2). Additionally, LC-3 assessment demonstrated increased accumulation, specifically LC-3-II, at all-time points and at all doses (Figure 7.1.3).

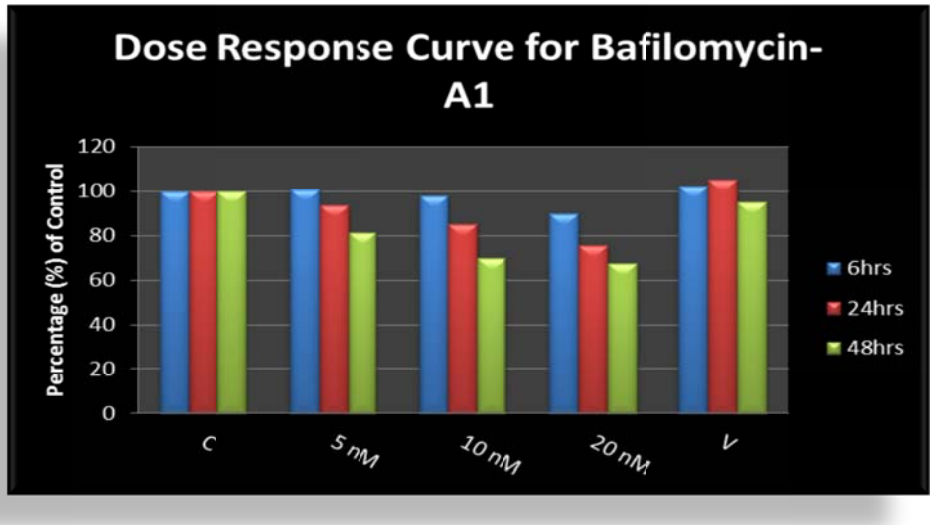

Figure 7.1.1: Effect of various Bafilomycin A1 concentrations on mitochondrial viability of 70-80% confluent H_9C_2s. H_9C_2 myoblasts were incubated with increasing concentrations of Bafilomycin A1 for 6, 24 and 48 hrs and their cell activities were assessed at these time points.

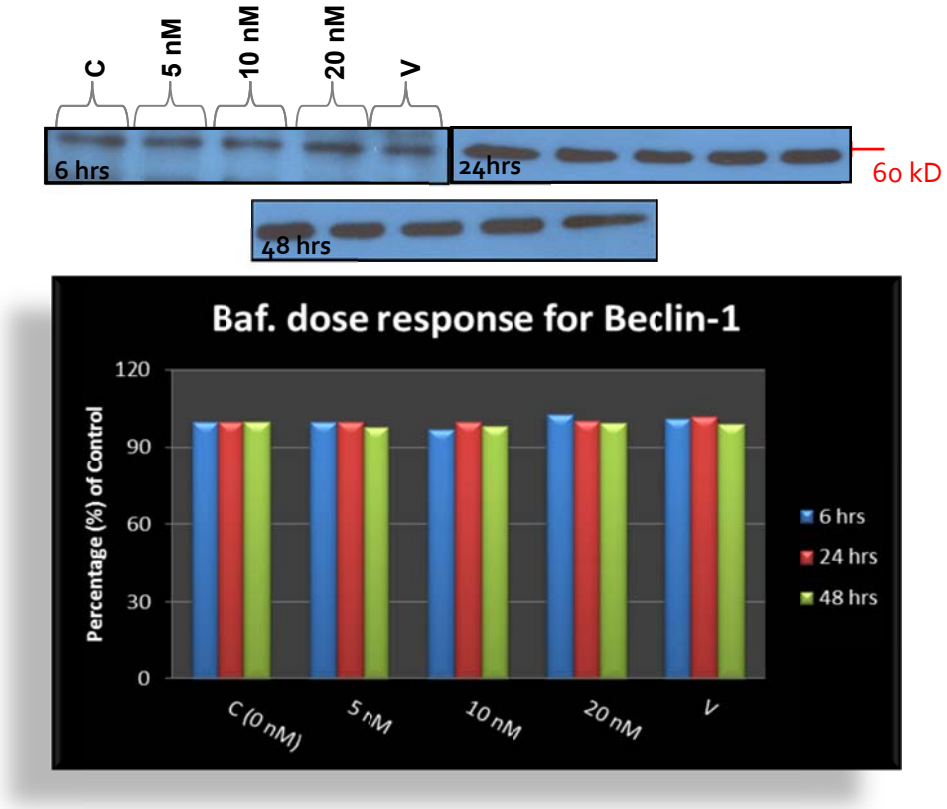

Figure 7.1.2: Immunoblot analysis and the relative quantification of Beclin-1 in the H_9C_2 cell line supplemented with various concentrations of Bafilomycin A1 for 6, 24 and 48 hrs.

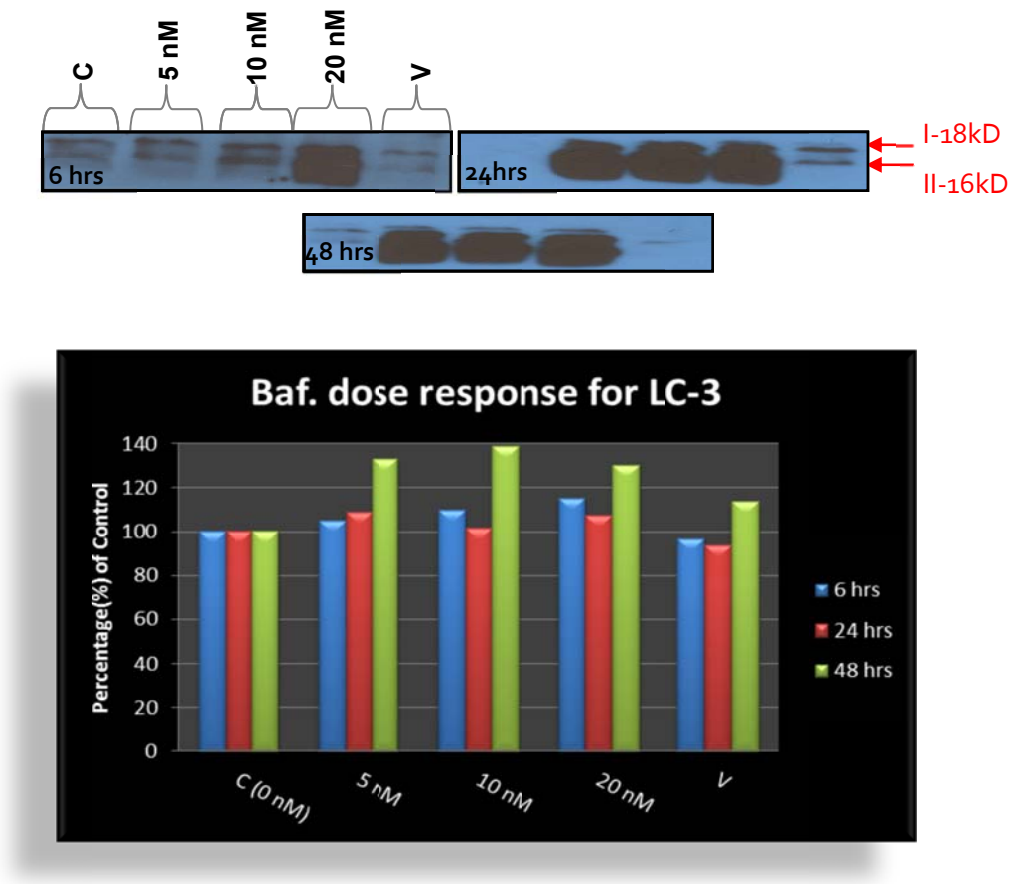

Figure 7.1.3: Immunoblot analysis and the relative quantification of LC-3 in the H_9C_2 cell line supplemented with various concentrations of Bafilomycin A1 for 6, 24 and 48 hrs.

From these results the concentration of 10 nM was deduced to be appropriate as it induced modest decreases in cell viability following shorter incubation times. The assessment of autophagic markers demonstrated a dose- and time-dependent increase in these proteins caused by the inhibition of autophagic activity. The following experiments will be conducted using this concentration (10 nM) of bafilomycin A1 at a time point of 6 hrs.

Appendix D – Supplementary Data (Section 4)

Assessment of Cell Death during combination treatment (Figure 8.1.1 - 3)

Assessment of cell death in the form of apoptosis and necrosis demonstrated a trend towards an increase in pyknosis in groups CR and CB when compared to the control. Necrosis evaluation also showed a trend towards an increase in group CB

whereas group CR showed a trend towards a decrease. No significant differences were however observed in any of the groups analysed. The groups treated with DXR were not analysed due to interference of DXR auto-fluorescence localised in the nuclei where both dyes are situated (see images below). Another problem encountered with analysis of the necrosis images was the fact that both PI and DXR fluoresce within the same light spectrum, and therefore an examiner was unable to differentiate whether what they observed was due to true PI fluorescence or true DXR fluorescence. Further experiments will however be conducted to assess both forms of cell death.

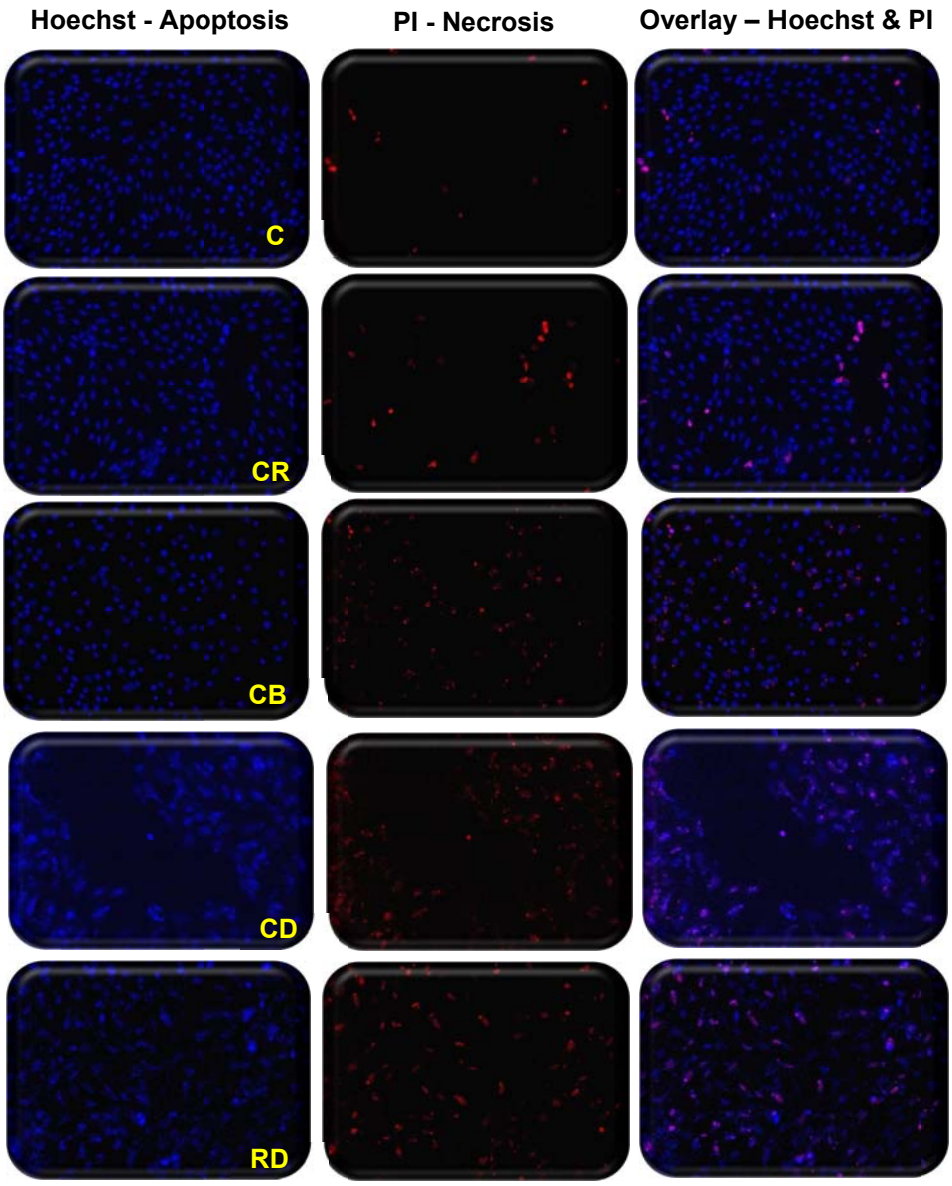

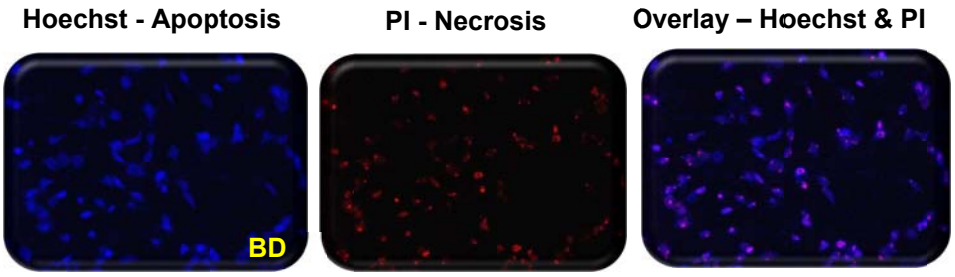

Figure 8.1.1: Effect of various treatment regimens on apoptosis and necrosis in H_9C_2 myoblasts. H_9C_2s were stained with both Hoechst 33342 (blue) and PI (red) and assessed for apoptosis and late apoptosis/necrosis using fluorescence microscopy. Abbreviations - **C**: control; **CR**: rapamycin, **CB**: bafilomycin A1, **CD**: DXR, **RD**: rapamycin and DXR, **BD**: bafilomycin A1 and DXR.

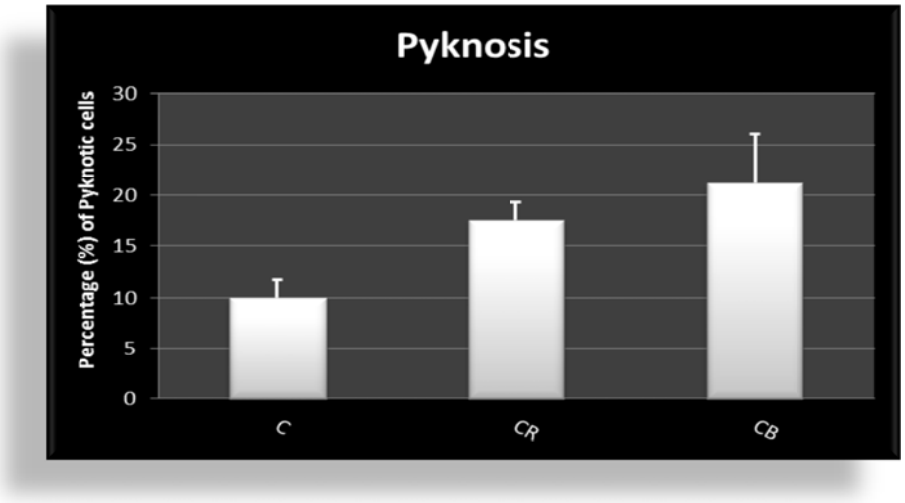

Figure 8.1.2: Effect of various treatment regimens on apoptotic cell death in H_9C_2 myoblasts. H_9C_2s were stained with Hoechst 33342 and apoptosis was assessed using fluorescence microscopy. At least 300 cells per experiment were assessed for signs of apoptosis. Results are presented as mean ± SEM ($n \geq 3$). Abbreviations - **C**: control; **CR**: rapamycin, **CB**: bafilomycin A1.

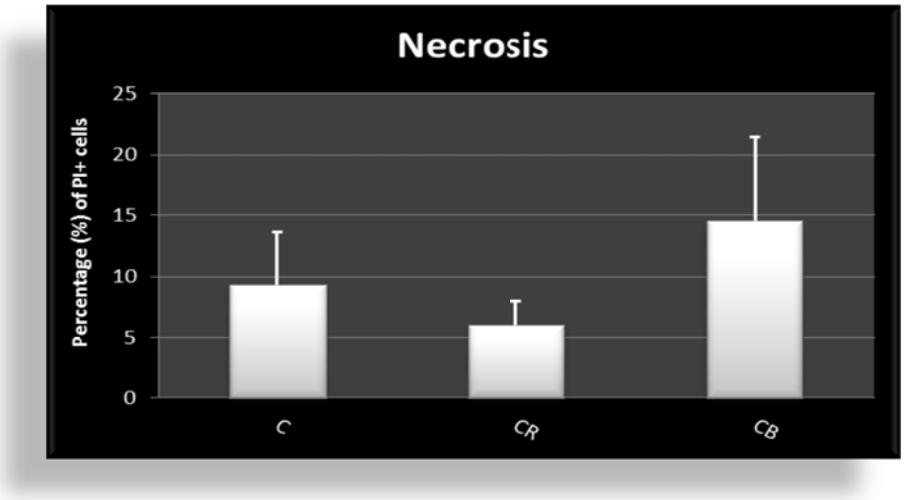

Figure 8.1.3: Effect of various treatment regimens on late apoptosis/necrosis in H_9C_2 myoblasts. H_9C_2s were stained with PI and necrotic cell death was assessed using fluorescence microscopy. At least 300 cells per experiment were assessed for signs of necrosis. Results are presented as mean ± SEM ($n \geq 3$). Abbreviations - **C**: control; **10**: **CR**: rapamycin, **CB**: bafilomycin A1.

Another technique used to assess apoptotic activity was western blotting. We needed to determine whether the enzyme activity observed in the above experiment was being translated into protein form. Significant increases in cleaved-caspase-3 were observed in groups CR [125.40 ± 1.34% ($p < 0.01$)], CB [121.90 ± 4.07% ($p < 0.01$)] and CD [131.00 ± 3.99% ($p < 0.001$)] when compared to the control (100%) (Figure 8.1.4). The upregulation (RD) or inhibition (BD) of autophagy in combination with DXR however did not appear to improve nor exacerbate the amount of c-caspase-3 produced when compared to group CD. Additionally, PARP cleavage (Figure 8.1.5) was also assessed in order to get a better understanding of the mechanism of this pathway as it is known that caspase-3 cleavage leads to PARP activation and thus execution of apoptosis. Although a trend towards an increase in cleaved-PARP (c-PARP) was observed in groups CR, CB and CD, a trend towards a decrease in c-PARP was observed in groups RD and BD. Nevertheless, these observations were insignificant.

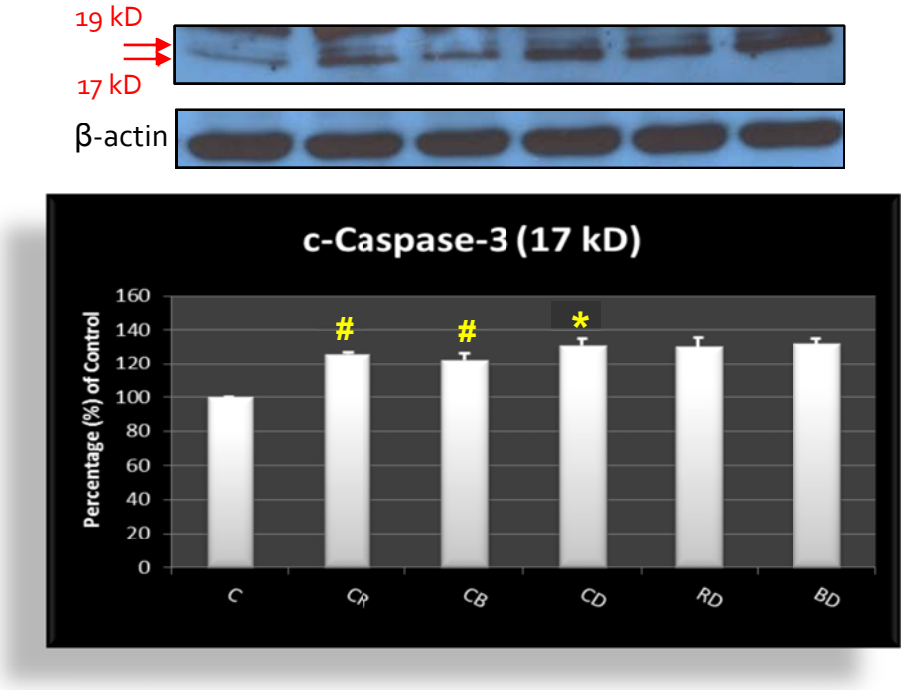

Figure 8.1.4: Immunoblot analysis and the relative quantification of cleaved-caspase-3 (c-caspase-3) in the H_9C_2 cell line supplemented with 50 nM rapamycin, 3 µM DXR for 24 hrs as well as 10 nM Bafilomycin A1 for 6 hrs. Results are presented as mean ± SEM (n = 3). $^{\#}P < 0.01$, $^{*}P < 0.001$ versus control. Abbreviations - **C**: control; **CR**: rapamycin, **CB**: bafilomycin A1, **CD**: DXR, **RD**: rapamycin and DXR, **BD**: bafilomycin A1 and DXR.

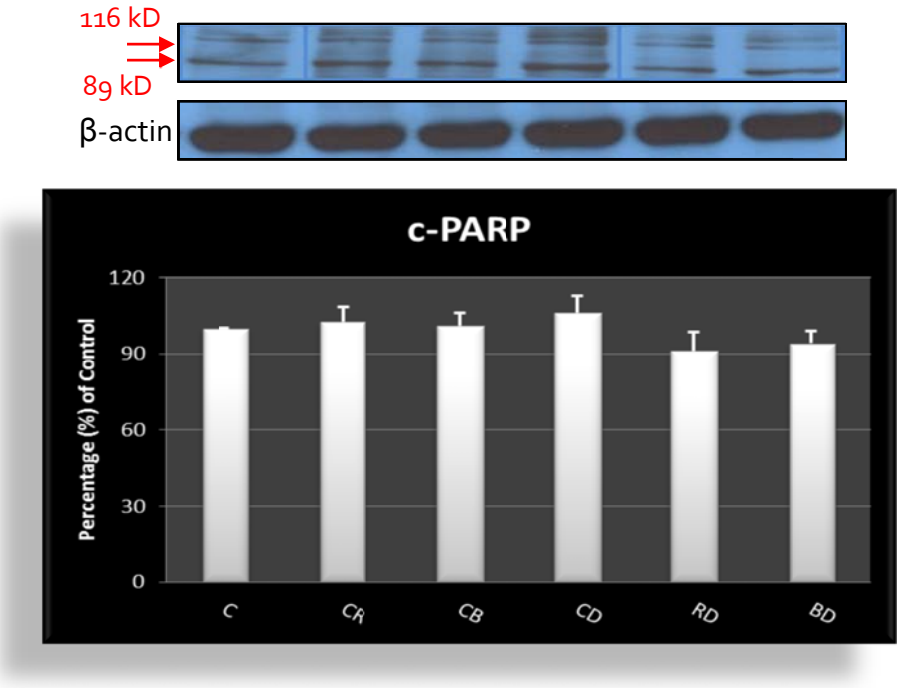

Figure 8.1.5: Immunoblot analysis and the relative quantification of cleaved-PARP (c-PARP) in the H_9C_2 cell line supplemented with 50 nM rapamycin, 3 µM DXR for 24 hrs as well as 10 nM Bafilomycin A1 for 6 hrs. Results are presented as mean ± SEM (n = 3). Abbreviations - **C**: control; **CR**: rapamycin, **CB**: bafilomycin A1, **CD**: DXR, **RD**: rapamycin and DXR, **BD**: bafilomycin A1 and DXR.

Lactate Dehydrogenase (LDH) Assay (Figure 8.1.6)

Another assay used to determine necrosis in this study included the LDH (lactate dehydrogenase) assay which quantitatively measures LDH, a stable cytosolic enzyme that is released during cell lysis. This assay is based upon the principal that the amount of LDH released by the cells during treatment is directly proportional to the amount of cell lysis taking place and thus necrosis. Results obtained from this assay were inconclusive as no significant differences were observed at any of the groups when compared to the control or group CD. Although this assay was performed to verify results acquired from the trypan blue exclusion technique, the pattern of results attained from these data varied vastly from that of the previous technique. While necrosis is a common irreversible form of cell death under stressful conditions, based on these findings, this type of cell death is present in varying amounts in the various treatment groups.

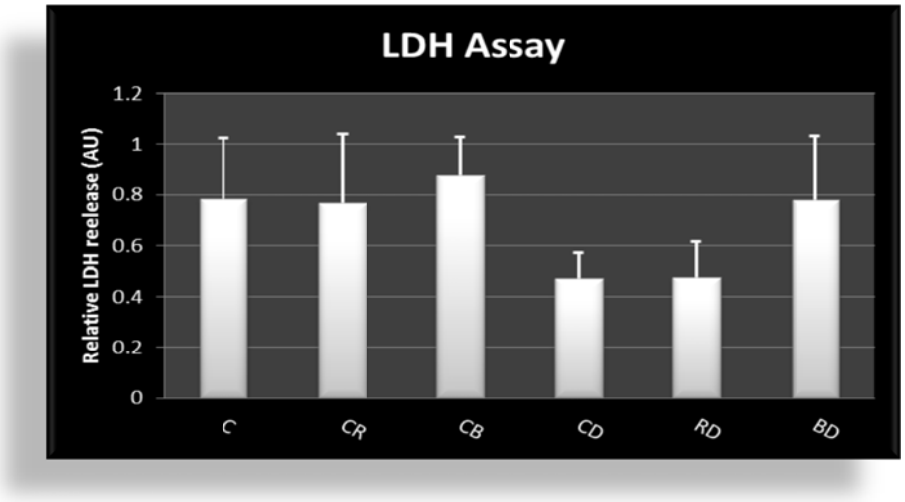

Figure 8.1.6: Effect of various treatment regimens on LDH release in H_9C_2s. H_9C_2 myoblasts were treated with 50 nM rapamycin, 3 µM DXR for 24 hrs as well as 10 nM Bafilomycin A1 for 6 hrs and LDH release was assessed. Results are presented as mean ± SEM (n = 3). Abbreviations - **C**: control; **CR**: rapamycin, **CB**: bafilomycin A1, **CD**: DXR, **RD**: rapamycin and DXR, **BD**: bafilomycin A1 and DXR.

Assessment of Ca^{2+} changes during combination treatment (Figure 8.1.7)

The toxicological significance of Ca^{2+} in this context has remained largely undefined. In order to determine the role of Ca^{2+} in cardiotoxicity, H_9C_2 cells were stained with

the Fura Ca^{2+} ratiometric indicator (Molecular Probes, F1221) and observed whether any changes in the ratio of the Fura Ca^{2+} ratiometric indicator were present. Results obtained only showed transient Ca^{2+} fluxes between the groups and no significance was observed. It should be noted that in this experiment only the ratiometric change and not the Ca^{2+} concentration was determine. Perhaps a better indicator to determine whether any changes had occurred would have been to measure free Ca^{2+} concentration within the cytosol of the cardiomyocytes with this technique.

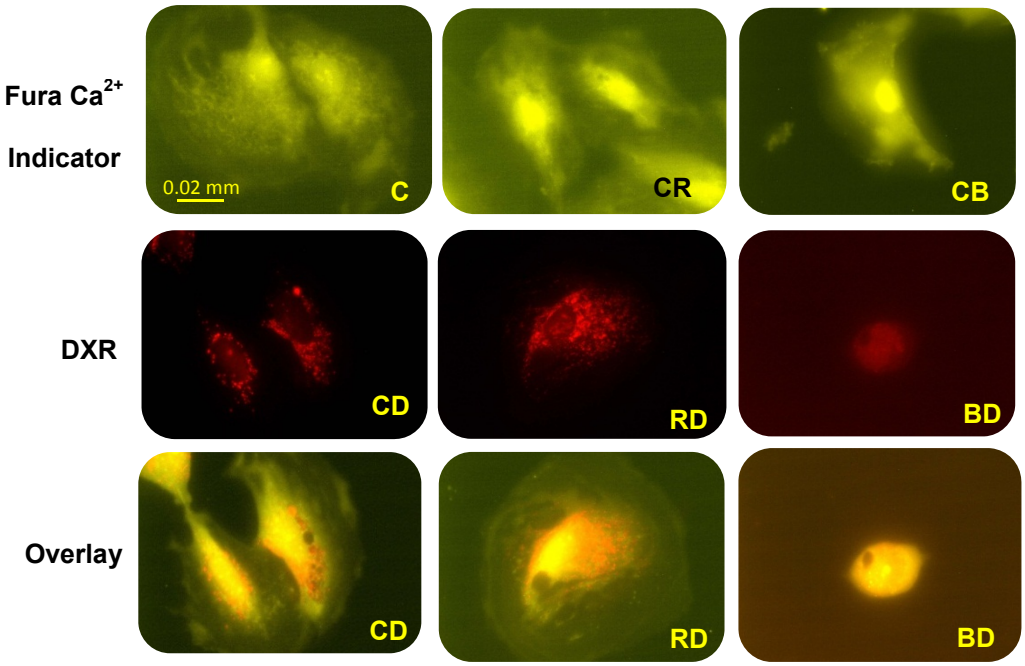

Figure 8.1.7 (a): Effect of various treatment regimens on Ca^{2+} homeostasis in H_9C_2 myoblasts. H_9C_2s were stained with the Fura Ca^{2+} ratiometric indicator and visualized using fluorescence microscopy ($n \geq 3$). Abbreviations - **C**: control; **CR**: rapamycin, **CB**: bafilomycin A1, **CD**: DXR, **RD**: rapamycin and DXR, **BD**: bafilomycin A1 and DXR. Magnification = 60X. Scale bar = 0.02 mm.

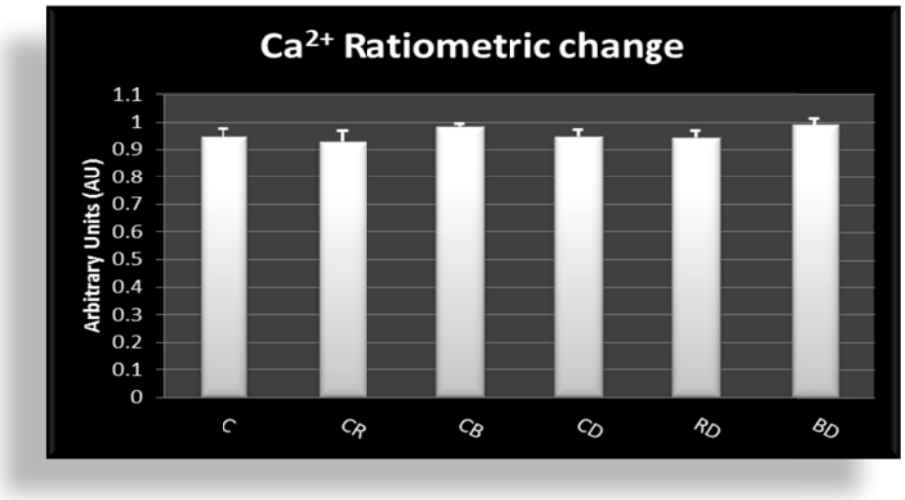

Figure 5.1.7 (b): Effect of various treatment regimens on Ca^{2+} homeostasis in H_9C_2 **m**yoblasts. H_9C_2s were stained with the Fura Ca^{2+} ratiometric indicator and assessed using fluorescence microscopy ($n \geq 3$). Abbreviations - **C**: control; **CR**: rapamycin, **CB**: bafilomycin A1, **CD**: DXR, **RD**: rapamycin and DXR, **BD**: bafilomycin A1 and DXR. Magnification = 60X. Scale bar = 0.02 mm.

Appendix E

The Red SR FLIVO dye (an apoptosis indicator) was injected into the tail vein of the mice 1 hr before animals were sacrificed. Following the sacrifice, hearts were rapidly excised and sectioned horizontally to allow freeze clamping for biochemical as well as histological analysis. Visualisation of the cardiac tissue through fluorescence microscopy ensued, however no fluorescence was detected through this method therefore western blotting was employed.

Appendix F

Protocol 1: Cell culture

- Before work was started on the hood, hands were washed up to the elbows and gloves were worn. Hands were sprayed with 70% alcohol each time before putting them inside the laminar flow to keep sterile
- 75 cm^2 flasks containing H_9C_2 myoblasts that were approximately 70-80% confluent were split into smaller 6-well plates or 25 cm^2 culture flasks containing ± $80x10^3$ or ± $20x10^4$ cells respectively for experimental purposes
- Cells were first washed with warm PBS (see Appendix G) to remove all traces of growth medium (GM) (see Appendix G) and were then loosened from the 75 cm^2 flask surface using trypsin (4 ml) which is a protease enzyme
- The flask was placed in a "shaking" incubator for 2-3 min at 37 ºC (Trypsin is only active at this temperature). Cells were checked to see if they have detached under a microscope. If the cells had not loosened, the bottom of the flask was gently tapped to help the process
- Once the cells have eventually loosened, warm GM (double the volume of trypsin, thus 8 ml) was added to the cells to neutralise the trypsin
- The cells/trypsin and medium were transferred to a 10 ml falcon tube and centrifuged at $15x10^3$ rpm for 3 min
- The supernatant (medium containing trypsin) was decanted and the pellet (cells) at the bottom of the tube was resuspended with 3 ml fresh GM using a pipette
- To determine the average number of cells, 20 µl from the cell suspension was pipetted onto a haemocytometer (see protocol 2)
- The number of cells per millilitre was determined using a simple calculation

Protocol 2: Cell counting using a haemocytometer

- The haemocytometer was first cleaned by wiping with 70% alcohol and then breathed on it to moisten the surface before placing a coverslip on top
- The coverslip was placed over the counting area on the haemocytometer and viewed under a microscope until Newton's rings appeared
- A sample (20 µl) of the resuspended cell solution was then aspirated onto the coverslip using a micropipette
- The cell suspension was allowed to fill the chamber by capillary action and both counting grids covered (see example below)

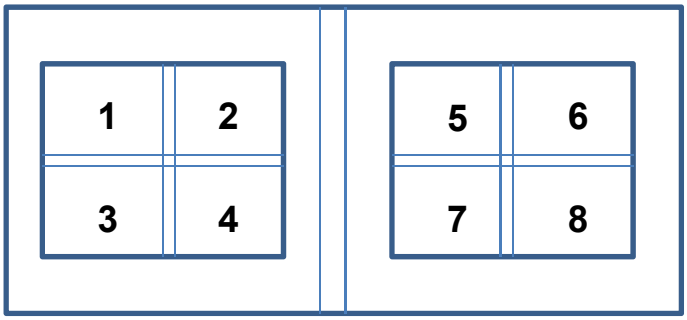

- The total number of cells was counted by counting areas 1 to 8 in both counting grids. The average number of cells was then calculated. This average was then multiplied by $1x10^4$ to get the number of cells per millilitre of the original cell suspension

Protocol 3: Cell Harvesting

- This process removes the cells from the plastic substrate and breaks cell-to-cell bonds as gently as possible
- The old medium was discarded either by careful decanting or with a sterile pipette and the monolayer of cells was washed quickly with ice cold PBS. This wash step was repeated three times to remove all traces of FBS

- The wash medium was decanted and then 250 µl (6-well plates) or 1000 µl (25 cm^2 flask) of RIPA buffer (see appendix G) was added to each well of the 6-well plate and flasks and placed on ice for 3-5 min
- The plates or flasks were swirled to make sure that the surface area was covered with the buffer
- After the time period had lapsed, the cells were scraped from the surface of each well and flask using a sterile cell scraper
- The buffer containing the cells was then pipetted into already chilled eppendorf tubes and stored at -80 °C until further experiments were carried out.

Protocol 4: Extraction of proteins from cell samples

- Work on ice at all times to avoid the denaturing of proteins
- Thawed cell samples (from protocol 3) were placed in chilled test tubes and sonicated. This process ruptures the cell walls in order to release proteins
- The metal piece of the sonicator was rinsed before and after use with distilled water
- After sonicating the cells, the cell solution was transferred into a chilled eppendorf tube and centrifuged at 4 ºC and $8x10^3$ rpm for 10 min.

Protocol 5: Protein determination with Bradford reagent

- Work on ice at all times to avoid the denaturing of proteins
- For protein determination, make a 1:5 dilution of the Bradford reagent (see Appendix G) using distilled water. This solution needs to be filtered twice using 2 pieces of filter paper. The Bradford reagent is light sensitive therefore remember to use foil or work in the dark room when filtering
- Once the Bradford reagent has been made, a standard curve needs to be made in 7 different eppendorf tubes as follows:

	Distilled water (dH_2O)	BSA (see Appendix G)	Bradford Reagent
1	0 µl	100 µl	900 µl
2	20 µl	80 µl	900 µl
3	40 µl	60 µl	900 µl
4	60 µl	40 µl	900 µl
5	80 µl	20 µl	900 µl
6	90 µl	10 µl	900 µl
7	100 µl	0 µl	900 µl (**BLANK**)

- Vortex the solutions thoroughly and let them stand in ice for ±5 min
- Zero the spectrophotometer using the blank and then read the absorbance values at 595 nm using the Simple Reads program
- Once the absorbance readings were recorded, the reading were transferred onto an Excel spreadsheet and a standard curve was created (see graph below)

Samples:

- Pipette 5 µl from each sample that was centrifuged into a new eppendorf tube and then add 95 µl distilled water and 900 µl Bradford reagent. Vortex solution and then read the absorbance values at 595 nm using the Simple Reads program
- Using excel, plot the standard curve with protein concentration on the x-axis and the mean OD on the y-axis (see example below). Add in the absorbance

values for the samples and determine final calculation for protein concentration in µl/ µg

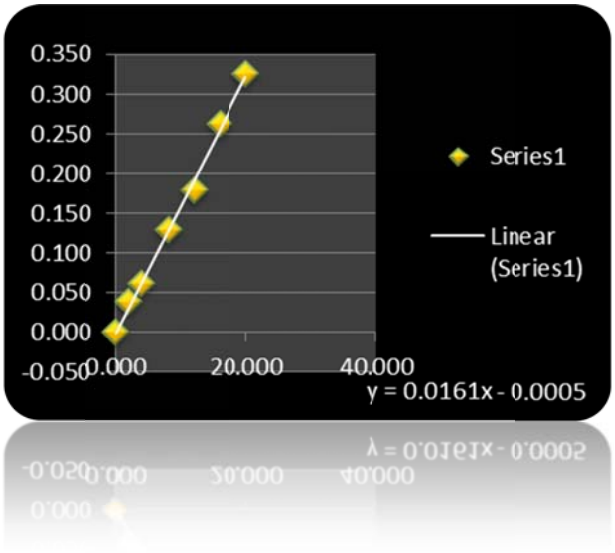

- Once the concentration of each sample has been worked out, pipette the desired amount into a new eppendorf tube and add the appropriate amount of sample buffer (see Appendix G)

Protocol 6: Western Blot Procedure

Preparation of assembly and gels

- Clean glass plates with 70% alcohol and place into assembly
- Place assembly onto plastic apparatus with rubber and firmly clip into place. Check for leaks with distilled water
- Mark on glass plate where separating gel comes to (1/2 cm below top of glass plate)
- Make up the separating gel (8%, 10%, 12% or 15%) (see Appendix G)
- Using a squeeze pipette, add separating gel to assembly into the side. Avoid making bubbles
- Add a few drops of iso-butanol to prevent oxidation of gel and to ensure a straight line with no meniscus
- Allow to set for 30 min

- Wash of iso-butanol with distilled water
- Make up the stacking gel (4%) (see Appendix G)
- Using a squeeze pipette, add stacking gel on top of separating gel. Immediately add the 10 well comb at an angle to prevent bubbles until the wells come to the end of the glass plates. Don't push in too deep and then take out
- Allow gel to set for 30 min. During this time prepare Running buffer and thaw your samples
- Denature samples by boiling at 50-70 ºC for 5 min. Punch a hole in each sample eppendorf to release pressure
- Centrifuge samples for ±10 sec at $5x10^3$ rpm.
- Remove combs carefully and rinse with distilled water. Drain excess water with blotting paper, being careful not to wipe away the wells
- Take glass off assembly stand and place onto U-shaped Core-latch and then click to secure
- Place the apparatus into tank and add Running buffer (see Appendix G) in the middle compartment just overflowing into the wells

Loading samples

- Place yellow well guide on top of apparatus in the middle compartment
- Using a 20 µl pipette, add 10 µl peqGOLD pre-stained marker in first well on the left and then your samples from the second well. Use a clean tip for every sample and marker
- Once all samples have been loaded, remove the well guide and add running buffer on the outer compartment up to ½ way from the bottom
- Place green lid on apparatus and attach electrodes – red to red and black to black
- Turn on electrophoresis machine and allow samples to run for 10 min at 400 mA and 100 V (fixed)
- Run samples for a second time for 50 min at 400 mA and 200 V

Transfer of proteins to membrane

- Soak PVDF membrane in methanol then rinse in distilled water and then soak in transfer buffer (see Appendix G) until needed
- Dip a piece of blotting paper in transfer buffer and place on the semi-dry apparatus
- Go back to gel apparatus and remove the U-shaped core-latch. Remove the glass plates and separate them very carefully to avoid tearing the gel. Cut off the wells (stacking gel) and place the remaining (separating) gel in transfer buffer
- Place the PVDF membrane on top of the blotting paper already on the semi-dry apparatus and then add the gel on top of membrane
- Finally, place another piece of blotting paper (dipped in transfer buffer) on top of the gel and roll out excess liquid thoroughly
- Close the apparatus and then supply power for electron transfer: 15V, 0.5A, 300W for 1 hr
- Once the time has elapsed, open semi-dry apparatus and remove the blotting papers on top carefully. Place membrane in methanol for a few minutes and allow to air dry completely
- Place membrane in blocking solution (see Appendix G) for a minimum period of 2 hr on the belly dancer on lowest setting or leave in the fridge (4 ºC) overnight

Specific binding of proteins

- Wash membrane 3X (5 min each) with TBS-tween (see Appendix G)
- Make primary antibody (see Appendix G) solution in a 50 ml falcon tube. Roll the membrane containing transferred proteins facing the inside and the marker facing the bottom and place inside the falcon tube
- Mix on the rotating machine in the corridor fridge for a minimum period of 8 hr or leave overnight
- Wash membrane 3X (5 min each) with TBS-tween

- Make secondary antibody (see Appendix G) solution in a 50 ml falcon tube and add to membrane. Mix on the belly dancer or tube roller on lowest setting for 1 hr

Exposure

- Wash membrane 3X (5 min each)
- Cut 2 pieces of transparent paper and tape them together on one side in a cassette (exposure tray)
- Mix ECL cocktails (500 µl solution **A** + 500 µl solution **B**) in falcon tube
- Drain excess liquid from membrane using tissue paper and add the ECL on the membrane and leave on for 1min
- Drain excess ECL from membrane and place membrane in between the transparencies. Remove the air bubbles
- In the dark room with the lights off, cut x-ray film and place on the exposure tray on top of the transparency. Place once and do not remove. Close exposure tray and leave for ± 5 min
- After the time elapsed, take out the x-ray film and place in developer for ± 5 min
- Rinse x-ray film thoroughly in water and then place in fixative for ± 5 min
- Rinse well and air dry

Stripping membranes

- Wash membrane 2X (5 min each) in dH_2O at room temperature
- Wash membrane 1X (5 min) in 0.2 M NaOH at room temperature
- Wash membrane 2X (5 min each) in dH_2O at room temperature
- Place membrane in blocking solution and carry on as usual for western blotting (This procedure completely removes all antibodies)

Protocol 7: MTT assay

Preparation of solutions

- 1% Isopropanol = 1 ml Concentrated HCl added to 99 ml Isopropanol
- % Triton = 0.1 ml Triton-X-100 made up to 100 ml using distilled water
- Isopropanol/ Triton solution in 50/1 ratio = 50 ml of 1% Isopropanol added to 1 mL 0.1% Triton
- 1% MTT (0.01 g/1 ml PBS) made fresh before use. This solution was covered in foil to protect against the light as it is light sensitive. It was then filtered to remove any excess granules that have not dissolved

Method

- The medium from the cells was gently discarded. These cells were not rinsed with PBS as the cells may loosen
- 1.5 ml PBS and 500 µl MTT solution was added to each well. This was done very slowly so that the cells did not loosen.
- The plate was then covered in foil and place in the incubator for 2 hr

If some cells have loosened:

- The contents of wells were transferred to 2 ml centrifuge tubes and spun down gently for 2 min at 1000 rpm
- The supernatant was discarded and 2 ml 'Isopropanol/Triton' solution was added to each pellet and the cells were resuspended. This resuspended solution was added back into wells were some cells may still be sticking to wells

If no cells loosened:

- The contents of the wells were discarded and 2 ml 'Isopropanol/Triton' solution was added to each well
- The plates were put on belly dancer shaker to mix for 5 min while still covered in foil. This loosens the cells from the bottom of the surface

- The content of each well was transferred to 2 ml eppendorf tubes and centrifuged for 2 min at 1400 rpm
- The absorbance values of the supernatant was read at 540 nm on the spectrophotometer, using Isopropanol/Triton solution as the blank
- If any of the absorbance values of the supernatants were greater than one, the supernatant was diluted with the Isopropanol/Triton solution

Protocol 8: Trypan Blue exclusion technique

- Trypan blue stock solution (0.4%) was prepared with PBS and stored in the dark room at 4 ºC (see appendix G)

Method

- Medium was removed from cells, washed with warm PBS and trypsinized as previously described
- Cell solution containing trypsin was neutralized using warm growth medium and centrifuged at 1300-1500 rpm for 3 min
- The cells (each well analysed separately) were then resuspended in 500 µl warmed PBS and 500 µl 0.4 % trypan blue solution and allowed to stand for 2-5 min prior to counting
- 50 µl of the resuspended solution was placed into the haemocytometer and counting was conducted utilising the Countess™ automated cell counter. Viable cells did not take up dye and non-viable cells took up dye and stained blue

Protocol 9: Hoechst 33342 and Propidium Iodide (PI) staining techniques

For this technique, cells were grown 8-chamber slides. Cells were grown and treated as previously described. The experiments were performed in the staining lab where there is minimal light.

Method

- Medium was removed from cells and washed 3X with sterile PBS (0.1 M)
- 100 µl of PI solution (see Appendix G) was added to each chamber and incubated for 20 min at 4 ºC
- PI solution was then removed and the cells were rinsed twice with sterile PBS
- A cold fixative (1:1 methanol/acetone), enough to cover the monolayer of cells, was then added to each chamber and incubated for 10 min at 4 ºC
- The fixative was removed and the coverslips were left to air dry completely for a further 10 min
- After the time had elapsed, 150 µl of Hoechst solution (see Appendix G) was added to each coverslip and incubated for 10 min at 4 ºC
- Hoechst solution was removed and the chambers containing cells were rinsed 5 times with sterile PBS to avoid or minimise background noise
- The chambers were allowed to dry before a small drop of fluorescent mounting medium was added
- The chambers were then covered with foil to protect from the light
- The chambers and their contents can now be viewed or stored at -20 ºC for up to 2 weeks

Protocol 10: CytoTox 96 non-radioactive cytotoxicity assay (LDH Assay)

For this technique, cells were grown and treated on 96-well flat-bottom (enzymatic assay) plates and LDH was measured as follows:

- 50 µl of the reconstituted substrate mix was added to each well (50 µl) of the plate. The plate was covered in foil to protect it from light and was incubated for 30 min at room temperature
- After the incubation time had elapsed, 50 µl of stop solution was added to each well of the plate. Any bubbles formed during this were popped using a syringe needle and absorbance was recorded at 490 nm using a plate reader.
- In addition, blank (containing only medium) wells were treated with the LDH assay. The values from these wells were subtracted from the wells containing cells to remove any background noise.

Protocol 11: Caspase-Glo 3/7 Assay

For this technique, cells were grown and treated on 96-well flat-bottom (enzymatic assay) plates and caspase activity was measured as follows:

- The Caspase-Glo 3/7 reagent was prepared (mix) following the manufacturer's instructions, and was allowed to equilibrate to room temperature
- The 96-well plates containing cells were removed from the incubator and allowed to equilibrate to room temperature
- 100 µl of the Caspase-Glo 3/7 reagent was added to each well (100 µl) of the plate. The plate was then covered
- The contents of the wells were mixed using a plate shaker at 300-500 rpm for 30 sec. Incubation followed for 30 min at room temperature
- The luminescence of each sample in the plate was measured using a plate-reading luminometer
- In addition, blank (containing only medium) wells were treated with the Caspase-Glo 3/7 reagent. The values from these wells were subtracted from the wells containing cells to remove any background noise.

Protocol 12: Proteasome-Glo Chymotrypsin-like Cell-based Assay

For this technique, cells were grown and treated on 96-well flat-bottom (enzymatic assay) plates and proteasome activity was measured as follows:

- The Proteasome-Glo Cell-based Reagent was prepared (by mixing) following the manufacturer's instructions, and was allowed to equilibrate to room temperature
- The 96-well plates containing cells were removed from the incubator and allowed to equilibrate to room temperature
- 100 µl of the Proteasome-Glo Cell-based Reagent was added to each well (100 µl) of the plate. The plate was then covered
- The contents of the wells were mixed using a plate shaker at 700 rpm for 2 min. Incubation followed for 10 min at room temperature
- The luminescence of each sample in the plate was measured using a plate-reading luminometer
- In addition, blank (containing only medium) wells were treated with the Proteasome-Glo Cell-based Reagent. The values from these wells were subtracted from the wells containing cells to remove any background noise.

Protocol 13: Haematoxylin and Eosin (H & E) staining technique

For this technique, mice cardiac tissue sections (8 µM) were made and placed on microscope slides. They were then stained as follows:

Method

- Xylene was added for 10 min
- Xylene was discarded and 100% ethanol was added for 15 sec
- 100% ethanol was discarded and 95% ethanol (see Appendix G) was added for 15 sec. This step is repeated twice

- 95% ethanol was discarded and 70% ethanol (see Appendix G) was added for 15 sec. This step is repeated twice
- 70% ethanol was discarded and coverslips were rinsed in distilled water
- Haematoxylin dye (see Appendix G) was then added for 3 min
- The microscope slides were rinsed in distilled water first and then in acid alcohol (see Appendix G)
- The microscope slides were rinsed in distilled water again and blued in Scott's tap water (see Appendix G)
- After this was done, the microscope slides were rinsed in distilled water before adding the eosin dye (see Appendix G) for 2 min
- After the time had elapsed, the microscope slides were rinsed for a final time in distilled water and then 70% ethanol was added for 15 sec
- 70% ethanol was discarded and 95% ethanol was added for 15 sec. This step is repeated twice
- 95% ethanol was discarded and 100% ethanol was added for 15 sec. This step is repeated twice
- 95% ethanol was discarded and xylene was added for 15 sec. This step was also repeated twice
- Finally the microscope slides were mounted with permanent labelled coverslips. Allow the mounting medium to dry before use

Protocol 14: Measurement of acidic vacuole accumulation

For this technique, cells were also grown and treated in 25 cm^2 tissue culture flasks as previously described (Protocol 1). The fluorescent dye LysoTracker was used to measure acidic vacuole (eg. lysosomes) accumulation in cells after treatment.

Method

- Growth medium was discarded and cells rinsed with warm (37 °C) sterile PBS
- Warm 0.25% trypsin-EDTA (3 ml) was added and cells were incubated until cells detached from the surface (2-3 min). Culture medium (double the volume

of trypsin used; 6 ml) was added to the cell suspension, which was then transferred to a 15 ml falcon tube, centrifuged for 3 min at 6000 x g.

- Medium was decanted and cells resuspended in 500 µl warm PBS. Lysotracker was directly added onto the unfixed cells, using a final concentration of 50 nM and incubated for 10 min
- Analysis followed on the flow cytometer (BD FACSAria I) immediately thereafter. A minimum of 10 000 events (cells) were collected and using the 488 nm laser and 590 nm (Abs. = 577 nm) emission filter, fluorescence intensity signal was measured using the geometric mean on the intensity histogram

Protocol 15: Measurement of intracellular and mitochondrial ROS production

For this technique, cells were also grown and treated in 25 cm^2 tissue culture flasks as previously described (Protocol 1). The intracellular and mitochondria specific fluorescent dyes DCF and MitoSOX were used to measure mitochondrial ROS production in cells after treatment.

Method

- Growth medium was discarded and cells rinsed with warm (37 °C) sterile PBS
- Warm 0.25% trypsin-EDTA (3 ml) was added and cells were incubated until cells detached from the surface (2-3 min). Culture medium (double the volume of trypsin used; 6 ml) was added to the cell suspension, which was then transferred to a 15 ml falcon tube, centrifuged for 3 min at 6000 x g.
- Medium was decanted and cells resuspended in 500 µl warm PBS. DCF and MitoSOX were directly added onto the unfixed cells, using a final concentration of 50 µmol/L and 5 µM respectively and incubated for 15 min
- Analysis followed on the flow cytometer (BD FACSAria I) immediately thereafter. A minimum of 10 000 events (cells) were collected and using the 488 nm laser and 510/580 nm excitation/emission filters, fluorescence intensity signal was measured using the geometric mean on the intensity histogram

- In addition, concentration of 100 µmol/L H_2O_2 was used as a positive control

Protocol 16: Measurement of mitochondrial load

For this technique, cells were also grown and treated in 25 cm^2 tissue culture flasks as previously described (Protocol 1). The mitochondria specific fluorescent dye Mitotracker was used to measure mitochondrial number in cells after treatment.

Method

- Growth medium was discarded and cells rinsed with warm (37 °C) sterile PBS
- Warm 0.25% trypsin-EDTA (3 ml) was added and cells were incubated until cells detached from the surface (2-3 min). Culture medium (double the volume of trypsin used; 6 ml) was added to the cell suspension, which was then transferred to a 15 ml falcon tube, centrifuged for 3 min at 6000 x g.
- Medium was decanted and cells resuspended in 500 µl warm PBS. Mitotracker was directly added onto the unfixed cells, using a final concentration of 25 nM and incubated for 15 min
- Analysis followed on the flow cytometer (BD FACSAria I) immediately thereafter. A minimum of 10 000 events (cells) were collected and using the 490/516 nm excitation/emission filters, fluorescence intensity signal was measured using the geometric mean on the intensity histogram

Protocol 17: Measurement of mitochondrial function

For this technique, cells were also grown and treated in 25 cm^2 tissue culture flasks as previously described (Protocol 1). The mitochondria membrane potential fluorescent dye JC-1 was used to measure mitochondrial function in cells after treatment.

Method

- Growth medium was discarded and cells rinsed with warm (37 °C) sterile PBS
- Warm 0.25% trypsin-EDTA (3 ml) was added and cells were incubated until cells detached from the surface (2-3 min). Culture medium (double the volume of trypsin used; 6 ml) was added to the cell suspension, which was then transferred to a 15 ml falcon tube, centrifuged for 3 min at 6000 x g.
- Medium was decanted and cells resuspended in 500 µl warm PBS. JC-1 was directly added onto the unfixed cells, using a final concentration of 5 µM and incubated for 15 min
- Analysis followed on the flow cytometer (BD FACSAria I) immediately thereafter. A minimum of 10 000 events (cells) were collected and using the 488 nm laser, emission was collected between 515-545 nm and 575-625 nm
- Fluorescence intensity signal was measured using the geometric mean on the intensity histogram

Protocol 18: Measurement of ER load

For this technique, cells were also grown and treated in 25 cm^2 tissue culture flasks as previously described (Protocol 1). The ER specific fluorescent dye ER-tracker was used to measure ER load in cells after treatment.

Method

- Growth medium was discarded and cells rinsed with warm (37 °C) sterile PBS
- Warm 0.25% trypsin-EDTA (3 ml) was added and cells were incubated until cells detached from the surface (2-3 min). Culture medium (double the volume of trypsin used; 6 ml) was added to the cell suspension, which was then transferred to a 15 ml falcon tube, centrifuged for 3 min at 6000 x g.
- Medium was decanted and cells resuspended in 500 µl warm PBS. ER-tracker were directly added onto the unfixed cells, using a final concentration of 100 nM and incubated for 10 min

- Analysis followed on the flow cytometer (BD FACSAria I) immediately thereafter. A minimum of 10 000 events (cells) were collected and using the 374/430-640 nm excitation/emission filters, fluorescence intensity signal was measured using the geometric mean on the intensity histogram

Protocol 19: Transfection (Silencing of mTOR)

- H_9C_2 cells were seeded on 12-well plates at a density that will allow the cells to reach a confluency level of 50% the very next day
- Remove medium from cells and replace it with 500 µl fresh serum-containing medium
- Add 100 µl of serum-free medium into a clean, sterile eppendorf tube
- Add 2 µl of transfection reagent into the tube. Mix by pipetting up and down and incubate at room temperature for 5 min
- Add the appropriate volume (6 µl of 10 µM stock SiRNA = 100 nM final concentration) of SiRNA into the tube. Mix by pipetting up and down gently and incubate at room temperature for 5 min
- Add the 100 µl mixture in the tube into the wells containing 500 µl medium all at once (not drop-wise). Agitate vigorously to disperse the SiRNA evenly but avoid spillage of medium from one well to another
- After 24 hr, the medium in the wells was replaced with fresh medium and the cells were allowed to continue proliferating until the desired confluency level

Protocol 20: Ca^{2+} staining technique

For this technique, cells were grown 8-chamber slides. Cells were grown and treated as previously described.

Method

- Prepare a 1–5 mM DMSO stock solution of the AM ester (Protocol provided by manufacturer)
- Dilute an aliquot of the DMSO stock solution into a suitable buffer (PBS). Use the minimum concentration of AM ester necessary to obtain an adequate

signal; typically as low as 0.1 µM. Mix well. Do not store the AM esters in aqueous solution for extended periods, as spontaneous hydrolysis will occur

- For adherent cells rinse off the medium and replace with a solution of the AM ester. Incubate for 15 min at 37 °C
- Wash the cells twice with PBS and then incubate for a further 30 min to allow complete de-esterification of intracellular AM esters

Appendix G

Growth Medium

- 500 ml Dulbecco's Modified Eagles Medium (DMEM)
- 56 ml Fetal Bovine Serum (FBS) (filtered first before used)
- 5.6 ml Penstrep

Growth Medium (without amino acids)

- 500 ml Dulbecco's Modified Eagles Medium (DMEM – no amino acids)
- 56 ml Dialysed FBS (filtered first before used – no amino acids)

X1 Phosphate Buffer Saline (PBS)-2 L

Dissolve the following in 1 L of water

- 16 g NaCl
- 0.4 g KCl
- 2.88 g Na_2HPO_4 (di Sodium hydrogen phosphate)
- 0.48 g KH_2PO_4 (potassium dihydrogen phosphate)

Adjust pH to 7.4, fill up to the 2 L mark with distilled water and sterilize by autoclaving

Trypan Blue dye

- Weight out 40 g trypan blue dye and dissolve this in 100 ml PBS
- Store away at 4 ºC

Propidium Iodide and Hoechst 33342 stain

- Dissolve 5 µl Propium iodide in 1000 µl sterile PBS
- Dissolve 5 µl Hoechst 33342 in 1000 µl sterile PBS
- These solutions are made fresh and must be kept on ice and away from light

10% Acid alcohol

- 10 ml 1% HCl dissolved in 1 L 70% alcohol

95% alcohol (1 L)

- Dilute 950 ml 100% ethanol with 50 ml distilled water

70% alcohol (1 L)

- Dilute 700 ml 100% ethanol with 300 ml distilled water

Harris Haematoxylin

- 5 g Harris haematoxylin
- 100 g Ammonium Alum
- 50 ml 100% ethanol
- 1 L distilled water
- 2.5 g mercury oxide

To prepare: Dissolve haematoxylin in ethanol and add the ammonium alum to distilled water and heat to boiling point. Immediately add the mercuric oxide and shake until the solution has a purple-black colour. Cool rapidly in the fridge

For staining: Filter before use and add 4 ml glacial acetic acid per 100 ml of haematoxylin

Eosin

Stock solution: dissolve 10 g eosin in 1 L distilled water

Working solution: 10 ml eosin stock solution dissolved in 90 ml distilled water. This must be prepared fresh

For staining: Add 2-3 drops of glacial acetic acid per 100 ml before use

Scott's Tap Water

- 3.5 g $NaHCO_3$
- 20 g $MgSO_4$
- 10 ml 37% Formalin
- 1 L tap water

To prepare: dissolve $NaHCO_3$ in the tap water first and then add $MgSO_4$ and formalin

DCF and **MitoSOX Red**

- Dissolve the 50 µg MitoSOX mitochondrial superoxide indicator in 13 µL of high-quality, anhydrous dimethylsulfoxide (DMSO) to make a 5 mM stock solution
- Dissolve the of 5 mM stock solution to a final working concentration (5 µM) in PBS
- Dissolve the DCF stock solution to a final working concentration (50 µmol/L) in PBS

LysoTracker Red

- Dissolve the of 1 mM stock solution to a final working concentration (50 nM) in PBS

MitoTracker Green

- Dissolve the lyophilized MitoTracker product in DMSO to a final concentration of 1 mM (stock solution)

- Dilute the 1 mM stock solution to the final working concentration (25 nM) in PBS

ER-Tracker Blue-White

- Dissolve the of 1 mM stock solution to a final working concentration (100 nM) in PBS

Fura ratiometric Ca^{2+} indicator

- Prepare a 1-5 mM DMSO stock solution of the AM esters
- Dilute an aliquot of the DMSO stock solution into a suitable buffer such as PBS. Use the minimum concentration (0.1-5 µM) of AM ester necessary to obtain an adequate signal
- Add one volume of aqueous AM ester dispersion to one volume of cell suspension or adherent cells
- Fluorescent images were then obtained and changes in the ratio were observed and calculated

RIPA buffer (100 ml)

- Prepare 50 mM Tris-HCl: add 790 mg Tris to 75 ml distilled water. Add 900 mg NaCl and stir. Adjust pH to 7.4 using HCl. Pour the prepared Tris-HCl into a 100 ml beaker. Add the following reagents in the beaker in the same order as they appear on the table

	Final Concentration	Volume
NP-40	1%	10 ml
Na-deoxycholate	0.25%	2.5 ml
EDTA	1 mM	1000 µl
Phenylmethylsulfonyl Flouoride (PMSF)	1 mM	1000 µl
Leupeptin	1 µg/ml	1 µl
SBTI-1	4 µg/ml	80 µl
Benzamidine	1 mM	100 µl

Na_3VO_4	1 mM	1000 µl
NaF	1 mM	500 µl

- Add 1000 µl Triton X-1000 to the solution and finally fill up to 100 ml with distilled water and mix thoroughly
- Aliquot 1000 µl of RIPA buffer into eppendorf tubes and store at -20 ºC

BSA (Bovine serum albumin 1 mg/ml)

- For 1 ml BSA, weight out 1mg BSA and add 1000 µl distilled water.
- For use during Western blotting, this BSA needs to be diluted. Pipette 100 µl from 1 mg/ml BSA in new eppendorf tube and add 400 µl distilled water
- Mix well

Bradford Reagent (1 L)

- Weight out 500 mg Coomassie Brilliant Blue G and add it to 250 ml 95% ethanol
- Add 500 ml phosphoric acid and mix well
- Fill up to 1 L with distilled water and store at 4 ºC
- For use during Western blotting, this solution needs to be filtered twice and then a 1:5 dilution needs to be made

3X Sample buffer

- Measure 33.3 ml stacking Tris (0.5 M) and place in a beaker
- Weigh out 8.8 g SDS and 20 g glycerol and place in the beaker
- Add a pinch of Bromo-phenol blue to the mixture
- Add and make up to 75.47 ml with distilled water

Tris pH 8.8 (500 ml)

- Weigh out 68.1 g Tris (1.124 M) and 1.5 g SDS (0.3%) and place in a beaker.

- Add 400 ml distilled water, stir and then adjust pH using HCl
- Add 100 ml distilled water to make the final volume to 500 ml

Tris pH 6.8 (500 ml)

- Weigh out 30.3 g Tris (0.5M) and 2g SDS (0.4%) and place in a beaker.
- Add 400 ml distilled water, stir and then adjust pH using HCl
- Add 100 ml distilled water to make the final volume to 500 ml

Tris pH 6.8 (100ml) for Sample buffer

- Weigh out 6.06 g Tris (0.5 M) and 4 ml 10%SDS and place in a beaker
- Add 80 ml distilled water, stir and then adjust pH using HCl
- Add 20 ml distilled water to make the final volume to 100 ml

10% Sodium dodecyl sulphate (SDS 500 ml)

- Weight out 50 g SDS and add 500 ml distilled water

10% Ammonium persulphate (1000 µl)

- Weight out 0.1 g APS into an eppendorf tube and add 1000 µl distilled water

6% acrylamide (separating) gel

Distilled water	2.6 ml
1.5 M Tris-HCl (pH 8.8)	1.3 ml
10% SDS	50 µl
Acrylamide	1.0 ml
10% APS	50 µl
Temed	4 µl

8% acrylamide (separating) gel

➢ Distilled water	➢ 2.3 ml
➢ 1.5 M Tris-HCl (pH 8.8)	➢ 1.3 ml
➢ 10% SDS	➢ 50 µl
➢ Acrylamide	➢ 1.3 ml
➢ 10% APS	➢ 50 µl
➢ Temed	➢ 3 µl

10% acrylamide (separating) gel

➢ Distilled water	➢ 3.85 ml
➢ 1.5 M Tris-HCl (pH 8.8)	➢ 2.5 ml
➢ 10% SDS	➢ 100 µl
➢ Acrylamide	➢ 2.5 ml
➢ 10% APS	➢ 50 µl
➢ Temed	➢ 5 µl

12% acrylamide (separating) gel

➢ Distilled water	➢ 3.35 ml
➢ 1.5 M Tris-HCl (pH 8.8)	➢ 2.5 ml
➢ 10% SDS	➢ 100 µl
➢ Acrylamide	➢ 3.0 ml
➢ 10% APS	➢ 50 µl
➢ Temed	➢ 5 µl

4% acrylamide (stacking) gel

➢ Distilled water	➢ 6.1 ml
➢ 0.5 M Tris-HCl (pH 6.8)	➢ 2.5 ml
➢ 10% SDS	➢ 100 µl

➢ Acrylamide	➢ 1.0 ml
➢ 10% APS	➢ 100 µl
➢ Temed	➢ 20 µl

Running buffer (1 L)

- Weight out 3.03 g Tris, 1.44 g Glycine and 1 g SDS into a 1 L beaker. Add 500 ml distilled water and stir until dissolved
- Fill up to 1 L with distilled water

10X TBS (5 L)

- Weight out 121 g Tris and 80 g NaCl into a 5 L beaker. Add 2.5 L distilled water and stir until dissolved.
- Adjust pH to 7.6 using HCl and then fill up to 5 L with distilled water
- For use in Western blotting, take a 1 L measuring cylinder and add 100 ml 10X TBS and dilute with 900 ml distilled water
- To make **TBST**, add 1 ml tween to 1 L diluted solution of TBS

Transfer Buffer

- In a 1 L cylinder, add 100 ml Biorad 10X TG buffer, 200 ml 100% methanol and 700 ml distilled water

Milk blocking solution (100 ml)

- Weight out 5 g non-fat dry instant milk powder into a beaker. Add 100 ml TBS and mix well
- Finally add 10 µl Tween and mix well. This is sufficient for only one gel

Primary (1º) antibody

- Pipette 5 µl 1º antibody in 5 ml TBST in a 50 ml falcon tube. This concentration is suitable for most 1º antibodies but others require a higher concentration

Secondary (2º) antibody

- Pipette 2.5 µl 2º antibody and 10 ml TBST in a 50 ml falcon tube

Stripping buffer (1 L)

- Dissolve 8 g NaOH in 1 L distilled water

Appendix H

Reagents	Catalogue Number	Company
Absolute alcohol	32221	Riedel deHaën
Agarose D-1 LE	39209080	Hispanagor
6-Aminohexanoic Acid	A7824	Sigma
Acrylamide	A3699	Sigma
Ammonium Alum	A2140	Sigma
Ammonium Persulphate (APS)	A3678	Sigma
Bafilomycin A1	1793	Sigma
Biorad 10X TG (Tris/Glycine) Buffer	1610771	Biorad
Bovine Serum Albumin (BSA)	A4503	Sigma
Bradford Reagent	B6916	Sigma
Bromophenol Blue	32400A	UnivAR
Caffeine	C0750	Sigma
Caspase-Glo 3/3 Assay	G8091	Promega
Coomassie Brilliant Blue G	27815	Fluka
Coverslips (18 X 18mm)	S1815	Sigma
CytoTox 96 non-radioactive cytotoxicity assay (LDH Assay)	G1780	Promega
Dako Fluorescent Mounting Media	S3023	DakoCytomation
Doxorubicin (DXR)	D1515	Sigma
Dulbecco's Modified Eagles medium (DMEM) + GlutaMAX-1	32430	Gibco
DMEM – no amino acids	CN3489	Highveld Biological
Eosin	32617	Riedel deHaën
ECL™ Western Blotting analysis system	RPN2108	Amersham Biosciences
ER-Tracker Blue-White	E12353	Molecular Probes, Invitrogen

Fetal Bovine Serum (FBS)	10270	Gibco
Dialyzed FBS	26400-044	Gibco
Formalin	HTS0-1-128	Sigma
Fura Ratiometric Calcium indicators	F1221	Molecular Probes, Invitrogen
Glacial Acetic Acid	UN2789	Merck
Glycerol	G5516	UnivAR
Glycine	G8898	Sigma
Harris haematoxylin	OB657122	Merck
Hoechst 33342	B2261	Sigma
Hydrochloric Acid (HCl)	UN1789	Merck
H_2O_2 (Perdrogen)	31642	Riedél-de Haën
Iso-butanol	UN1212	Merck
Isopentane	1071771000	Merck
Isopropanol 31	461-1	Sigma
JC-1	T3168	Invitrogen
LysoTracker Red	L7528	Molecular Probes, Invitrogen
Magnesium Sulphate (MgSO4)	M2643	Sigma
Manual X-ray Developer	9X23018	Axim
Manual X-ray Fixative	9X23013	Axim
Mercuric Oxide	21-335-7	Sigma
Methanol	UN1250	Merck
MG132 (Z-Leu-Leu-Leu-al)	C2211	Sigma
Microscope slides (25 X 75 mm)	S8400	Sigma
MitoSOX Red	M36008	Molecular Probes, Invitrogen
MitoTracker Green	M7514	Molecular Probes, Invitrogen
MTT (Thiazolyl Blue Tetrazolium Bromide)	M5655-16	Sigma
PecqGold prestained protein	27-2110	Peqlab

Marker		
Penicillin-Streptomyin Solution	P4333	Sigma
Phenol solution	P5447	Sigma
Phosphoric Acid	P5811	Merck
Ponceau S solution	P7170	Sigma
Precision plus protein dual colour standards	161-0374	Bio-Rad
Propidium Iodide (PI)	P4170	Sigma
Proteasome-Glow Chymotrypsin-like Cell-based Assay	G8622	Promega
Rapamycin	R8781	Sigma
Rapid Mounting Media for Microscopy	UN1866	Merck
SiRNA (mTOR)	6381	Cell Signalling
Sodium Dodecyl Sulphate (SDS)	L3771	Sigma
Sodium Hydrogen carbonate (NaHCO3)	AC006329.500	Merck
SR FLIVO *in vivo* apoptosis kit	983	ImmunoChemistry Technologies
Temed	T9281	Sigma
FuGENE Transfection Reagent	11814443001	Roche
Triton X-100	X-100	Sigma
Trizma-base	93304	Fluka
Trypan Blue dye	T6146	Sigma
0.25% Trypsin-EDTA Solution	T4049	Sigma
Tween 20	P5927	Sigma
Xylol	UN1307	Merck

Primary Antibodies

	Catalogue Number	Company Name
Cleaved-caspase-3	9665	Cell Signalling
Cleaved-PARP	9541S	Cell Signalling
Bax	2772	Cell Signalling
Bcl2	2827	Cell Signalling
Beclin-1	3738	Cell Signalling
LC-3B	2775	Cell Signalling
Anti-P62 protein	03-GP62-C	American Research Products
p-FoxO1/FoxO3a	9464	Cell Signalling
T-FoxO3a	9467	Cell Signalling
MAFbx	Sc-33782	Santa Cruz Biotechnotology
Anti-MuRF-1/TRIM 63	IMX-3924	Imgenex
Anti-ubiquitin (P4D1)	3936	Cell Signalling
p-Akt	9275	Cell Signalling
T-Akt	9272	Cell Signalling
p-mTOR	2971L	Cell Signalling
T-mTOR	2983	Cell Signalling
B-actin	4967	Cell Signalling

Secondary Antibodies

	Catalogue Number	Company Name
ECL Anti-rabbit IgG, Horseradish peroxidase linked whole antibody	NA 934V	Amersham Life Science
Peroxidase labelled anti-mouse antibody	NIF 825	Amersham Life Science
Anti-goat IgG (H & L) (Donkey)	605-703-125	Rockland

Paper and Film

	Catalogue Number	Company Name
Hyperfilm	28-9068-36	Amersham Biosciences
Immobilon™ P transfer membrane (PVDF)	IPVH00010	Millipore
Paper (Blotting) Sheets	06-134	Lasec

References

1. Loos, B. 2009. Cell death in hypoxic injury: signaling mechanisms and dynamics in the decision making process. *Stellenbosch: SUN PReSS* (Thesis)
2. Scherz-Shouval, R., Zvulun, E. 2007. ROS, mitochondria and the regulation of autophagy. *TRENDS in cell Biology*. 17: 422-427